SCREENING PATTERN EFFECT ON PRINT USING FLEXOGRAPHY AND SCREEN PRINTING

Thesis submitted by

Soumen Basak

Doctor of Philosophy (Engineering)

Department of Printing Engineering
Faculty Council of Engineering & Technology
Jadavpur University
Kolkata, India
2025

JADAVPUR UNIVERSITY

KOLKATA – 700 032, INDIA

INDEX NO. 290/23/E

1. **Title of the Thesis:** Screening pattern effect on print using flexography and screen printing
2. **Name, Designation & Institute of the Supervisor/s:**

Kanai Chandra Paul
Professor
Department of Printing Engineering
Jadavpur University
Kolkata

3. **List of Publications**

1. Soumen Basak, Saritha P.C and Kanai Chandra Paul, “Optimization of flexographic process parameters using taguchi’s grey relational analysis technique” in Acta Graphica, ISSN 0353-4707 (Tisak), ISSN 1848-3828 (Online), Vol. 32, No. 2, September, 2024, pp 68-83.
2. Soumen Basak, Saritha P.C and Kanai Chandra Paul, “Print quality optimization in screen printing by AM and FM screening using Taguchi’s Grey Relational Analysis technique” in Journal of Graphic Engineering and Design, ISSN 2217-379X, ISSN (Online) 2217-9860, Vol. 16, No. 1, March, 2025, pp 39-50.
3. Soumen Basak, Saritha P.C, Alenrex Maity and Kanai Chandra Paul, “Machine learning approach to predict the dot gain of flexographic prints” in Acta Graphica, ISSN 0353-4707 (Tisak), ISSN 1848-3828 (Online), Vol. 33, No. 1, March, 2025, pp 34-43.
4. Soumen Basak, Saritha P.C and Kanai Chandra Paul, “Application of box behnken design to optimize some parameters for flexographic printing process” in Acta Graphica, ISSN 0353-4707 (Tisak), ISSN 1848-3828 (Online), Vol. 33, No. 2, June, 2025, pp 44-59.
5. Soumen Basak, Saritha P.C, Alenrex Maity and Kanai Chandra Paul, “Prediction of dot gain in flexographic color printing using machine learning”, Journal of Graphic Engineering and Design. (Accepted)

Soumen Basak
10.10.2025

10/10/2025

6. Soumen Basak, Saritha P.C, Alenrex Maity and Kanai Chandra Paul, “Comparison of machine learning models for hue error prediction in flexographic process color printing”, Journal of Print and Media Technology Research. (Accepted)

Soumen Basak
10.10.2025

10/10/2025

“Statement of Originality”

I, Soumen Basak (Index No. 290/23/E) registered on April 13, 2023 do hereby declare that this thesis entitled “Screening pattern effect on print using flexography and screen printing” contains literature survey and original research work done by the undersigned candidate as part of Doctoral studies.

All information in this thesis have been obtained and presented in accordance with existing academic rules and ethical conduct. I declare that, as required by these rules and conduct, I have fully cited and referred all materials and results that are not original to this work.

I also declare that I have checked this thesis as per the “Policy on Anti Plagiarism, Jadavpur University, 2019”, and the level of similarity as checked by iThenticate software is 4%.

Soumen Basak
10.10.2025

Signature of Candidate

Date:

10/10/2025

Certified by Supervisor:

(Signature with date, seal)

Professor
Department of Printing Engineering
Jadavpur University, Salt-lake Campus
Kolkata - 700 098

CERTIFICATE FROM THE SUPERVISOR

This is to certify that the thesis entitled “Screening pattern effect on print using flexography and screen printing” submitted by Shri Soumen Basak, who got his name registered on April 13, 2023 for the award of Ph. D. (Engg.) degree of Jadavpur University is absolutely based upon his own work under the supervision of me and that neither his thesis nor any part of the thesis has been submitted for any degree/diplom or any other academic award anywhere before.

10/10/2025

.....

Signature of the Supervisor

and date with Office Seal

Professor
Department of Printing Engineering
Jadavpur University, Salt-lake Campus
Kolkata - 700 098

Acknowledgements

When I started my Ph. D. journey, I did not anticipate the wonderful experiences that lay ahead of me. After completing this, I have realised, I could not finish this monumental task without extreme help and moral support of some people who made my dream true.

Firstly, I want to express my gratitude to my guide Prof. Kanai Chandra Paul for his exceptional academic knowledge along with his guidance and encouragement. Then I want to thank all the faculty members and staff of Printing Engineering Department for their support. I would also like to thank everyone of Jadavpur University associated with my work in every possible way.

In this occasion, I would like to remember my parents and in-laws who are now no more. But it is they who inculcated the seeds of academic dream in me, and their joys knew no bounds if they could live to see this day. I want to dedicate this Ph. D. thesis in remembrance of their holy memory.

Lastly, I want to express my deepest gratitude to my wife Mrs. Trishna Basak, who has been my pillar of strength throughout ups and downs of this journey. I would like to thank my daughter Ms. Souti Basak, for her constant persuasion and encouragement. Their belief in me has made this day possible.

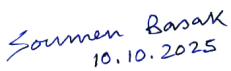

Soumen Basak

Contents

List of Figures

List of Tables

Chapter 1
Introduction

1.1 Preliminaries

Printing is one of the greatest inventions of mankind. Mass communication becomes easier due to this invention.

The conventional printing techniques can be divided into different categories like letterpress, flexography, gravure, lithography and screen printing. Flexography and screen printing both are direct printing process [1].

1.2 Flexography Printing

In flexography printing, the image areas are raised above the non-image areas. When an inked roller is passed over the image carrier, the ink only adheres to the raised image areas leaving the lower areas uninked. The inked image is transferred under pressure onto the printing substrate. A flexible rubber or photopolymer plates are used. A liquid type or low viscosity ink is transferred to the printing plate via an anilox roller which is evenly screened with cells [2].

Flexography printing employs anilox roller having engraved cells look like screen in appearance. Screen printing uses screen mesh on which screened and lined images are formed is similar to screen. This type of screen like effect affects print quality on substrate [26].

Flexography is a roll to roll relief printing technique which uses liquid ink and flexible photopolymer or rubber printing plate to produce quality image onto a wide variety of substrates such as paper, paperboard, plastic films, foils, laminations etc. [18]. Figure 1.1 represents the schematic diagram of flexography printing unit.

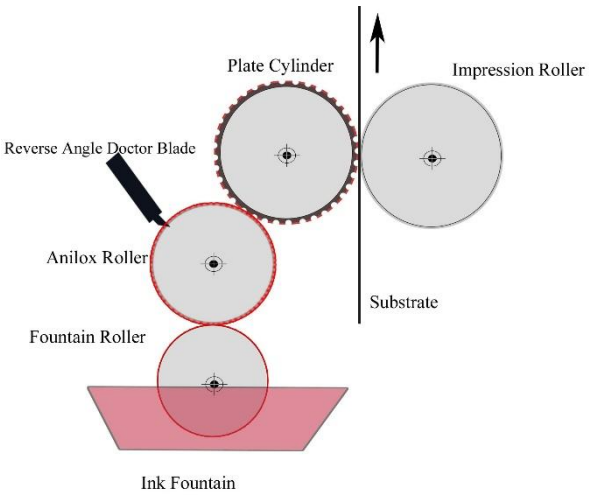

Figure 1.1: Schematic diagram of flexography printing unit

The flexography printing employs anilox roller inking system and it acts as the fundamental part of the printing unit for efficient transmitting and metering of ink from the ink fountain to the printing plate. The characteristics of cells engraved on the surface of anilox roller determine the quantity of ink to be supplied to the printing plate. So, the quality of flexography print ultimately depends on the surface properties of the anilox roller. Figure 1.2 represents the schematic diagram of anilox roller.

Figure 1.2: Schematic diagram of anilox roller [25]

The remarkable distinctiveness of flexography printing technique to deliver quality image onto a wide variety of surfaces makes it as a suitable printing technique for a wide application like commercial printing, packaging, publication printing etc. Nowadays, the key part of the printing of the paper related to the packaging

applications are carried out by flexography printing because of its excellence in printability together with cost-effective nature and simplicity when compared to other printing techniques. Various researches and studies are going on in the industry and academic institutions to investigate more into the factors related to the flexography printing.

1.3 Screen Printing

Screen printing is a stencil printing process. The image and non-image areas are formed on a woven mesh screen. Image areas are open while non-image areas are blocked using a light hardened coating. Ink is poured into the upper surface of the screen, then spread across it and pushed through the open mesh with a squeegee and transfers onto the different type of substrates. This is the only type of printing that prints through the image carrier rather than from it [26].

One of the more adaptable printing techniques among the traditional printing methods is screen printing, which prints using an image carrier in the form of a stencil. The stencil can be made on a screen mesh using photographic techniques and printing is accomplished by using a squeegee to force ink through opening of the stencil onto the substrates. Regardless of the surface textures and shapes, a variety of substrates, including paper, paperboard, glass, plastics, metals, ceramics, etc. can be used to print on them. Figure 1.3 shows the schematic diagram of the screen printing unit.

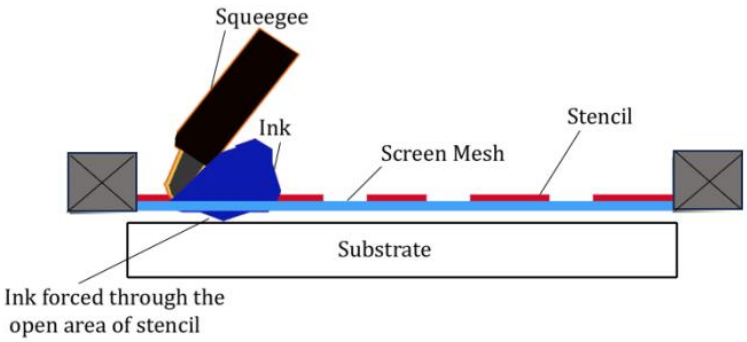

Figure 1.3: Schematic diagram of screen printing unit

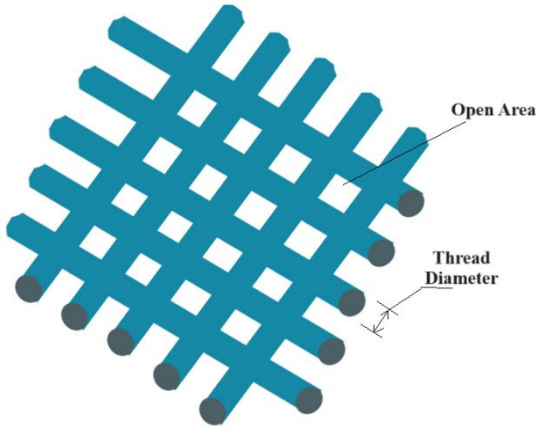

Figure 1.4: Woven structure of screen mesh

Figure 1.4 shows the schematic of the woven screen mesh on which images are formed by photomechanical process using light sensitive coating.

1.4 Taguchi Grey Relational Analysis

Taguchi grey relational analysis technique is an optimization technique in engineering and manufacturing process that combines Taguchi method and Grey Relational Analysis (GRA) to solve complex multi-response optimization problems. Taguchi method was developed by Dr. Genechi Taguchi which focuses on improving the quality of product and processes by minimizing variability through robust design. GRA technique was introduced by Deng Julong from Grey System Theory.

The printing industry has always been facing with various challenges in their working environment and that may have contained several multi-criteria based decision making problems to be solved. In such cases, the approach of taking advantages of the Taguchi's grey relational analysis technique is appreciable one.

The general methods that go through the different steps are as following:

- Design of experiments with Taguchi method
- Conducting experiments
- Data collection
- Data preprocessing
- Grey relational grade generation
- Ranking the experiments

For this purpose, the following equations are generally used like normalization of performance index data, deviation sequence, grey relational co-efficient and grey relational grade.

Normalization of Performance Index Data

- For beneficial attributes (higher is better),

$$X_i^*(k) = \frac{X_i(k) - \min X_i(k)}{\max X_i(k) - \min X_i(k)}$$

- For non-beneficial attributes (lower is better),

$$X_i^*(k) = \frac{\max X_i(k) - X_i(k)}{\max X_i(k) - \min X_i(k)}$$

where,

$Xi^*(k)$ = Normalized value of i^{th} data of 'k' responses

$Xi(k)$ = Actual value of i^{th} data of 'k' responses

$\min Xi(k)$ = Lowest value of $X_i(k)$ for 'k' responses

$\max X_i(k)$ = Highest values of $X_i(k)$ for 'k' responses

Deviation Sequence

- Deviation Sequence is given by the equation,

$$\Delta i(k) = X_0^m(k) - X_i^*(k)$$

where,

$\Delta i(k)$ = Deviation sequence of i^{th} data for 'k' responses

$X_0^m(k)$ = Maximum value among the $Xi(k)$ elements of 'k' responses

$X_i^*(k)$ = Normalized value of performance index of 'k' responses

Grey Relational Co-efficient

- Grey Relational Co-efficient is given by the equation,

$$\xi_i(k) = \frac{\Delta_{min} - \xi\Delta_{max}}{\Delta_i(k) + \xi\Delta_{max}}$$

where,

$\xi i(k)$ = Grey relational co-efficient of i^{th} data for 'k' responses

Δ_{min} = Minimum value obtained from deviation sequence

Δ_{max} = Maximum value obtained from deviation sequence

$\Delta i(k)$ = Deviation sequence of i^{th} data for ‘k’ responses

Dynamic Distinguished Co-efficient (ξ) = 0-1

For multiple decision-making criteria, the value can take as 0.5.

Grey Relational Grade

- Grey Relational Grade is given by the equation,

$$\Upsilon_i = \frac{1}{n}\sum_{k=1}^{n} \xi_i(k)$$

where,

Υi = Grey relational grade of i^{th} data for ‘k’ responses

n = Number of data responses

$\xi i(k)$ = Grey relational co-efficient of i^{th} data for ‘k’ responses

Dot Gain

It is the measure of how different the halftone dot size is reproduced in relation to the original dot given at the input.

Dot Gain (%) = % Dot Area of Printed Dot - % Dot Area of Target Dot

Hue Error

It is the measure of degree of contamination of the printed ink in the aspects of change in hue of the color.

$$\text{Hue Error} = \frac{D_M - D_L}{D_H - D_L} \times 100$$

where,

D_H = Highest solid ink density

D_M = Medium solid ink density

D_L = Lowest solid ink density

Print Contrast

- It indicates that how well a printing system reproduces image detail in particular tonal regions, especially shadow region.

$$\text{Print Contrast} = \frac{D_S - D_T}{D_S} \times 100$$

where,

D_S = Solid ink density (solid areas)

D_T = Solid ink density (tinted areas)

Solid Ink Density

It is the measurement of how much ink is deposited onto a printed patch of the substrate during the printing process.

Taguchi grey relational analysis technique can be applied in flexography and screen printing to find optimal printing conditions that enhance print quality and reduce defects.

Taguchi grey relational analysis technique can be used to optimize and analyze the optical print density, dot gain, hue error and print contrast in the flexography printing. To optimize the above parameters, the anilox cell count, halftone dot shape and type of substrates in the print quality of flexography printing are targeted.

In screen printing, Taguchi grey relational analysis technique is used to optimize parameters such as solid ink density, dot gain, hue error and print contrast. To optimize these parameters, different screen mesh count, the impact of AM and FM halftone in the print quality on both coated and uncoated paper grades are considered.

1.5 Box Behnken Design

Box Behnken Design (BBD) is a Response Surface Methodology (RSM) technique, a powerful statistical tool is used by fitting a quadratic model to experimental data for process optimization. It was developed by George E. P. Box and Donald Behnken in 1960.

The Box Behnken experimental designs for response surface methods use the following steps:

- The factors (input parameters) have to be defined and their three levels (low (-1), centre point (0) and high (+1)) have to be mentioned.
- After that, a design matrix is generated by the software with specific combinations of factor levels.
- Then experiments are carried out at these specified design points.
- Next, the experimental results are analysed using statistical methods such as ANOVA for identification of significant variables and interactions and development of the quadric model.
- Finally, the model is used for prediction of optimal conditions for the process.

The number of experimental run, N for BBD experiment can be found out using the following formula:

$$N = 2k(k-1) + C$$

where,

k = number of factors

C = number of centre points in the design

The main advantage of this process is fewer experimental runs. This design is most widely used in engineering applications.

Figure 1.5 shows the basic structure of BBD.

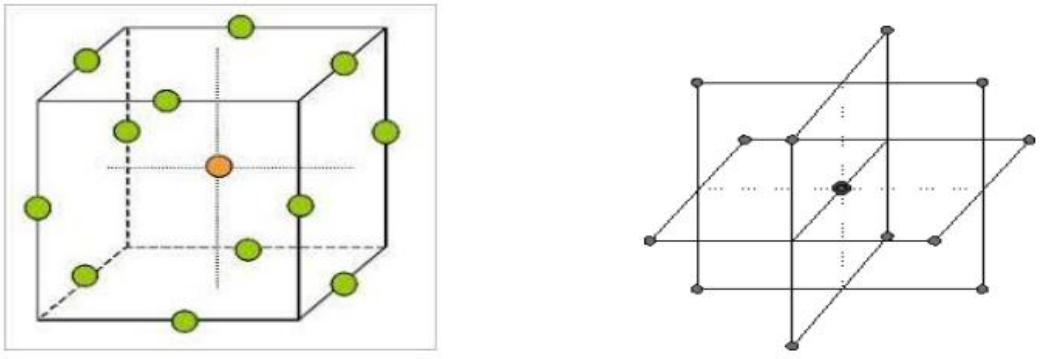

Figure 1.5: Basic structure of BBD

In flexography printing, BBD can be used to optimize key process parameters such as three kinds of anilox roller screen rulings, three grades of paper substrates with different smoothness, and three levels of halftone dot percentages. The dot gain and print contrast are taken as the output responses that denote the degree of accomplishment of print quality.

Key process parameters that can be optimized using BBD in screen printing include three types of screen meshes, three classes of paper substrates with varying smoothness and three degrees of halftone dot percentages. The output responses that indicate the level of print quality are the dot gain and print contrast.

1.6 Machine Learning

Predictive modeling is very important in modern statistics, data science and machine learning. It consists of developing algorithms which are able to make predictions based on historical and current data. In early 20^{th} century, statistical forecasting techniques were used. With the invention of computers, these techniques have become more complex, from which predictive modeling is originated. Nowadays, predictive modeling is used all over industries to improve decision making and process automation.

There are two types of predictive modeling viz. regression and classification. Regression is used to predict continuous numerical values, e.g. the future price of a product. In comparison to regression, classification is used to predict discrete categorical outcomes, e.g. to detect a spam email. The selection of regression and classification depends on target variables. Mathematical robustness, adaptability and flexibility of regression make it suitable for numerical prediction tasks.

Regression analysis is particularly designed for modeling the relationship between one or more independent variables i.e. features and a dependent continuous variable i.e. target. Its main objective is to quantify the magnitude and direction of these relationships and offer a predictive function that converts input values to numerical outputs.

Regression models– specifically different modern types of machine learning models are best in the following situations:

- Non-linear pattern capturing (e.g. support vector machines regression, decision tree)
- Auto learning feature interactions without explicit programming
- Dealing with large sets of predictors with varying scales and distributions
- Offering generalizable models which perform well on unknown data

In regression, target variable is continuous. Its output is real-valued numerical prediction e.g. predicting next week's average rainfall. Here loss functions are Mean Squared Error (MSE), Root Mean Squared Error (RMSE), Mean Absolute Error (MAE) and R^2.

Some commonly used machine learning algorithms are Linear Regression, Decision Tree Regression, Random Forest Regression, Extreme Gradient Boosting or XG Boost Regression, Support Vector Machines Regression, Neural Network Learning Algorithms etc. These machine learning algorithms give better performance regarding accuracy, training time, parameters, data points etc. and most commonly used techniques.

1.6.1 Linear Regression

This is a well known regression technique as well as one of the most widely used machine learning modeling strategies. With this method, the independent variable(s) can be discrete or continuous, the dependent variable is continuous and the regression line has a linear form. Using the best fit straight line, linear regression establishes a link between the dependent variable and one or more independent variables that are referred to as the regression line. Using the provided predictor variable(s), one can use the regression equation to predict the value of the target variable. An expansion of simple linear regression is multiple linear regression models in which a response variable acts as a linear function of two or more predictor variables. Linear regression gives best result in case of quick, interpretable baseline for simple linear relationships.

Mathematical formulation:

The equation for a multiple linear regression model is:

$$y = \alpha_0+\alpha_1x_1+\alpha_2x_2+\ldots\ldots\ldots+\alpha_nx_n+\varepsilon$$

where,

y = Dependent (target) variable

$x_1, x_2, \ldots\ldots, x_n$ = Independent (predictor) variables

α_0 = Intercept term (value of y when all predictors are zero)

$\alpha_1, \alpha_2, \ldots\ldots\ldots, \alpha_n$ = Coefficients (weights) assigned to each predictor

ε = Error term, representing the difference between the observed and predicted values

1.6.2 Decision Tree Regression

It is a non-parametric supervised learning method. Both the regression and the classification challenges make use of decision tree learning techniques. The decision tree classifies the instances by sorting the tree from the root to a few leaf nodes. Starting at the root node of tree and working along the branch that corresponds to the attribute value, instances are categorized by examining the attribute defined by that node. The most widely used criterion for splitting is 'gini' for the gini impurity and 'entropy' for the information gain. When non-linear problems, where interpretability and quick prototyping are important, the decision tree is suitable.

Mathematical formulation:

A decision tree regression intends to minimize the Mean Squared Error (MSE) within each region after splitting.

For example, a dataset D containing N samples with target values $d_1, d_2, \ldots, d_N$, the MSE for a node is expressed as:

$$\mathrm{MSE} = \frac{1}{N}\sum_{i=1}^{N}\left(d_i - \bar{d}\right)^2$$

where, $\bar{d}$ is the mean of the target values in that node.

1.6.3 Random Forest Regression

It is a well known ensemble classification method both in machine learning and data science with a wide range of applications. This technique employs 'parallel ensembling'

which fits multiple decision tree classifiers concurrently on various subsamples of the data set. The final result is determined by majority voting or averages. As a result, it reduces the issue of overfitting and raises control and prediction accuracy. It blends random feature selection with bootstrap aggregation or bagging to create a sequence of decision trees with controlled variation. It fits well for both continuous and categorical variables and may be adjusted for both regression and classification issues. Random forest is used for large datasets requiring accuracy and robustness without much hyper parameter tuning.

Mathematical formulation:

A Random Forest contains Q decision trees, each trained on a different bootstrap sample from the dataset. Say,

$D = (x_1,y_1),(x_2,y_2),\ldots,(x_N,y_N)$ be the training data.

R_q be the q^{th} decision tree model.

For each tree:

1. A bootstrap sample D_q is obtained from D (sampling with replacement).
2. Only a random subset of features k (where $k < p$, the total number of features) is considered at each split.

The prediction for a new input x is:

$$\hat{y} = \frac{1}{Q}\sum_{q=1}^{Q} R_q(x)$$

1.6.4 XG Boost Regression

It is a technique for ensemble learning that builds a final model from a set of individual models usually decision trees. In the same way that neural networks employ gradient descent to improve weights, the gradient is used to minimize the loss function. A variation of gradient boosting is called Extreme Gradient Boosting (XG Boost) which considers more precise approximations while choosing the optimal model. It computes the second order gradients of the loss function to minimize loss and achieve advanced regularization. This reduces overfitting and increases the generalization and

performance of the model. XG Boost can process large sized datasets efficiently and interprets results quickly. High-stakes prediction tasks when accuracy is critical and availability of computational resources are the criterions for choosing the XG boost.

Mathematical formulation:

Say, a dataset is given as,

$D = (x_1,y_1),(x_2,y_2),\ldots,(x_N,y_N)$

and a model that predicts $\hat{y}_i$, the objective function is given as,

$$\mathcal{L}(\phi) = \sum_{i=1}^{N} \left(m(y_i, \hat{y}_i) + \sum_{r=1}^{R} \Omega(f_r) \right)$$

where,

$m(y_i,\hat{y}_i)$ is a differentiable loss function (e.g., Mean Squared Error for regression).

f_r represents the r^{th} decision tree.

$\Omega(f) = \alpha T + \frac{1}{2}\beta \sum_{j=1}^{T} w_j^2$ is the regularization term

where,

T = number of leaves,

w_j= weight of leaf j,

α and β are regularization parameters.

The trees are constituted additively, updating predictions as:

$$\hat{y}_i^{(k)} = \hat{y}_i^{(k-1)} + \eta f_k(x_i)$$

Where η is the learning rate controlling the contribution of each new tree.

1.6.5 Support Vector Machines Regression

The support vector machines (SVM) regression algorithm is also a well employed technique in regression and classification tasks. They are able to handle nonlinear relationships and high-dimensional data. The algorithm mostly uses the vector machine approach in the particular application procedure to finish the predetermined data

analysis work. In order to optimize the data information, the SVM algorithm will simultaneously examine the data to be processed using the automatic support of the SVM. To enhance the scientific quality of the final data analysis results, it gathers numerous sets of analysis samples during the analysis process and identifies the sample data of the boundary value. The algorithm identifies the largest possible separation hyper plane between the many classes present in the target feature. SVM is best used when small to medium datasets with complex non-linear boundaries are involved.

Mathematical formulation:

The main objective is for approximation of the target function $f(x)$ so that deviations from the true values y fall within a pre-defined tolerance ϵ. Any prediction error smaller than ϵ is not considered, which leads to the ε-insensitive loss function:

$$L_\epsilon(y, f(x)) = \max\left(0,\ |y - f(x)| - \epsilon\right)$$

The optimization problem can be defined as,

$$\min_{W,b,Y_i,Y_i^*} \frac{1}{2}\|W\|^2 + C\sum_{i=1}^{n}(Y_i + Y_i^*)$$

subject to,

$$y_i - (w, \eta(x_i) + b) \leq \epsilon + Y_i$$

$$(w.\eta(x_i) + b) - y_i \leq \epsilon + Y_i^*$$

$$Y_i, Y_i^* \geq 0$$

where,

w → weight vector in feature space

b → bias term

η(x) → transformation into higher dimensional feature space (via kernel trick)

C → regularization constant controlling the penalty for errors larger than ϵ

Y_i, Y_i^* → slack variables allowing for error tolerance beyond ϵ

Support vector machines regression can deal with nonlinear relationships using the **kernel trick**, which skips explicit computation of the transformation $\eta(x)$ by defining a kernel function $K(x_i, x_j)$ that represents the dot product in feature space:

$$K(x_i,x_j) = \eta(x_i).\ \eta(x_j)$$

1.6.6 Neural Network Algorithms

The term neural network describes a system that mimics how information is transmitted by humans, classifying various facts into a single neuron, and linking those neurons via the internet to perform sophisticated memory tasks. Still, this evolving process of data analysis serves as the foundation for the neural network algorithm. The algorithm is made up of several linked nodes in a layered structure. These nodes stand in for the actual neurons of human brain. Every distinct neuron has a high level of authenticity, and the data can finish the external output process. It resembles how the human body advances, pauses and then takes off. Setting the output threshold after the weighting coefficient has been chosen will make data analysis and computation easier. This increases the overall orderliness of the numerical analysis process. The machines can utilize this adaptive approach to learn from their errors and keep getting better. Neural networks are generally considered for very large dataset which contains highly non-linear relationships, and predictive accuracy is given priority over interpretability.

Mathematical formulation:

A feedforward neural network with L layers can be written as,

$$\hat{y} = f(x;\omega) = W^{(L)}\,\alpha\Big(W^{(L-1)}\,\alpha\big(\dots\alpha(W^{(1)}x + b^{(1)})\dots\big) + b^{(L-1)}\Big) + b^{(L)}$$

where,

x = Input feature vector

$W^{(L)}$, $b^{(L)}$ = Weights and biases for layer L

α = Non-linear activation function (ReLU, sigmoid, tanh)

$\hat{y}$ = Predicted continuous value

ω = All learnable parameters of the network

Machine learning (ML) has emerged as a powerful tool to optimize and automate flexography printing. By learning patterns from historical and real-time data, ML enables process optimization, quality control, predictive maintenance and fault detection.

Machine learning models such as linear regression, decision tree, random forest regression, XG boost regression, SVM regression and neural network (NN) algorithm are used for data analysis and performance assessment can predict print quality metrics like dot gain, hue error on process parameters.

Related published research papers available were reviewed to find the gaps in the assessment of printing parameters and input variables both in flexography and screen printing and were given in Chapter 2.

1.7 Research Problem

This thesis examines screening pattern effect on print using flexography and screen printing. In flexography printing, anilox roller looks like screen and in screen printing, screen mesh also looks like screen. There is huge effect of these screen-like anilox roller [6, 8] and screen mesh [32] on print quality [13, 23]. Screening involves converting continuous tone images into halftones consisting of a series of dots of varying size or spacing. Main types of screening are AM, FM and Hybrid. The quality and visual output of flexography printing are significantly affected by the choice of screening pattern [9, 10]. Nowadays, the flexography printing is widely used for packaging and label printing and the screening pattern directly affects tonal range, image clarity, color consistency and the overall print appearance as well as print quality. The screening pattern is a critical factor in the flexography printing that affects everything from image fidelity to print consistency, considering the substrate characteristics [14, 17], anilox roller, halftone dot shape and ink which ensures optimal print performance.

Screen printing involves using a mesh screen to transfer ink onto a substrate. The mesh screen is coated with a stencil and areas of the stencil allow ink to pass through while others block it. In this process, the screen acts as a filter and the ink is pushed through it using a squeegee. The screening pattern refers how the image is broken down into dots on the screen. The size, shape and frequency of these dots are essential in defining the

final printed image, particularly when printing images with tonal variation. The screen mesh count and dot size also influence the amount of ink deposited. The screening pattern is also a crucial factor in the screen printing that affects print quality considering different types of substrates [28] and different screen mesh rulings.

1.8 Research Objectives

The objectives of this research are:

1. To print an ideal grey scale step wedge of dot coverage varying from 5% to 100% with AM, FM and Hybrid dots considering different anilox roller screen rulings onto different grades of substrates using flexography printing.

2. To print an ideal grey scale step wedge consisting of both AM and FM dots varying from 5% to 100% considering different screen mesh rulings onto different grades of substrates using screen printing.

3. To study and analyze the prints of flexography and screen printing.

Taguchi Grey Relational Analysis, Box Behnken Design and Machine Learning are used to analyze the various print quality parameters such as solid ink density, dot gain, print contrast and hue error.

This thesis is organised as follows:

In Chapter 1, Introduction is given.

Chapter 2 describes the Literature Review.

In Chapter 3, Taguchi Grey Relational Analysis of Prints is discussed.

Chapter 4 presents Box Behnken Design of Prints.

Chapter 5 consists of Machine Learning of Prints.

Chapter 6 deals with Conclusions and Future Scopes.

Figure 1.6 and Figure 1.7 represent the flexography and screen printing samples those were used in the thesis work.

Figure 1.6: Flexography printing sample

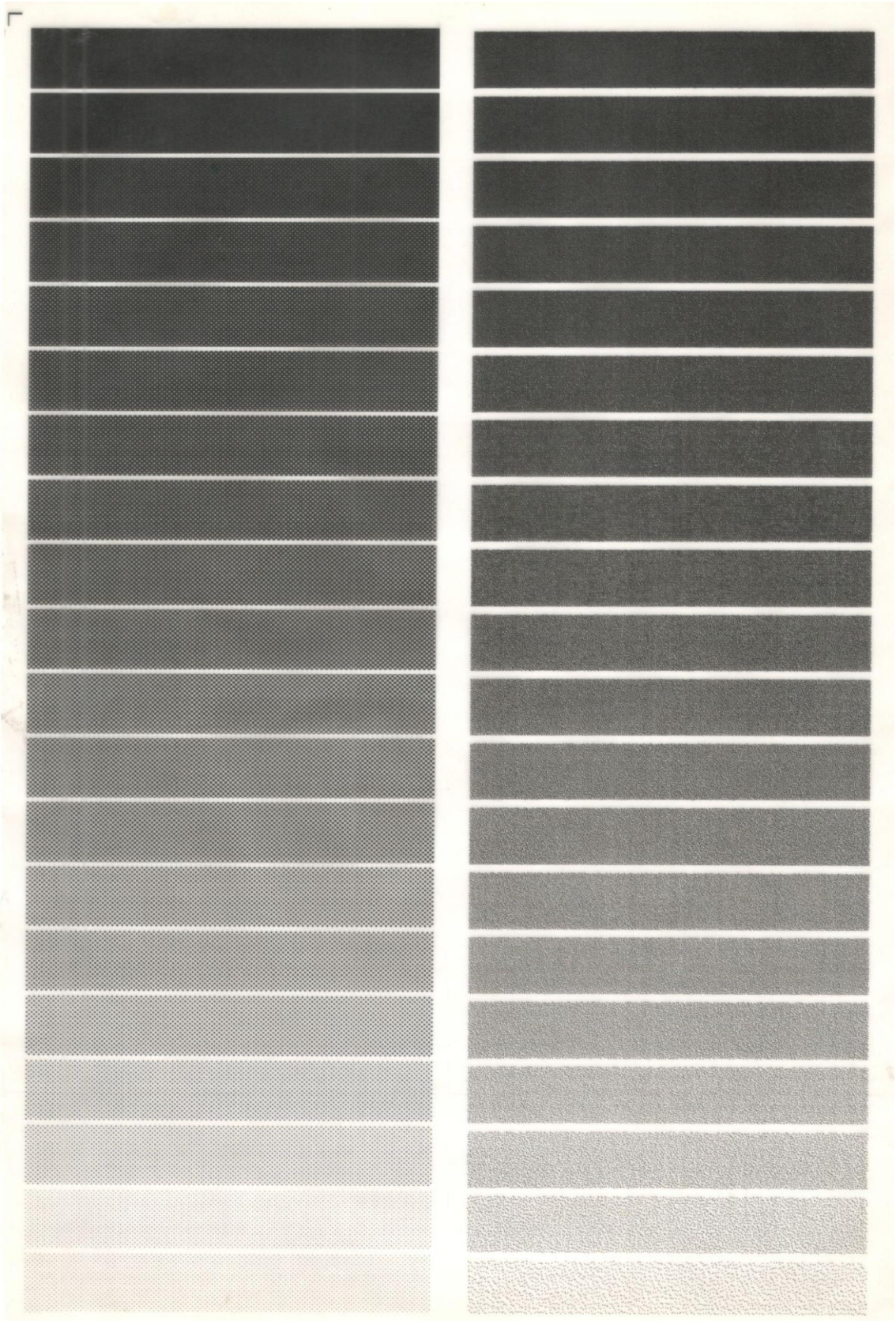

Figure 1.7: Screen printing sample

Chapter 2

Literature Review

2.1 Flexography Printing

Conventional printing techniques are divided into two groups – direct and indirect. Major direct printing processes are letterpress, flexography, gravure and screen printing. Offset printing falls under indirect printing category [1].

Image areas are raised above the non-image areas in flexography printing. Image carriers are generally flexible rubber or photopolymer which when comes in contact with inked roller, the ink only transfers to the image areas leaving the non-image areas uninked. Then the image is transferred onto the substrate under pressure. Anilox roller which is evenly screened with cells plays a vital role to transfer the liquid low viscosity ink to the printing plate [2].

The direct printing method known as flexographic printing that uses a rotary relief image carrier that is sufficiently flexible to transfer printing ink to a broad range of substrates, including paper, paperboards, plastic films, foils, etc. [3].

A small amount of pressure is sufficient in flexography to move ink from the plate to the substrate at the printing nip [4].

In flexographic halftone printing, it is clear that the anilox frequency at the final print affects both the lower and higher screen rules of the plate image. The finer anilox roll is needed to maintain a cell aperture smaller than the minimum reproducible plate dot. The dot becomes steadier as it gets deeper, which reduces the tone value increase [5].

The amount of ink to be applied to the substrate was greatly influenced by the specifications for the anilox roller cell engraving, which in turn had an impact on the optical density and halftone reproduction of the finished print. The anilox cell capacity was the main factor that determined print quality, but other factors such as the cell's shape were also discovered to have an impact [6].

The assessment of print quality is probably going to make use of quantitative studies such as dot gain, dot area, print contrast, and others. The correctness of the dot replication in the graphic reproduction is monitored using the dot gain and dot area parameters. The degree to which shadow features are accurately depicted on the final print is indicated by the print contrast value [7].

In the flexographic printing process, the anilox ruling frequency is varied from the finer to coarser screen frequency to get the final image to be printed well. The anilox roller cells are responsible to carry the required amount of ink into the printing unit to print the each and every halftone dot properly as per the requirements of printing. The anilox cell size opening smaller than that of the minimum dot size of halftone to be printed will bring better print result in flexography. The dot gain issues may increase by increasing the plate image screen frequency and decreasing cell count of anilox roller [8].

The flexographic printing has some limitations to handle shadow areas and finer dots in highlight areas in the reproduction by using solitary AM screening. The FM screening method in highlight and shadow will bring better result than AM [9].

The technique adopting FM-AM-Hybrid technology with flexography will brighten the situation as well. This technique employs FM screening method in both highlight as well as shadow areas and AM screening method on rest of the tonal areas of the image [10].

Screening technology can eliminate the tonal transmission deficiencies in the printing in terms of better highlight details, smoother gradient, exact tonal value reproduction etc. [11].

The use of FM dots at 0% to 10%, AM dots at 10% to 75% and FM dots again at 75% to 100% in the tonal areas of a graphic reproduction on substrate like PVC can empower flexographic print quality to an optimum level [12].

The halftone dot deformation can cause irregularities in print quality, including a sudden increase in the tone value or loss of highlight tones. The increase in dot coverage may occur due to the wear of the polymer plate, which caused the side shoulders of the dot to become a part of the printing surface. The correct ratio of the

anilox roller line screen to the line ruling of the printing plate is important in order to ensure a minimum dot size in print [13].

The printability and print quality of flexographic printing is dependent on the surface smoothness of the substrate. The ink absorption and spreading are influenced by the surface texture of substrate. The elastic deformation tendency of printing plate at high pressure leads to unpredictable dot deformation and ink spread [14].

The dot gain or tonal value increase (TVI) indicates the increase of dot size in the final print than that of the original dot size given at the input. The print contrast indicates the accuracy of halftone reproduction at the shadow areas of a print [15].

The assessment of print contrast at 70% or 75% tonal areas are the most common practice followed in the industry. The hue error indicates the shift in the real hue of the ink that is printed on the substrate. It may occur mainly due to the contamination of ink at the press condition, or the optical behaviour associated with the substrate, viewing conditions etc. [16].

The most popular and effective way to get the high print quality is to coordinate with the ISO 12647-6 standard's objective values. However, a specific combination of ink, anilox roller, printing plates, printing substrates, and printing machine determines how the production process is characterised. As a result, there are no suitable characterisation implementation methods that would consider each of these factors and specify the precise values for every potential combination. Therefore, it is critical that the set of qualitative data or the process characterization should match with the expectations of the customers. The rapid growth of the flexographic industry with innovative technological solutions in every aspect of the production process makes it impossible to create a suitable standard [17].

With the flexible relief printing plates, a tiny amount of printing pressure at the printing nip is just enough to transfer the ink from the plate onto the substrate that have a wide range of surface textures [18].

In flexographic printing, the anilox roller cell engraving specifications are a major factor in determining how much ink should be supplied to the substrate. This, in turn affects the optical density and halftone reproduction of the final print [19].

The flexography may create halftone dot sizes with percentage coefficients of variation (% CV) of 19.64 in highlight picture areas [20].

The uncoated paper has open fibre textures that accelerate ink solvents seep through it and reduce print density. The coating surface that permits the fibre pores of paper to contract during printing preventing ink from penetrating [21].

A thicker coating layer in halftone prints produces a surface with fewer surface peak features, reducing apparent dot gain by minimizing surface light scattering [22].

Print density is more in smooth surface paper whereas print density is found to drop abruptly in rough surface paper substrates [23].

A crucial first step toward obtaining consistent color on press is measuring and managing the color as well as the contamination levels of printing inks. No ink in the practical situations is ideal in nature. Based on the manufacturing reasons or from the processing or working environment, the chance of contamination of actual hue of the ink is prominent in the real printing world. Hue error is a percentage that indicates how much one process color ink has been contaminated by another [24].

2.2 Screen Printing

Screen printing is known as stencil printing process. Images are transferred through the woven screen mesh onto the different types of substrates by using squeegee. Images are formed by photomechanical process. Screen mesh looks like screen which has huge impact on print quality [26].

In comparison to other printing methods, screen printing is relatively easy to print on any desired material. However, in order to get the right design with the correct print detail, print resolution, coverage and hand feel etc., it is necessary to select the right mesh count and ink system for a particular design type. A higher mesh count resulted in high accuracy in design with less ink consumption, good hand feels and good background coverage. On the other hand, a lower mesh count resulted in poor background coverage, poor print detail and poor print sharpness. There is no significant change in color speed performance of the printed material with the change in mesh count [27].

The material that plans to print is equally important as the specifics of our screen print process. The composition, structure and characteristics of the printed items along with the composition, viscosity and other properties of ink, all contribute to the quality of the screen printed matter [28].

The screen printing is one of the versatile printing technologies among the conventional printing method that utilizes a stencil type image carrier for the printing function. The stencil is attachable over a screen mesh and the printing can be done by forcing ink through the stencil opening by a squeegee on to the substrate. The printing technique is suitable to print on a wide range of substrate like paper, paperboard, glass, plastics, metals, ceramics etc. irrespective of their surface textures and shape [29].

The print quality assessment is probable with the quantitative analysis of dot gain, dot area, print contrast, hue error etc. The dot gain and dot area values monitor the dot reproduction accuracy of the graphic reproduction at the final print. The print contrast value represents the accuracy of reproducing shadow details on the final print. The hue error represents the percentage of change in actual hue in the final print [30].

In halftone reproduction, the size of halftone dot should be larger than that of the opening area of the screen mesh used otherwise dot loss or lack of image details in the final print will be the result. This is a common factor applicable to both AM and FM mode of halftone printing via screen printing process. Moreover, the halftone dot reproduction by screen printing is somewhat thoughtful in terms of screen mesh characteristics, accuracy of stencil preparation method, type of stencil used, characteristics of ink, squeegee pressure etc.

In graphic reproduction process, the FM dots are better in highlight and shadow areas and also give better print results in those areas but fails in middle-tone, while the AM dots are better in middle-tone areas to give the better results [31].

The characteristic of the screen mesh used is a major factor that influences the quality of printed elements in screen printing. The commonly used screen mesh is nylon, polyester, stainless steel etc. in the industrial purposes. For screen mesh, the screen thread diameter and the open area of mesh are the two major critical parameters that describe the degree of reproducibility of halftone dots via screen printing method. According to the studies, the fabric with more thread per linear distance is capable to

produce high print quality. At the same time, it should have enough open area to guide the passage of average pigment size of the ink through it to the substrate. Smaller thread diameter builds up finer screen mesh [32].

2.3 Taguchi Grey Relational Analysis

Genichi Taguchi, Japanese engineer and statistician introduced the Taguchi method in the 1950's which can be statistically useful to improve the quality of output in variety of manufacturing applications. The Taguchi method of quality control approach is effective to eradicate variances occurs in the production process before its occurrence [33].

Grey Relational Analysis (GRA) is a method to find out the degree of correlation of variables associated with a process and it is developed by Deng Julong in 1982. The grey relational grade will give indication on the degree of correlation between the actual performances in relation to the target performance [34].

GRA method is better to solve multiple conditions based decision making activities. The Taguchi based GRA model is a better solution to the various field of manufacturing process in engineering like quality control, optimization etc. [35].

The Taguchi method acts as a better concept for the improvement of quality of product and process involved in a manufacturing process. Taguchi's concept of robust design indicates the design which gives the production of goods with less sensitive responses towards the factors that causes variability in the manufacturing process [36].

The Taguchi method is a better approach to apply in the industrial production activities that will entirely modify the outlook of production process on quality improvement and error free performance aspects [37].

2.4 Box Behnken Design

Box Behnken Design (BBD) was developed in 1960 by George E. P. Box and Donald Behnken. It is an experimental design and second order quadratic nonlinear model of the Response Surface Methodology. An experimental matrix required for the combination of the process parameter conditions is created by the Box Behnken Design. The design aids in the development of the quadratic response surface model which is

employed in response value estimation and prediction, and also a common technique in the optimization of industrial processes and products [38].

The Box Behnken experimental designs for Response Surface Methods feature the following:

- Each factor is set at three equally spaced levels usually coded as −1, 0, +1.
- The treatment combinations are positioned at the centre and at the midpoints of the process space's edges.
- A quadratic model or one with squared terms, products of two components, linear terms and an intercept.
- The ratio of experimental points to coefficients should be judicious usually within the range of 1.5 to 2.6.

The estimation variance mostly depends primarily on the distance from the centre [39].

To conduct an experiment with BBD, just three levels and a minimum of three components are needed. These patterns can be rotated or at least almost rotated. The main effect, interaction effect and quadratic effect are all optimized with their support. The Box Behnken Design with three factors e.g. consists of three blocks, two of which are modified using the four potential combinations of high and low [40].

The number of Experimental Run, N with BBD can be calculated using the formula:

$$N = 2k(k-1) + C$$

where,

k = number of factors

C = number of centre points in the design

The efficiency of the experimental design = (Number of coefficients in the estimated model) / (Number of experiments or run). The Box Behnken Design is a strong choice for response surface methodology since it allows for the following: (i) quadratic model parameter estimate, (ii) sequential design construction, (iii) model lack of fit detection and (iv) block usage [41].

BBD experimental design is used by most industry sectors to optimize their goods or processes. Response Surface Methodology or Response Surface Modeling (RSM), is a commonly utilized technique for response optimization. The response surface methodology is a set of practical and efficient mathematical and statistical tools for creating, enhancing, and optimizing processes and/or products by improving the operational elements. Using this approach the link between one or more response variables (dependent variables) and many explanatory variables (independent variables) is examined statistically to optimize the response or product [42].

An essential component of Response Surface Methodology (RSM) is design of experiments (DoE), which aims to identify the points at which response should be assessed. When employing the response surface methodology, two stages are required: 1) creating an approximation function and 2) designing an experiment plan [43].

The BBD lacks any points at the vertices of the experimental region, it is acknowledged as a special three level design. Both the centre points and the midpoints of the edges should be used in a BBD. Because face points are frequently easier to execute than extreme (corner) points, a BBD uses them instead. The Box Behnken Design is often rotational or almost rotatable and can be used to a variety of variables, from three to twenty one [44].

In comparison to central composite designs with an equal number of elements, Box Behnken Designs frequently have fewer design points and can be executed at a lower cost. Nevertheless, they are not appropriate for sequential trials since they lack an embedded factorial design. The main benefit is that it addresses the question of where the borders of the experiment should be, specifically avoiding combinations of treatments that are too extreme [45].

The BBD is more efficient than CCD and FFD [46].

The design is not considering the vertices of the cube, so that it can avoid situations under which the experiments done at extreme conditions or the responses at these extreme conditions. This can eliminate unsatisfactory results. The BBD offers block orthogonality which means the effects themselves are orthogonal to the block effects or it will not affect parameter estimates [47].

Analysis of variance (ANOVA) is a statistical tool which helps to identify the deviation of mean of experimental parameters. ANOVA helps to determine the actual state of the performance statistics of experimental parameters, errors, uncontrolled parameters etc. and also to crisscross the competence of the experimental model against the responses [48].

2.5 Machine Learning

Flexographic printing is an impact printing technique that transfers printing ink to a variety of substrates such as paper, paperboards, plastic films, foils and more, using a rotary relief image carrier that is suitably flexible [49].

A subfield of computer science and artificial intelligence is called machine learning that focuses on using data and algorithms to simulate human learning processes and progressively increase their accuracy [50].

Machine learning is a group of algorithms that are learned from data and/or experiences as opposed to being deliberately coded. Every task requires a different collection of algorithms and these algorithms identify patterns to carry out particular tasks. There are four popular techniques used to train machine learning algorithms [51].

Machine learning models are created and taught using algorithms. These are the kinds of steps that a machine learning model picks up through observation and followed by the application of the same method. Through training, machine learning algorithms are able to become a better version of themselves [52].

The machine learning, which teaches machines how to learn from their past experiences and make judgments on their own when necessary. Making computer programs before hand, without the need for human involvement is the primary goal of machine learning. Train and make decision by any machine with the help of pattern, prediction, input and past experience, the machine is designed to be able to make decisions automatically without involving a human in the process and thus produces the appropriate results [53].

Machine learning techniques educate computers to perform tasks that people perform on a daily basis with ease and naturalness. Raw data is fed into a machine learning model, which interprets it and predicts the output based on its understanding of the input data [54].

The ideas of machine learning have started around the era of 1950’s by Alan Turing. Rather than being explicitly coded, machine learning is a collection of algorithms that are taught from data and/or experiences. A distinct set of algorithms is needed for each activity and these algorithms detect habits to carry out specific operations [55].

The algorithms that make up machine learning teach computers to do things that humans do on a regular basis with ease and naturalness [56].

Machine learning is a technique where the output is obtained by using the current input data. The machine is trained using labelled data. It takes labelled inputs and maps it to the known outputs. Machines are trained using well labelled training data and on the basis of that data the output is predicted (remember the input data, formulate features, predict) [57].

The output classification and regression supervised learning are the two categories of supervised learning [58].

This method does not provide output data. The relationships and connections among the data are used to facilitate learning. Also, there are no training data for unsupervised learning. The unlabelled data is used to train the machine. It understands patterns and trends in the data and discovers the output. The unsupervised learning comes in two flavours: association and clustering [59].

When the amount of labelled data is smaller than that of unlabelled data, both supervised and unsupervised learning are insufficient. In these situations, relatively little information about them is inferred from the unlabelled data. Fewer labelled data than anticipated data are present in semi-supervised learning [60].

In this type of learning, agents pick up new skills through reward systems. While there are start and finish points, the agent's objective is to take the quickest and most accurate route to the destination. Positive reinforcement is given to the agent when they follow the right procedures. However, using the incorrect methods will have unfavourable effects. Learning takes place when pursuing the objective. It uses an agent and an environment to produce actions and rewards. There is no pre-defined target variable. It follows trial and error method to arrive at the desired solution [61].

Chapter 3

Taguchi Grey Relational Analysis of Prints

3.1 Preliminaries

There are many printing processes used for different purposes. In this study, two different printing processes viz. flexography and screen printing processes were considered. Both these processes utilize the screened input devices in addition to screened images. In flexography printing, screened anilox roller is used in the inking system and in screen printing, screened mesh is used for stencil preparation [3]. These play an important role in image quality of the print. The Taguchi method of quality control approach is an effective method to minimise the variances in the production process before its occurrence [33]. The Taguchi based GRA method is one of the effective solution to the various field of manufacturing process in engineering like quality control, optimization etc. [35]. The dot gain may increase by increasing the plate image screen frequency and decreasing cell count of anilox roller [8]. The FM screening method in highlight and shadow will bring better result than AM [9, 31]. Dot gain, dot area, print contrast and other quantitative analysis are likely to be used in the evaluation of print quality [15]. Hue error is calculated to quantify and regulate the level of impurity in printing inks [16]. Smoother paper can increase print density, but an increase in substrate surface roughness can also result in a sudden decrease in print density [23]. A higher mesh count in screen printing resulted in high accuracy in design with less ink consumption. A lower mesh count in screen printing resulted in poor background coverage, poor print detail and print sharpness [27].

Taguchi Grey Relational Analysis was done by using the same process steps and equations mentioned in Chapter 1, subsection 1.4.

3.2 Flexography Printing

3.2.1 Objective of the Study

In flexography printing, Taguchi Grey Relational Analysis (GRA) technique has been used to optimize parameters such as solid ink density, dot gain, hue error and print

contrast. To optimize these parameters, the anilox cell count, halftone dot shape and type of substrates in the print quality on both coated and uncoated paper grades are considered.

3.2.2 Experimental Methods

The experiment was conducted by printing an ideal grey scale step wedge of dot coverage varying from 5% to 100% with both AM square and AM round dot onto two grades of substrates - coated paper and uncoated paper. As the anilox roller acts as the core of flexography printing to deliver exact print quality, three different kinds of anilox roller rulings were 700 lpi (275.6 c/cm), 1000 lpi (393.7 c/cm) and 1300 lpi (Lines Per Inch) (511.8 c/cm) (Cells Per Centimeter) were employed to obtain prints. The engraved cells chosen for the printing has 60º hexagonal in geometry. The printing of paper was done in flexography printing machine, OMET LAB230 Iflex (printing speed – 35 m/min, nip pressure – 3 mm) with black color uv ink. The plate used was photopolymer plate of 1.14 mm thickness with magnetic backing.

Each element of the specified samples of printed sheets are subjected to visual analysis with a Digital microscope (LEICA, S8APO) followed by the quantitative optical property measurement using Spectro densitometer (X-Rite Spectro Eye and TECHKON GmbH Spectro Dens). The collected data were systematically processed and the print quality assessment was carried out by concentrating onto some major print parameters such as solid ink density, hue error, dot gain and print contrast.

In the computation process, 30%, 50% and 70% (that represents highlight, middle-tone and shadow areas respectively) step wedges are targeted for the analysis of solid ink density, dot gain, hue error and the print contrast.

The experimental variable parameters were substrate, dot shape and anilox ruling and the quality assessment parameters were solid ink density, dot gain, hue error and print contrast, the Taguchi’s orthogonal array for grey relational analysis was performed considering the input variables and quality assessment parameters.

Figure 3.1 shows flow chart of the process adopted to optimize the parameters to obtain print as per requirement.

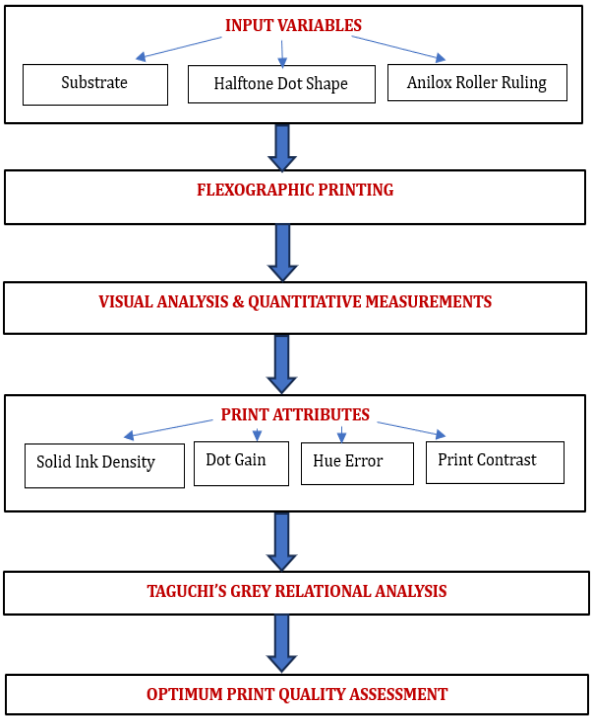

Figure 3.1: Flow chart of the process adopted to optimize the parameters using Taguchi's GRA analysis

3.2.3 Taguchi Grey Relational Analysis

The Table 3.1 shows the experimental variables and the quality assessment parameters taken for the Taguchi's GRA relational analysis.

Table 3.1: Elements of performance index array for Taguchi's grey relational analysis

Experiment No.	Experimental Variables	Factors
1	Coated Paper-Round Dot-700 LPI Anilox	Solid Ink Density
2	Coated Paper-Round Dot-1000 LPI Anilox	Dot Gain
3	Coated Paper-Round Dot-1300 LPI Anilox	Hue Error
4	Uncoated Paper-Round Dot-700 LPI Anilox	Print Contrast
5	Uncoated Paper-Round Dot-1000 LPI Anilox	

6	Uncoated Paper-Round Dot-1300 LPI Anilox	
7	Coated Paper-Square Dot-700 LPI Anilox	
8	Coated Paper-Square Dot-1000 LPI Anilox	
9	Coated Paper-Square Dot-1300 LPI Anilox	
10	Uncoated Paper-Square Dot-700 LPI Anilox	
11	Uncoated Paper-Square Dot-1000 LPI Anilox	
12	Uncoated Paper-Square Dot-1300 LPI Anilox	

3.2.4 Results

The optical properties of the prints obtained under different conditions are measured using X-Rite Spectro Eye (solid ink density, hue error, dot gain and print contrast) and TECHKON GmbH SpectroDens (opacity, whiteness) and the optical data plotted are shown vide Figures 3.2-3.6.

Figure 3.2 shows the Tonal reproduction curve of the prints under different conditions.

Figure 3.3 shows the variations in dot gain at different dot percentage of the original under different conditions.

Figure 3.4 shows the variations in hue errors of the prints at different dot percentages of dot areas.

Figure 3.5 shows the variations of print contrast of the different prints at different percentage of dot area of the original.

Figure 3.6 shows the bar charts of solid ink density of the different prints at different experimental variables.

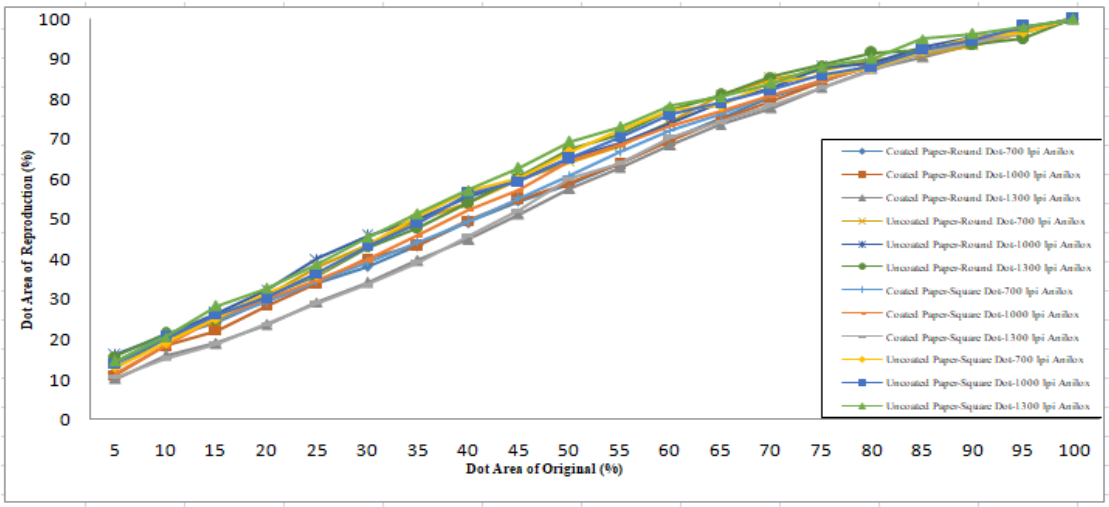

Figure 3.2: Tonal reproduction curve for dot area

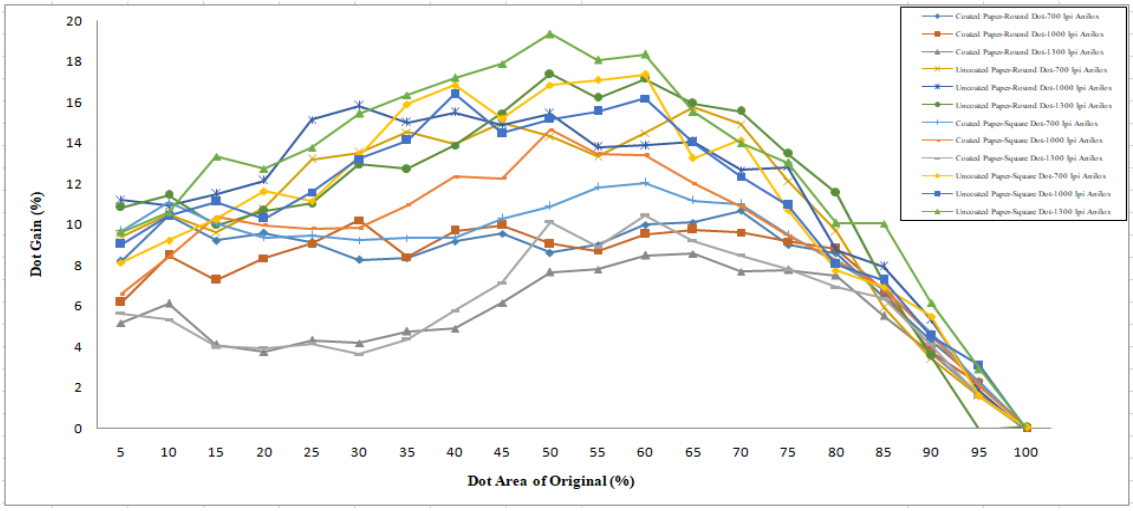

Figure 3.3: Variation in dot gain with respect to percentage dot area of the original

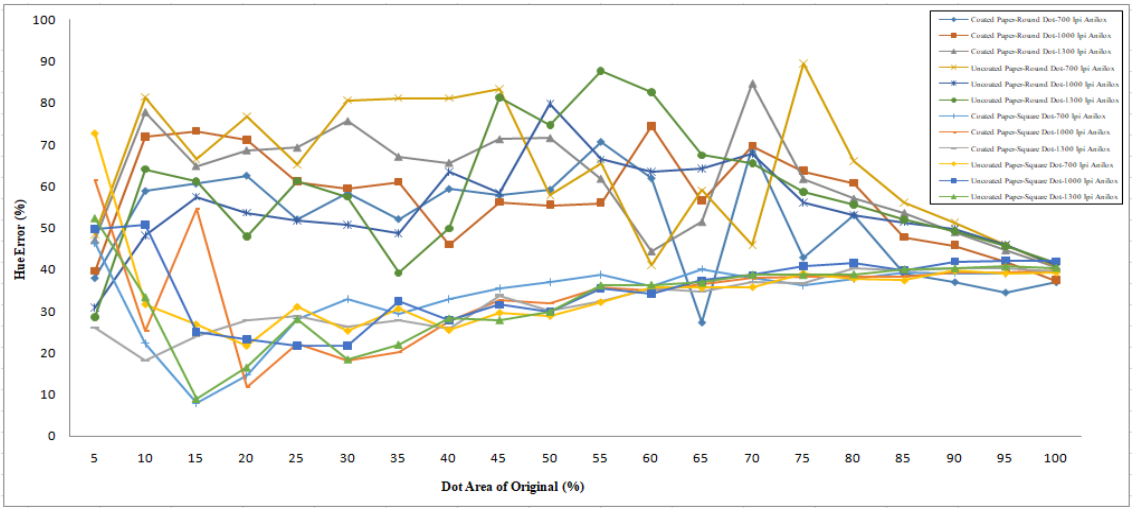

Figure 3.4: Variation in hue error with percentage dot area of the original

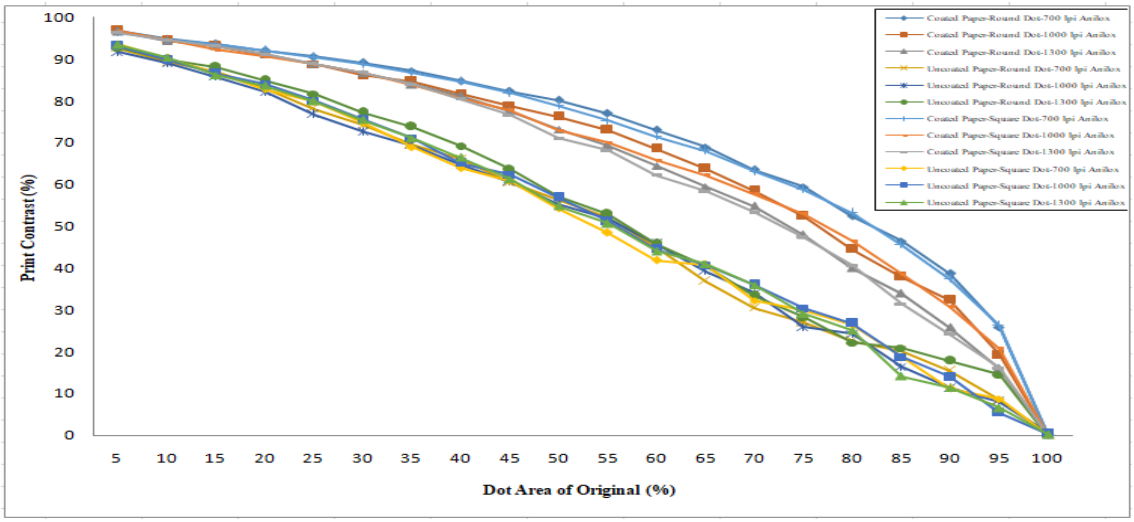

Figure 3.5: Variation in print contrast with respect to percentage dot area of the original

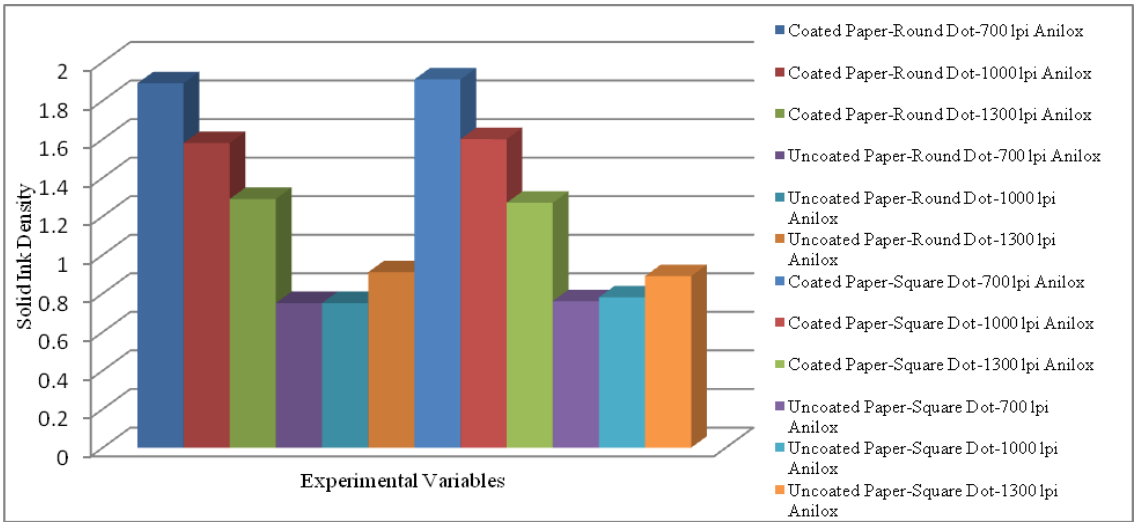

Figure 3.6: Bar charts of solid ink density with respect to different experimental variables

Taguchi's grey relational analysis for the collected data is carried out and the grey relational grade is calculated. As per the grade the test prints are prioritized under ranking based on different parameters such as solid ink density, dot gain, hue error and print contrast.

The various stages of Taguchi's grey relational analysis process are tabulated as-normalization (Table 3.2), deviation sequence (Table 3.3), grey relational co-efficient (Table 3.4).

Table 3.2: Normalised table of performance index

Exp. No.	Solid Ink Density	Dot Gain at 30%	Dot Gain at 50%	Dot Gain at 70%	Hue Error at 30%	Hue Error at 50%	Hue Error at 70%	Print Contrast at 30%	Print Contrast at 50%	Print Contrast at 70%
1	1.00	0.70	0.90	0.64	0.36	0.43	0.37	1.00	1.00	1.00
2	0.71	0.54	0.82	0.76	0.11	0.16	0.00	0.82	0.84	0.85
3	0.47	1.00	1.00	1.00	0.48	0.00	0.35	0.85	0.74	0.74
4	0.00	0.19	0.37	0.04	0.77	0.84	0.96	0.10	0.07	0.00
5	0.00	0.00	0.29	0.36	0.88	0.98	0.98	0.00	0.05	0.12
6	0.13	0.27	0.11	0.00	0.94	0.98	0.95	0.29	0.11	0.09
7	1.00	0.57	0.69	0.61	0.35	0.49	0.35	0.97	0.95	0.99
8	0.74	0.53	0.41	0.62	0.00	0.45	0.83	0.84	0.73	0.83
9	0.45	0.98	0.74	0.89	0.37	0.16	0.41	0.84	0.64	0.69
10	0.02	0.24	0.20	0.18	1.00	0.94	0.96	0.14	0.00	0.04
11	0.05	0.25	0.32	0.48	0.90	1.00	1.00	0.18	0.09	0.18
12	0.13	0.06	0.00	0.24	1.00	0.99	0.94	0.17	0.02	0.16

Table 3.3: Deviation sequence

Exp. No.	Solid Ink Density	Dot Gain at 30%	Dot Gain at 50%	Dot Gain at 70%	Hue Error at 30%	Hue Error at 50%	Hue Error at 70%	Print Contrast at 30%	Print Contrast at 50%	Print Contrast at 70%
1	0.00	0.30	0.10	0.36	0.64	0.57	0.63	0.00	0.00	0.00
2	0.29	0.46	0.18	0.24	0.89	0.84	1.00	0.18	0.16	0.15

3	0.53	0.00	0.00	0.00	0.52	1.00	0.65	0.15	0.26	0.26
4	1.00	0.81	0.63	0.96	0.23	0.16	0.04	0.90	0.93	1.00
5	1.00	1.00	0.71	0.64	0.12	0.02	0.02	1.00	0.95	0.88
6	0.87	0.73	0.89	1.00	0.06	0.02	0.05	0.71	0.89	0.91
7	0.00	0.43	0.31	0.39	0.65	0.51	0.65	0.03	0.05	0.01
8	0.26	0.47	0.59	0.38	1.00	0.55	0.17	0.16	0.27	0.17
9	0.55	0.02	0.26	0.11	0.63	0.84	0.59	0.16	0.36	0.31
10	0.98	0.76	0.80	0.82	0.00	0.06	0.04	0.86	1.00	0.96
11	0.95	0.75	0.68	0.52	0.10	0.00	0.00	0.82	0.91	0.82
12	0.87	0.94	1.00	0.76	0.00	0.01	0.06	0.83	0.98	0.84

Table 3.4: Grey relational co-efficient

Exp. No.	**Solid Ink Density**	**Dot Gain at 30%**	**Dot Gain at 50%**	**Dot Gain at 70%**	**Hue Error at 30%**	**Hue Error at 50%**	**Hue Error at 70%**	**Print Contrast at 30%**	**Print Contrast at 50%**	**Print Contrast at 70%**
1	1.00	0.63	0.83	0.58	0.44	0.47	0.44	1.00	1.00	1.00
2	0.63	0.52	0.73	0.68	0.36	0.37	0.33	0.74	0.76	0.77
3	0.48	1.00	1.00	1.00	0.49	0.33	0.43	0.77	0.66	0.66
4	0.33	0.38	0.44	0.34	0.68	0.76	0.93	0.36	0.35	0.33
5	0.33	0.33	0.41	0.44	0.80	0.96	0.96	0.33	0.34	0.36
6	0.36	0.41	0.36	0.33	0.90	0.96	0.90	0.41	0.36	0.36

7	1.00	0.54	0.62	0.56	0.43	0.49	0.44	0.94	0.90	0.98
8	0.66	0.51	0.46	0.57	0.33	0.48	0.74	0.76	0.65	0.74
9	0.48	0.96	0.66	0.81	0.44	0.37	0.46	0.75	0.58	0.62
10	0.34	0.40	0.38	0.38	1.00	0.89	0.93	0.37	0.33	0.34
11	0.35	0.40	0.42	0.49	0.83	1.00	1.00	0.38	0.36	0.38
12	0.37	0.35	0.33	0.40	1.00	0.97	0.89	0.38	0.34	0.37

Based on the grey relational co-efficient, the grey relational grading and ranking of experiments are given in the Table 3.5-3.15. According to Taguchi's grey relational analysis, the highest value of grey relational grade that indicates the better performance.

Table 3.5: Grey relational grade and ranking for solid ink density

Rank	**Experimental Variables**	**Grey Relational Grade**	**Experiment No.**
1	Coated Paper-Round Dot-700 LPI Anilox	1.000	1
2	Coated Paper-Square Dot-700 LPI Anilox	1.000	7
3	Coated Paper-Square Dot-1000 LPI Anilox	0.657	8
4	Coated Paper-Round Dot-1000 LPI Anilox	0.632	2
5	Coated Paper-Round Dot-1300 LPI Anilox	0.483	3
6	Coated Paper-Square Dot-1300 LPI Anilox	0.475	9
7	Uncoated Paper-Square Dot-1300 LPI Anilox	0.365	12
8	Uncoated Paper-Round Dot-1300 LPI Anilox	0.364	6

9	Uncoated Paper-Square Dot-1000 LPI Anilox	0.345	11
10	Uncoated Paper-Square Dot-700 LPI Anilox	0.338	10
11	Uncoated Paper-Round Dot-1000 LPI Anilox	0.334	5
12	Uncoated Paper-Round Dot-700 LPI Anilox	0.333	4

Table 3.6: Grey relational grade and ranking for 30% dot gain

Rank	**Experimental Variables**	**Grey Relational Grade**	**Experiment No.**
1	Coated Paper-Round Dot-1300 LPI Anilox	1.000	3
2	Coated Paper-Square Dot-1300 LPI Anilox	0.957	9
3	Coated Paper-Round Dot-700 LPI Anilox	0.627	1
4	Coated Paper-Square Dot-700 LPI Anilox	0.537	7
5	Coated Paper-Round Dot-1000 LPI Anilox	0.521	2
6	Coated Paper-Square Dot-1000 LPI Anilox	0.515	8
7	Uncoated Paper-Round Dot-1300 LPI Anilox	0.407	6
8	Uncoated Paper-Square Dot-1000 LPI Anilox	0.401	11
9	Uncoated Paper-Square Dot-700 LPI Anilox	0.397	10
10	Uncoated Paper-Round Dot-700 LPI Anilox	0.381	4
11	Uncoated Paper-Square Dot-1300 LPI Anilox	0.348	12
12	Uncoated Paper-Round Dot-1000 LPI Anilox	0.333	5

Table 3.7: Grey relational grade and ranking for 50% dot gain

Rank	Experimental Variables	Grey Relational Grade	Experiment No.
1	Coated Paper-Round Dot-1300 LPI Anilox	1.000	3
2	Coated Paper-Round Dot-700 LPI Anilox	0.827	1
3	Coated Paper-Round Dot-1000 LPI Anilox	0.731	2
4	Coated Paper-Square Dot-1300 LPI Anilox	0.656	9
5	Coated Paper-Square Dot-700 LPI Anilox	0.616	7
6	Coated Paper-Square Dot-1000 LPI Anilox	0.459	8
7	Uncoated Paper-Round Dot-700 LPI Anilox	0.443	4
8	Uncoated Paper-Square Dot-1000 LPI Anilox	0.423	11
9	Uncoated Paper-Round Dot-1000 LPI Anilox	0.414	5
10	Uncoated Paper-Square Dot-700 LPI Anilox	0.384	10
11	Uncoated Paper-Round Dot-1300 LPI Anilox	0.359	6
12	Uncoated Paper-Square Dot-1300 LPI Anilox	0.333	12

Table 3.8: Grey relational grade and ranking for 70% dot gain

Rank	Experimental Variables	Grey Relational Grade	Experiment No.
1	Coated Paper-Round Dot-1300 LPI Anilox	1.000	3
2	Coated Paper-Square Dot-1300 LPI Anilox	0.814	9

3	Coated Paper-Round Dot-1000 LPI Anilox	0.676	2
4	Coated Paper-Round Dot-700 LPI Anilox	0.581	1
5	Coated Paper-Square Dot-1000 LPI Anilox	0.568	8
6	Coated Paper-Square Dot-700 LPI Anilox	0.560	7
7	Uncoated Paper-Square Dot-1000 LPI Anilox	0.489	11
8	Uncoated Paper-Round Dot-1000 LPI Anilox	0.439	5
9	Uncoated Paper-Square Dot-1300 LPI Anilox	0.395	12
10	Uncoated Paper-Square Dot-700 LPI Anilox	0.379	10
11	Uncoated Paper-Round Dot-700 LPI Anilox	0.342	4
12	Uncoated Paper-Round Dot-1300 LPI Anilox	0.333	6

Table 3.9: Grey relational grade and ranking for 30% hue error

Rank	**Experimental Variables**	**Grey Relational Grade**	**Experiment No.**
1	Uncoated Paper-Square Dot-700 LPI Anilox	1.000	10
2	Uncoated Paper-Square Dot-1300 LPI Anilox	1.000	12
3	Uncoated Paper-Round Dot-1300 LPI Anilox	0.896	6
4	Uncoated Paper-Square Dot-1000 LPI Anilox	0.832	11
5	Uncoated Paper-Round Dot-1000 LPI Anilox	0.804	5
6	Uncoated Paper-Round Dot-700 LPI Anilox	0.682	4

7	Coated Paper-Round Dot-1300 LPI Anilox	0.488	3
8	Coated Paper-Square Dot-1300 LPI Anilox	0.444	9
9	Coated Paper-Round Dot-700 LPI Anilox	0.439	1
10	Coated Paper-Square Dot-700 LPI Anilox	0.434	7
11	Coated Paper-Round Dot-1000 LPI Anilox	0.360	2
12	Coated Paper-Square Dot-1000 LPI Anilox	0.333	8

Table 3.10: Grey relational grade and ranking for 50% hue error

Rank	**Experimental Variables**	**Grey Relational Grade**	**Experiment No.**
1	Uncoated Paper-Square Dot-1000 LPI Anilox	1.000	11
2	Uncoated Paper-Square Dot-1300 LPI Anilox	0.974	12
3	Uncoated Paper-Round Dot-1000 LPI Anilox	0.962	5
4	Uncoated Paper-Round Dot-1300 LPI Anilox	0.962	6
5	Uncoated Paper-Square Dot-700 LPI Anilox	0.894	10
6	Uncoated Paper-Round Dot-700 LPI Anilox	0.760	4
7	Coated Paper-Square Dot-700 LPI Anilox	0.494	7
8	Coated Paper-Square Dot-1000 LPI Anilox	0.478	8
9	Coated Paper-Round Dot-700 LPI Anilox	0.468	1

10	Coated Paper-Round Dot-1000 LPI Anilox	0.373	2
11	Coated Paper-Square Dot-1300 LPI Anilox	0.372	9
12	Coated Paper-Round Dot-1300 LPI Anilox	0.333	3

Table 3.11: Grey relational grade and ranking for 70% hue error

Rank	**Experimental Variables**	**Grey Relational Grade**	**Experiment No.**
1	Uncoated Paper-Square Dot-1000 LPI Anilox	1.000	11
2	Uncoated Paper-Round Dot-1000 LPI Anilox	0.962	5
3	Uncoated Paper-Round Dot-700 LPI Anilox	0.926	4
4	Uncoated Paper-Square Dot-700 LPI Anilox	0.926	10
5	Uncoated Paper-Round Dot-1300 LPI Anilox	0.904	6
6	Uncoated Paper-Square Dot-1300 LPI Anilox	0.893	12
7	Coated Paper-Square Dot-1000 LPI Anilox	0.742	8
8	Coated Paper-Square Dot-1300 LPI Anilox	0.459	9
9	Coated Paper-Round Dot-700 LPI Anilox	0.441	1
10	Coated Paper-Square Dot-700 LPI Anilox	0.437	7
11	Coated Paper-Round Dot-1300 LPI Anilox	0.435	3
12	Coated Paper-Round Dot-1000 LPI Anilox	0.333	2

Table 3.12: Grey relational grade and ranking for 30% print contrast

Rank	Experimental Variables	Grey Relational Grade	Experiment No.
1	Coated Paper-Round Dot-700 LPI Anilox	1.000	1
2	Coated Paper-Square Dot-700 LPI Anilox	0.939	7
3	Coated Paper-Round Dot-1300 LPI Anilox	0.768	3
4	Coated Paper-Square Dot-1000 LPI Anilox	0.762	8
5	Coated Paper-Square Dot-1300 LPI Anilox	0.753	9
6	Coated Paper-Round Dot-1000 LPI Anilox	0.739	2
7	Uncoated Paper-Round Dot-1300 LPI Anilox	0.413	6
8	Uncoated Paper-Square Dot-1000 LPI Anilox	0.379	11
9	Uncoated Paper-Square Dot-1300 LPI Anilox	0.377	12
10	Uncoated Paper-Square Dot-700 LPI Anilox	0.367	10
11	Uncoated Paper-Round Dot-700 LPI Anilox	0.357	4
12	Uncoated Paper-Round Dot-1000 LPI Anilox	0.333	5

Table 3.13: Grey relational grade and ranking for 50% print contrast

Rank	Experimental Variables	Grey Relational Grade	Experiment No.
1	Coated Paper-Round Dot-700 LPI Anilox	1.000	1
2	Coated Paper-Square Dot-700 LPI Anilox	0.901	7
3	Coated Paper-Round Dot-1000 LPI Anilox	0.756	2

4	Coated Paper-Round Dot-1300 LPI Anilox	0.658	3
5	Coated Paper-Square Dot-1000 LPI Anilox	0.646	8
6	Coated Paper-Square Dot-1300 LPI Anilox	0.584	9
7	Uncoated Paper-Round Dot-1300 LPI Anilox	0.360	6
8	Uncoated Paper-Square Dot-1000 LPI Anilox	0.356	11
9	Uncoated Paper-Round Dot-700 LPI Anilox	0.350	4
10	Uncoated Paper-Round Dot-1000 LPI Anilox	0.344	5
11	Uncoated Paper-Square Dot-1300 LPI Anilox	0.338	12
12	Uncoated Paper-Square Dot-700 LPI Anilox	0.333	10

Table 3.14: Grey relational grade and ranking for 70% print contrast

Rank	**Experimental Variables**	**Grey Relational Grade**	**Experiment No**
1	Coated Paper-Round Dot-700 LPI Anilox	1.000	1
2	Coated Paper-Square Dot-700 LPI Anilox	0.975	7
3	Coated Paper-Round Dot-1000 LPI Anilox	0.765	2
4	Coated Paper-Square Dot-1000 LPI Anilox	0.743	8
5	Coated Paper-Round Dot-1300 LPI Anilox	0.659	3
6	Coated Paper-Square Dot-1300 LPI Anilox	0.615	9
7	Uncoated Paper-Square Dot-1000 LPI Anilox	0.380	11

8	Uncoated Paper-Square Dot-1300 LPI Anilox	0.374	12
9	Uncoated Paper-Round Dot-1000 LPI Anilox	0.361	5
10	Uncoated Paper-Round Dot-1300 LPI Anilox	0.355	6
11	Uncoated Paper-Square Dot-700 LPI Anilox	0.343	10
12	Uncoated Paper-Round Dot-700 LPI Anilox	0.333	4

Table 3.15: Overall grey relational grade and ranking

Rank	**Experimental Variables**	**Grey Relational Grade**	**Experiment No.**
1	Coated Paper-Round Dot-700 LPI Anilox	0.738	1
2	Coated Paper-Square Dot-700 LPI Anilox	0.689	7
3	Coated Paper-Round Dot-1300 LPI Anilox	0.682	3
4	Coated Paper-Square Dot-1300 LPI Anilox	0.613	9
5	Coated Paper-Square Dot-1000 LPI Anilox	0.590	8
6	Coated Paper-Round Dot-1000 LPI Anilox	0.589	2
7	Uncoated Paper-Square Dot-1000 LPI Anilox	0.561	11
8	Uncoated Paper-Square Dot-1300 LPI Anilox	0.540	12
9	Uncoated Paper-Square Dot-700 LPI Anilox	0.536	10
10	Uncoated Paper-Round Dot-1300 LPI Anilox	0.535	6
11	Uncoated Paper-Round Dot-1000 LPI Anilox	0.529	5
12	Uncoated Paper-Round Dot-700 LPI Anilox	0.491	4

3.2.5 Discussions

The GRA index of print considering different input variables in terms of solid ink density, dot gain, hue error and print contrast are given in Tables 3.5-3.15.

It has been found from Table 3.5 that the grey relational grade is higher on coated paper than uncoated paper and grey relational grade is higher for lower anilox screen ruling in coated paper in case of solid ink density. But in case of uncoated paper, the result is just opposite. This may be due to poor bottoming of the image on the paper as the surface of the paper is uneven.

It has been observed vide Tables 3.6-3.8 considering dot gains at 30%, 50% and 70% dot area that 1300 lpi anilox ruling frequency produces minimum dot gain in highlight, midtone and shadows on coated paper for image made up of round shape AM dots.

The dot gains are different under different conditions due to screen frequency of anilox ruling, paper textures and dot pattern.

It is found from Tables 3.9-3.11 that hue error is minimum on uncoated paper in highlight for both 700 lpi and 1300 lpi anilox ruling frequency. Hue error is minimum in midtone and shadow on uncoated paper for 1000 lpi anilox ruling frequency. However, the hue errors on coated paper in highlight, midtone and shadow are different so far as anilox ruling frequency is concerned. The dot shape also has an influence on the hue error. Square dot shape produces minimum hue error as compared to round dot shape.

Tables 3.12-3.14 show the GRA index of the print for print contrast. It is observed that 700 lpi anilox ruling frequency produces maximum print contrast in highlight, midtone and shadow on coated paper. Lower anilox ruling frequency and round shape dot provide the best print contrast on coated paper.

Table 3.15 shows the overall grey relational grade and ranking of the print considering the input variable and output print parameters such as solid ink density, dot gain, hue error and print contrast. It has been found that 700 lpi anilox ruling frequency will provide high print quality followed by 1300 lpi anilox ruling frequency. It is also found

that images made up of round shape dot will be produced better on coated paper in flexography.

It has been observed from Figure 3.3 that dot gain of prints on coated paper utilizing 1300 lpi screen frequency and round shape dot pattern of the image is minimum followed by dot gain of prints on coated paper adopting 1300 lpi anilox screen ruling using square shape dots of the image. The dot gain is maximum on uncoated paper utilizing 1300 lpi anilox ruling of images containing square shape dots.

It was observed from Figure 3.4 that hue errors are minimum for uncoated paper as compared to coated one irrespective of anilox screen ruling frequency and dot shapes.

It has been observed from Figure 3.5 that the print contrast is lower in uncoated paper as compared to coated paper. It is also observed that the print contrast value is increasing with increasing value of anilox ruling for uncoated paper and print contrast is decreasing with increasing value of anilox ruling for coated paper.

It has been observed from Figure 3.6 that lower the anilox screen ruling, higher will be the ink deposit on the substrate.

The microscopic view of both round and square dot (at 30%, 50% and 70% tonal areas) of the prints are illustrated in Figures 3.7-3.12 for the better understanding of the tonal reproduction at each case.

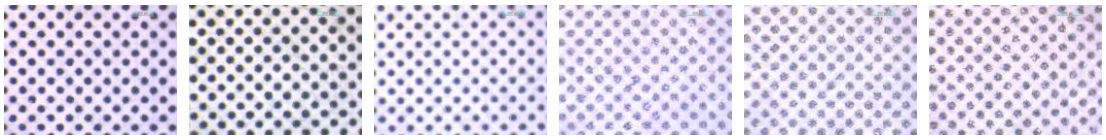

Figure 3.7: Microscopic view of Round dot at 30% dot area

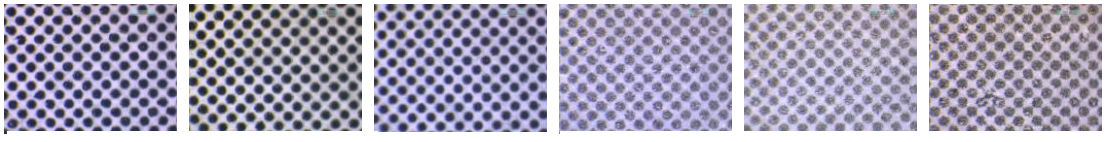

Figure 3.8: Microscopic view of Round dot at 50% dot area

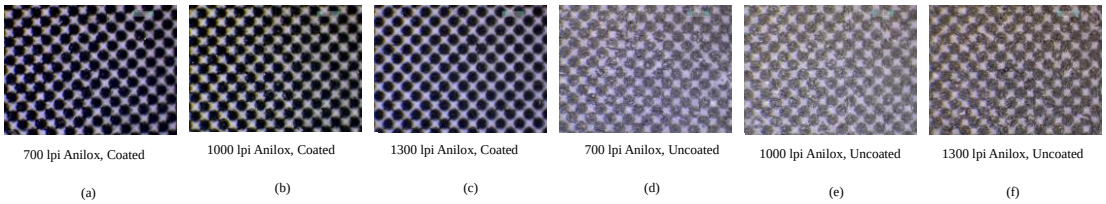

Figure 3.9: Microscopic view of Round dot at 70% dot area

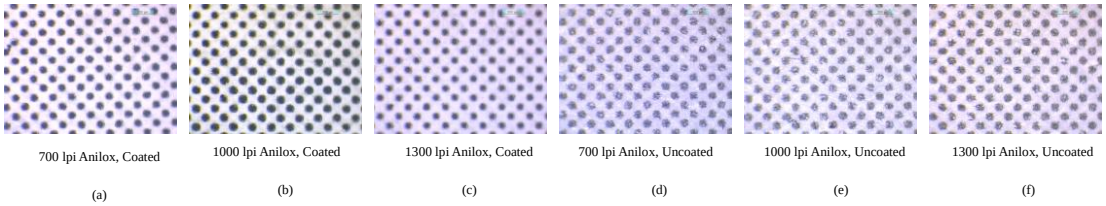

Figure 3.10: Microscopic view of Square dot at 30% dot area

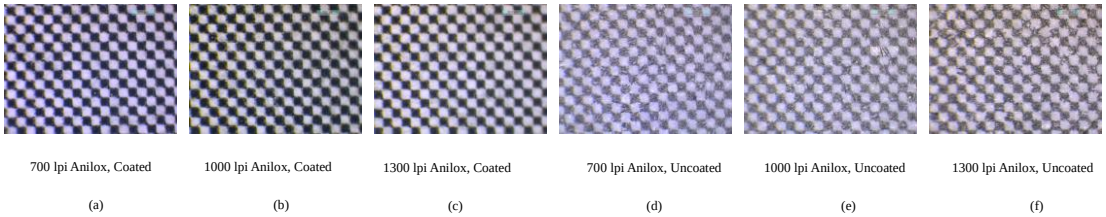

Figure 3.11: Microscopic view of Square dot at 50% dot area

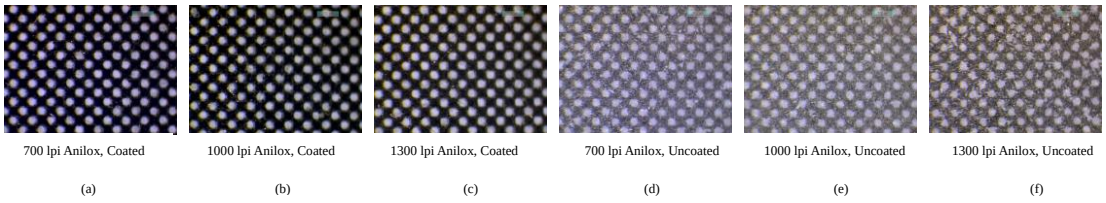

Figure 3.12: Microscopic view of Square dot at 70% dot area

Figures 3.7-3.9 indicate that dot gain is minimum in print of 1300 lpi anilox screen ruling on coated paper with round dot. This confirms the Taguchi GRA analysis as given in Tables 3.6-3.8.

Comparing Figures 3.7-3.9 and Figures 3.10-3.12, it has been observed that the overall print quality is best at 700 lpi anilox screen ruling on coated paper with round dot which also confirms the Taguchi GRA analysis vide Table 3,15.

3.2.6 Conclusions

In the present work, the research was conducted on flexography printing with three variable factors: coated and uncoated paper, round and square shaped halftone dots and three different anilox roller rulings. It has been found that optimum print quality is

obtained when print is taken on coated paper at 700 lpi anilox ruling if the image is made of round dot considering dot gain as factor affecting print quality.

It is also found that if hue error is considered as print quality index, optimum result can be obtained on uncoated paper using square dot but it behaves differently in different percentage dot areas so far as print contrast is concerned, coated paper with 700 lpi screen ruling will produce highest print quality. As a whole, 700 lpi screen ruling will produce highest print quality on coated paper if the image is composed of round dots. The print quality has been analysed on the basis of the assessment of print parameters: solid ink density, dot gain, hue error and print contrast using Taguchi's grey relational analysis. The results showed that the flexographic print quality is dependent on the factors such as surface characteristics of substrate, geometrical shape of the halftone dots used and the anilox cell rulings. Also, this study showed the scope of implementation of Taguchi's grey relational analysis in the decision making process associated with the print quality assessment in flexography.

3.3 Screen Printing

3.3.1 Objective of the Study

To find the influence of factors such as screen mesh ruling, AM and FM halftone dots, coated and uncoated paper grades etc. on the print quality of screen printing. The attainment of best quality is assessed by Taguchi's Grey Relational Analysis (GRA) method.

3.3.2 Experimental Methods

The research was conducted by printing an ideal grey scale image consisting of both AM and FM dots onto both coated and uncoated paper by screen printing method. Three different screen mesh ruling such as 100 lpi, 120 lpi and 140 lpi (lines per inch) were used to form the stencils.

The stencils consisting of halftone grey scale were fixed in flatbed semiautomatic screen printing machine: ATOM 1520, APL Machinery Pvt. Ltd. and prints were obtained on both coated and uncoated papers. The printed samples were subjected to the visual inspection by Digital microscope (LEICA, S8APO) and the quantitative optical

properties were measured by Spectro densitometer (such as X-Rite Spectro Eye & TECHKON GmbH Spectro Dens).

The 30%, 50% and 70% tonal areas (representing highlight area, middle-tone area and shadow area respectively) were considered for quantitative assessment of the print quality. The solid ink density, dot gain, hue error and print contrast etc. of these tonal values were analysed with Taguchi's grey relational analysis. The sequential flow chart of the Taguchi's GRA process is shown in the illustration Figure 3.13.

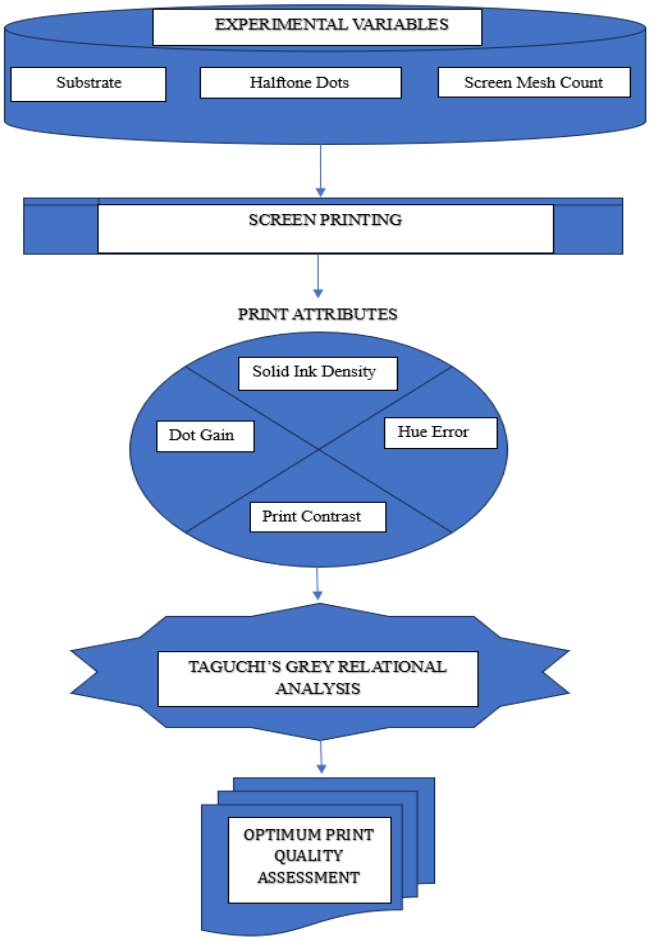

Figure 3.13: Sequential flow chart of the Taguchi's GRA process

3.3.3 Taguchi Grey Relational Analysis

The Table 3.16 represents the list of input variables taken for the process and the various parameters of the prints considered for assessing the print quality. These were taken as the key elements in the Taguchi's grey relational analysis of this research work.

Table 3.16: Elements taken for Taguchi's grey relational analysis

Experiment No.	Experimental Variables	Parameters
1	Coated Paper, 100 lpi Mesh, AM Dot	Solid Ink Density Dot Gain Hue Error Print Contrast
2	Coated Paper, 120 lpi Mesh, AM Dot	
3	Coated Paper, 140 lpi Mesh, AM Dot	
4	Coated Paper, 100 lpi Mesh, FM Dot	
5	Coated Paper, 120 lpi Mesh, FM Dot	
6	Coated Paper, 140 lpi Mesh, FM Dot	
7	Uncoated Paper, 100 lpi Mesh, AM Dot	
8	Uncoated Paper, 120 lpi Mesh, AM Dot	
9	Uncoated Paper, 140 lpi Mesh, AM Dot	
10	Uncoated Paper, 100 lpi Mesh, FM Dot	
11	Uncoated Paper, 120 lpi Mesh, FM Dot	
12	Uncoated Paper, 140 lpi Mesh, FM Dot	

3.3.4 Results

The Figures 3.14-3.18 graphically represent the output responses such as dot area, dot gain, hue error, print contrast and solid ink densities of reproduced image against the target dot percentage that ranging from 5% to 100% dot coverage with an incremental step of 5%.

The Figure 3.14 and Figure 3.15 shows the dot area curve and followed by dot gain curve respectively. These curves show that the dot area of printed sample is comparatively higher for FM dots on uncoated paper with 100 lpi mesh count. This

represents the higher dot gain associated with uncoated paper with lower mesh count and FM dot combination in screen printing process. Meanwhile, the AM dot print on coated paper with 140 lpi mesh count gives a better dot area reproduction when comparing to all other cases. This implies that higher the mesh count lesser will be the dot gain and also the AM dots with smooth textured substrate also facilitates the attainment of optimum dot gain. Lower mesh count with FM dots is a poor choice in screen printing. Because the larger mesh openings of screen at lower mesh count will facilitate considerable loss of FM dot details on the stencil over the mesh and there will be high dot gain issues in the final reproduction due to larger openings. Also, the uncoated paper facilitates the unpredictable dot gain due to the undesirable ink absorption on to its porous structure and unevenness of the surfaces. Also, there is a chance of optical dot gain due to the light scattering effects from the paper surface. It has been observed that at highlight areas up to 15%, there is loss of dots with 140 lpi and 120 lpi mesh count in case of AM dots. This may be due to the inability of the screen mesh to carry the finer sized AM dots at those highlight areas. Meanwhile the FM dots performed in a better way at the highlight and shadow areas only in the case of higher mesh count.

The Figure 3.16 shows the graphical representation of hue error of print. The overall hue error is minimum for prints on coated paper with AM dots using 140 lpi screen mesh. The hue error remains constant till the 40% dot area. The higher hue error value is obtained for uncoated paper especially at the middle-tone areas. However, the hue error is the indicator of purity of ink in the print and it is influenced by press conditions, and the spectral behaviour of the ink and substrate used.

The Figure 3.17 shows the print contrast curve, in which the best print contrast is obtained for AM dot print on coated paper with 140 lpi mesh count and the lowest print contrast is found on the FM dot print on uncoated paper with 100 lpi mesh count. The print contrast represents the accuracy of tonal reproduction in contrast with the shadow details. The higher mesh count of screen with AM dot and smooth textured substrate improves the print contrast of screen printing. The print contrast is near about zero beyond 85% dot area in all the cases.

Figure 3.18 is a bar graph that shows the solid ink densities reproduced on the print, among which the more vibrant color of solid ink coverage is obtained for FM dots on

coated paper with low mesh count. It was also observed that lower the screen mesh count, higher will be the ink deposit on the substrate.

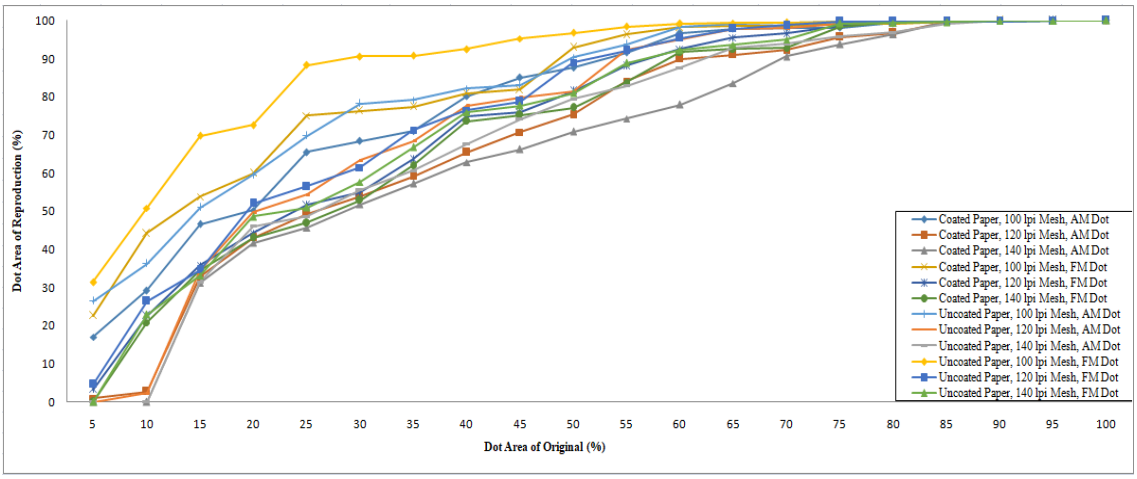

Figure 3.14: Tonal reproduction curve for dot area

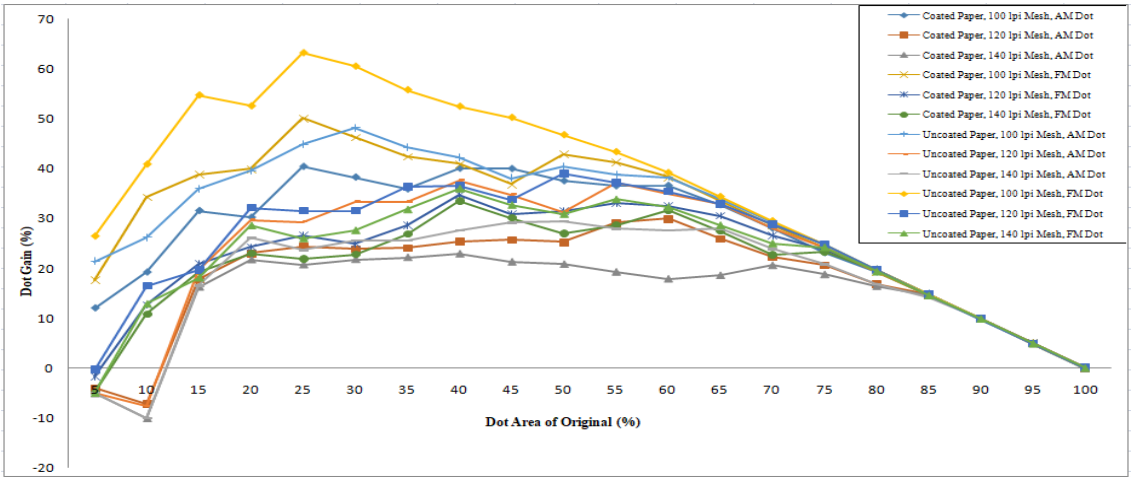

Figure 3.15: Variation in dot gain with respect to percentage dot area of the original

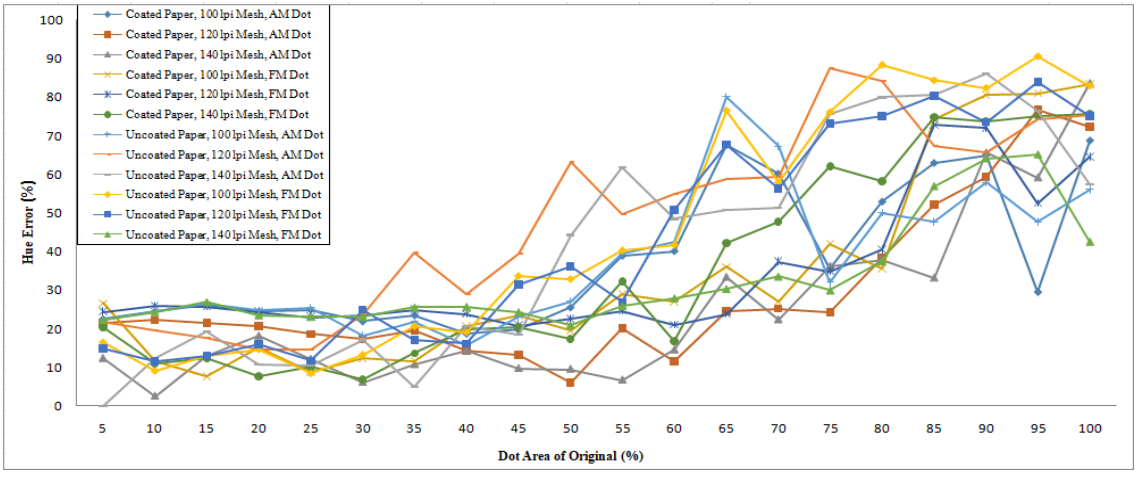

Figure 3.16: Variation in hue error with percentage dot area of the original

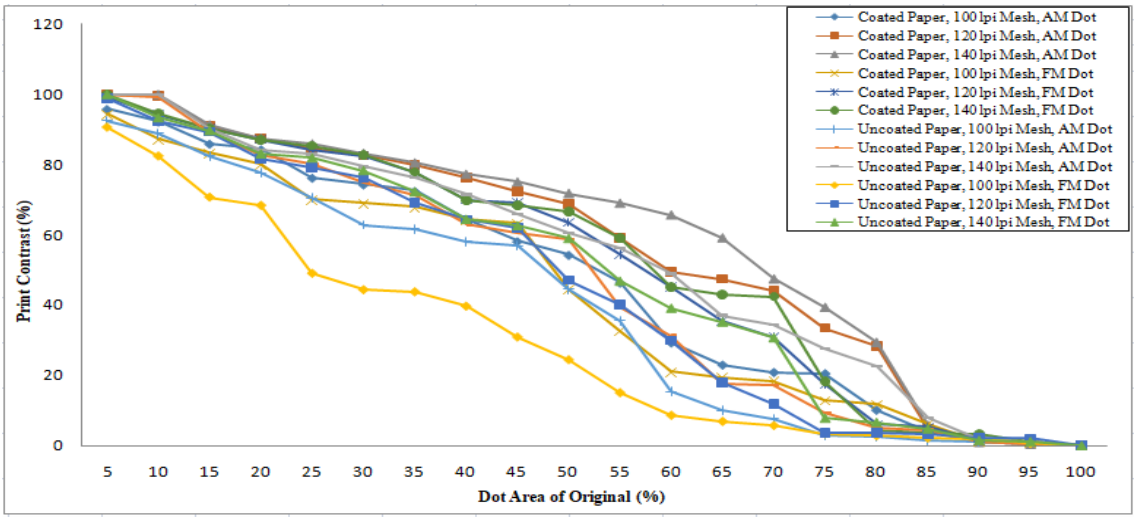

Figure 3.17: Variation in print contrast with percentage dot area of the original

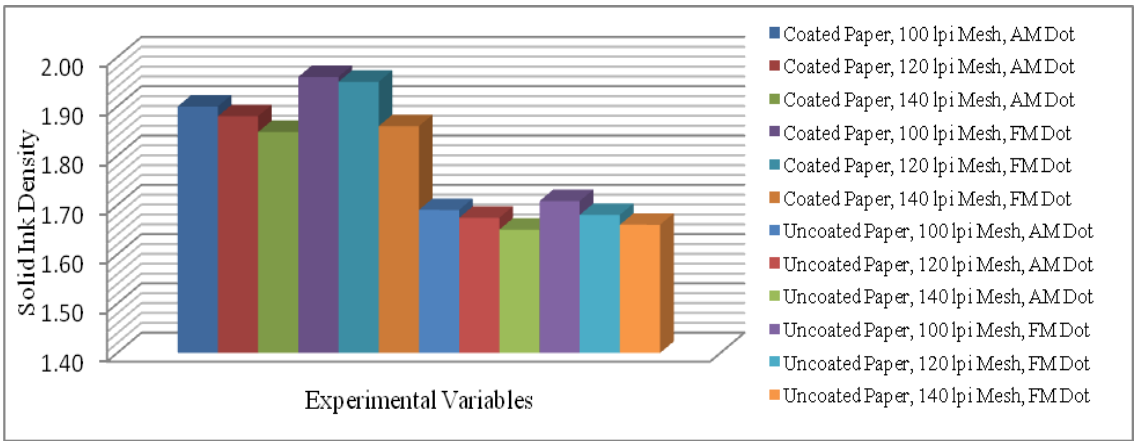

Figure 3.18: Bar charts of solid ink density with respect to different experimental variables

The Taguchi's grey relational analysis is carried out in various stages such as normalization of data (shown in Table 3.17), calculation of deviation sequence (shown in Table 3.18), calculation of grey relational co-efficient (shown in Table 3.19). Based on quality assessment parameters such as solid ink density, dot gain, hue error and print contrast, each experimental approaches are ranked (vide shown in Table 3.20 to Table 3.30) and among which the highest grey relational analysis (GRA) score indicates the best print quality.

Table 3.17: Normalised data of performance index

Experiment No.	Solid Ink Density	Dot Gain at 30%	Dot Gain at 50%	Dot Gain at 70%	Hue Error at 30%	Hue Error at 50%	Hue Error at 70%	Print Contrast at 30%	Print Contrast at 50%	Print Contrast at 70%
1	0.81	0.57	0.35	0.16	0.16	0.66	0.16	0.77	0.63	0.36
2	0.74	0.94	0.83	0.81	0.40	1.00	0.94	0.98	0.93	0.92
3	0.64	1.00	1.00	1.00	1.00	0.94	1.00	1.00	1.00	1.00
4	1.00	0.37	0.15	0.10	0.67	0.76	0.90	0.63	0.42	0.30
5	0.97	0.92	0.59	0.32	0.07	0.71	0.67	0.98	0.83	0.60
6	0.68	0.97	0.76	0.75	0.97	0.80	0.44	0.99	0.89	0.88
7	0.13	0.32	0.25	0.02	0.35	0.63	0.00	0.47	0.42	0.05
8	0.08	0.70	0.60	0.17	0.06	0.00	0.18	0.79	0.72	0.27
9	0.00	0.90	0.67	0.63	0.41	0.33	0.36	0.90	0.76	0.68
10	0.19	0.00	0.00	0.00	0.62	0.53	0.21	0.00	0.00	0.00
11	0.10	0.75	0.30	0.08	0.00	0.47	0.24	0.82	0.48	0.15
12	0.03	0.85	0.61	0.50	0.10	0.74	0.75	0.87	0.73	0.60

Table 3.18: Deviation sequence

Experiment No.	Solid Ink Density	Dot Gain at 30%	Dot Gain at 50%	Dot Gain at 70%	Hue Error at 30%	Hue Error at 50%	Hue Error at 70%	Print Contrast at 30%	Print Contrast at 50%	Print Contrast at 70%
1	0.19	0.43	0.65	0.84	0.84	0.34	0.84	0.23	0.37	0.64
2	0.26	0.06	0.17	0.19	0.60	0.00	0.06	0.02	0.07	0.08

3	0.36	0.00	0.00	0.00	0.00	0.06	0.00	0.00	0.00	0.00
4	0.00	0.63	0.85	0.90	0.33	0.24	0.10	0.37	0.58	0.70
5	0.03	0.08	0.41	0.68	0.93	0.29	0.33	0.02	0.17	0.40
6	0.32	0.03	0.24	0.25	0.03	0.20	0.56	0.01	0.11	0.12
7	0.87	0.68	0.75	0.98	0.65	0.37	1.00	0.53	0.58	0.95
8	0.92	0.30	0.40	0.83	0.94	1.00	0.82	0.21	0.28	0.73
9	1.00	0.10	0.33	0.37	0.59	0.67	0.64	0.10	0.24	0.32
10	0.81	1.00	1.00	1.00	0.38	0.47	0.79	1.00	1.00	1.00
11	0.90	0.25	0.70	0.92	1.00	0.53	0.76	0.18	0.52	0.85
12	0.97	0.15	0.39	0.50	0.90	0.26	0.25	0.13	0.27	0.40

Table 3.19: Grey relational co-efficient

Experiment No.	**Solid Ink Density**	**Dot Gain at 30%**	**Dot Gain at 50%**	**Dot Gain at 70%**	**Hue Error at 30%**	**Hue Error at 50%**	**Hue Error at 70%**	**Print Contrast at 30%**	**Print Contrast at 50%**	**Print Contrast at 70%**
1	0.72	0.54	0.44	0.37	0.37	0.59	0.37	0.69	0.57	0.44
2	0.66	0.90	0.74	0.72	0.46	1.00	0.89	0.96	0.88	0.86
3	0.58	1.00	1.00	1.00	1.00	0.89	1.00	1.00	1.00	1.00
4	1.00	0.44	0.37	0.36	0.60	0.68	0.83	0.58	0.46	0.42
5	0.94	0.86	0.55	0.42	0.35	0.63	0.60	0.97	0.74	0.56
6	0.61	0.95	0.67	0.67	0.94	0.72	0.47	0.98	0.82	0.81
7	0.36	0.42	0.40	0.34	0.44	0.57	0.33	0.49	0.46	0.34

8	0.35	0.63	0.55	0.38	0.35	0.33	0.38	0.70	0.64	0.41
9	0.33	0.84	0.60	0.58	0.46	0.43	0.44	0.84	0.68	0.61
10	0.38	0.33	0.33	0.33	0.57	0.51	0.39	0.33	0.33	0.33
11	0.36	0.67	0.42	0.35	0.33	0.49	0.40	0.73	0.49	0.37
12	0.34	0.77	0.56	0.50	0.36	0.66	0.67	0.80	0.65	0.55

Table 3.20: Grey relational grade and ranking for solid ink density

Rank	**Experimental Variables**	**Grey Relational Grade**	**Experiment No.**
1	Coated Paper, 100 lpi Mesh, FM Dot	1	4
2	Coated Paper, 120 lpi Mesh, FM Dot	0.939394	5
3	Coated Paper, 100 lpi Mesh, AM Dot	0.72093	1
4	Coated Paper, 120 lpi Mesh, AM Dot	0.659574	2
5	Coated Paper, 140 lpi Mesh, FM Dot	0.607843	6
6	Coated Paper, 140 lpi Mesh, AM Dot	0.580524	3
7	Uncoated Paper, 100 lpi Mesh, FM Dot	0.380835	10
8	Uncoated Paper, 100 lpi Mesh, AM Dot	0.364706	7
9	Uncoated Paper, 120 lpi Mesh, FM Dot	0.356322	11
10	Uncoated Paper, 120 lpi Mesh, AM Dot	0.351474	8
11	Uncoated Paper, 140 lpi Mesh, FM Dot	0.340659	12
12	Uncoated Paper, 140 lpi Mesh, AM Dot	0.333333	9

Table 3.21: Grey relational grade and ranking for 30% dot gain

Rank	Experimental Variables	Grey Relational Grade	Experiment No.
1	Coated Paper, 140 lpi Mesh, AM Dot	1	3
2	Coated Paper, 140 lpi Mesh, FM Dot	0.945868	6
3	Coated Paper, 120 lpi Mesh, AM Dot	0.898934	2
4	Coated Paper, 120 lpi Mesh, FM Dot	0.860275	5
5	Uncoated Paper, 140 lpi Mesh, AM Dot	0.836995	9
6	Uncoated Paper, 140 lpi Mesh, FM Dot	0.768237	12
7	Uncoated Paper, 120 lpi Mesh, FM Dot	0.666259	11
8	Uncoated Paper, 120 lpi Mesh, AM Dot	0.626478	8
9	Coated Paper, 100 lpi Mesh, AM Dot	0.538942	1
10	Coated Paper, 100 lpi Mesh, FM Dot	0.441564	4
11	Uncoated Paper, 100 lpi Mesh, AM Dot	0.423592	7
12	Uncoated Paper, 100 lpi Mesh, FM Dot	0.333333	10

Table 3.22: Grey relational grade and ranking for 50% dot gain

Rank	Experimental Variables	Grey Relational Grade	Experiment No.
1	Coated Paper, 140 lpi Mesh, AM Dot	1	3
2	Coated Paper, 120 lpi Mesh, AM Dot	0.743286	2

3	Coated Paper, 140 lpi Mesh, FM Dot	0.674287	6
4	Uncoated Paper, 140 lpi Mesh, AM Dot	0.60192	9
5	Uncoated Paper, 140 lpi Mesh, FM Dot	0.563111	12
6	Uncoated Paper, 120 lpi Mesh, AM Dot	0.552834	8
7	Coated Paper, 120 lpi Mesh, FM Dot	0.550254	5
8	Coated Paper, 100 lpi Mesh, AM Dot	0.43576	1
9	Uncoated Paper, 120 lpi Mesh, FM Dot	0.416692	11
10	Uncoated Paper, 100 lpi Mesh, AM Dot	0.398931	7
11	Coated Paper, 100 lpi Mesh, FM Dot	0.370185	4
12	Uncoated Paper, 100 lpi Mesh, FM Dot	0.333333	10

Table 3.23: Grey relational grade and ranking for 70% dot gain

Rank	**Experimental Variables**	**Grey Relational Grade**	**Experiment No.**
1	Coated Paper, 140 lpi Mesh, AM Dot	1	3
2	Coated Paper, 120 lpi Mesh, AM Dot	0.720117	2
3	Coated Paper, 140 lpi Mesh, FM Dot	0.669859	6
4	Uncoated Paper, 140 lpi Mesh, AM Dot	0.575611	9
5	Uncoated Paper, 140 lpi Mesh, FM Dot	0.50187	12
6	Coated Paper, 120 lpi Mesh, FM Dot	0.424586	5

7	Uncoated Paper, 120 lpi Mesh, AM Dot	0.375753	8
8	Coated Paper, 100 lpi Mesh, AM Dot	0.372034	1
9	Coated Paper, 100 lpi Mesh, FM Dot	0.358086	4
10	Uncoated Paper, 120 lpi Mesh, FM Dot	0.352903	11
11	Uncoated Paper, 100 lpi Mesh, AM Dot	0.338944	7
12	Uncoated Paper, 100 lpi Mesh, FM Dot	0.333333	10

Table 3.24: Grey relational grade and ranking for 30% hue error

Rank	**Experimental Variables**	**Grey Relational Grade**	**Experiment No.**
1	Coated Paper, 140 lpi Mesh, AM Dot	1	3
2	Coated Paper, 140 lpi Mesh, FM Dot	0.94	6
3	Coated Paper, 100 lpi Mesh, FM Dot	0.602564	4
4	Uncoated Paper, 100 lpi Mesh, FM Dot	0.566265	10
5	Uncoated Paper, 140 lpi Mesh, AM Dot	0.460784	9
6	Coated Paper, 120 lpi Mesh, AM Dot	0.456311	2
7	Uncoated Paper, 100 lpi Mesh, AM Dot	0.435185	7
8	Coated Paper, 100 lpi Mesh, AM Dot	0.373016	1
9	Uncoated Paper, 140 lpi Mesh, FM Dot	0.356061	12
10	Coated Paper, 120 lpi Mesh, FM Dot	0.350746	5

11	Uncoated Paper, 120 lpi Mesh, AM Dot	0.348148	8
12	Uncoated Paper, 120 lpi Mesh, FM Dot	0.333333	11

Table 3.25: Grey relational grade and ranking for 50% hue error

Rank	**Experimental Variables**	**Grey Relational Grade**	**Experiment No.**
1	Coated Paper, 120 lpi Mesh, AM Dot	1	2
2	Coated Paper, 140 lpi Mesh, AM Dot	0.888199	3
3	Coated Paper, 140 lpi Mesh, FM Dot	0.715	6
4	Coated Paper, 100 lpi Mesh, FM Dot	0.677725	4
5	Uncoated Paper, 140 lpi Mesh, FM Dot	0.655963	12
6	Coated Paper, 120 lpi Mesh, FM Dot	0.632743	5
7	Coated Paper, 100 lpi Mesh, AM Dot	0.593361	1
8	Uncoated Paper, 100 lpi Mesh, AM Dot	0.574297	7
9	Uncoated Paper, 100 lpi Mesh, FM Dot	0.514388	10
10	Uncoated Paper, 120 lpi Mesh, FM Dot	0.486395	11
11	Uncoated Paper, 140 lpi Mesh, AM Dot	0.428144	9
12	Uncoated Paper, 120 lpi Mesh, AM Dot	0.333333	8

Table 3.26: Grey relational grade and ranking for 70% hue error

Rank	Experimental Variables	Grey Relational Grade	Experiment No.
1	Coated Paper, 140 lpi Mesh, AM Dot	1	3
2	Coated Paper, 120 lpi Mesh, AM Dot	0.889328	2
3	Coated Paper, 100 lpi Mesh, FM Dot	0.830258	4
4	Uncoated Paper, 140 lpi Mesh, FM Dot	0.667656	12
5	Coated Paper, 120 lpi Mesh, FM Dot	0.6	5
6	Coated Paper, 140 lpi Mesh, FM Dot	0.471698	6
7	Uncoated Paper, 140 lpi Mesh, AM Dot	0.438596	9
8	Uncoated Paper, 120 lpi Mesh, FM Dot	0.39823	11
9	Uncoated Paper, 100 lpi Mesh, FM Dot	0.387263	10
10	Uncoated Paper, 120 lpi Mesh, AM Dot	0.378151	8
11	Coated Paper, 100 lpi Mesh, AM Dot	0.373134	1
12	Uncoated Paper, 100 lpi Mesh, AM Dot	0.333333	7

Table 3.27: Grey relational grade and ranking for 30% print contrast

Rank	Experimental Variables	Grey Relational Grade	Experiment No.
1	Coated Paper, 140 lpi Mesh, AM Dot	1	3
2	Coated Paper, 140 lpi Mesh, FM Dot	0.97837	6
3	Coated Paper, 120 lpi Mesh, FM Dot	0.967088	5

4	Coated Paper, 120 lpi Mesh, AM Dot	0.961473	2
5	Uncoated Paper, 140 lpi Mesh, AM Dot	0.835247	9
6	Uncoated Paper, 140 lpi Mesh, FM Dot	0.798154	12
7	Uncoated Paper, 120 lpi Mesh, FM Dot	0.734116	11
8	Uncoated Paper, 120 lpi Mesh, AM Dot	0.700236	8
9	Coated Paper, 100 lpi Mesh, AM Dot	0.685541	1
10	Coated Paper, 100 lpi Mesh, FM Dot	0.575144	4
11	Uncoated Paper, 100 lpi Mesh, AM Dot	0.486471	7
12	Uncoated Paper, 100 lpi Mesh, FM Dot	0.333333	10

Table 3.28: Grey relational grade and ranking for 50% print contrast

Rank	**Experimental Variables**	**Grey Relational Grade**	**Experiment No.**
1	Coated Paper, 140 lpi Mesh, AM Dot	1	3
2	Coated Paper, 120 lpi Mesh, AM Dot	0.879562	2
3	Coated Paper, 140 lpi Mesh, FM Dot	0.820181	6
4	Coated Paper, 120 lpi Mesh, FM Dot	0.741233	5
5	Uncoated Paper, 140 lpi Mesh, AM Dot	0.677953	9
6	Uncoated Paper, 140 lpi Mesh, FM Dot	0.648809	12
7	Uncoated Paper, 120 lpi Mesh, AM Dot	0.644314	8

8	Coated Paper, 100 lpi Mesh, AM Dot	0.573083	1
9	Uncoated Paper, 120 lpi Mesh, FM Dot	0.488219	11
10	Coated Paper, 100 lpi Mesh, FM Dot	0.463068	4
11	Uncoated Paper, 100 lpi Mesh, AM Dot	0.462986	7
12	Uncoated Paper, 100 lpi Mesh, FM Dot	0.333333	10

Table 3.29: Grey relational grade and ranking for 70% print contrast

Rank	**Experimental Variables**	**Grey Relational Grade**	**Experiment No.**
1	Coated Paper, 140 lpi Mesh, AM Dot	1	3
2	Coated Paper, 120 lpi Mesh, AM Dot	0.861357	2
3	Coated Paper, 140 lpi Mesh, FM Dot	0.805676	6
4	Uncoated Paper, 140 lpi Mesh, AM Dot	0.612611	9
5	Coated Paper, 120 lpi Mesh, FM Dot	0.555078	5
6	Uncoated Paper, 140 lpi Mesh, FM Dot	0.554395	12
7	Coated Paper, 100 lpi Mesh, AM Dot	0.439206	1
8	Coated Paper, 100 lpi Mesh, FM Dot	0.41748	4
9	Uncoated Paper, 120 lpi Mesh, AM Dot	0.407046	8
10	Uncoated Paper, 120 lpi Mesh, FM Dot	0.369722	11

11	Uncoated Paper, 100 lpi Mesh, AM Dot	0.344066	7
12	Uncoated Paper, 100 lpi Mesh, FM Dot	0.333333	10

Table 3.30: Grey relational grade and ranking for overall performance

Rank	Experimental Variables	Grey Relational Grade	Experiment No.
1	Coated Paper, 140 lpi Mesh, AM Dot	0.946872	3
2	Coated Paper, 120 lpi Mesh, AM Dot	0.806994	2
3	Coated Paper, 140 lpi Mesh, FM Dot	0.762878	6
4	Coated Paper, 120 lpi Mesh, FM Dot	0.66214	5
5	Uncoated Paper, 140 lpi Mesh, FM Dot	0.585491	12
6	Uncoated Paper, 140 lpi Mesh, AM Dot	0.580119	9
7	Coated Paper, 100 lpi Mesh, FM Dot	0.573608	4
8	Coated Paper, 100 lpi Mesh, AM Dot	0.510501	1
9	Uncoated Paper, 120 lpi Mesh, AM Dot	0.471777	8
10	Uncoated Paper, 120 lpi Mesh, FM Dot	0.460219	11
11	Uncoated Paper, 100 lpi Mesh, AM Dot	0.416251	7
12	Uncoated Paper, 100 lpi Mesh, FM Dot	0.384875	10

3.3.5 Discussions

The GRA index score for solid ink density is shown in Table 3.20 indicates that the coated grade paper has the ability to reproduce better solid ink density by screen printing using different types of dots and mesh count than that of uncoated paper. The smooth surface texture of the coated paper enhances the excellent reproduction of solid

ink density in all cases. But for uncoated paper, the irregular and matt surface texture diminishes such effects due to the uneven distribution of ink over the uncoated surface as well the undesirable light scattering effects from the paper. At lower screen mesh count, the ink deposition on the substrate will be more in screen printing than that of higher screen mesh count. Here the 100 lpi screen mesh count can reproduce better solid ink densities than that of 140 lpi mesh count. The lower the screen meshes count more will be the mesh open areas, so the ink flow will be more and the heavier ink deposition will be the result. Also, at solid ink density deposition, the printed sample with FM dots offers higher optical densities than that of AM dots as shown in Table 3.20. The AM dot with low mesh count is also capable to deliver heavy ink deposition, but the FM dots are comparatively capable to give more vibrant colors than AM at solid densities.

The Table 3.21 shows the GRA index ranking for 30% dot gain, and it is noticed that the print quality of screen printing is highly dependable to the mesh count. Higher the screen mesh count better will be the reproduction of finer details. The higher screen mesh count facilitates the better carrying of fine dot details of stencil over the mesh and also controls the ink flow through the mesh opening during printing. At higher mesh count such as 140 lpi and 120 lpi, both coated paper and uncoated paper grades can reproduce the 30% tonal area better than that of 100 lpi mesh count. The 100 lpi screen mesh comparatively contains larger mesh opening and so fails to accurately carry the finer details of stencil on the mesh as well as to control the ink flow through the mesh during printing. The AM dots on coated paper with 140 lpi mesh count gives the best result. Even though, the FM dots at higher screen mesh count also works better at 30% dot area.

The GRA index ranking for 50% dot gain shown are in Table 3.22 which indicates that the higher screen mesh count can control the dot gain at those middle-tones than that of lower mesh count. Also, with higher screen mesh count the AM dots will perform better than FM dots especially in these middle-tone areas. FM dots show undesirable random shift of tonal values at this middle-tone than AM dots. Also, the surface irregularities and porosity of uncoated paper always provides a tendency to undesirably absorb the ink and that will increase the chance of dot gain.

The GRA ranking of 70% dot gain as shown in Table 3.23 indicates that the higher mesh count of screen printing can reproduce better shadow details effectively. The AM dots printed on coated paper with 140 lpi mesh count gives the best result. Higher the screen mesh count better will be the ink flow through the mesh in printing and also better the halftone dot details on stencil over the mesh.

The Tables 3.24-3.26 are showing the GRA ranking of hue error at 30%, 50% and 70% tonal areas respectively. Higher the mesh count, lower will be the hue error irrespective of percentage dot area. It is observed that hue error is minimum in the case of AM dots in highlight, midtone and shadows. However, the hue error depends on the printing conditions, purity of ink, spectral behaviour of the substrate etc.

The Tables 3.27-3.29 show the GRA index ranking for print contrast at 30%, 50% and 70% tonal areas respectively. All the cases indicate that, higher the mesh count better will be the print contrast. Lowering the mesh count will reduce the print contrast of reproduction. The AM dot print with 140 lpi screen mesh count on coated grade paper shows the superior print contrast in all the cases. At higher screen mesh count the coated paper provides greater print contrast than uncoated grade. The print contrast indicates the accuracy of tonal area reproduction or shadow details in contrast with the solid area ink density.

The overall GRA index based ranking given in Table 3.30 indicates that, at 140 lpi screen mesh count, the coated paper with AM dots is comparatively best in the print quality by considering the criteria like solid ink densities, dot gain, hue error and the print contrast. The result shows the importance of mesh count in screen printing in distinction with the type of substrate and the halftone mode of reproduction employed in the printing process.

As per the results, the screen mesh with higher thread counts such as 140 lpi is capable to produce better print quality in screen printing than that of screen mesh with 120 lpi and 100 lpi mesh count. The screen mesh with high thread count indicates the less open area and its capability to hold more stencil details over the mesh than that of screen with lower mesh count. Also, the lesser open area of 140 lpi screen mesh facilitates the better control over the ink flow through the mesh and thereby reduces the chance of dot gain under the circumstance of high squeegee pressure and low viscous screen printing ink.

Also, it is noticed that, the irregular surface textured substrate such as uncoated paper in such cases will accelerates the occurrence of undesirable dot gain at lower mesh count in screen printing.

It is also observed that the mode of halftone screening process such as AM and FM dots employed in the printing process influences the print quality. Comparing AM with FM print quality in the result, it is found that the AM dot pattern gives the best print results at 30%, 50% and 70% tonal areas than FM dots. This indicates that AM dots in middle-tone areas can produce better details in screen printing.

The FM dots are capable to reproduce vibrant color than AM dots but show an undesirable random shift of tonal values from highlight to shadow region. This leads to the loss of details at the middle-tones considerably. At the same time, the AM dots are better in reproducing middle-tone gradations when comparing with FM dot reproduction. The problem faced by FM dots in this kind may be due to its fine size and the randomly distributed feature that all made it less likely capable to the various features of screen printing process like complications of stencil making process, mesh opening, stencil adhesion requirements with the screen, squeegee pressure, ink pigment particle size and its viscosity.

The microscopic view of the dot reproduction is shown vide in Figures 3.19-3.24 that gives a better understanding about the nature of dot reproduction of both AM and FM dots on coated and uncoated grade paper at different screen mesh count.

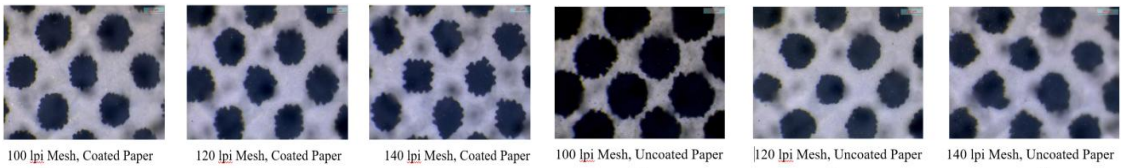

Figure 3.19: Microscopic view of AM dot at 30% dot area

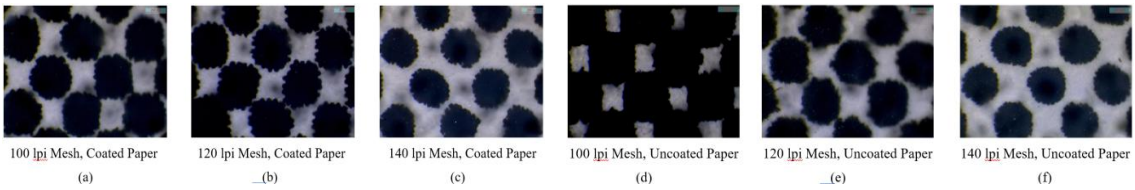

Figure 3.20: Microscopic view of AM dot at 50% dot area

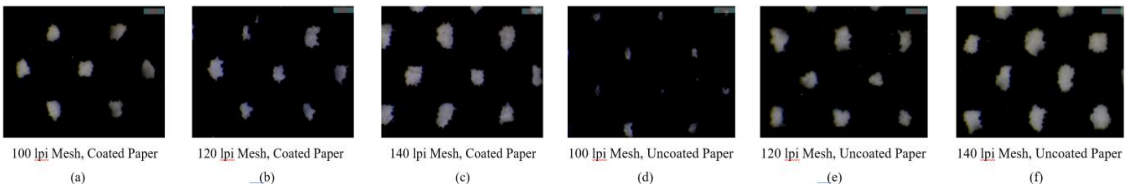

Figure 3.21: Microscopic view of AM dot at 70% dot area

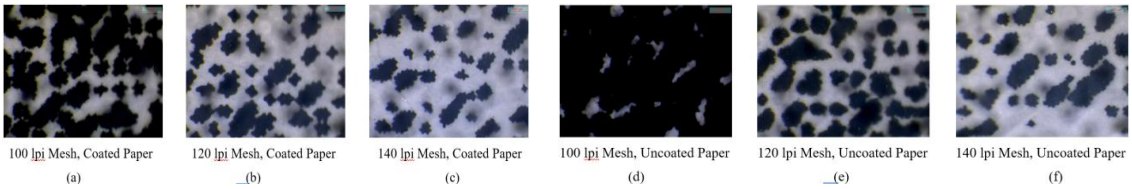

Figure 3.22: Microscopic view of FM dot at 30% dot area

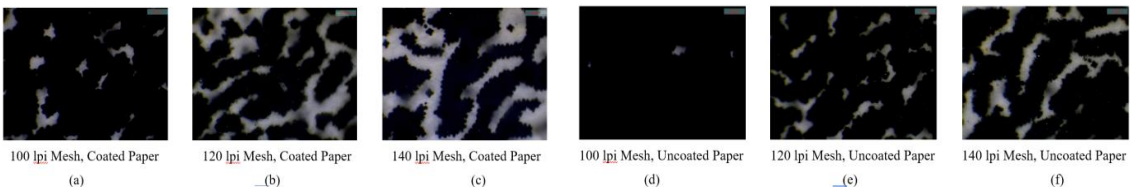

Figure 3.23: Microscopic view of FM dot at 50% dot area

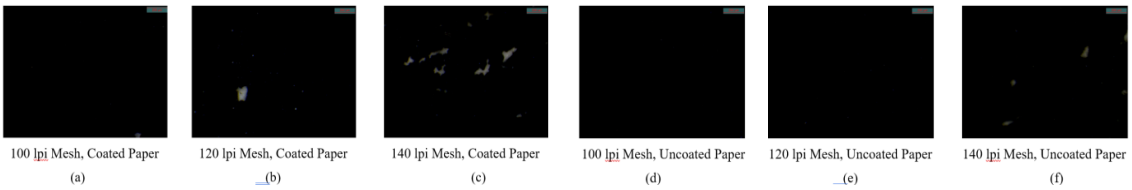

Figure 3.24: Microscopic view of FM dot at 70% dot area

Figures 3.19a-3.19f represent the microscopic image (enlarged to 80x) of 30% dot area printed on both coated and uncoated paper substrates produced by different combinations of screen mesh. The image is made up of AM dots only. Figure 3.19c shows that 140 lpi screen mesh on coated paper provides the sharp image with uniform ink distribution which confirms the Taguchi's GRA ranking made in the analysis. Figure 3.19b represents image printed through 120 lpi on coated images are darker in appearance and hence it confirms the analysis made by Taguchi's GRA method which is the second best.

Figures 3.20a-3.20f show the microscopic images of 50% dot area of print made up of AM dots on both coated and uncoated papers by using stencils made on different screen meshes. Figure 3.20c shows 140 lpi mesh gives the best print quality as compared to others. This confirms the Taguchi's GRA analysis results as obtained.

Figures 3.21a-3.21f represent the microscopic images of 70% dot area of print of grey scale formed with AM dots taken on both coated and uncoated paper substrates through the stencils formed on different screen meshes. Figure 3.21c shows the minimum dot gain as compared to others. This confirms the Taguchi's GRA analysis as given in Table 3.23 and Table 3.30.

Figures 3.22a-3.22f are the microscopic images of the prints of 30% dot area obtained through stencils made on different lpi screen mesh adopting FM dots. The pictures show dot gain is minimum in print of 140 lpi mesh on coated paper but dots are irregular in shape in all the cases.

Figures 3.23a-3.23f represent the microscopic images of prints obtained through stencils made on different lpi screen mesh by using FM screening. These shows that dots are not at all clear and gain is more in all the cases.

Figures 3.24a-3.24f are the microscopic images of 70% dot area of FM dots through the stencils made on different lpi screen meshes. This shows dot gain is minimum in case of 140 lpi mesh on coated paper vide Figure 3.22c which confirms the Taguchi's GRA analysis.

3.3.6 Conclusions

The experimental study conducted with this research work was designed in such a way to find the influence of AM and FM dots on coated and uncoated paper under three different screen mesh ruling in the screen printing process. The print quality assessment was done through the scientific approach of Taguchi's grey relational analysis by considering the major factors influencing the print quality such as solid ink density, dot gain, hue error and print contrast. The tonal reproduction curve at 5% to 100% dot coverage is plotted for dot area, dot gain, hue error and the print contrast. Moreover, this research work employed the systematic implementation of Taguchi's grey relational analysis technique in the print quality assessment in a most reliable and meaningful way.

The results show that the screen printing quality is dependent on the screen mesh count. Printing with a high screen mesh count on smooth surface paper will give the best result in screen printing. The AM dots will work better in the middle-tone region with a good

tonal value transition from highlight to shadow region. Meanwhile, the FM dots are capable to give the vibrant color especially at the solid density regions than that of AM dots but fail to reproduce the middle-tone densities with a smooth tonal transition. There is a huge shift of tonal value are obtained at the middle-tones for FM dots. The accurate reproduction of FM dots in screen printing is dependent on the mesh count and some other crucial factors like adaptation with proper stencil making process, adhesion with screen mesh, squeegee pressure, ink parameters etc. The printing on uncoated paper with low mesh count will leads to high dot gain and it is a poor choice for high quality precision works.

Chapter 4

Box Behnken Design of Prints

4.1 Preliminaries

Different types of impact and non-impact printing processes are adopted for specific purposes considering the different benefits, costs, limitations of the processes. Out of these, two screen like effects based printing processes viz. flexography and screen printing were considered for the study [3]. Box Behnken Design (BBD) is used to optimize the goods in terms of quality as well as production process [42]. Analysis of Variance (ANOVA) is used to determine the actual state of the performance statistics of experimental parameters, errors and uncontrolled parameters etc. along with crisscrossing the competence of the experimental model against the responses [48]. The dot gain increases in flexographic halftone printing in proportion to drops in anilox roll line frequency and increase in plate image screen frequency [8]. The print contrast describes the accuracy of halftone reproduction at the shadow areas of a print [15]. Spreading of ink on the print surface is directly correlated with the paper smoothness or roughness [14]. Studies show that fabrics with a higher thread count per linear distance can produce prints with excellent quality [32].

For Box Behnken Design, the same process steps and equations were used, mentioned in Chapter 1, subsections 1.4 and 1.5.

4.2 Flexography Printing

4.2.1 Objective of the Study

This study is an experimental and statistical approach to determine the optimum process parameters for flexography print quality that can be achieved with AM square shaped halftone dots on three grades of paper with different roughness under three anilox roller rulings.

4.2.2 Experimental Methods

The experiment was conducted by printing an ideal grey scale image with AM square dots onto three grades of paper substrates such as coated, uncoated and calendared papers having different smooth textures or roughness. The roughnesses of the paper substrates were measured by Gurley 4340 automatic densometer & smoothness tester using contact method and given in Table 4.1. As the anilox roller acts as the core of flexography printing process to deliver exact print quality, three different kinds of anilox roller screen rulings such as 700 lpi (BCM 4.1), 1000 lpi (BCM 3.9) and 1300 lpi (BCM 3.8) (lines per inch) were employed at each print trials. The engraved cells have chosen for the work that features 60º hexagonal in geometry. The printing work was executed in flexography printing machine, OMET LAB230 Iflex with black color uv ink. The plates used are photopolymer plate of 1.14 mm thickness with magnetic backing. The plate used is Dupont make and the hardness of the finished plate is 45 shore A^0. The printing speed (35 m/min), nip pressure (3 mm), room temperature (23^0c) and ink parameters are kept constant throughout the printing process. The ink used in the printing process is liquid ink. The values of the viscosity and surface tension of the ink used are 2.5 poise and 36 x 10^{-3} N/m.

4.2.2.1 Measurements and Data Collection

Each element of the specified samples of printed sheets are subjected to visual inspection with a Digital microscope (LEICA, S8APO) followed by the quantitative optical property measurement using Spectro densitometer (such as X-Rite Spectro Eye and TECHKON GmbH Spectro Dens). The quality analysis on the collected data followed by optimization of process parameters were done with the response surface methodology such as Box Behnken Design (BBD). In the computation process, 30%, 50% and 70% (that represents highlight, middle-tone and shadow areas respectively) tonal areas are targeted for the analysis of response such as dot gain and print contrast. The planning of experiment with Box Behnken Design has been performed with Minitab 17 statistical software.

Table 4.1 shows different process parameters or factors, their values, corresponding levels and the response variable such as dot gain considering in this analysis process.

Table 4.1: Process parameters or factors and their levels

Factors	Unit	Symbol	Levels			Responses
			1	2	3	
Anilox Roller Screen Rulings	Lines per inch (lpi)	A	700	1000	1300	Dot Gain & Print Contrast
Paper Roughness	Millilitre per minute (ml/min)	B	36	109	182	
Dot Percentage	Percentage (%)	C	30	50	70	

The influence of experimental variable parameters such as substrate, dot percentage and anilox roller screen rulings in flexography printing corresponding to the possible dot gain and print contrast are investigated in the analysis part with ANOVA and regression analysis process.

4.2.2.2 Box Behnken Design

The BBD design includes the following features:

- 3 factors with 3 levels.
- 1 base block and 3 centre points.
- 1 replicate with 15 base runs.
- Total of 1 block and 15 experimental runs.

The Table 4.2 represents the design table of BBD. The design represents the values 1 and -1 corresponding to high and low levels of factors. The 0 represents the centre point or the middle level value of factors. As per BBD, the total experimental run is 15.

Table 4.2: Design table of BBD

Run	Blk	A	B	C
1.	1	-1	-1	0

2.	1	1	-1	0
3.	1	-1	1	0
4.	1	1	1	0
5.	1	-1	0	-1
6.	1	1	0	-1
7.	1	-1	0	1
8.	1	1	0	1
9.	1	0	-1	-1
10.	1	0	1	-1
11.	1	0	-1	1
12.	1	0	1	1
13.	1	0	0	0
14.	1	0	0	0
15.	1	0	0	0

4.2.3 Results

As per the Box Behnken approach the conduct of experiments and the measurement of output responses at each experimental runs are prepared as shown in the Table 4.3. The Analysis of Variance (ANOVA) and regression analysis of the data are performed in detail. Table 4.3 represents the input data which were selected and measured with instruments for the purpose of BBD. Anilox roller screen rulings, paper roughness and

dot percentage data were selected during the printing of the jobs. Dot gains were measured and calculated. Print contrast data were also measured from the printed copy using X-Rite Spectro Eye.

Table 4.3: Dot gain and print contrast response at each experimental run

Run Order	**Factor 1: A** **Anilox Rulings (lpi)**	**Factor 2: B** **Paper Roughness (ml/min)**	**Factor 3: C** **Dot Percentage (%)**	**Dot Gain (%)**	**Print Contrast (%)**
1.	700	36	50	15	76
2.	1300	36	50	10	71
3.	700	182	50	29	46
4.	1300	182	50	25	48
5.	700	109	30	13	81
6.	1300	109	30	13	78
7.	700	109	70	14	44
8.	1300	109	70	12	41
9.	1000	36	30	9	87
10.	1000	182	30	30	64
11.	1000	36	70	11	58

12.	1000	182	70	19	27
13.	1000	109	50	17	60
14.	1000	109	50	17	60
15.	1000	109	50	17	60

4.2.3.1 Graphical Analysis

The graphical plots of the BBD results are given at Figures 4.1-4.13. The residual data of experiments, main effects and interaction effects of factors over responses, contour plots, 3D surface plots, 3D scatterplot of process parameters etc. are plotted in detail.

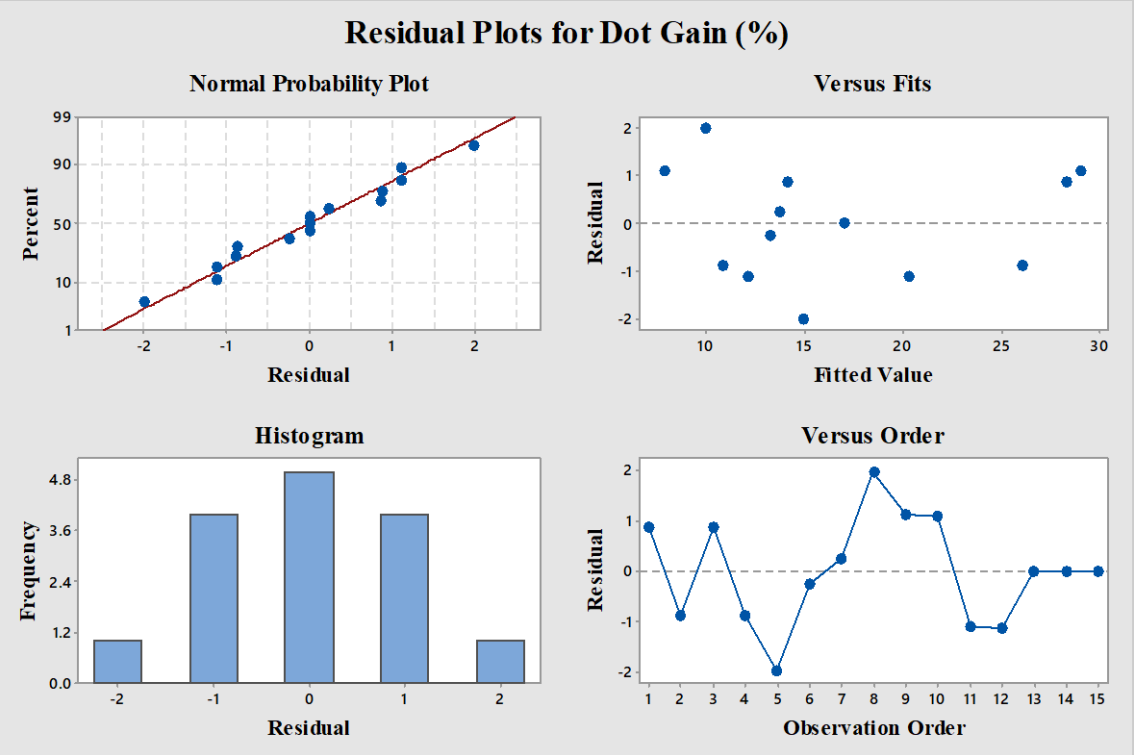

Figure 4.1: Residual plots for dot gain

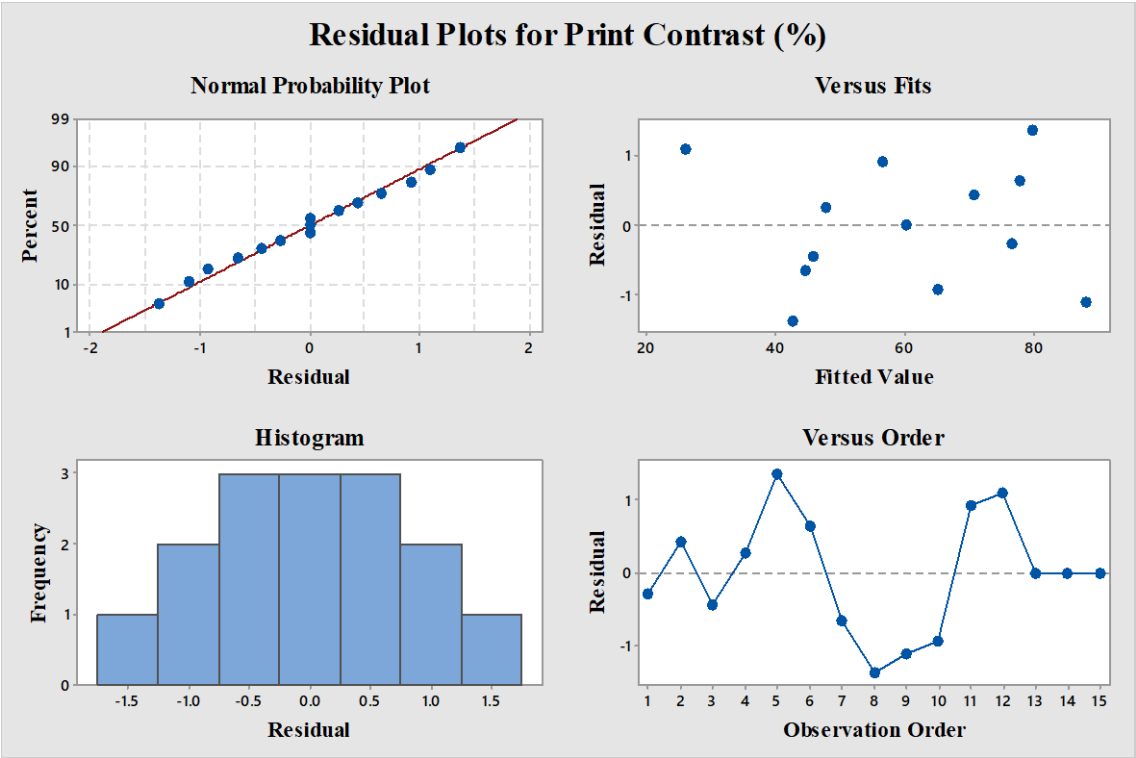

Figure 4.2: Residual plots for print contrast

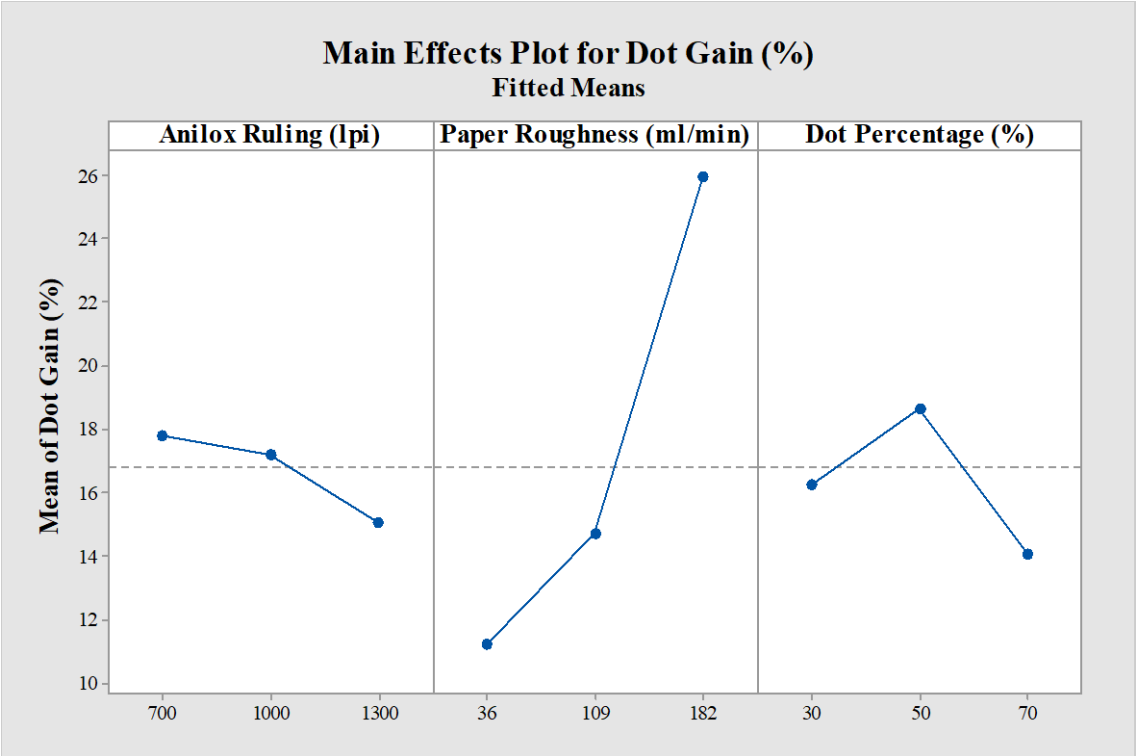

Figure 4.3: Main effect plot for dot gain

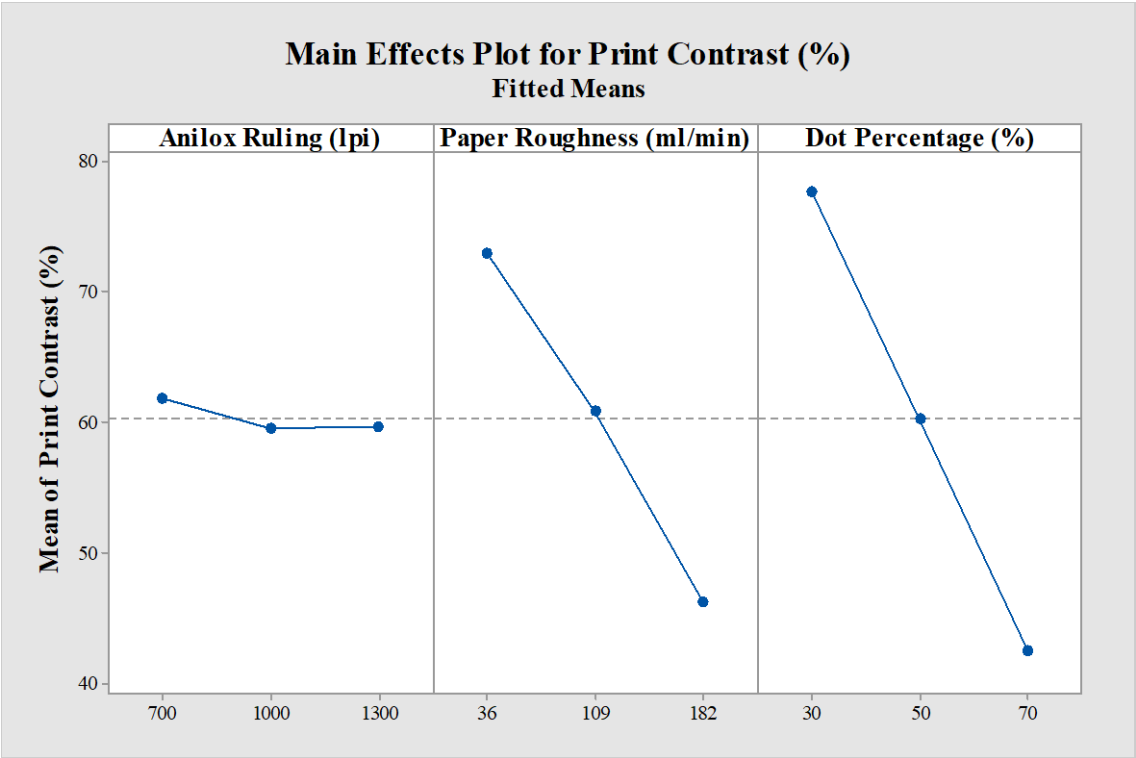

Figure 4.4: Main effect plot for print contrast

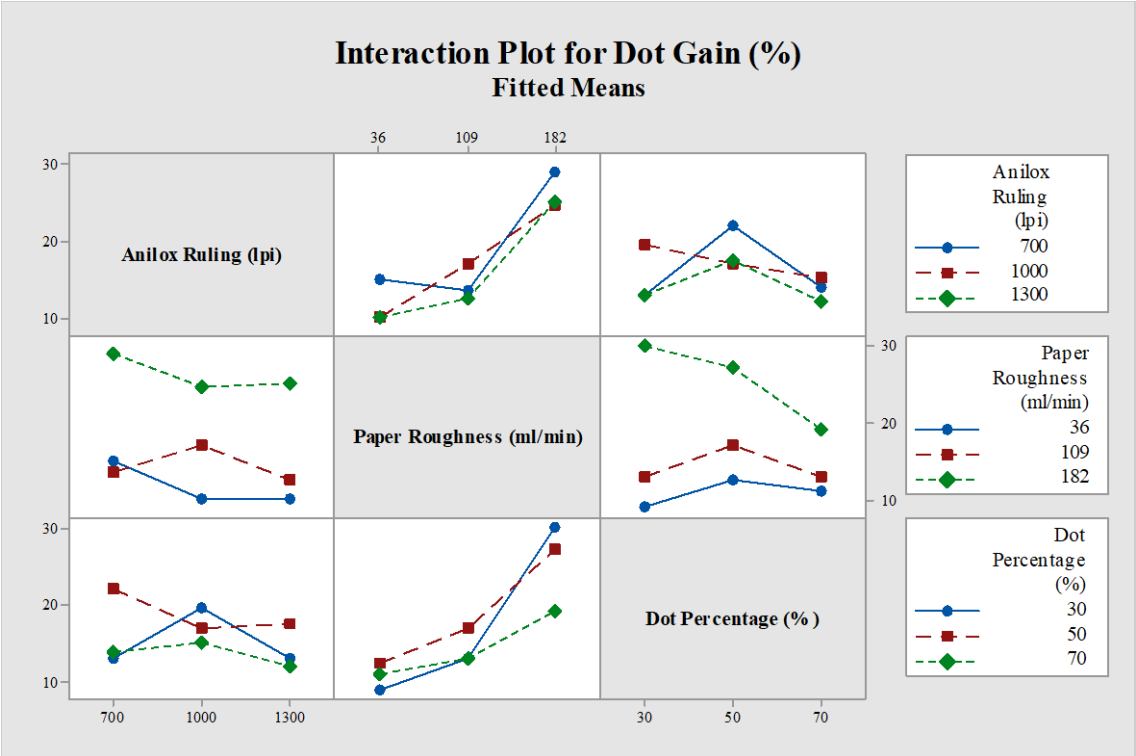

Figure 4.5: Interaction plot for dot gain

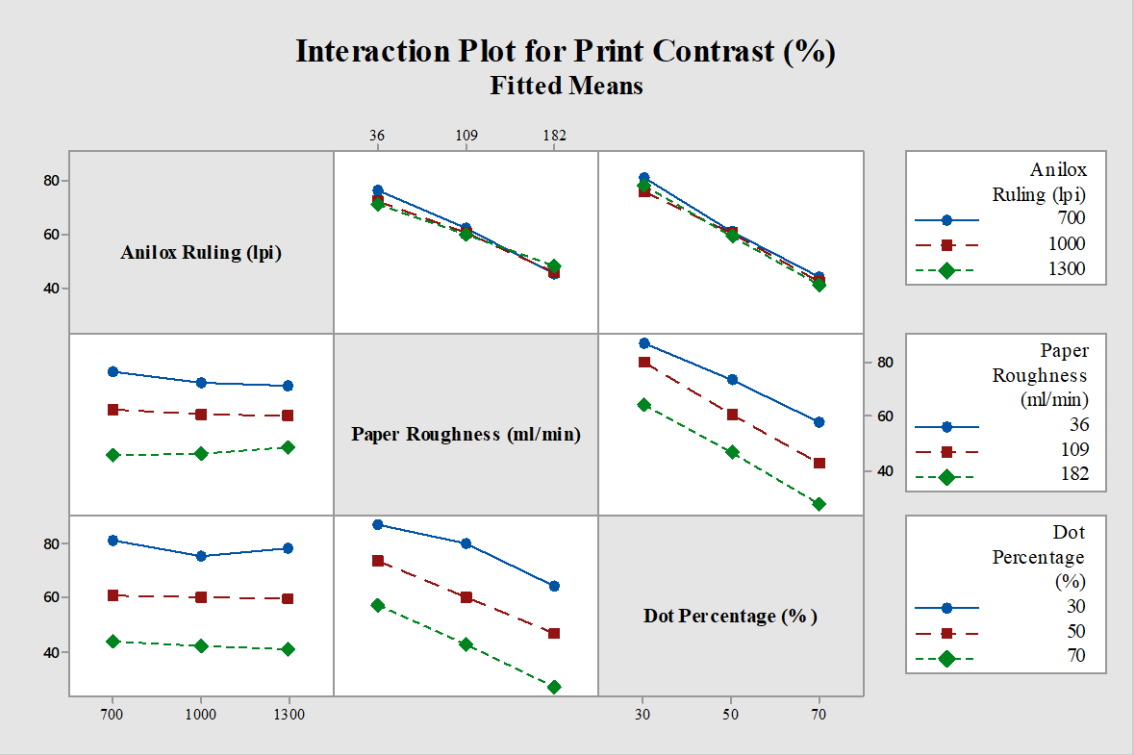

Figure 4.6: Interaction plot for print contrast

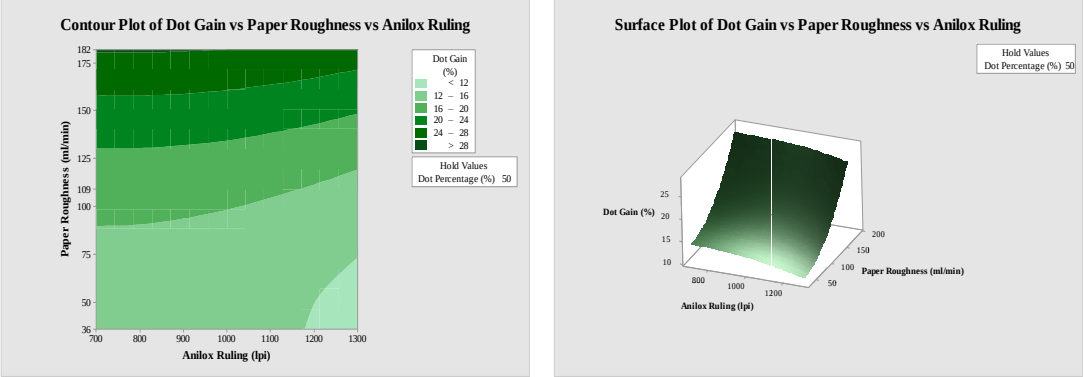

Figure 4.7: Contour plot (left) and Surface plot (right) shows dot gain against paper roughness and anilox roller screen rulings

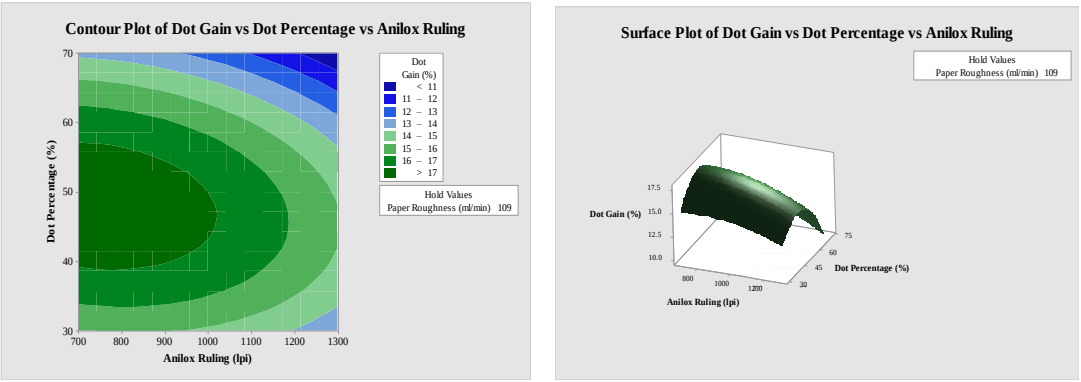

Figure 4.8: Contour plot (left) and Surface plot (right) shows dot gain against dot percentage and anilox roller screen rulings

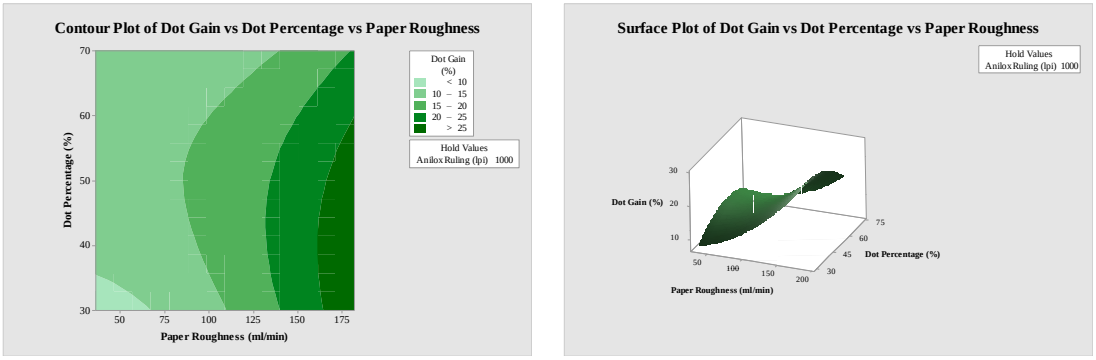

Figure 4.9: Contour plot (left) and Surface plot (right) shows dot gain against dot percentage and paper roughness

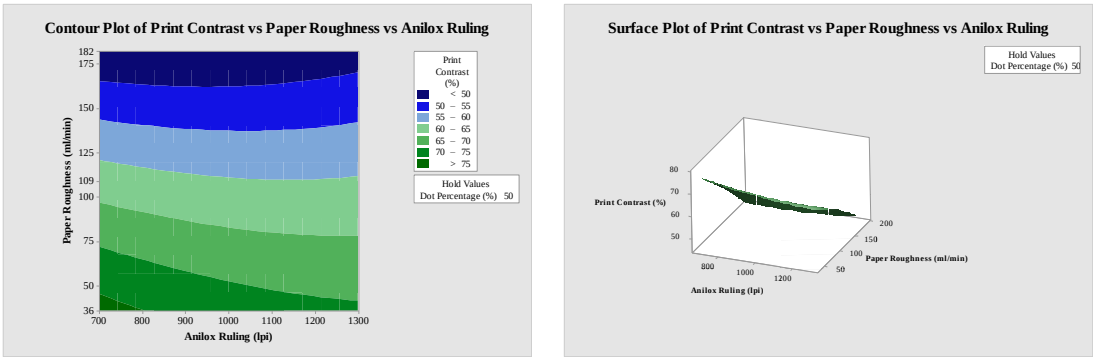

Figure 4.10: Contour plot (left) and Surface plot (right) shows print contrast against paper roughness and anilox roller screen rulings

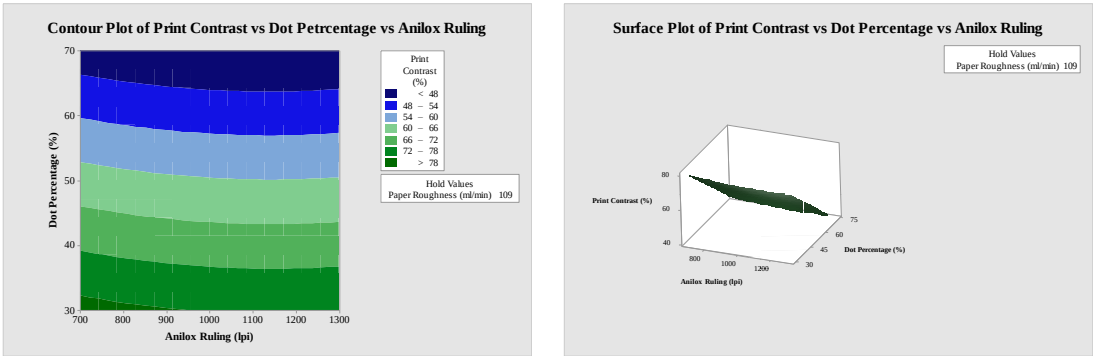

Figure 4.11: Contour plot (left) and Surface plot (right) shows print contrast against dot percentage and anilox roller screen rulings

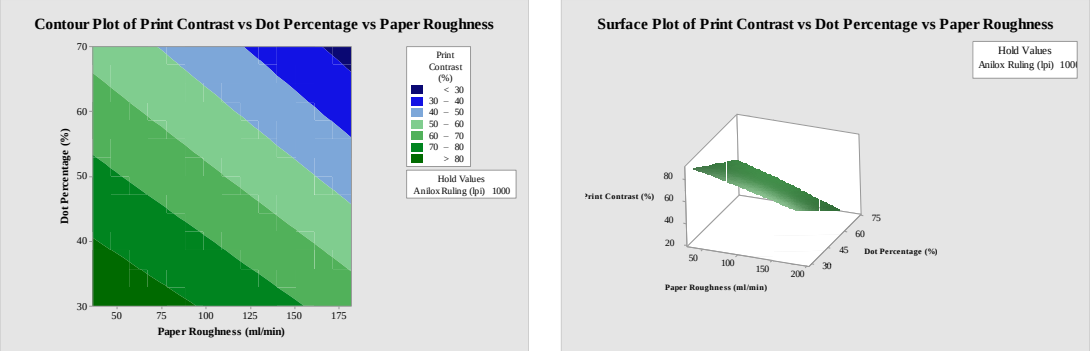

Figure 4.12: Contour plot (left) and Surface plot (right) shows print contrast against dot percentage and paper roughness

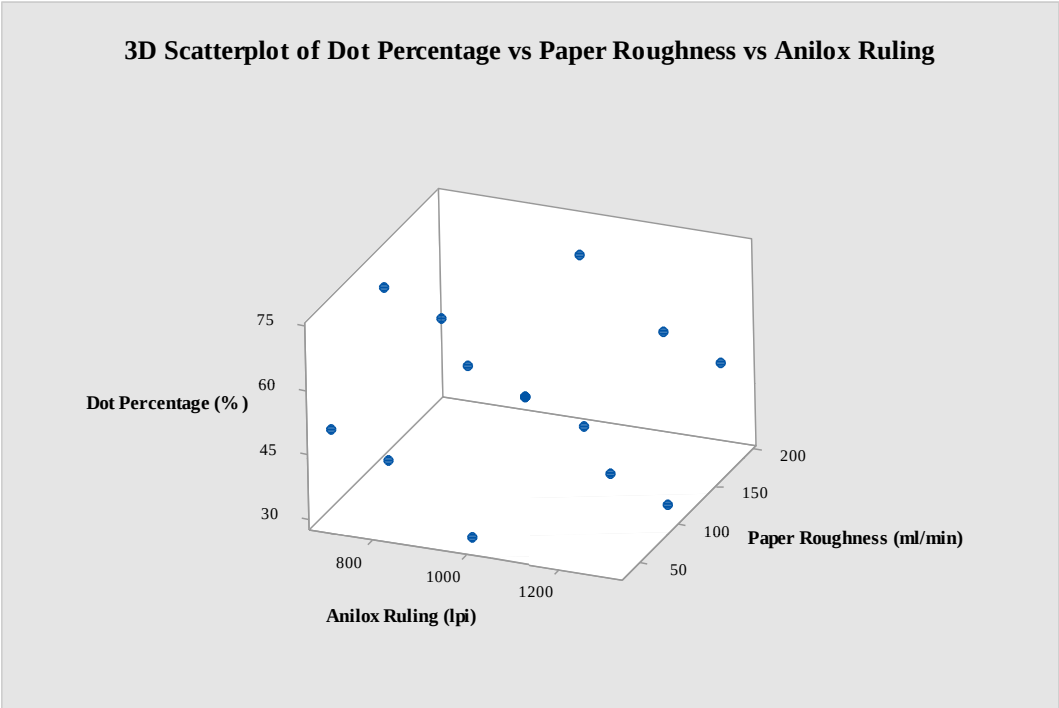

Figure 4.13: 3D scatterplot illustrates correlation between dot percentage, paper roughness and anilox roller screen rulings

4.2.3.2 Regression Analysis

The Tables 4.4-4.7 represent the ANOVA results of this experimental study that shows the response surface regression of dot gain and print contrast against various process parameters such as anilox roller screen rulings, paper roughness and halftone dot percentages.

Table 4.4: ANOVA result for dot gain

Source	**DF**	**Adj SS**	**Adj MS**	**F-Value**	**P-Value**
Regression	9	595.619	66.180	20.60	0.002
Linear	3	456.492	152.164	47.35	0.000
A	1	15.120	15.120	4.71	0.082
B	1	431.427	431.427	134.26	0.000
C	1	9.945	9.945	3.09	0.139
Square	3	96.149	32.050	9.97	0.015
A*A	1	2.067	2.067	0.64	0.459
B*B	1	47.682	47.682	14.84	0.012
C*C	1	39.045	39.045	12.15	0.018
2-Way Interaction	3	42.979	14.326	4.46	0.071
A*B	1	0.251	0.251	0.08	0.791
A*C	1	1.000	1.000	0.31	0.601
B*C	1	41.728	41.728	12.99	0.015
Residual Error	5	16.066	3.213		
Lack-of-Fit	3	16.066	5.355		
Pure Error	2	0.000	0.000		
Total	14	611.686			

Model Summary:

S 1.79256

R-sq 97.37%

R-sq(adj) 92.65%

R-sq(pred) 57.97%

Table 4.5: Coded co-efficients for dot gain

Term	Effect	Coef	SE Coef	T-Value	VIF
Constant		17.00	1.03	16.43	
A	-2.750	-1.375	0.634	-2.17	1.00
B	14.687	7.344	0.634	11.59	1.00
C	-2.230	-1.115	0.634	-1.76	1.00
A*A	-1.496	-0.748	0.933	-0.80	1.01
B*B	7.187	3.594	0.933	3.85	1.01
C*C	-6.504	-3.252	0.933	-3.49	1.01
A*B	0.501	0.250	0.896	0.28	1.00
A*C	-1.000	-0.500	0.896	-0.56	1.00
B*C	-6.460	-3.230	0.896	-3.60	1.00

Regression Equation for Dot Gain,

Dot Gain (%) = -22.2 + 0.0150 A + 0.0528 B + 1.082 C - 0.000008 A*A
+ 0.000674 B*B - 0.00813 C*C + 0.000011 A*B - 0.000083 A*C - 0.002212 B*C (4.1)

Table 4.6: ANOVA result for print contrast

Source	**DF**	**Adj SS**	**Adj MS**	**F-Value**	**P-Value**
Regression	9	3964.94	440.55	236.82	0.000
Linear	3	3924.83	1308.28	703.28	0.000
A	1	8.81	8.81	4.74	0.081
B	1	1436.81	1436.81	772.38	0.000
C	1	2479.21	2479.21	1332.73	0.000
Square	3	10.22	3.41	1.83	0.259
A*A	1	4.50	4.50	2.42	0.181
B*B	1	4.85	4.85	2.60	0.167
C*C	1	0.10	0.10	0.05	0.826
2-Way Interaction	3	29.89	9.96	5.36	0.051
A*B	1	15.09	15.09	8.11	0.036
A*C	1	0.00	0.00	0.00	0.961
B*C	1	14.80	14.80	7.95	0.037
Residual Error	5	9.30	1.86		
Lack-of-Fit	3	9.30	3.10		
Pure Error	2	0.00	0.00		
Total	14	3974.24			

Model Summary:

S 1.36391

R-sq 99.77%

R-sq(adj) 99.34%

R-sq(pred) 96.26%

Table 4.7: Coded co-efficients for print contrast

Term	**Effect**	**Coef**	**SE Coef**	**T-Value**	**VIF**
Constant		60.341	0.787	76.63	
A	-2.099	-1.050	0.482	-2.18	1.00
B	-26.803	-13.402	0.482	-27.79	1.00
C	-35.208	-17.604	0.482	-36.51	1.00
A*A	2.207	1.103	0.710	1.55	1.01
B*B	-2.291	-1.146	0.710	-1.61	1.01
C*C	-0.328	-0.164	0.710	-0.23	1.01
A*B	3.884	1.942	0.682	2.85	1.00
A*C	0.070	0.035	0.682	0.05	1.00
B*C	-3.847	-1.923	0.682	-2.82	1.00

Regression Equation for Print Contrast,

Print Contrast (%) = 139.3 - 0.0380 A - 0.1595 B - 0.701 C + 0.000012 A*A -
0.000215 B*B - 0.00041 C*C + 0.000089 A*B + 0.000006 A*C - 0.001317 B*C (4.2)

Based on Box Behnken response surface model, the regression equation for the dot gain and print contrast are generated as equation 4.1 and 4.2 respectively and represented vides Figures 4.14 & 4.15 respectively.

4.2.3.3 Optimization for Responses

As per the Box Behnken Design of response surface methodology, the optimum values found for the responses such as dot gain and print contrast are given at Table 4.8 and in Figures 4.14-4.15.

Table 4.8: Summary of optimization result

Response	**Target**	**Optimal Solution of Process Parameters**	**Optimal Fit of Response**
Dot Gain (%)	To Minimize	Factor A: Anilox Roller Screen Rulings = 1300 lpi Factor B: Paper Roughness = 36 ml/min Factor C: Dot Percentage = 30%	6.01 % under 95% CI
Print Contrast (%)	40%	Factor A: Anilox Roller Screen Rulings = 740.18 lpi Factor B: Paper Roughness = 127.07 ml/min Factor C: Dot Percentage = 70 %	40 % under 95% CI
	60%	Factor A: Anilox Roller Screen Rulings = 700 lpi Factor B: Paper Roughness = 174.31 ml/min Factor C: Dot Percentage = 37.38 %	60 % under 95% CI

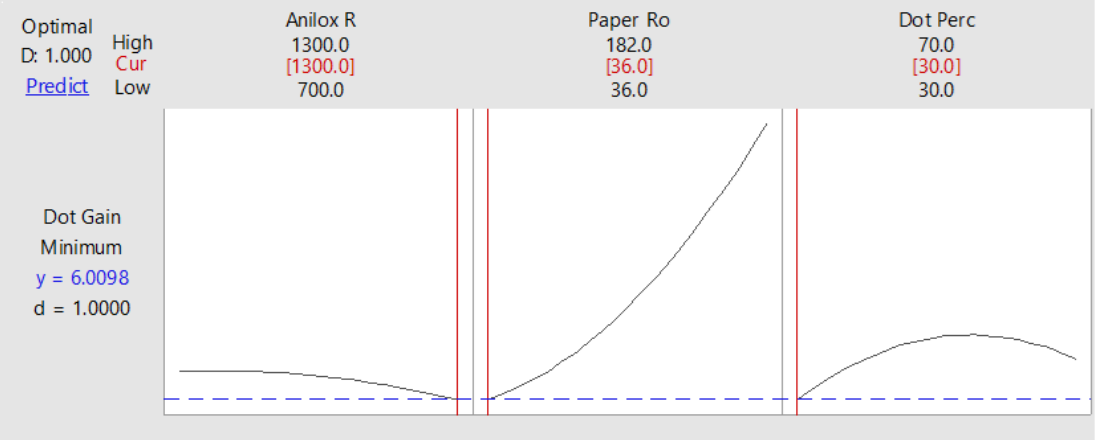

Figure 4.14: Optimization result for dot gain

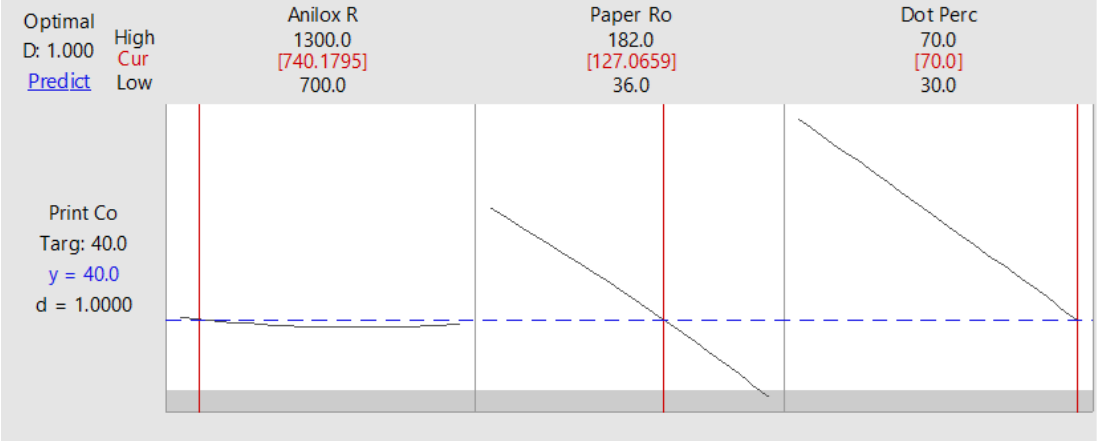

Figure 4.15: Optimization result for 40% print contrast as target

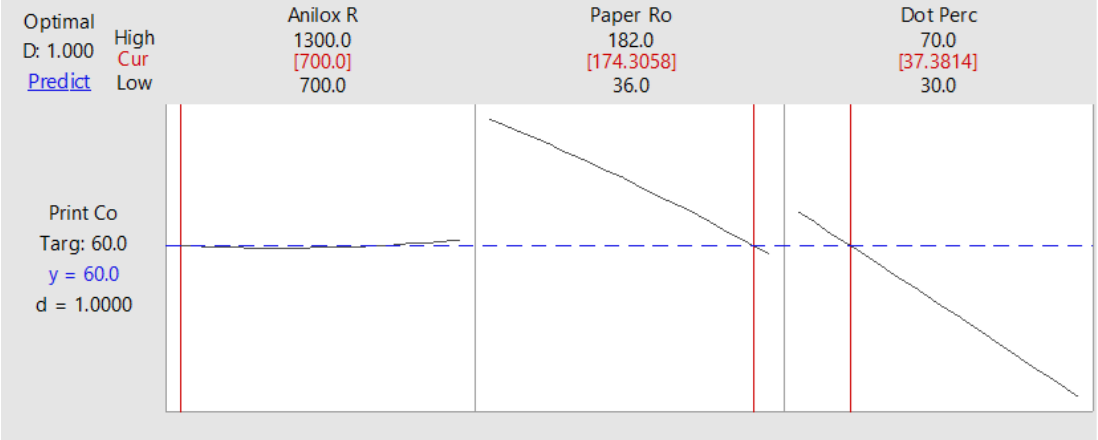

Figure 4.16: Optimization result for 60% print contrast as target

4.2.4 Discussions

The Figures 4.1-4.2 shows the residual plots for dot gain and print contrast respectively. Each plot represents the appropriateness of linear model with the experimental data by evaluating the discrepancy between projected value by the regression model and actual

observed value. In normal probability plot, the departure of data points from the straight line indicates the shift of response from normal distribution. In versus fits plot, the deviation of data points from the dash line represents the shift of observed value of response against the estimated regression line or the line of best fit. The data point on dash line indicates zero residuals. The non linearity, unequal errors, outliers can be visualized from the plotted data points. The histogram shows the normal distribution of residuals. Versus order plot shows the correlation of errors in the sequence and it is related with the appropriateness of data collection in the experimental process. Data point on regression line means there is no serial correlation. Ideally the points should fall randomly on both sides of regression line rather than recognizable pattern.

The Figure 4.3 shows the relative strength of each factor against mean value of dot gain. The contribution of each factor to the dot gain is given separately. Steeper the line more will be the main effect. The paper roughness levels contribute dot gain comparatively than other factors.

In the Figure 4.4, the paper roughness and dot percentage shows more effects towards print contrast than anilox roller screen rulings.

The Figure 4.5 shows the interaction between factors that contribute to dot gain. At all levels of anilox roller screen rulings, the paper with rough surface texture contributes higher dot gain especially at 50% tonal areas. The effect of paper roughness is more throughout the process. The coated paper at 30% tonal area contributes less dot gain but at uncoated grade paper it is high. At 50% tonal region the dot gain is high for all grades of paper but more for uncoated grade paper.

In the Figure 4.6, at all levels of anilox roller screen rulings, the print contrast is high for smoother grade paper.

The Figure 4.7 shows how the dot gain varies with change in anilox roller screen rulings and paper roughness while keeping the dot percentage as hold value. Based on the regression equation, the dot gain is minimum around 1300 lpi anilox roller screen rulings and paper roughness of 36 ml/min. The dot gain is maximum at lower anilox roller screen rulings with paper roughness around 182 ml/min. This implies the fact that at lower anilox roller screen rulings the quantity of ink supply will be more than that with the anilox roller of higher screen rulings. At the same time, the surface irregularity

of the substrate also influences dot gain at a considerable extent. Higher the paper roughness more will be the ink penetration into the paper than that of the desirable level. This will increase the dot size at print than the required size. Also, the paper surface roughness promotes uneven ink distribution over the paper at printing.

The Figure 4.8 shows the attainment of dot gain based on the changing levels of anilox roller screen rulings with different dot percentages while holding out the paper roughness value. The contour plot and surface plot that visualizes the chance of higher dot gain at middle-tone areas of square shaped halftone dots with lower anilox roller screen rulings.

The Figure 4.9 shows the variation of dot gain against various dot percentages and paper roughness with anilox roller screen rulings as hold value. The chance of dot gain is there at both highlight and middle-tone areas when printing on paper having high roughness values. For smoother or coated paper, the dot gain is minimum around 30% tonal regions.

The Figures 4.10-4.12 show the attainment of print contrast against any of the two factors at a time while keeping the third factor levels as hold values. The print contrast from 40-60% represents an ideal range of print contrast. This indicates the print reproduction with expanded tonal range and well reproduced image details at the shadow areas. From the graphical data it is found that the paper roughness shows a greater influence in controlling print contrast. Higher the paper roughness greater will be the dot gain and thus the image details will be lost at shadow areas. This implies to a low print contrast. The high anilox roller screen rulings enhance precision in ink metering and thus promote more controlled inking over shadow areas. Also, in order to analyze the print contrast, analysis of data points at shadow areas say 70-100% tonal region will be accountable.

The 3D scatterplot given in Figure 4.13 shows the visual information on the correlation between the process parameters such as dot percentage, paper roughness and anilox roller screen rulings involved in the experiment. This plot helps to visualize the direction, strength and linearity of relationship among variables.

The ANOVA result for the dot gain shown in Table 4.4 gives Sum of Square, R-sq as 97.37%. This implies that the regression model explains 97.37% of all variability in the

dataset. It is the measure of the power of the model that suggests the fact that the dot gain variable is capable of well explaining the variance in the dependent variable. The model does fit the data well and the model is more predictive. For factors B, B*B, C*C and B*C there is significant linear relationship with dot gain is found from the Table 4.4.

Similarly, Table 4.6 shows the ANOVA result for the print contrast. The Sum of Square, R-sq is 99.77% that suggests the independent variable is capable of well explaining the variance in the dependent variable. The model does fit the data well and is more predictive. For the factors such as B, C, A*B and B*C there is significant linear relationship with print contrast.

The Tables 4.5-4.7 show the coded co-efficients of regression equations for both dot gain and print contrast respectively. The regression co-efficient, Coef expresses the strength and direction of the association between predictor and the response variable in the regression equation, which are actually the numbers that multiply the term values in model equation. The standard error of the co-efficient, SE Coef calculates the variation in co-efficient estimations. The estimate is more accurate when smaller the standard error.

The Variance Inflation Factor (VIF) shown in Tables 4.5-4.7 is always found below 1.5 that indicates the less occurrence of multi-collinearity in the regression models.

4.2.5 Conclusions

A mathematical model with three factors based on Box Behnken Design, was utilized to optimize the process parameters for flexography printing's evaluation of print contrast and dot gain. The BBD model permits an easy way to generate a higher order response surface using fewer experimental runs. A total of fifteen experimental runs were carried out and both the dot gain and print contrast responses were recorded. The BBD is executed with Minitab 17 statistical software and the graphical analysis and regression analysis are done. The graphical analysis shows the influence of different factors over dot gain and print contrast. The result is analyzed in detail with main effect plot, interaction plot, contour plots, surface plots etc. In the regression analysis part, main, squared, and interaction components are created. To identify which of the components are more important, a 95% confidence level was used.

The influence of paper roughness and anilox roller screen rulings influence the dot gain of flexography print as shown in Figures 4.7-4.9. The dot area percentage with square dots at middle-tone areas are found more sensitive to dot gain. This effect will be more with the choice of low anilox roller screen rulings together with rough textured substrate in the printing process as controlled transfer of a liquid ink is essential to the flexography printing process as shown in Figure 4.9. The optimum level of process parameters in this experimental process are identified as anilox roller with higher line rulings and substrate with smooth surface finish are better for halftone dot reproduction with flexography. It has been found from Figures 4.10-4.12, print contrast is affected by the choice of anilox roller screen rulings, paper roughness and percentage dot area. It has been found that print contrast varies from 40%-60% which indicates good tonal range and well reproduced image details at shadow areas. The roughness of the paper also influences the print contrast. Higher the paper roughness, lower will be the print contrast. The square dot around 50% tonal regions promotes dot gain in an undesirable way, and so the dot shapes other than square dots will be a better choice around 50% tonal regions.

4.3 Screen Printing

4.3.1 Objective of the Study

This study uses an experimental and statistical methodology to find the best process parameters for screen printing quality using FM square shaped halftone dots on three types of paper having varying levels of surface roughness under three screen mesh rulings at three tonal areas of a print such as 30%, 50% and 70% respectively.

4.3.2 Experimental Methods

The experiment was conducted by printing an ideal grey scale image made of FM dots onto three grades of paper substrates having different smooth textures or roughness levels. Three different kinds of screen mesh rulings such as 100 lpi, 120 lpi and 140 lpi (lines per inch) were adopted at each print trial. The printing work was executed in screen printing machine ATOM 1520, APL Machinery Pvt. Ltd with black ink. The printing pressure, room temperature and ink parameters were kept constant throughout the printing process.

4.3.2.1 Measurements and Data Collection

The quantitative evaluation of the dot gain and print contrast are done at the 30%, 50%, and 70% tonal areas of the print which correspond to the highlight, middle-tone, and shadow areas, respectively. A digital microscope (LEICA, S8APO) is used to visually analyse each component of the designated printed sheet samples. A Spectro-densitometer (X-Rite Spectro Eye and TECHKON GmbH Spectro Dens) is then used to quantify the optical properties quantitatively. Using response surface methodologies like the Box Behnken Design, the quality analysis of the gathered data was followed for the optimization of process parameters. Using Minitab 17 software, the output data were analysed.

The Table 4.9 illustrates different process parameters or factors, their values, associated levels and the response variable such as dot gain considering in this analytical procedure.

Table 4.9: Process parameters and their levels

Factors	**Unit**	**Symbol**	**Levels**			**Responses**
			1	**2**	**3**	
Mesh Ruling	Lines per inch (lpi)	A	100	120	140	Dot Gain & Print Contrast
Paper Roughness	Millilitre per minute (ml/min)	B	36	109	182	
Dot Percentage	Percentage (%)	C	30	50	70	

The ANOVA and regression analysis were used to examine the impact of experimental variable parameters, such as substrate smoothness level, dot percentage, and screen mesh ruling on dot gain and print contrast in the screen printing process.

4.3.2.2 Box Behnken Design

The BBD design table is shown in Table 4.10. The values 1 and -1, which stands for high and low levels of factors, are represented in the design. The middle level value or centre point of the factors is represented by the zero. The entire experimental run, according to BBD is 15.

Table 4.10: BBD table

Run	Blk	A	B	C
1.	1	0	0	0
2.	1	-1	0	-1
3.	1	0	-1	1
4.	1	-1	0	1
5.	1	0	1	-1
6.	1	1	0	1
7.	1	1	-1	0
8.	1	0	0	0
9.	1	0	-1	-1
10.	1	0	1	1
11.	1	1	1	0

12.	1	-1	-1	0
13.	1	0	0	0
14.	1	1	0	-1
15.	1	-1	1	0

4.3.3 Results

The experimentation and output response measurements for each trial run are prepared in accordance with the Box Behnken Design (BBD), as indicated in Table 4.11. The data are subjected to a thorough regression analysis and analysis of variance (ANOVA). The Box Behnken Design is used for DoE optimization, and the outcomes are summarized.

Table 4.11: Dot gain and print contrast response at each experimental run

Run Order	**Factor 1: A** **Mesh Ruling (lpi)**	**Factor 2: B** **Paper Roughness (ml/min)**	**Factor 3: C** **Dot Percentage (%)**	**Dot Gain (%)**	**Print Contrast (%)**
1	120	109	50	38.52	62.98
2	100	109	30	59.79	61.42
3	120	36	70	26.62	30.77
4	100	109	70	29.67	12.99
5	120	182	30	31.47	76.19

6	140	109	70	28.54	29.78
7	140	36	50	27.08	66.67
8	120	109	50	38.52	62.98
9	120	36	30	24.91	82.56
10	120	182	70	28.75	11.90
11	140	182	50	30.88	59.04
12	100	36	50	42.89	44.39
13	120	109	50	38.52	62.98
14	140	109	30	29.45	84.35
15	100	182	50	46.77	24.47

4.3.3.1 Graphical Analysis

The Figures 4.17-4.28 show the graphical plots of the BBD results. The residual data of experiments, main effects and interaction effects of factors over responses, contour plots, 3D surface plots, 3D scatter plot of process parameters etc. are all meticulously plotted.

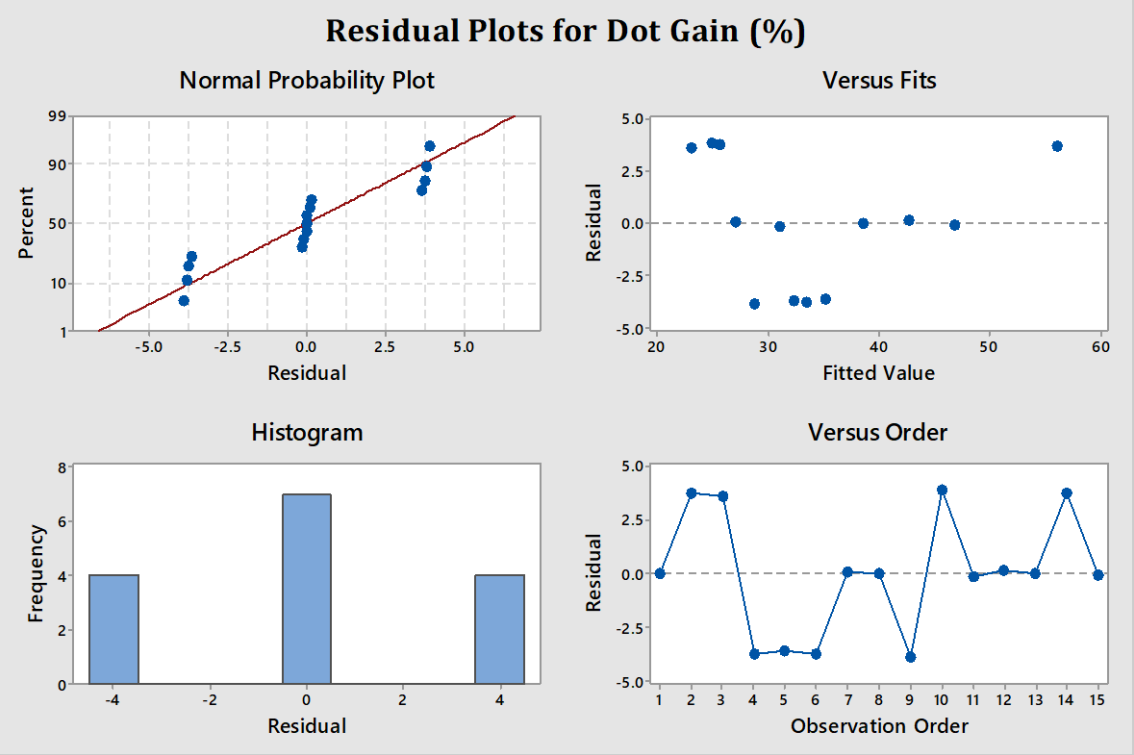

Figure 4.17: Residual plots for dot gain

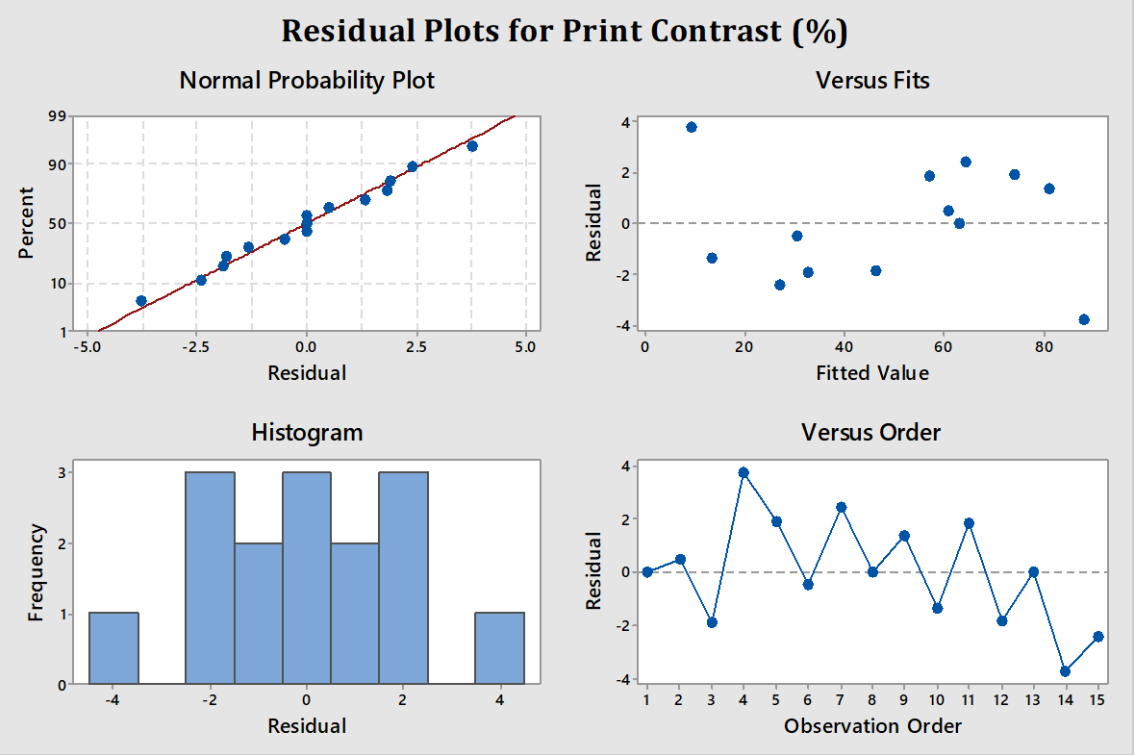

Figure 4.18: Residual plots for print contrast

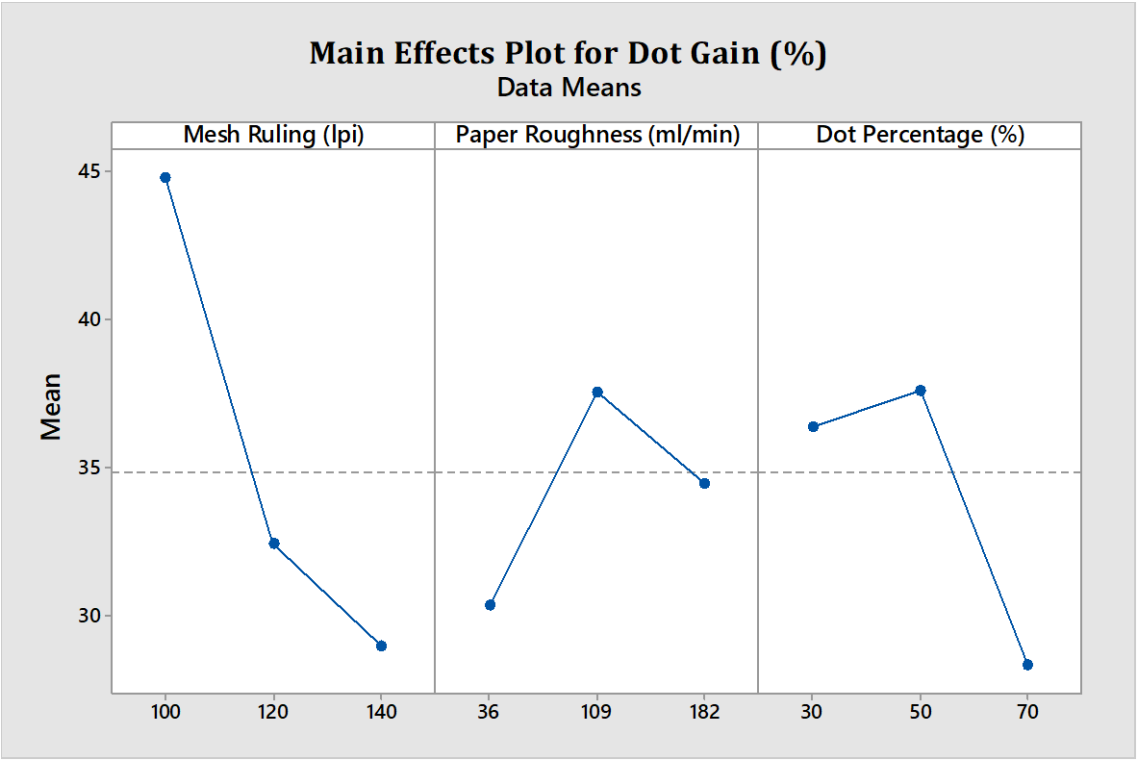

Figure 4.19: Main effects plot for dot gain

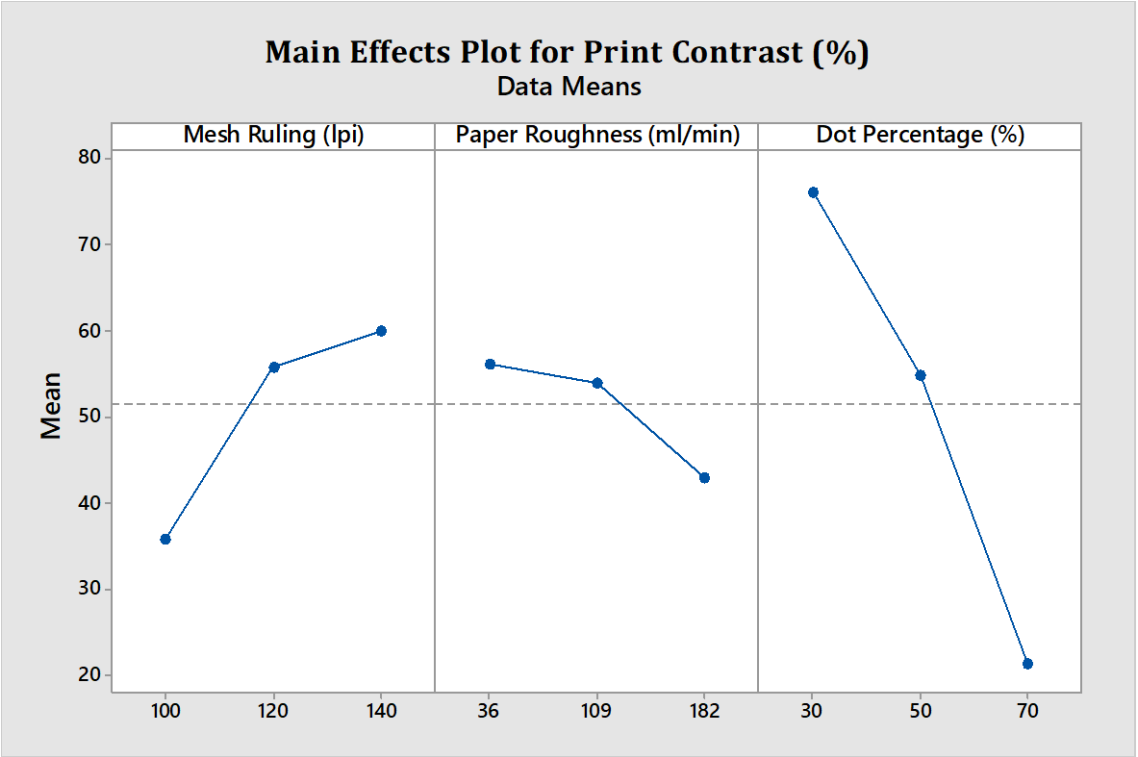

Figure 4.20: Main effects plot for print contrast

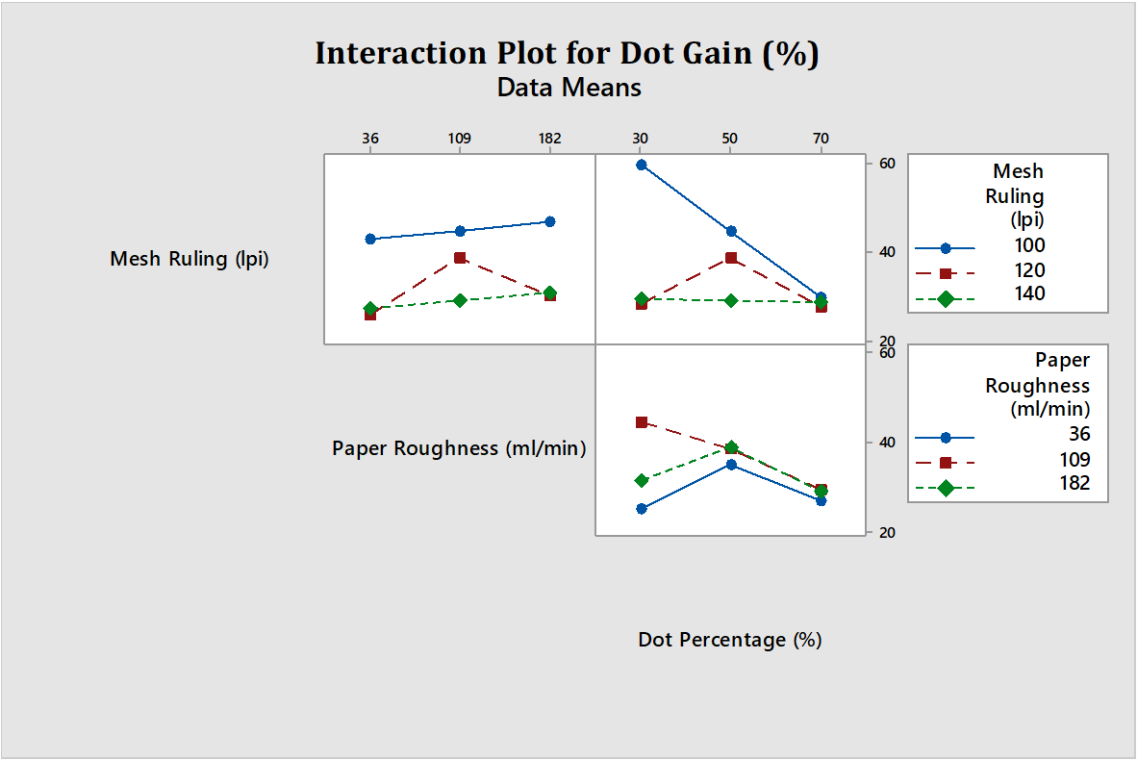

Figure 4.21: Interaction plot for dot gain

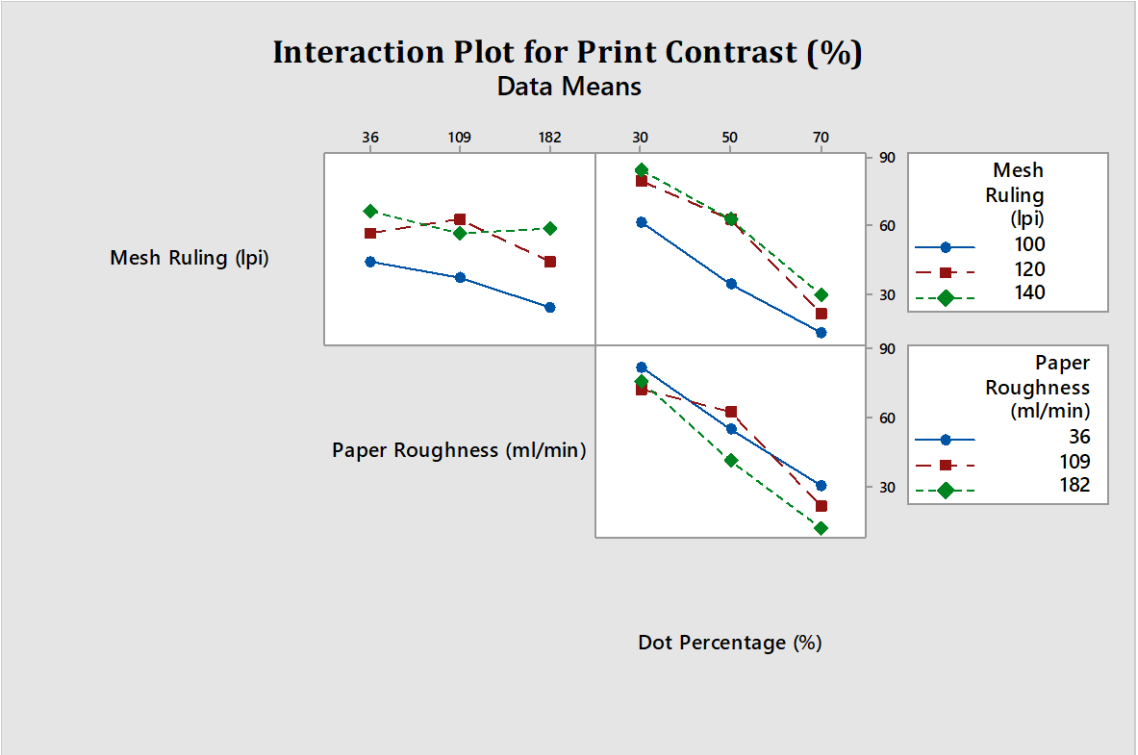

Figure 4.22: Interaction plot for print contrast

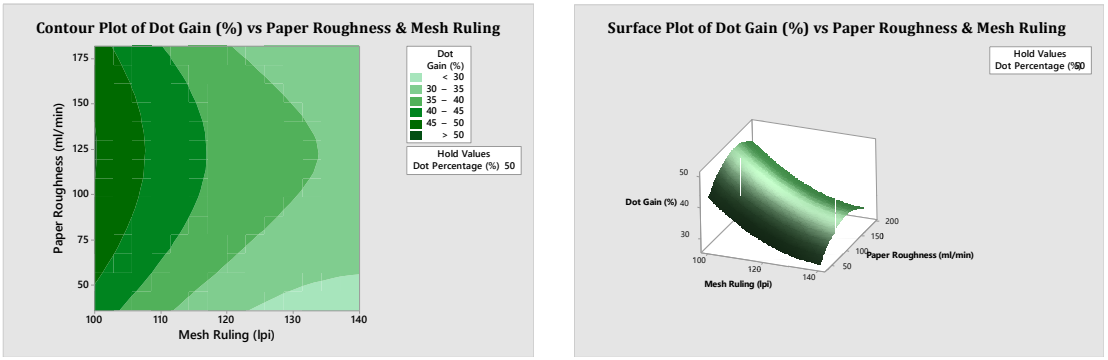

Figure 4.23: Contour plot (left) and Surface plot (right) shows dot gain against paper roughness and mesh ruling

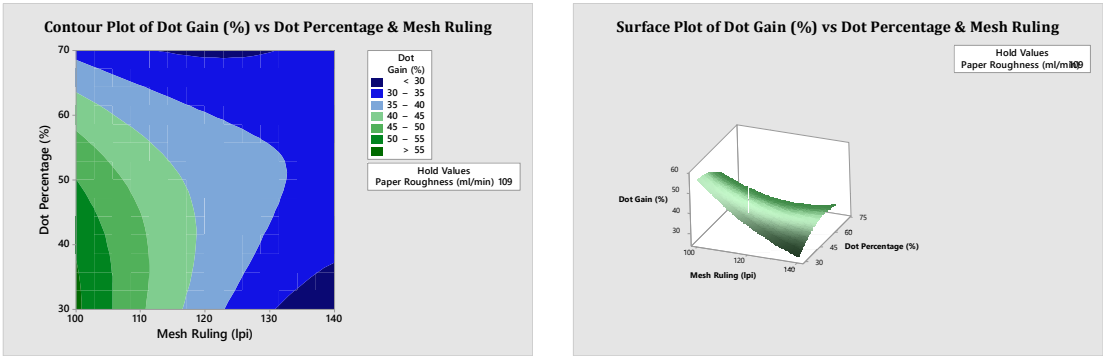

Figure 4.24: Contour plot (left) and Surface plot (right) shows dot gain against dot percentage and mesh ruling

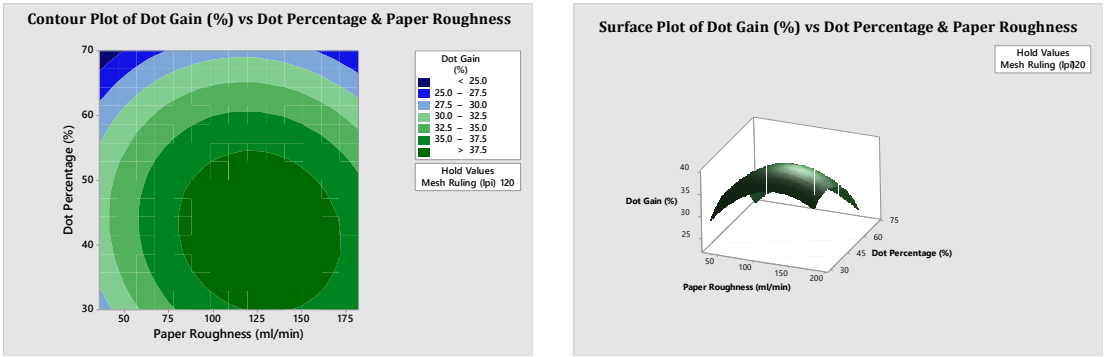

Figure 4.25: Contour plot (left) and Surface plot (right) shows dot gain against dot percentage and paper roughness

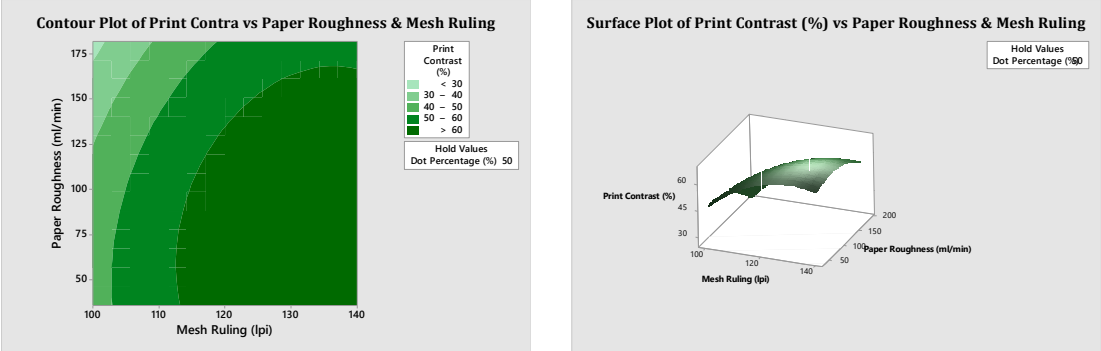

Figure 4.26: Contour plot (left) and Surface plot (right) shows print contrast against paper roughness and mesh ruling

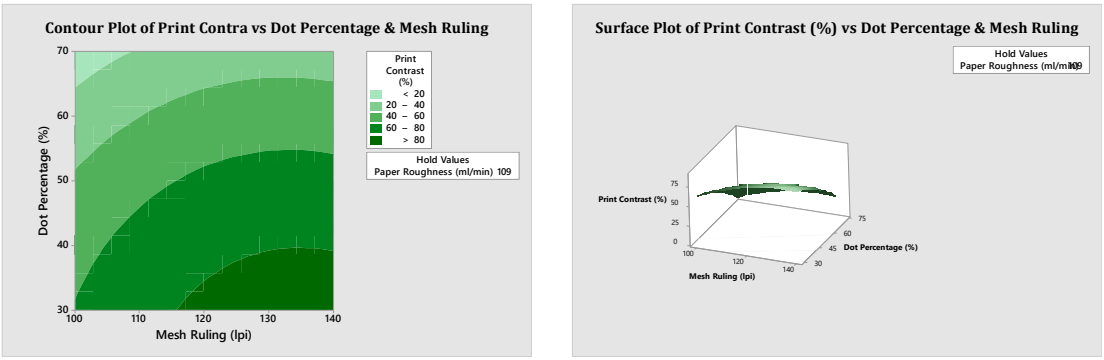

Figure 4.27: Contour plot (left) and Surface plot (right) shows print contrast against dot percentage and mesh ruling

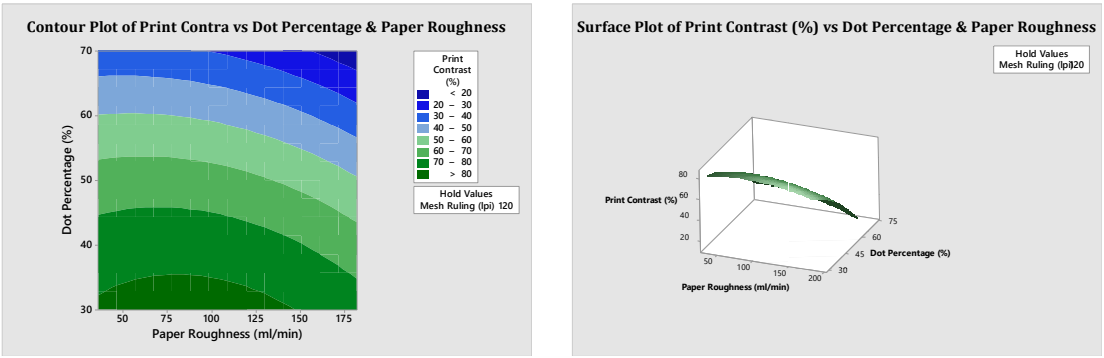

Figure 4.28: Contour plot (left) and Surface plot (right) shows print contrast against dot percentage and paper roughness

4.3.3.2 Regression Analysis

The ANOVA results, which display the response surface regression of dot gain and print contrast against several process parameters including screen mesh ruling, paper roughness, and halftone dot percentages, are displayed in Tables 4.12-4.14.

Table 4.12: ANOVA result for dot gain

Source	**DF**	**Adj SS**	**Adj MS**	**F-Value**	**P-Value**
Regression	9	1143.46	127.051	5.63	0.036
Linear	3	660.70	220.233	9.76	0.016
A	1	498.82	498.822	22.11	0.005
B	1	33.53	33.532	1.49	0.277
C	1	128.34	128.344	5.69	0.063
Square	3	264.65	88.218	3.91	0.088
A*A	1	49.25	49.248	2.18	0.200
B*B	1	102.67	102.669	4.55	0.086
C*C	1	104.21	104.213	4.62	0.084
2-Way Interaction	3	218.11	72.702	3.22	0.120
A*B	1	0.00	0.001	0.00	0.994
A*C	1	213.20	213.196	9.45	0.028
B*C	1	4.91	4.910	0.22	0.660
Residual Error	5	112.78	22.557		
Lack-of-Fit	3	112.78	37.595	*	*

Pure Error	2	0.00	0.000		
Total	14	1256.24			
Model Summary: S 4.74939 R-sq 91.02% R-sq(adj) 74.86% R-sq(pred) 0.00%					

Regression Equation for Dot Gain,

Dot Gain (%) = 285 - 3.50 A + 0.283 B - 0.980 C + 0.00913 A*A - 0.000990 B*B

- 0.01328 C*C - 0.00001 A*B + 0.01825 A*C - 0.00076 B*C (4.3)

Table 4.13: ANOVA result for print contrast

Source	**DF**	**Adj SS**	**Adj MS**	**F-Value**	**P-Value**
Regression	9	8108.73	900.97	76.72	0.000
Linear	3	7513.21	2504.40	213.26	0.000
A	1	1165.42	1165.42	99.24	0.000
B	1	348.26	348.26	29.66	0.003
C	1	5999.53	5999.53	510.88	0.000
Square	3	509.33	169.78	14.46	0.007

A*A	1	284.64	284.64	24.24	0.004
B*B	1	114.01	114.01	9.71	0.026
C*C	1	184.24	184.24	15.69	0.011
2-Way Interaction	3	86.18	28.73	2.45	0.179
A*B	1	37.73	37.73	3.21	0.133
A*C	1	9.45	9.45	0.81	0.411
B*C	1	39.01	39.01	3.32	0.128
Residual Error	5 107107	58.72	11.74		
Lack-of-Fit	3	58.72	19.57	*	*
Pure Error	2	0.00	0.00		
Total	14	8167.45			

Model Summary:

S	3.42687
R-sq	99.28%
R-sq(adj)	97.99%
R-sq(pred)	88.50%

Regression Equation for Print Contrast,

Print Contrast (%) = -311.0 + 5.83 A - 0.009 B + 1.091 C - 0.02195 A*A -
0.001043 B*B - 0.01766 C*C + 0.00210 A*B - 0.00384 A*C - 0.00214 B*C (4.4)

Equation 4.3 and equation 4.4 respectively provide the regression equations for the dot gain and print contrast, derived from the Box Behnken response surface model.

4.3.3.3 Optimization for Responses

The optimum values for the responses such as dot gain and print contrast, were discovered using the Box Behnken Design of response surface methodology. These values are shown in Table 4.14 and vide Figure 4.29. Using Box Behnken response surface model, the regression equation for the dot gain and print contrast are generated as equation 4.3 and 4.4 respectively.

Table 4.14: Summary of multiple response optimization

Response	**Target**	**Optimal Solution of Process Parameters**	**Optimal Fit of Response**
Dot Gain (%)	Minimum	Factor A: Mesh Ruling = 138.79 lpi Factor B: Paper Roughness = 87.62 ml/min Factor C: Dot Percentage = 30%	24.79% under 95% CI
Print Contrast (%)	Maximum		88.03% under 95% CI

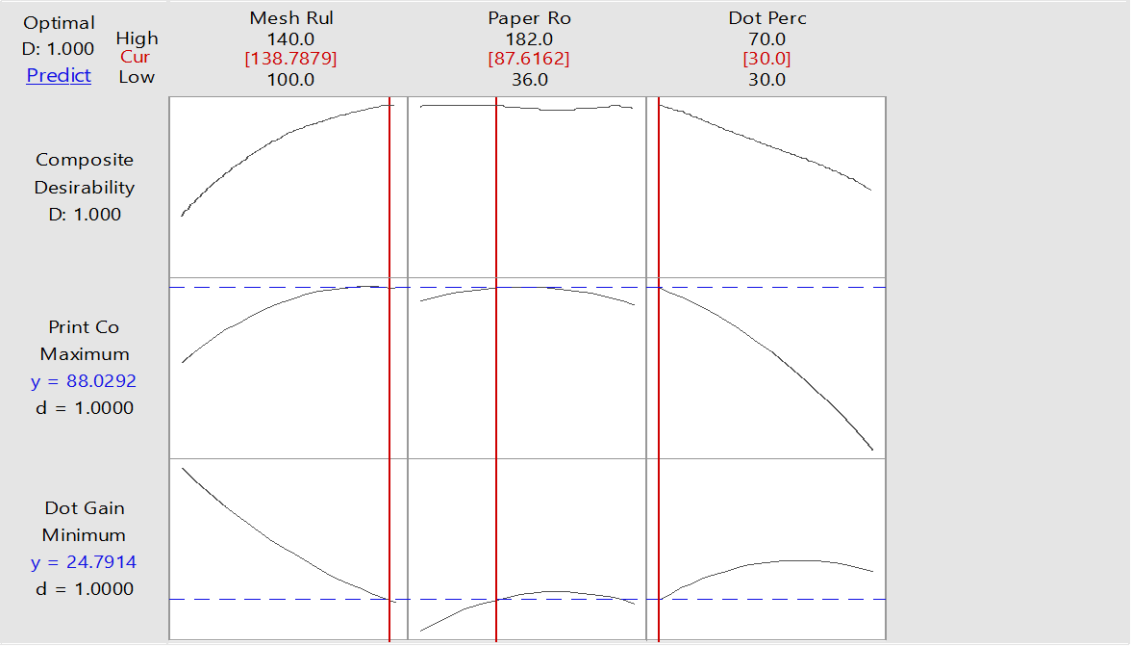

Figure 4.29: Optimization result for multi-response prediction

4.3.4 Discussions

Figures 4.17-4.18 show the residual plots for print contrast and dot gain respectively. Each plot shows how well the liner model matches the experimental data by contrasting the projected value of the regression model with the actual observed value. In a normal probability plot, a shift in the response from the normal distribution is indicated by the divergence of datapoints from the straight line. The datapoints divergence from the dashed line in a versus fits plot indicates the displacement of the observed response value against the estimated regression line or the line of best fit. The datapoints that are displayed make it possible to visualize outliers, unequal errors, and nonlinearity. The histogram shows the normal distribution of the residuals. The association between sequence errors and the appropriateness of data collection during the experimental procedure is depicted in the versus order image. When a data point on the regression line is present, there is no serial correlation. The points should preferably fall arbitrarily on both sides of the regression line rather than following a noticeable pattern.

In Figures 4.19-4.20, the relative intensities of each element are displayed against the mean dot gain value and print contrast respectively. The dot gain seems to be minimum when mesh ruling count as well as paper smoothness level increases. At shadow areas the dot gain for FM is found to be minimum than that of highlight and middle-tones

vide Figure 4.19. The print contrast is maximum when the mesh count and paper smoothness increases. Also, the print contrast is far better at the shadow areas.

The interaction plots shown in Figures 4.21-4.22 that illustrate the achievement of dot gain and print contrast respectively based on the effect of interaction between two factors while holding the third one as hold value.

The Figures 4.23-4.24 represent the contour plot and surface plot that visualizes the inter relationships between factors. The response values are represented by contours in a contour plot, which shows the x- and y-factors or predictors plotted on the x- and y-scales. In a contour plot, the darker areas correspond to greater z-values. The slope in that direction is shown by the distance between the contours, a small distance denotes a sharp slope and a large distance denotes a gentle slope. In surface plot, the height of the surface represents the value of the function.

The Table 4.12 indicates that, based on ANOVA result for dot gain, the mesh ruling count is found as the most significant factor in achieving better print result with screen printing process with FM dots. The mesh ruling and dot percentage as per two way interaction effect shows a significant effect in dot gain. As per Table 4.13, for promoting better print contrast at the screen printing output with FM dots, the three factors are significantly influencing. The ANOVA results show Sum of Square or R-sq as 91.02% & 99.28% respectively for dot gain and print contrast. This implies that the level of fitness of model with the data is well and is found as more predictive.

Table 4.14 and Figure 4.29, presents an overview of the optimal solutions for multi-responses, including dot gain and print contrast. According to the findings, 24.79 % is found as the optimum level of dot gain and 88.03% value for print contrast at 95% confidence interval (CI). The ideal process parameter values for this are determined to be: 138.79 lpi of mesh ruling, 87.62 ml/min of paper roughness and at 30% tonal regions.

4.3.5 Conclusions

In order to improve the process parameters for the evaluation of print contrast and dot gain in screen printing, a mathematical model comprising three elements based on Box Behnken Design was employed. With fewer experimental runs, a higher order response

surface can be easily generated through the BBD model. The dot gain and print contrast responses were recorded throughout a total of fifteen experimental runs. Minitab 17 software was used to carry out the BBD, and regression and graphical analysis were performed. The graphical analysis illustrates how many parameters affect print contrast and dot gain. Using surface, contour, interaction, main effects, and other plots, the outcome was thoroughly examined.

The screen mesh ruling plays a major role in the occurrence of dot gain in screen printing. Higher the screen mesh ruling, higher will be the dot gain especially for FM halftone dots. The mesh opening size must be capable to carry each individual halftone dots of the stencil for the accurate result in printing. Otherwise, the dot loss over the screen mesh will occur and it further causes dot gain and also it will influence the print contrast too. The undesirable tonal shift from highlight to middle-tones and immediately to the shadow areas are also observed with the screen printing result with FM dots. Also, the dot gain and print contrast are found to be influenced by the surface roughness level of the substrates used. The roughness of the surface can accelerate the rate of ink absorption and increase of dot gain. In this experimental method, a substrate with smoother surface finish and a higher screen mesh ruling are the ideal levels of process parameters which can be used with the screen printing process in order to get a good quality print.

Chapter 5

Machine Learning of Prints

5.1 Preliminaries

Machine learning for prediction of dot gains and hue errors of flexography printing were carried out and the results confirmed with statistical method. Machine learning was also performed for screen printing to predict the print quality in terms of dot gain. A distinct set of algorithms is required for each activity and these algorithms are used for detecting habits to accomplish specific operations [51, 55]. Well labelled training data are used to train the machines and the output is predicted on that basis of data [57]. The assessment of print quality is probably going to make use of quantitative studies such as dot gain, dot area, print contrast and others [30]. The level of impurity in printing inks is computed, quantified and regulated by using hue error [16].

Machine Learning was performed by using the similar process steps and equations mentioned in Chapter 1, subsections 1.4 and 1.6.

5.2 Flexography Printing

5.2.1 Flexography Black and White Prints for Dot Gain

5.2.1.1 Objective of the Study

The machine learning is something that comes into contact with our everyday life. This research examines the application of machine learning technique in the estimation and prediction of flexography single color print quality. This aims to implement supervised machine learning techniques such as linear regression, decision tree and random forest regression algorithms in the most efficient way possible using with python tool. The experimental background comprises the flexography printing on 114 tonal gradations on both coated and uncoated paper under three different anilox roller ruling.

5.2.1.2 Experimental Methods

The flexography printing were carried out with three input variables such as paper substrates with two different roughness levels, anilox rollers with three different line rulings and square shaped AM halftone dots with 114 dot area levels. The anilox roller rulings were selected as 700 lpi (275.6 lines/cm), 1000 lpi (393.7 lines/cm) and 1300 lpi (lines per inch) (511.8 lines/cm). The paper roughnesses were chosen as 36 ml/min and 182 ml/min. The engraved anilox cells had the features of 60º hexagonal in geometry, volume of cells (BCM 4.1 (700 lpi), BCM 3.9 (1000 lpi), BCM 3.8 (1300 lpi)), distortion factor (1.3%) with same mounting tape. The flexography printing machine such as OMET LAB230 Iflex (printing speed – 35 m/min, nip pressure – 3 mm) with black colour uv ink were employed for the printing. The photopolymer plate (manufacturer – Dupont) with thickness of 1.14 mm magnetic backing was used as the printing image carrier. The parameters such as nip pressure, printing speed, room temperature and ink features were kept constant throughout the printing process.

5.2.1.2.1 Measurements and Data Collection

The output response was taken as dot gain for the assessment of print quality. So, the quantitative measurement of output parameters was done with Spectro densitometer such as X-Rite Spectro Eye instrument. The visual inspection of printed area was observed with a Digital microscope such as LEICA S8APO. The input datasets for the machine learning algorithms were created from the readings up to 114 different prints. The split ratio of training to test dataset was taken as 7:3. The collected data were given as input to the python program to process with machine learning algorithms.

The Table 5.1 shows different process parameters or factors, their values, corresponding levels and the response variable such as dot gain etc. that are considering in the analysis process.

Table 5.1: Parameters background at flexography printing

Factors	Unit	Symbol	Levels	Response
Anilox Ruling	Lines per inch (lpi)	A	700, 1000, 1300	Dot Gain

Paper Roughness	Millilitre per minute (ml/min)	B	36, 182	
Dot Percentage	Percentage (%)	C	5% to 100 % with 5% increments.	
Halftone Dot Shape	-	D	Square Shape	

5.2.1.2.2 Programming to Train the Model

The programming code to perform the machine learning algorithms such as linear regression, decision tree and random forest regression are done with python programming language. The influence of input parameters over the output response are evaluated with machine learning techniques and the accuracy are compared with each technique.

5.2.1.3 Dataset

Some samples of black dataset have been given in Table 5.2.

Table 5.2: Black dataset

Paper_Roughness	**Anilox_Roll_Ruling**	**Dot_Percentage**	**Dot_Gain**
36	700	5	10
36	1000	5	7
36	1300	5	6
182	700	5	10
182	1000	5	9
182	1300	5	8

36	700	10	11
36	1000	10	8
36	1300	10	5
182	700	10	11
182	1000	10	10
182	1300	10	9

5.2.1.4 Results

The result obtained at the machine learning algorithms at python programming execution are given at Tables 5.3-5.4. The summary of dataset as Table 5.3 and the loss functions of various algorithms as Table 5.4 are given. Loss functions are generally used to assess the performance of various machine learning techniques.

Table 5.3: Summary of dataset

	Paper Roughness	**Anilox Roller Ruling**	**Dot Percentage**	**Dot Gain**
count	114.000000	114.000000	114.000000	114.000000
mean	109.000000	1000.000000	50.000000	10.245614
std	73.322297	246.030432	27.507039	4.103876
min	36.000000	700.000000	5.000000	2.000000
30%	36.000000	700.000000	25.000000	8.000000

50%	109.000000	1000.000000	50.000000	10.000000
70%	182.000000	1300.000000	75.000000	13.000000
max	182.000000	1300.000000	95.000000	19.000000
Shape of data	(114, 4)			
Shape of split data	The shape of X_train: (85, 3)			
	The shape of X_test: (29, 3)			
	The shape of Y_train: (85, 3)			
	The shape of Y_test: (29, 3)			

Table 5.4: Loss functions of various techniques

Machine Learning Algorithm	**MSE**	**RMSE**	**MAE**	**R^2**
Linear Regression (LR)	9.5271	3.0836	2.5686	0.13
Decision Tree Regression (DT)	1.5969	1.2637	0.9472	0.8538
Random Forest Regression (RF)	0.5952	0.7715	0.5960	0.9455

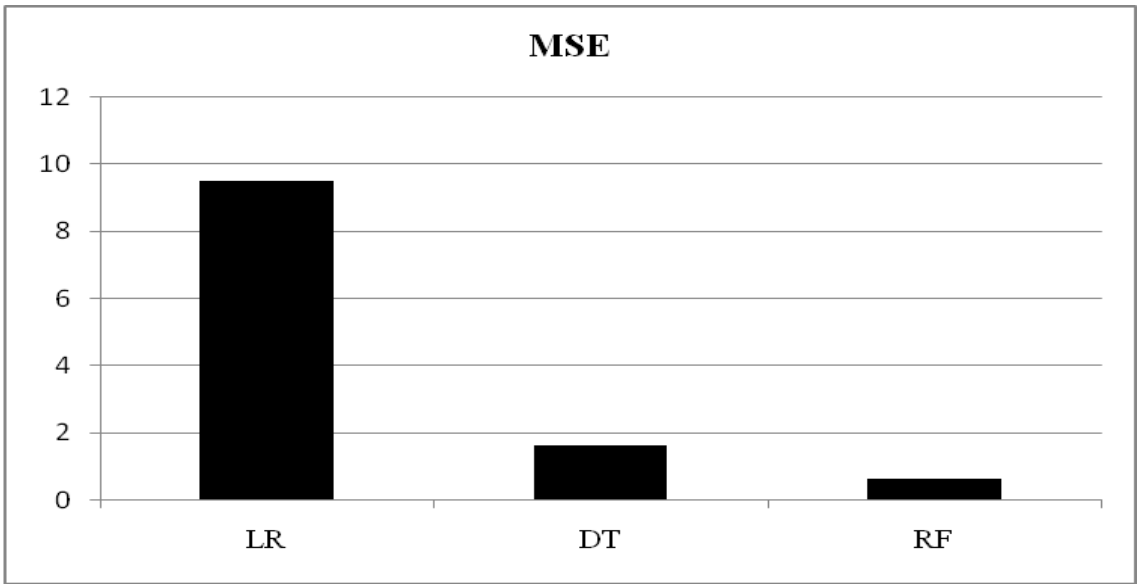

Figure 5.1: Bar chart of MSE values for different machine learning algorithms

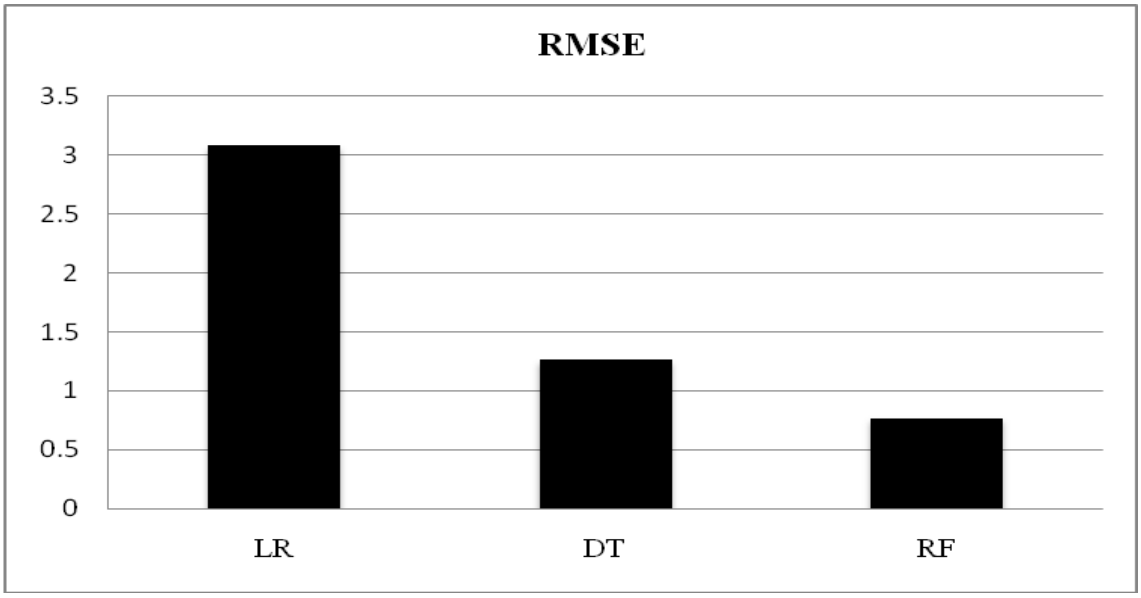

Figure 5.2: Bar chart of RMSE values for different machine learning algorithms

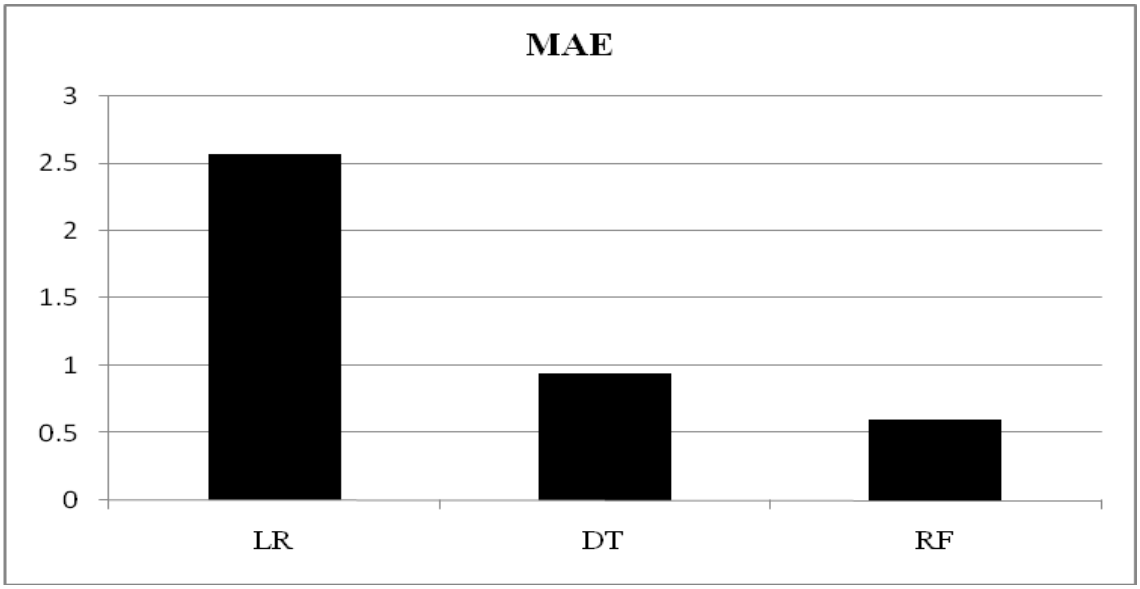

Figure 5.3: Bar chart of MAE values for different machine learning algorithms

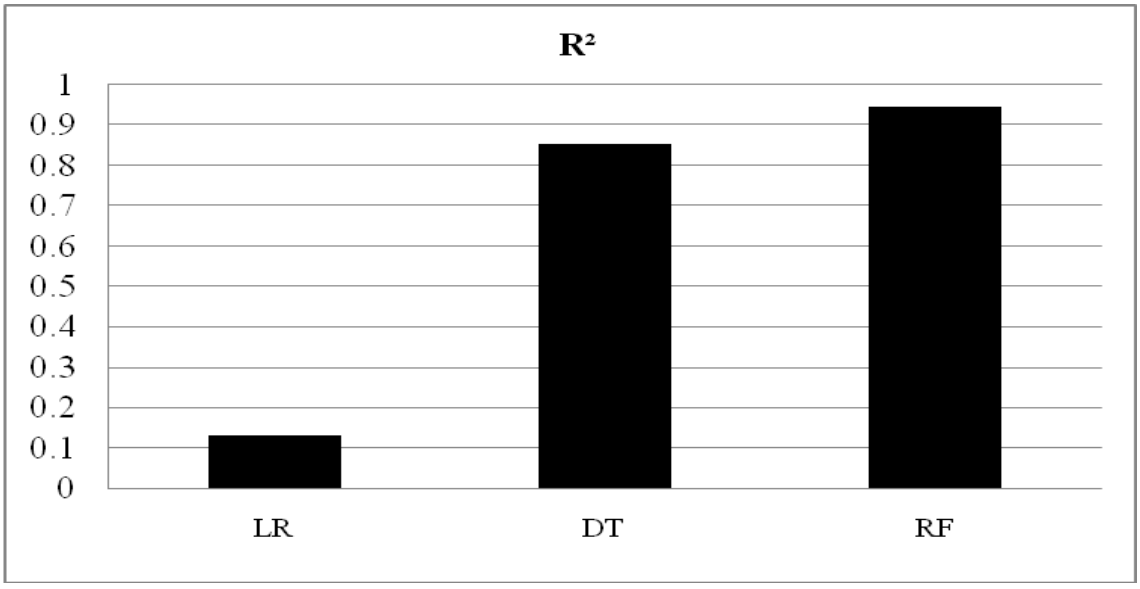

Figure 5.4: Bar chart of R^2 score for different machine learning algorithms

Figure 5.1 shows the Mean Squared Error (MSE) for three different machine learning algorithms used for prediction of dot gain in black and white flexography printing. It measures the average squared difference between the actual values and predicted values. Lower value of MSE indicates the accuracy of the model. It has been found that MSE is the lowest for the random forest regression (RF) compared to linear regression (LR) and decision tree regression (DT). This means that random forest regression (RF) is the best method for the prediction of dot gain in the present work.

Figure 5.2 represents the Root Mean Squared Error (RMSE) for the different machine learning algorithms adopted for prediction of dot gain. RMSE signifies the average square root of the mean of the squared difference between predicted and actual values. It has been observed that RMSE is least for random forest regression (RF) which implies that it is best for this prediction.

Figure 5.3 shows the bar chart of Mean Absolute Error (MAE) for the different machine learning algorithms used for prediction of dot gain. MAE implies the average magnitude of the differences between actual values and predicted values. Lower MAE value indicates a more accurate model. It has been found that MAE value is the lowest for random forest regression (RF). This indicates that random forest regression (RF) is the best model for this prediction.

Figure 5.4 represents the R-squared (R^2) values for three different machine learning algorithms adopted for this prediction of dot gain. It signifies the proportion of variance in the target variables that can be explained by the independent variables. A higher R^2 value closer to 1 is the better fit. The more the R^2 value the better is the prediction. It has been observed that R^2 value for the random forest regression (RF) method is maximum and close to 1 which means that this method is the best for the prediction of dot gain in this present work. The loss functions of different machine learning algorithms shown in Table 5.4 were derived by considering the values given in Figures 5.1-5.4.

The loss functions states the capability of the developed model to forecast the result from the given input variables.

5.2.1.4.1 Graphical Analysis

The graphical plots that demonstrate the nature of distribution of datasets, residuals found at the analysis part and the relationship among various parameters associated with the experimental process. The Figures 5.5-5.15 have been plotted using Minitab 17 statistical software.

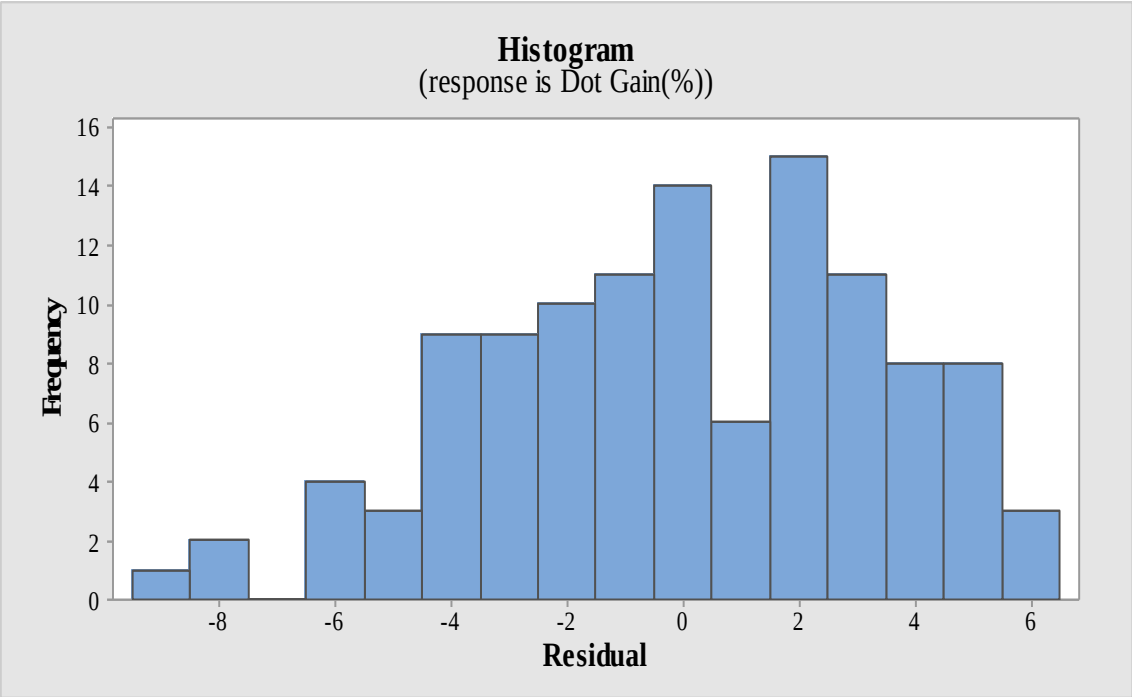

Figure 5.5: Residual plot for dot gain in histogram

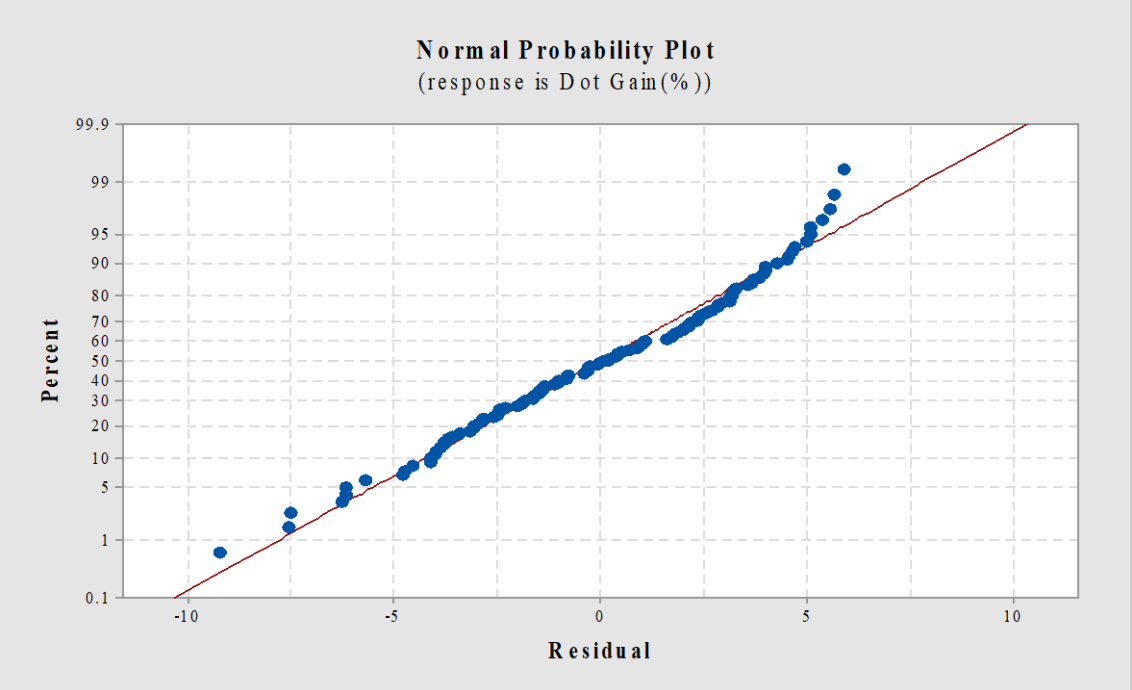

Figure 5.6: Normal probability plot for dot gain

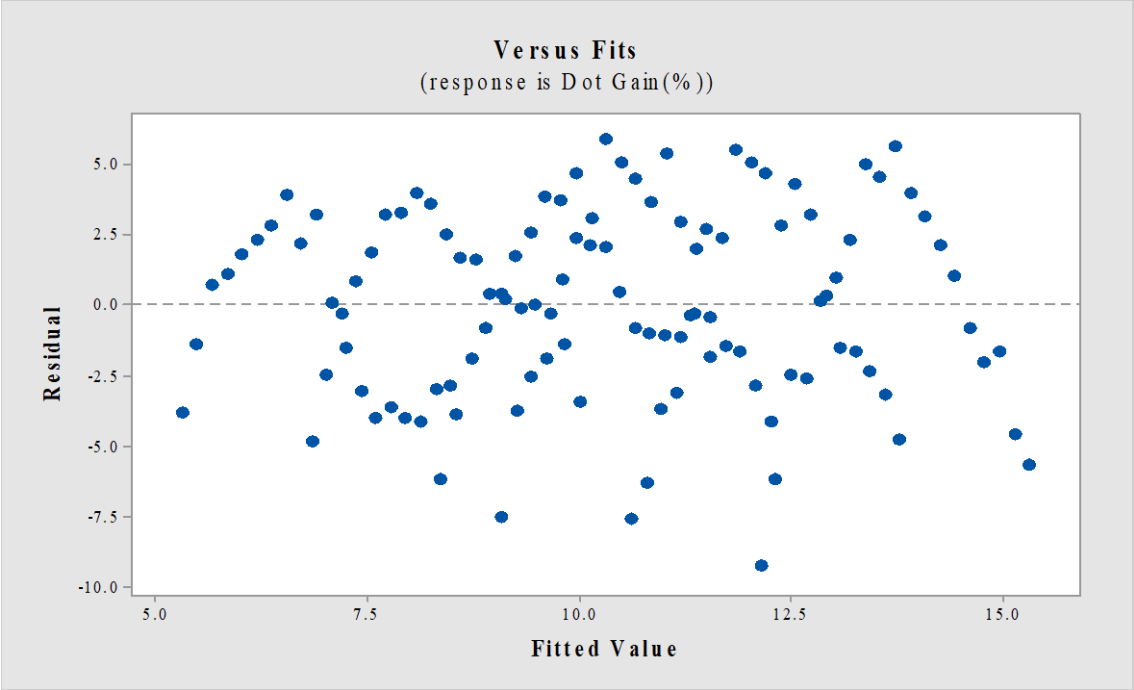

Figure 5.7: Versus fit plot for dot gain

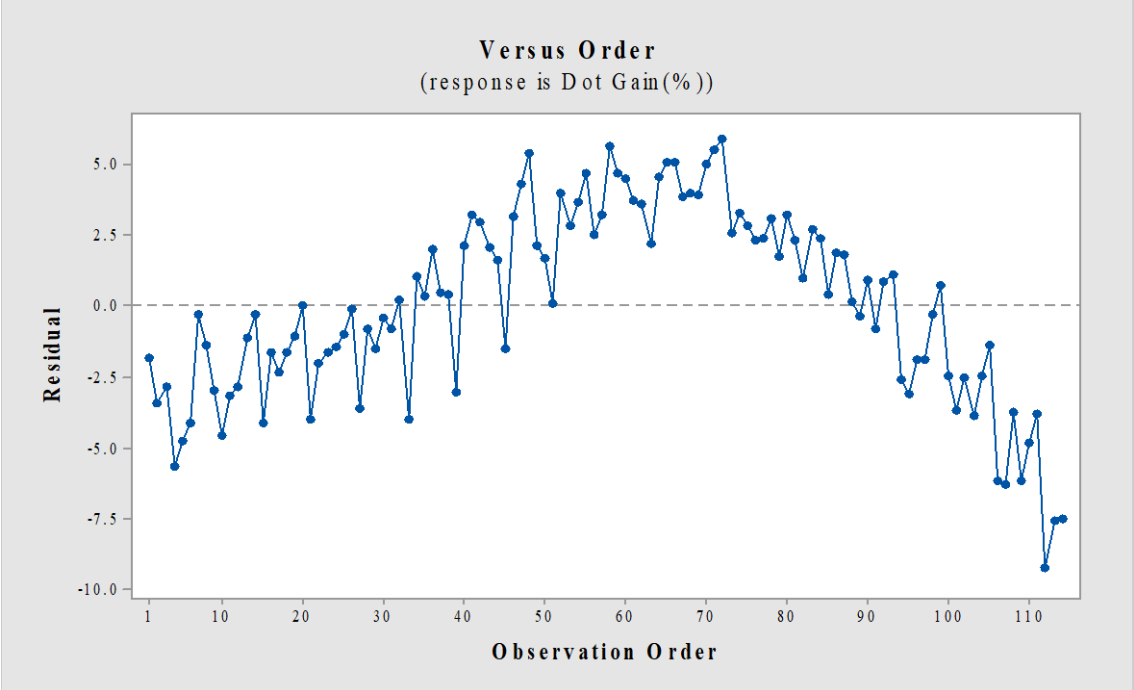

Figure 5.8: Versus order plot for dot gain

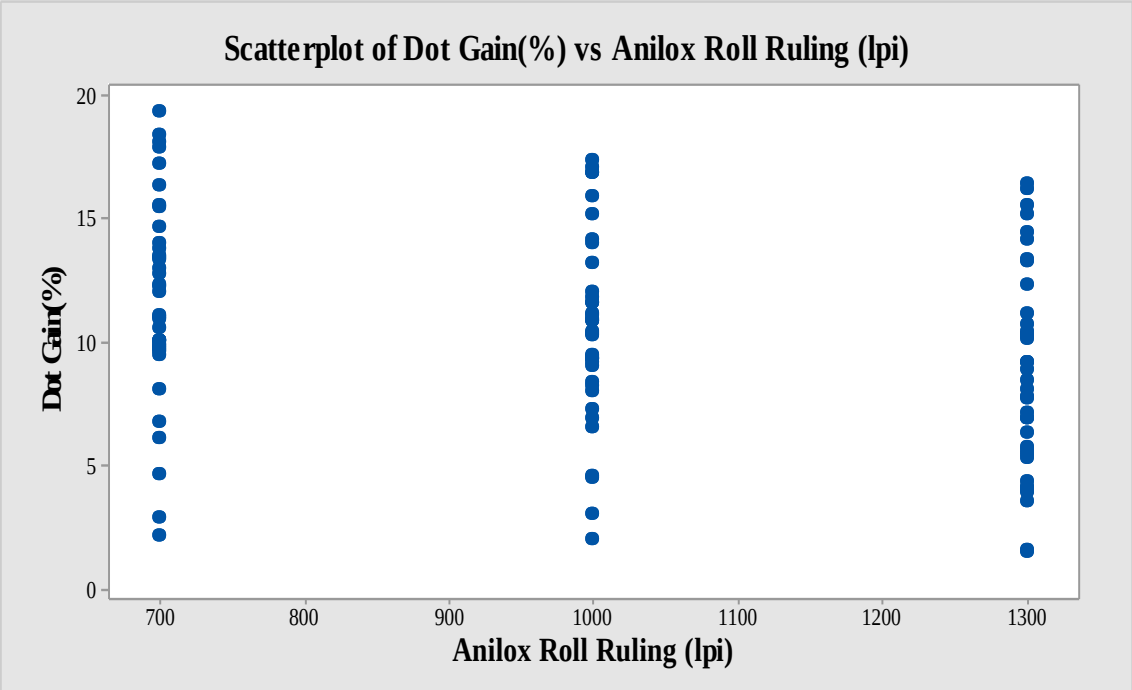

Figure 5.9: Scatterplot of dot gain vs anilox roller ruling

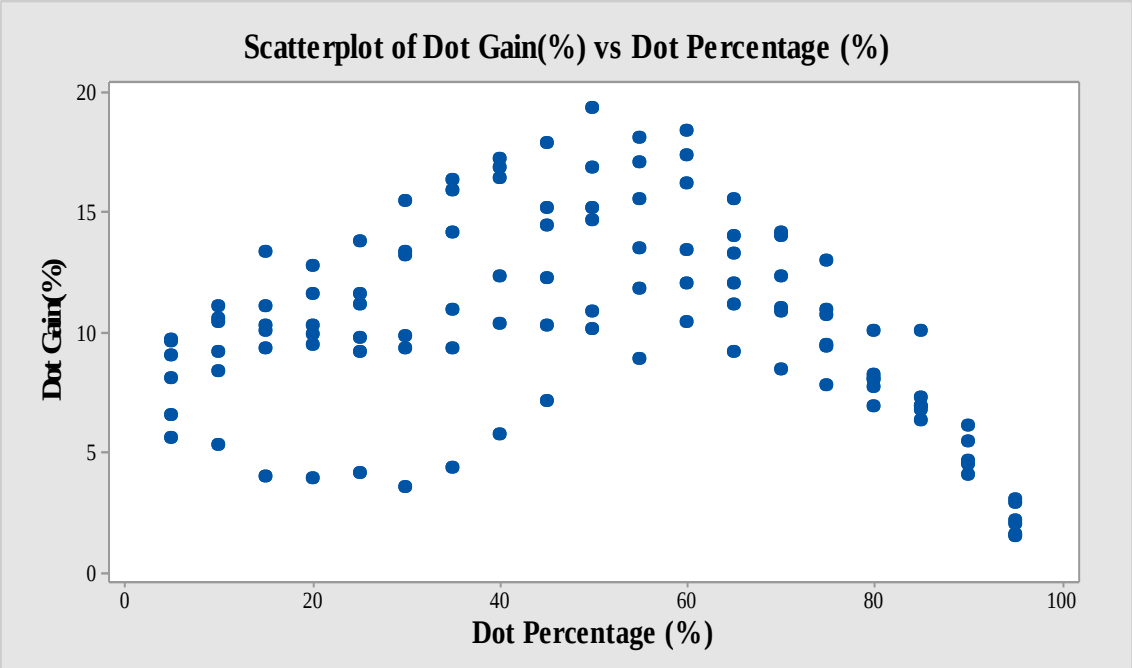

Figure 5.10: Scatterplot of dot gain vs dot percentage

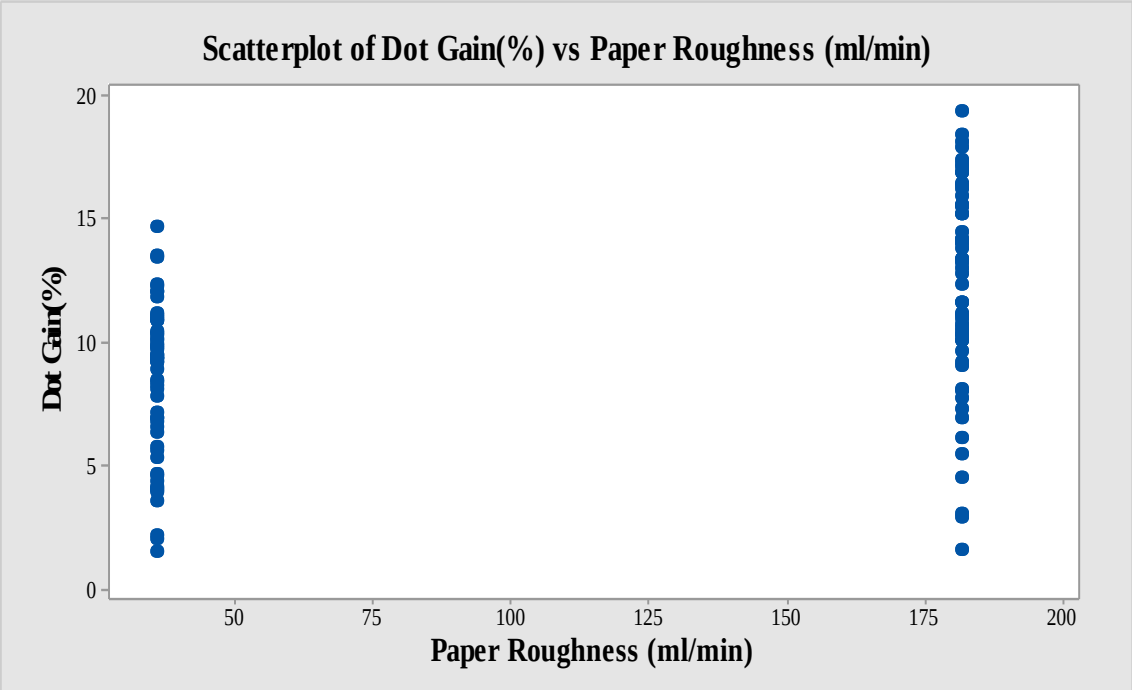

Figure 5.11: Scatterplot of dot gain vs paper roughness

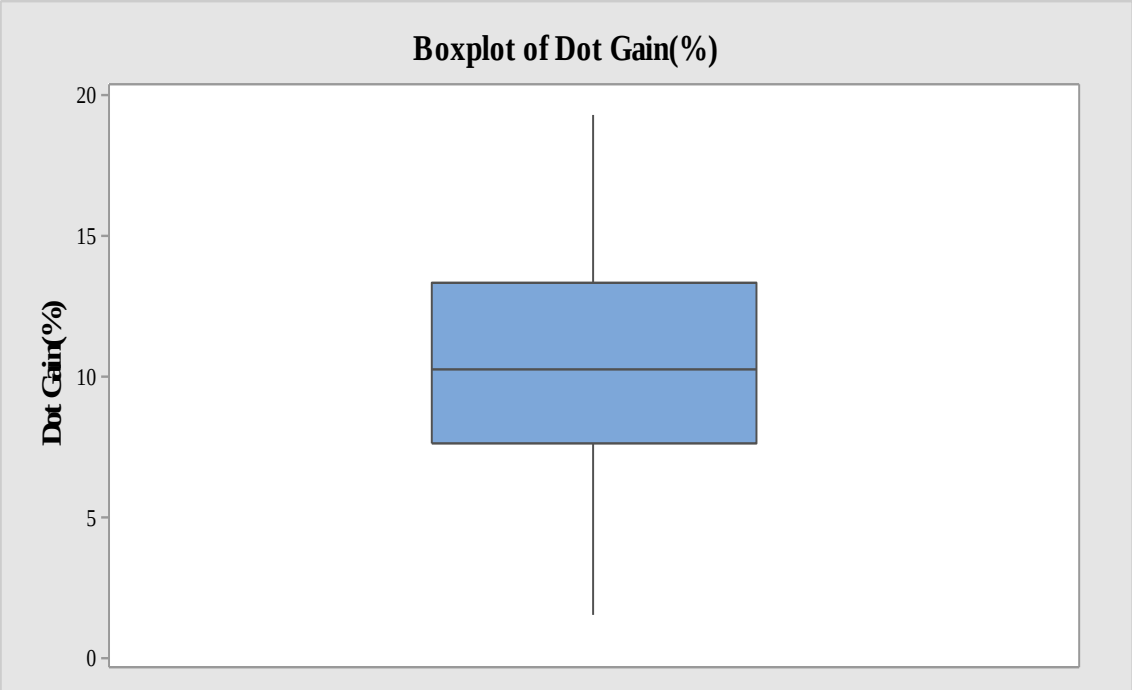

Figure 5.12: Boxplot of dot gain

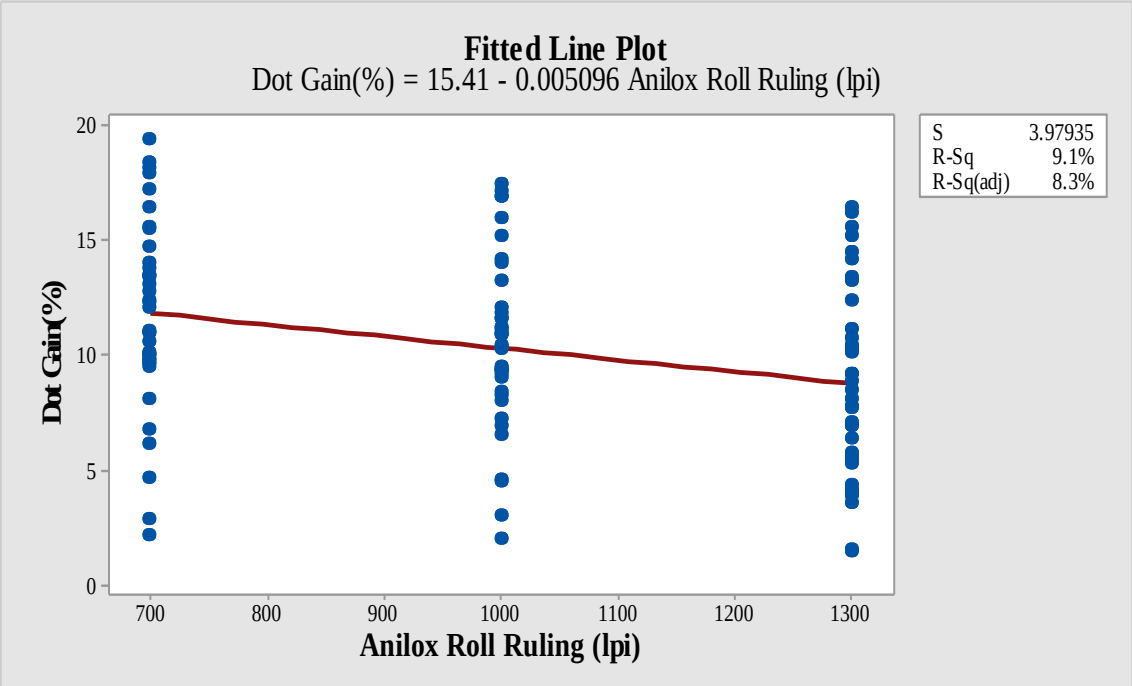

Figure 5.13: Fitted line plot for dot gain vs anilox roll ruling

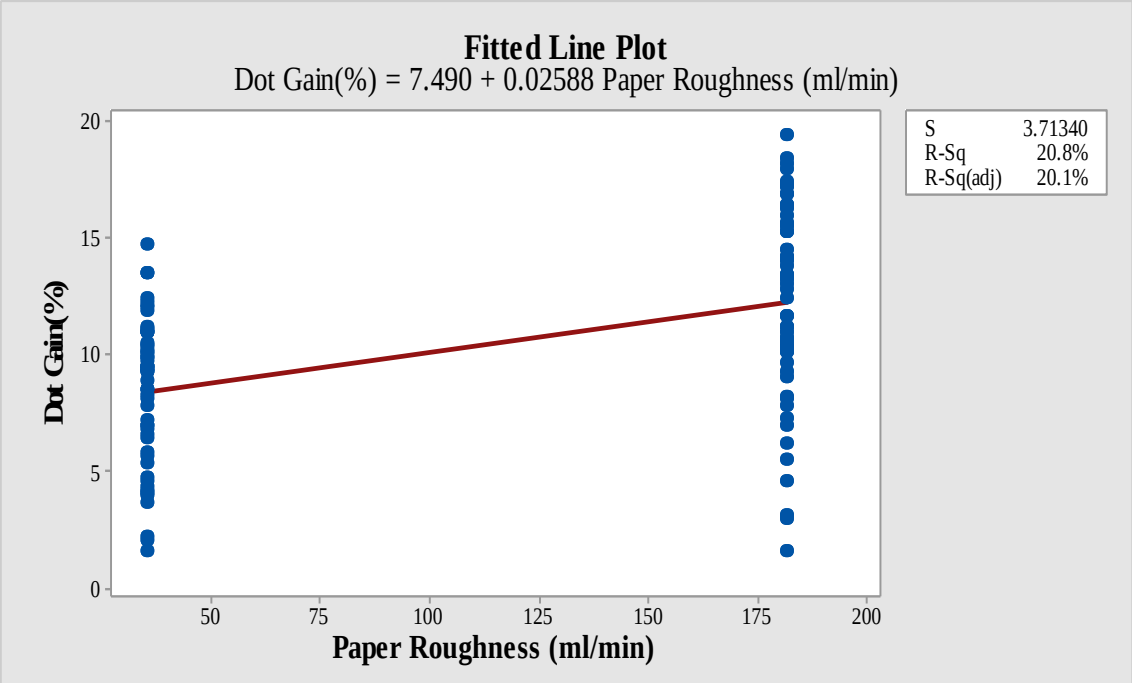

Figure 5.14: Fitted line plot for dot gain vs paper roughness

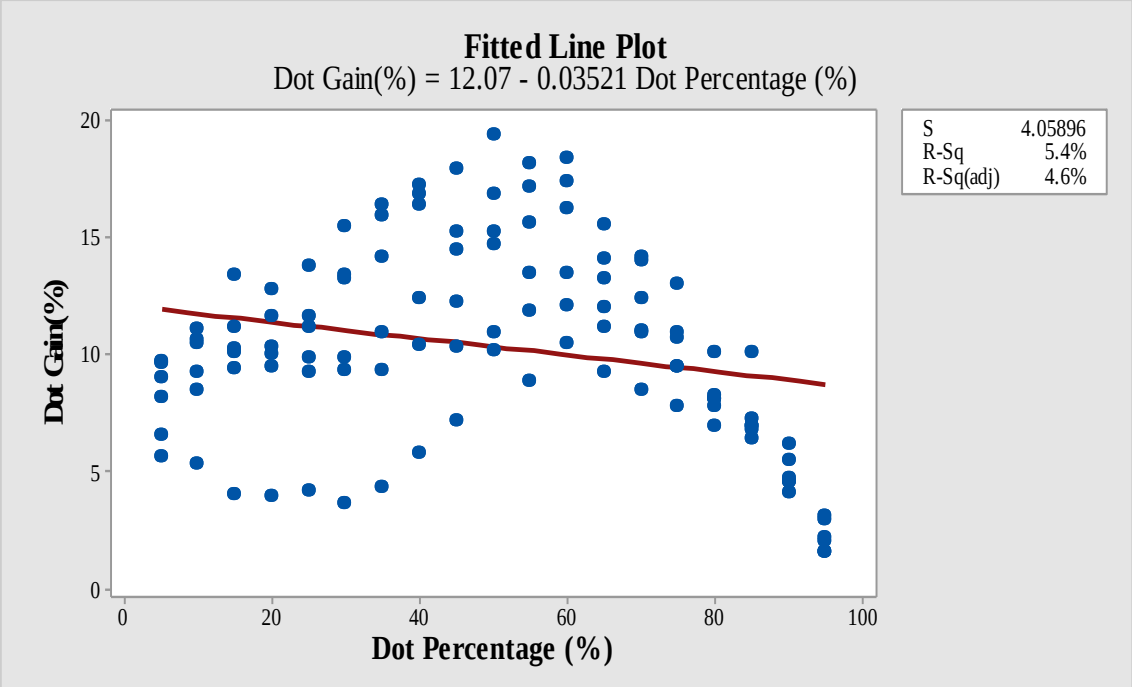

Figure 5.15: Fitted line plot for dot gain vs dot percentage

5.2.1.5 Discussions

The Table 5.4 comprises the result that shows the random forest regression algorithm is comparatively better in the prediction of accuracy than linear regression and decision tree algorithms. The random forest regression is an ensemble learning technique that actually combines the predictions from several decision trees to generate a single, more reliable forecast, so that the accuracy and reliability of this algorithm will be more. When linear and decision tree regression utilizes a single model for prediction, the random forest uses several decision trees instead. The linear regression will be more accurate if the relationship between variables is linear only so that the linear regression is often less effective than random forest method. For a decision tree algorithm, each decision tree has a significant variance, but when aggregated them all at once, the variance that results is reduced because each decision tree is perfectly trained on that specific sample data. This method adopted by the random forest make it stronger and more adaptable for regression related problems. It is simpler to use, less dependent on the training set and is more accurate. It works well with big datasets with plenty of attributes, outliers, noisy characteristics and missing data are all handled by it. The main python machine learning library is called sklearn. It offers a large selection of tools for building, preprocessing, assessing, and applying machine learning models.

The Figure 5.5 is the histogram plot for the residuals found in the analysis part. The normal distribution of residuals is found somewhat asymmetrical at some points. The Figure 5.6 represents the normal probability plot that shows the visual data regarding the deviation of response from normal distribution. The Figure 5.7 shows the versus fit plot that represents the non-linearity, outliers and undesirable errors associated with the dataset found from the experimental process. The Figure 5.8 indicates the appropriateness of data collection and serial correlation of errors in the experimental sequence.

The Figure 5.9 is a scatterplot that indicates the possibility of decreasing the dot gain with increasing anilox roller ruling in flexography printing. The scatterplot of Figure 5.10 illustrates that, for square dots the occurrence of dot gain is more at middle-tone areas of the print.

The Figure 5.11 tells the fact that the dot gain will be more if the substrate has high porous texture. The Figure 5.12 is a boxplot of dot gain showing the locality, skewness and spread of data through their quartiles. The whiskers extending from the box represents the variability outside the quartiles.

The Figures 5.13-5.15 are fitted line plots that represent the estimated value of regression function between response and input variables as per linear regression.

5.2.1.6 Conclusions

The various sectors of the work are organized as background information on flexography printing and machine learning, delves into supervised techniques using the python language, outliers the proposed model for data analytics, addresses performance evaluation, examination on result analysis.

The implementation of machine learning algorithms with three different supervised learning algorithms such as linear regression, decision tree regression and random forest regression are carried out. The result shows that the random forest regression having the better efficiency based on the prediction of accuracy of the model.

The graphical plot shows the nature of distribution of datasets and the relationships between output response and input variables associated with the flexography printing experiment.

5.2.2 Flexography Color Prints for Dot Gain

5.2.2.1 Objective of the Study

Establishing a machine learning system to forecast dot gain in the flexography color printing is the aim of study.

5.2.2.2 Experimental Methods

Different paper samples having varying paper roughness were printed by flexography printing varying different input parameters such as anilox screen rulings. Effects of varying dot percentages on different colored dot gain were also considered. Prints were taken in four process colors separately on two sets of different paper samples. Table 5.5 displays the three input variables that were selected for the research. In the present research, dot gain was used as the response variable.

Table 5.5: Parameters in the study

Factors	**Unit**	**Symbol**	**Levels**	**Response**
Anilox Ruling	Lines per inch (lpi)	A	900, 1200	Dot Gain
Paper Roughness	Millilitre per minute (ml/min)	B	76, 109	
Dot Percentage	Percentage (%)	C	4% to 100 % with 4% increments	
Halftone dot shape	-	D	Square Shaped AM dot	

The anilox roller screen rulings used in the work had lines per inch (lpi) of 900 and 1200 respectively. The chosen roughness levels for the paper were 76 and 109 milliliters per minute. The roughness was measured using Roughness tester (Bendtsen type) following IS 1060 (Part 5/ Sec 20) RA2018. The engraved anilox roller cells were 60º hexagonal in form. The Gallus ECS flexography printing machine which uses process color inks of cyan (C), magenta (M), yellow (Y) and black (K), was utilized for

the printing. The inks used were solvent based liquid inks and have viscosity of 300 cp. A photopolymer plate (manufacturer – Dupont, type of the plate – digital solid photopolymer, plate production process – laser engraving process) with a magnetic backing and of 1.14 mm thickness was used as the printing image carrier. All of the parameters including the ink characteristics (uv ink), room temperature (23^0c), printing speed (35 m/min) and nip pressure (3 mm), were kept constant during the printing process.

5.2.2.2.1 Measurements and Data Collection

The print quality score was determined using the output response. As a result, the output parameters were quantitatively measured using the X-Rite Spectro Eye Spectro-densitometer. Visual examination of the printed area was done using a digital microscope, the LEICA-S8APO. The machine learning algorithms employed the readings of 100 print trials of input datasets for every color. It is expected that the split ratio of the training to test dataset is 7:3. The collected data is fed into the python program, which processes it using machine learning techniques.

5.2.2.3 Dataset

Some samples of cyan, magenta, yellow and black dataset have been given in Tables 5.6-5.9.

Table 5.6: Cyan dataset

Paper_Roughness	**Anilox_Roll_Ruling**	**Dot_Percentage**	**Dot_Gain**
76	900	4	7.18
76	1200	4	5.07
109	900	4	12.05
109	1200	4	9.89

76	900	8	13.14
76	1200	8	9.34
109	900	8	16.12
109	1200	8	14.13
76	900	12	18.01
76	1200	12	12.88
109	900	12	19.49
109	1200	12	21.16

Table 5.7: Magenta dataset

Paper_Roughness	**Anilox_Roll_Ruling**	**Dot_Percentage**	**Dot_Gain**
76	900	4	7.46
76	1200	4	5.17
109	900	4	12.46
109	1200	4	9.99
76	900	8	11.73
76	1200	8	11.51

109	900	8	16.74
109	1200	8	14.3
76	900	12	15.27
76	1200	12	14.97
109	900	12	20.29
109	1200	12	21.41

Table 5.8: Yellow dataset

Paper_Roughness	**Anilox_Roll_Ruling**	**Dot_Percentage**	**Dot_Gain**
76	900	4	5.41
76	1200	4	5.6
109	900	4	8.02
109	1200	4	12.97
76	900	8	9.98
76	1200	8	8.24
109	900	8	12.69
109	1200	8	15.45

76	900	12	13.81
76	1200	12	12.41
109	900	12	16.6
109	1200	12	19.42

Table 5.9: Black dataset

Paper_Roughness	**Anilox_Roll_Ruling**	**Dot_Percentage**	**Dot_Gain**
76	900	4	5.04
76	1200	4	9.17
109	900	4	12.27
109	1200	4	15.86
76	900	8	9.29
76	1200	8	12.99
109	900	8	16.46
109	1200	8	19.45
76	900	12	10.99
76	1200	12	16.12

109	900	12	19.92
109	1200	12	22.37

5.2.2.4 Results

The Tables 5.11-5.16 display the results of different machine learning techniques for each of the C, M, Y and K process colors. The evaluation instrument for comparison is the loss functions of different algorithms for every color. Loss functions measure the performance accuracy of different machine learning techniques. The capacity of the developed model is used to predict the result based on the given input variables. The Table 5.10 shows the splitting of dataset.

Table 5.10: Splitting of dataset

Shape of data	(100, 4)
Shape of split data	The shape of X_train: (75, 3)
	The shape of X_test: (25, 3)
	The shape of Y_train: (75, 3)
	The shape of Y_test: (25, 3)

Table 5.11: Loss functions of dot gain with linear regression algorithm

Process Color	**Linear Regression (LR)**			
	MSE	RMSE	MAE	R^2
Cyan	76.9796	8.7738	6.6254	0.0347

Magenta	75.4535	8.6864	6.6426	0.164
Yellow	62.5017	7.9058	5.9712	0.0545
Black	62.5586	7.9097	6.0685	0.0718

Table 5.12: Loss functions of dot gain with decision tree regression algorithm

Process Color	**Decision Tree Regression (DT)**			
	MSE	RMSE	MAE	R^2
Cyan	8.7184	2.9527	2.2271	0.8907
Magenta	6.7242	2.8931	2.1725	0.9073
Yellow	6.0501	2.4597	1.7292	0.9085
Black	7.1567	2.6752	2.2341	0.8938

Table 5.13: Loss functions of dot gain with random forest regression algorithm

Process Color	**Random Forest Regression (RF)**			
	MSE	RMSE	MAE	R^2
Cyan	2.9381	1.7141	1.2644	0.9632
Magenta	1.5403	1.2411	0.9413	0.9829
Yellow	3.0955	1.7594	1.4247	0.9532
Black	3.9517	1.9879	1.4614	0.9414

Table 5.14: Loss functions of dot gain with XG boost regression algorithm

Process Color	**XG Boost Regression (XGB)**			
	MSE	RMSE	MAE	R^2
Cyan	3.6584	1.9127	1.35	0.9541
Magenta	1.4106	1.1877	0.8311	0.9844
Yellow	1.9435	1.3941	1.1186	0.9706
Black	2.888	1.6994	1.3164	0.9572

Table 5.15: Loss functions of dot gain with support vector machines regression algorithm

Process Color	**Support Vector Machines Regression (SVM)**			
	MSE	RMSE	MAE	R^2
Cyan	41.3552	6.4308	5.1188	0.4814
Magenta	43.8853	6.6246	5.2003	0.5138
Yellow	35.8777	5.9898	4.5985	0.4572
Black	35.3264	5.9436	4.2382	0.4759

Table 5.16: Loss functions of dot gain with neural network algorithm

Process Color	**Neural Network (NN)**			
	MSE	RMSE	MAE	R^2
Cyan	0.2831	0.5321	0.3723	0.972
Magenta	0.0595	0.244	0.1712	0.974
Yellow	0.179	0.4231	0.3125	0.9725
Black	0.441	0.6641	0.491	0.9714

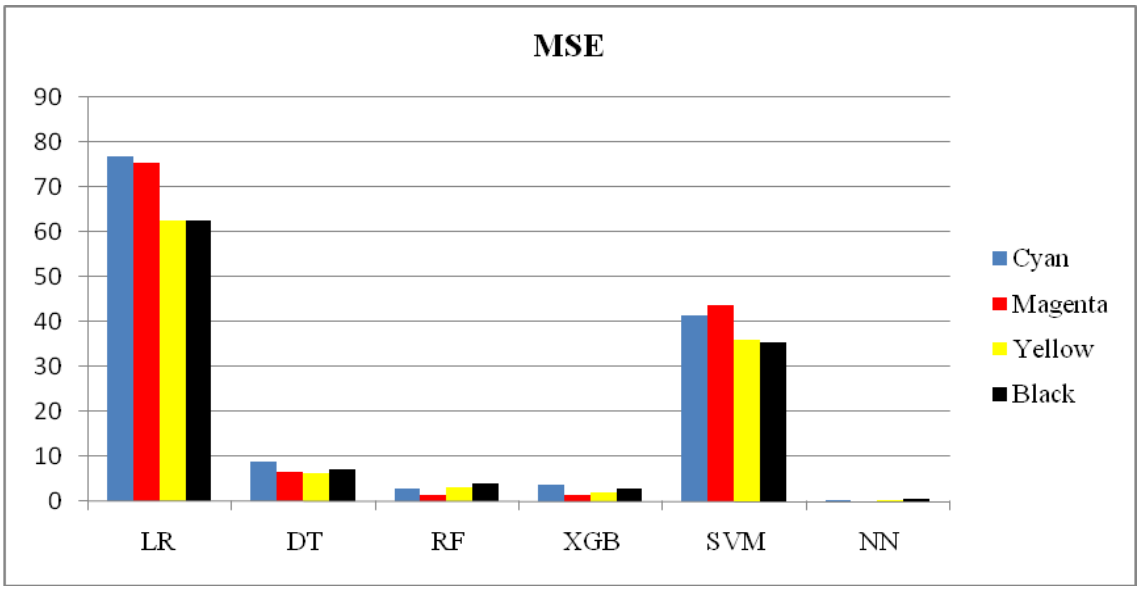

Figure 5.16: Bar chart of MSE values for different machine learning algorithms

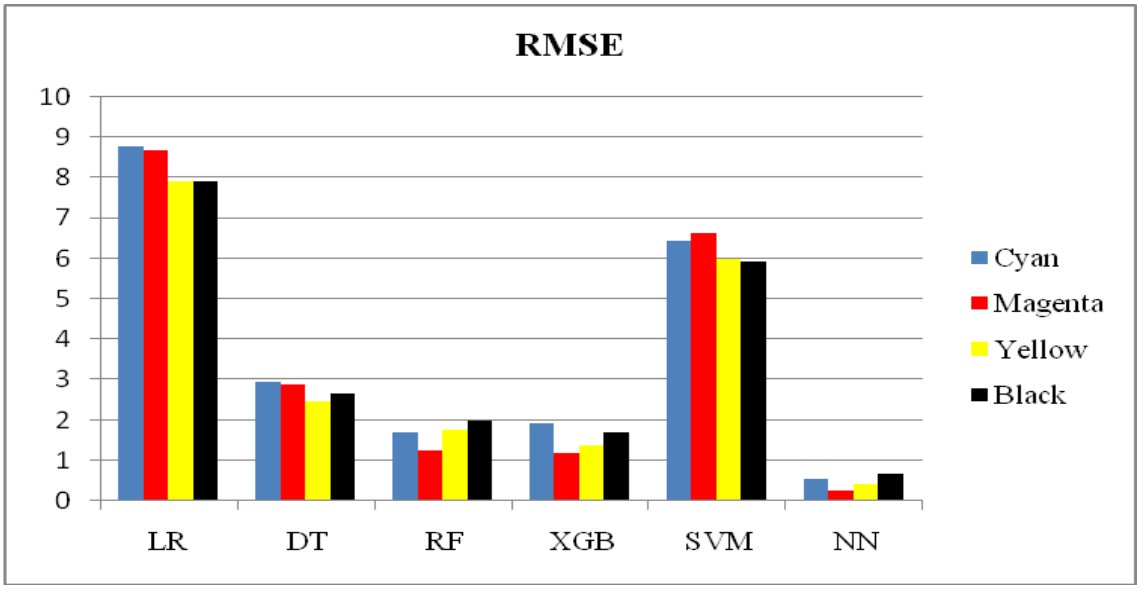

Figure 5.17: Bar chart of RMSE values for different machine learning algorithms

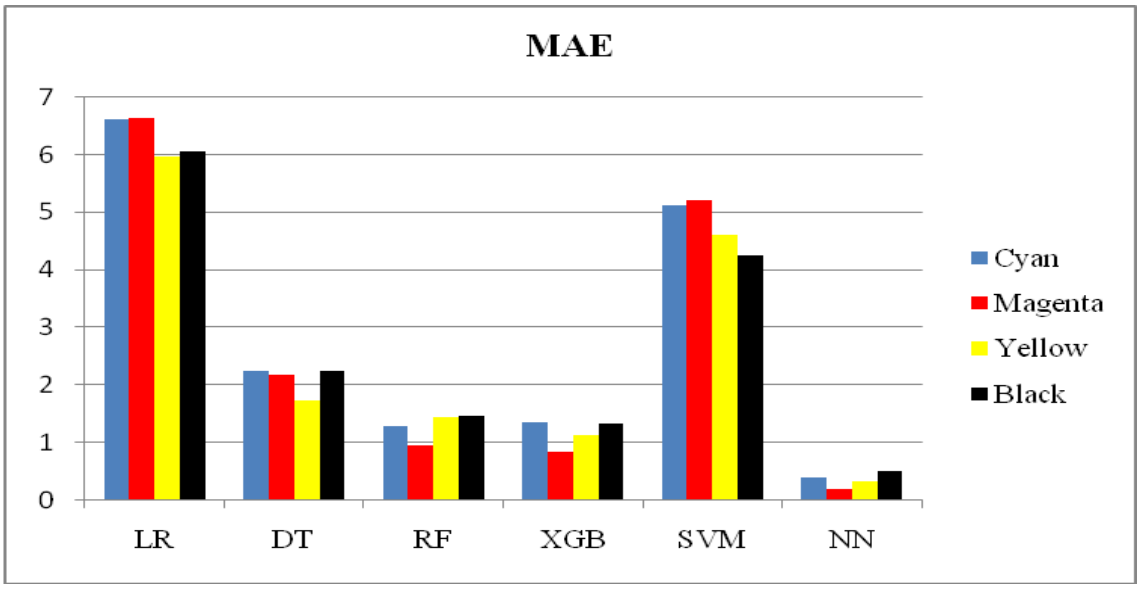

Figure 5.18: Bar chart of MAE values for different machine learning algorithms

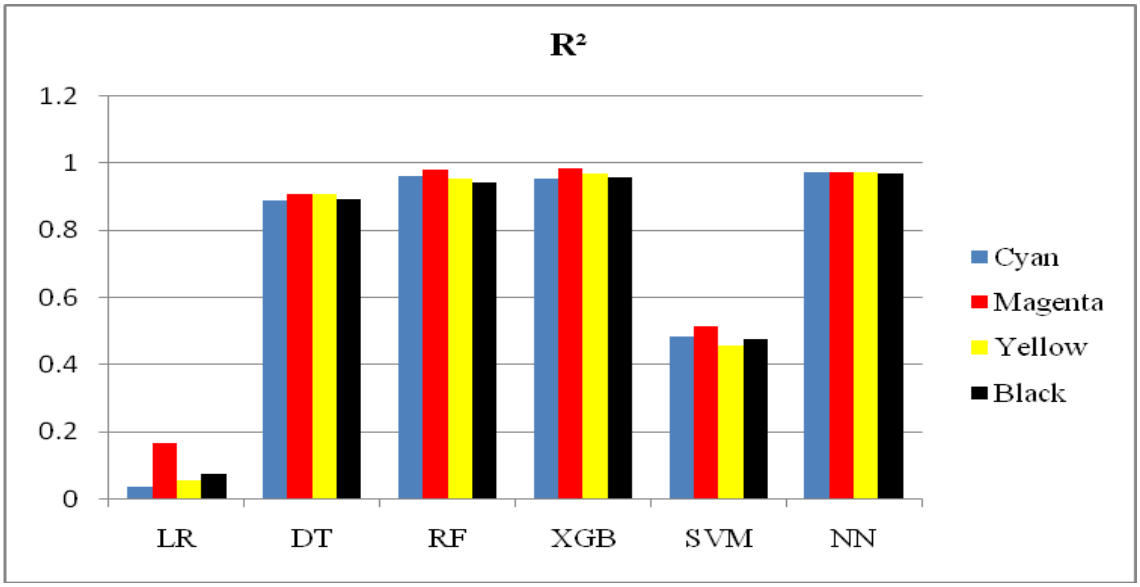

Figure 5.19: Bar chart of R^2 score for different machine learning algorithms

Figure 5.16 shows the Mean Squared Error (MSE) for the different machine learning algorithms adopted for prediction of color dot gain in flexography printing process. MSE signifies the average squared difference between the actual values and predicted values by a model. A lower value of MSE indicates the accuracy of the model to be used for prediction. It has been found that MSE is lowest in neural network (NN) which implies it is the best model for prediction out of the models considered.

Figure 5.17 represents the Root Mean Squared Error (RMSE) for the different machine learning algorithms. RMSE quantifies the differences between the predicted values and actual values. It has been observed that RMSE is least for neural network (NN) which implies it is best for this prediction.

Figure 5.18 shows the bar chart of Mean Absolute Error (MAE) for the different machine learning algorithms adopted for prediction. MAE measures the average absolute differences between the actual and the predicted values. It has been found that MAE value is the lowest for the Neural Network. This means that neural network (NN) is the best of all the machine learning algorithms considered for the prediction of dot gain in the present work.

Figure 5.19 represents the bar chart of R^2 values for the different machine learning algorithms adopted for the prediction of color dot gain. It indicates the percentage of variation in the target variables that can be obtained by the independent variables. The

maximum value of R^2 is 1. The higher the R^2 value, the better is the prediction. It has been found that R^2 value for the neural network (NN) method is maximum and near about 1 which implies that this method is the best for the prediction of color dot gain in the current investigation. The loss functions of different machine learning algorithms given in Tables 5.11-5.16 were decided by considering the values given in Figures 5.16-5.19.

5.2.2.4.1 Graphical Analysis

The graphical depictions display the interplay among the various experimental factors that was identified during the analysis stage. The Figures 5.20-5.27 display the main effects plot of each experimental factor over dot gain of original data and predicted data obtained by neural network and the Figures 5.28-5.35 displays the interaction effects of original experimental data as well as predicted data. The Figures 5.20-5.35 have been plotted using Minitab 17 statistical software.

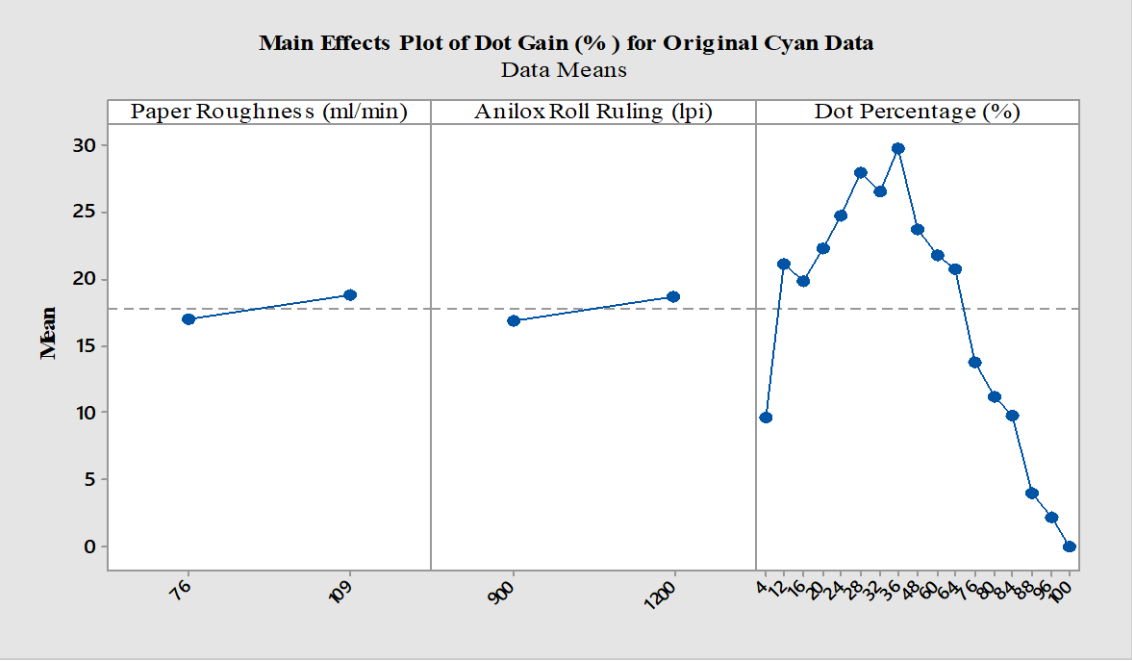

Figure 5.20: Main effects plot of dot gain for original cyan data

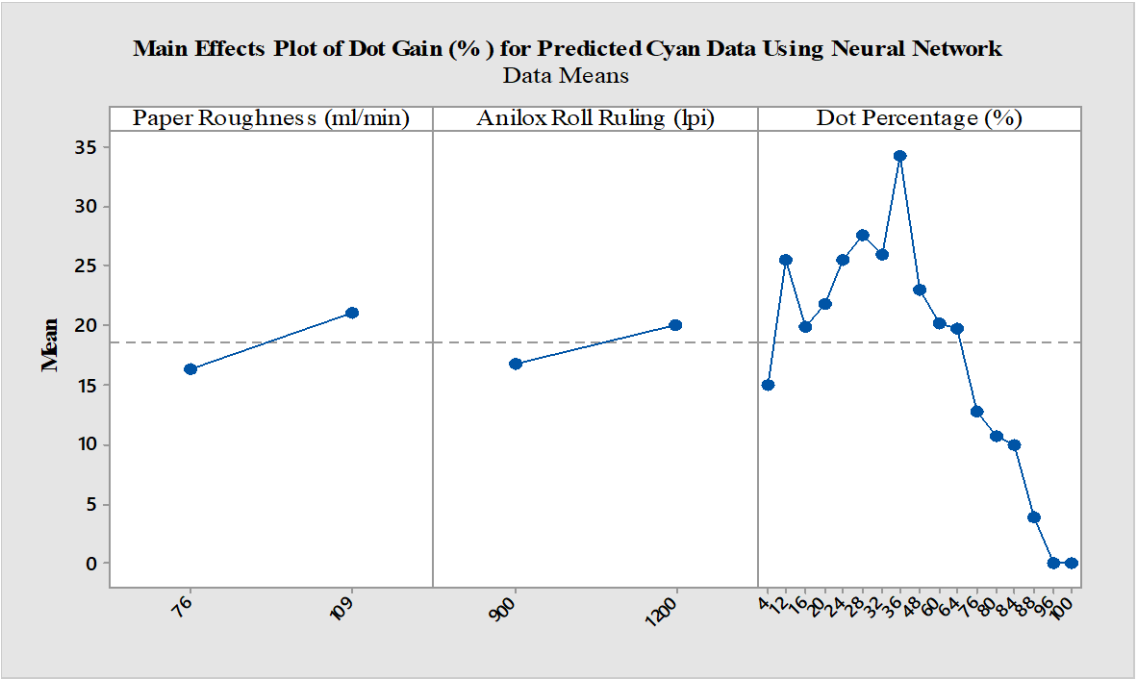

Figure 5.21: Main effects plot of dot gain for predicted cyan data using neural network

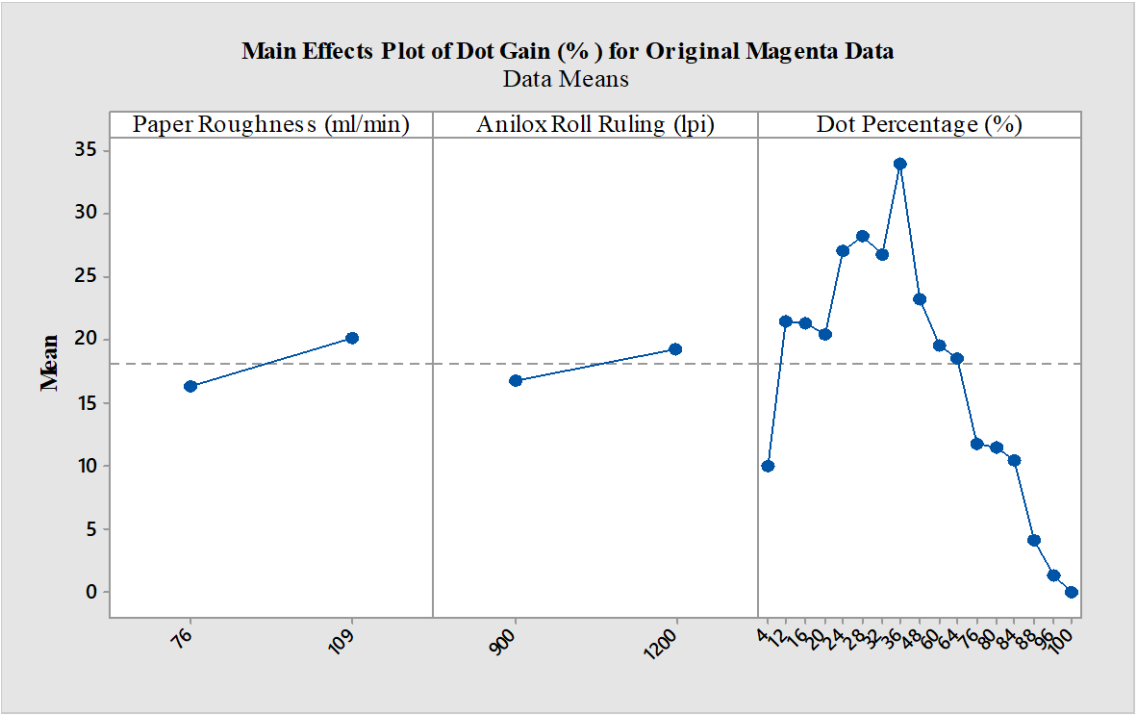

Figure 5.22: Main effects plot of dot gain for original magenta data

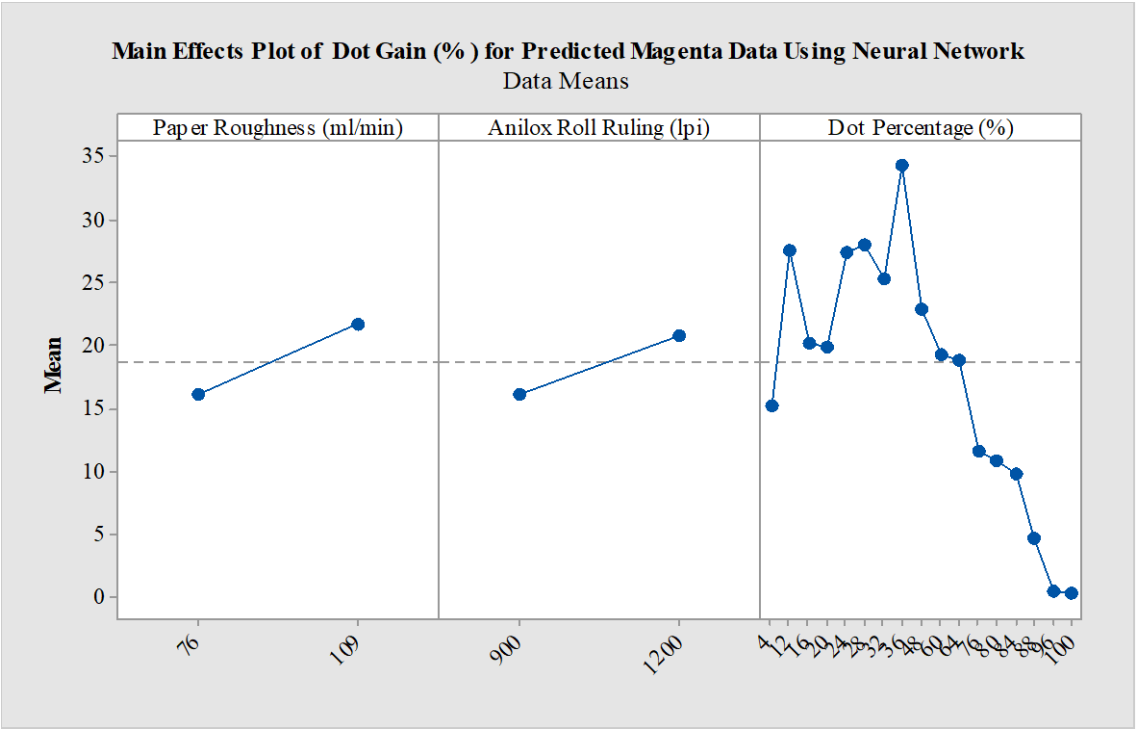

Figure 5.23: Main effects plot of dot gain for predicted magenta data using neural network

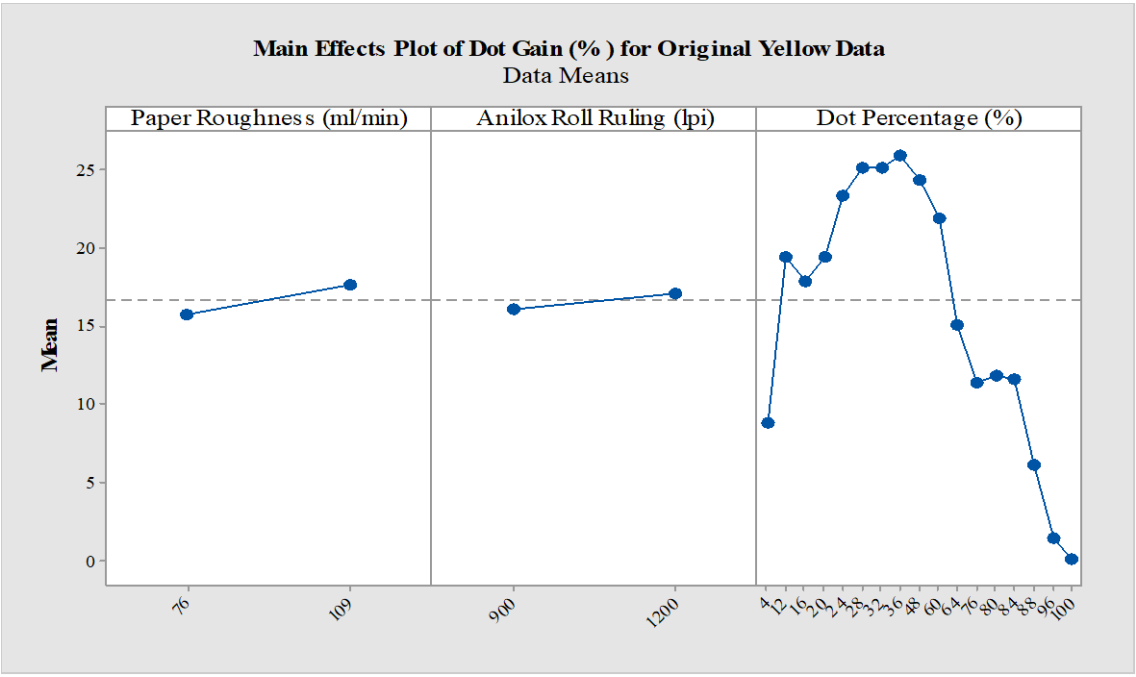

Figure 5.24: Main effects plot of dot gain for original yellow data

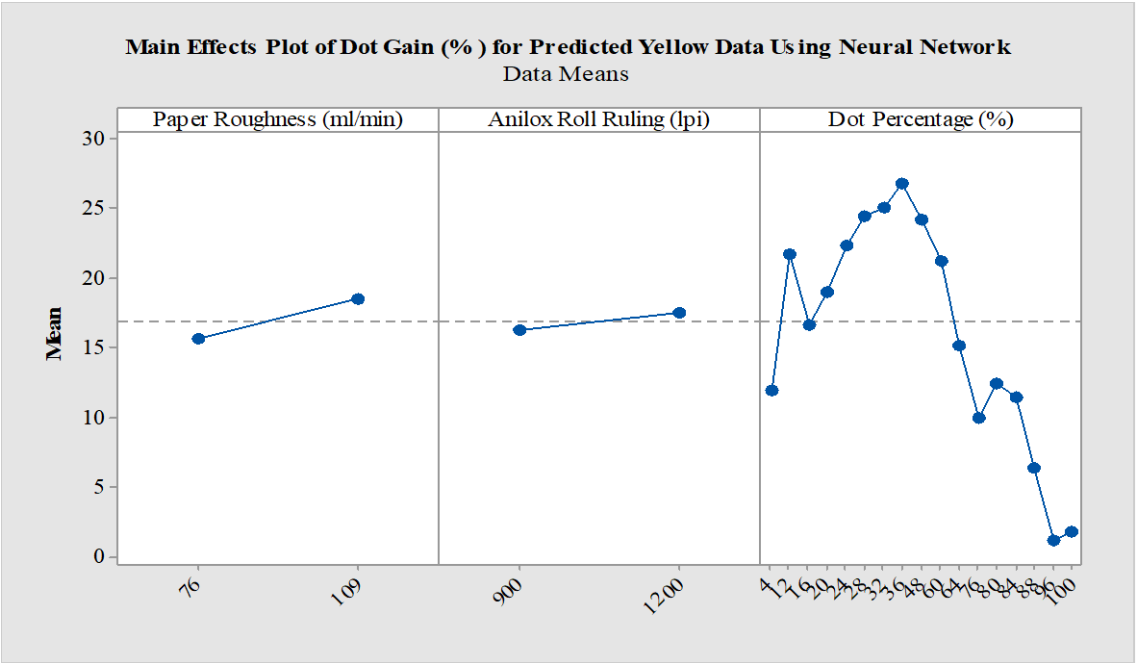

Figure 5.25: Main effects plot of dot gain for predicted yellow data using neural network

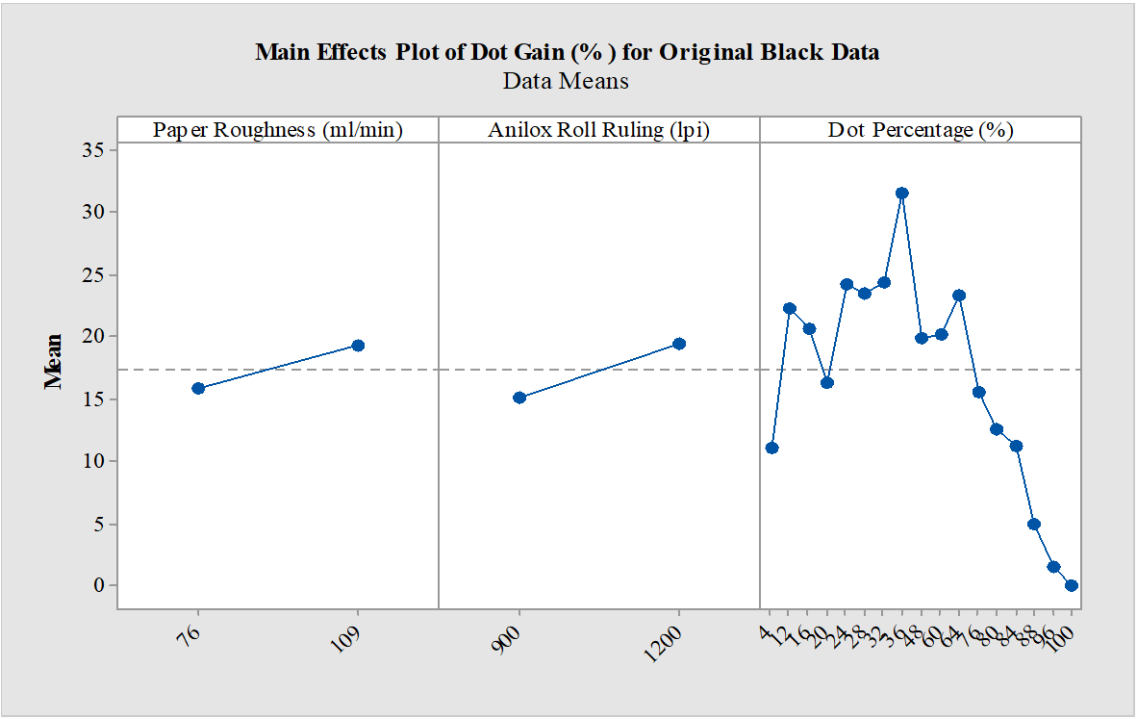

Figure 5.26: Main effects plot of dot gain for original black data

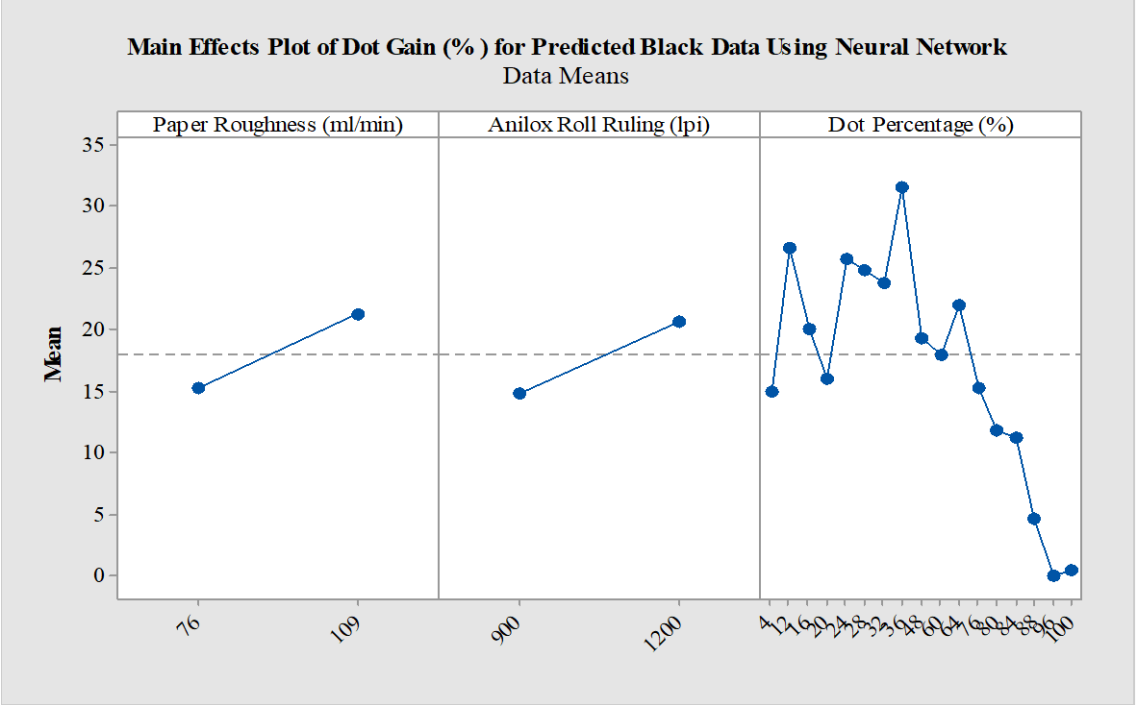

Figure 5.27: Main effects plot of dot gain for predicted black data using neural network

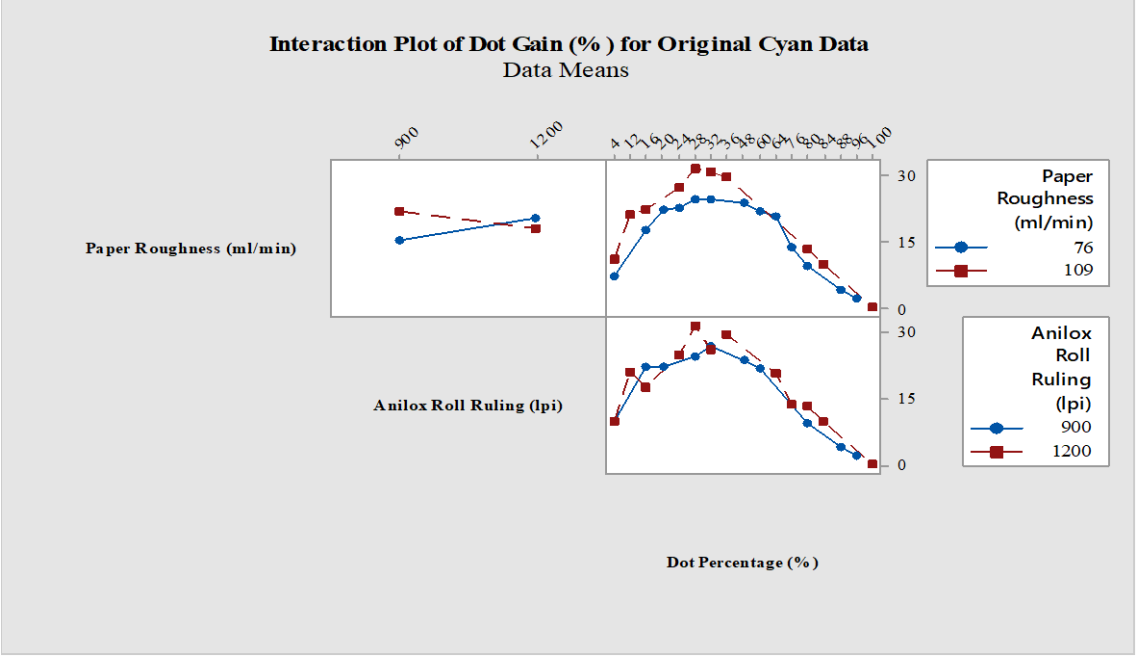

Figure 5.28: Interaction plot of dot gain for original cyan data

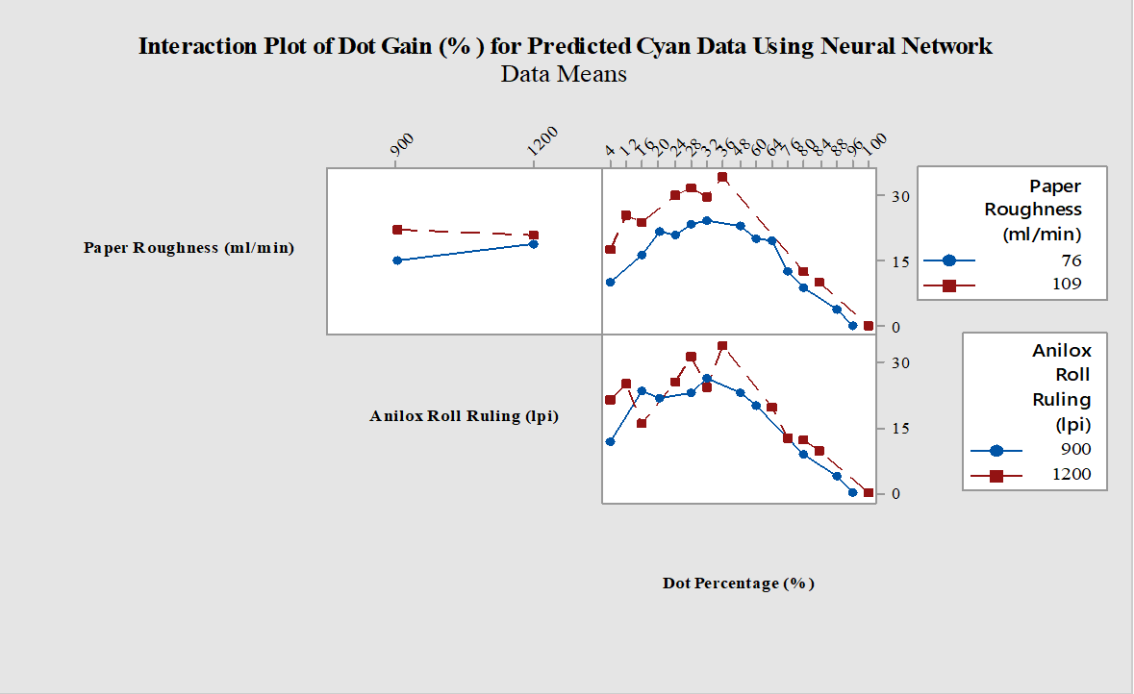

Figure 5.29: Interaction plot of dot gain for predicted cyan data using neural network

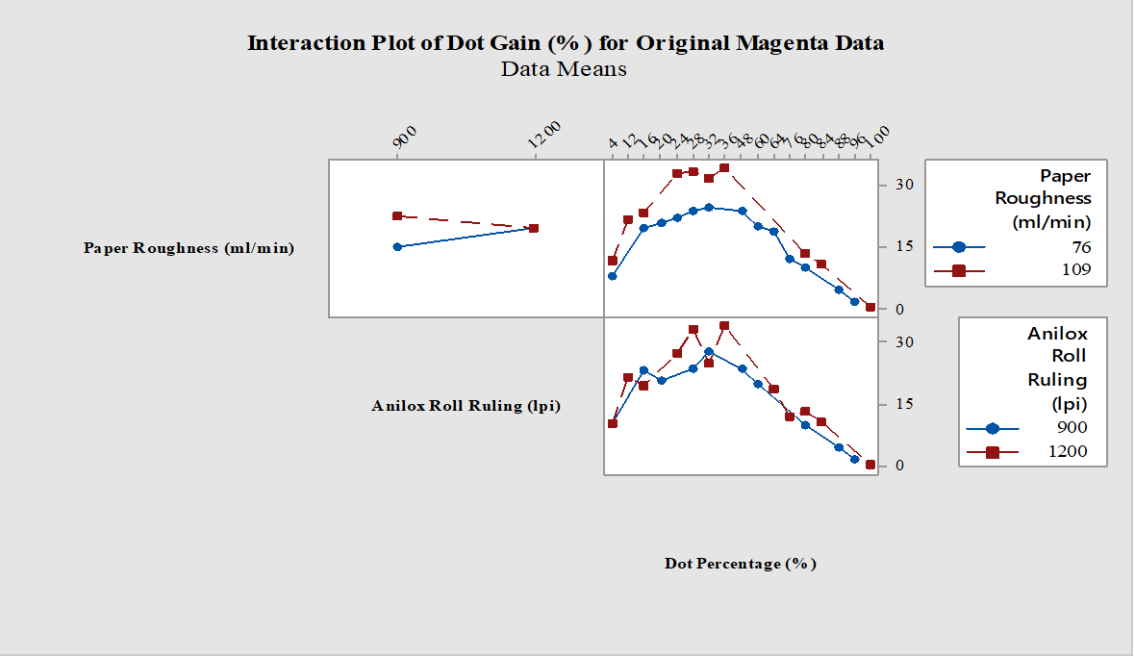

Figure 5.30: Interaction plot of dot gain for original magenta data

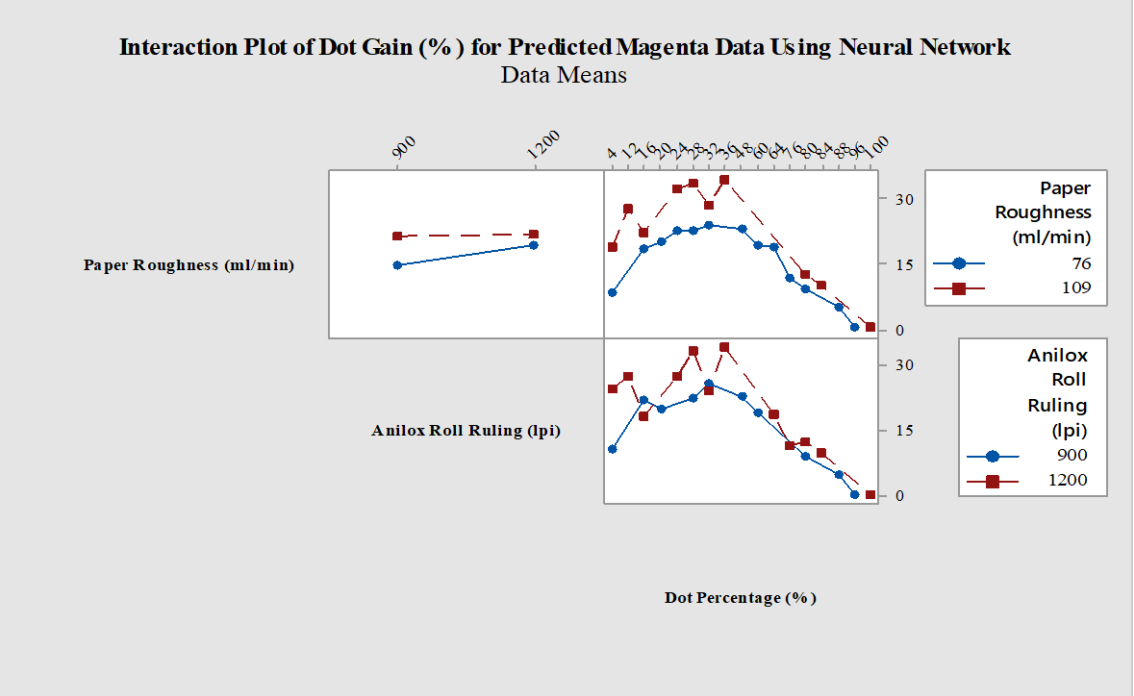

Figure 5.31: Interaction plot of dot gain for predicted magenta data using neural network

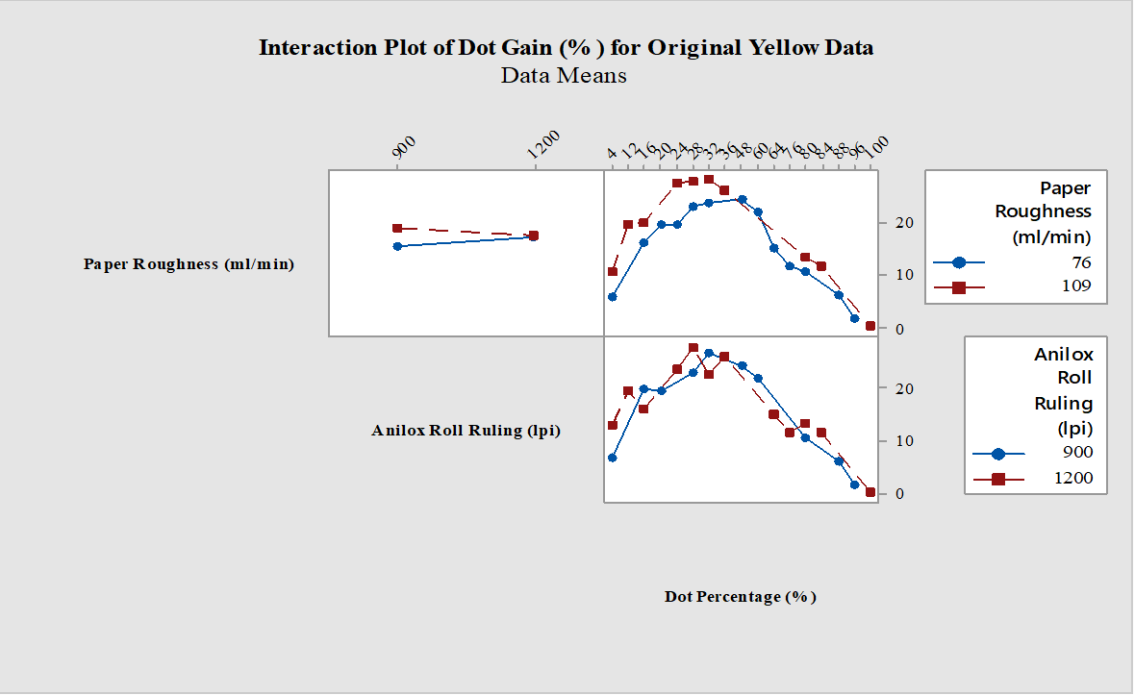

Figure 5.32: Interaction plot of dot gain for original yellow data

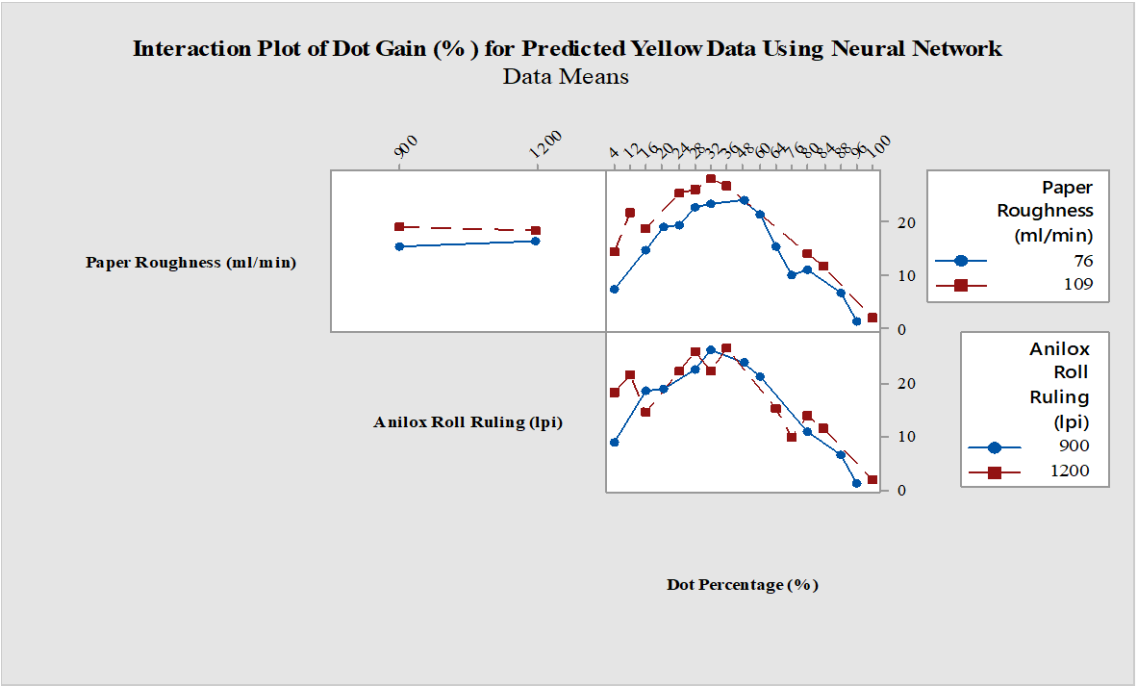

Figure 5.33: Interaction plot of dot gain for predicted yellow data using neural network

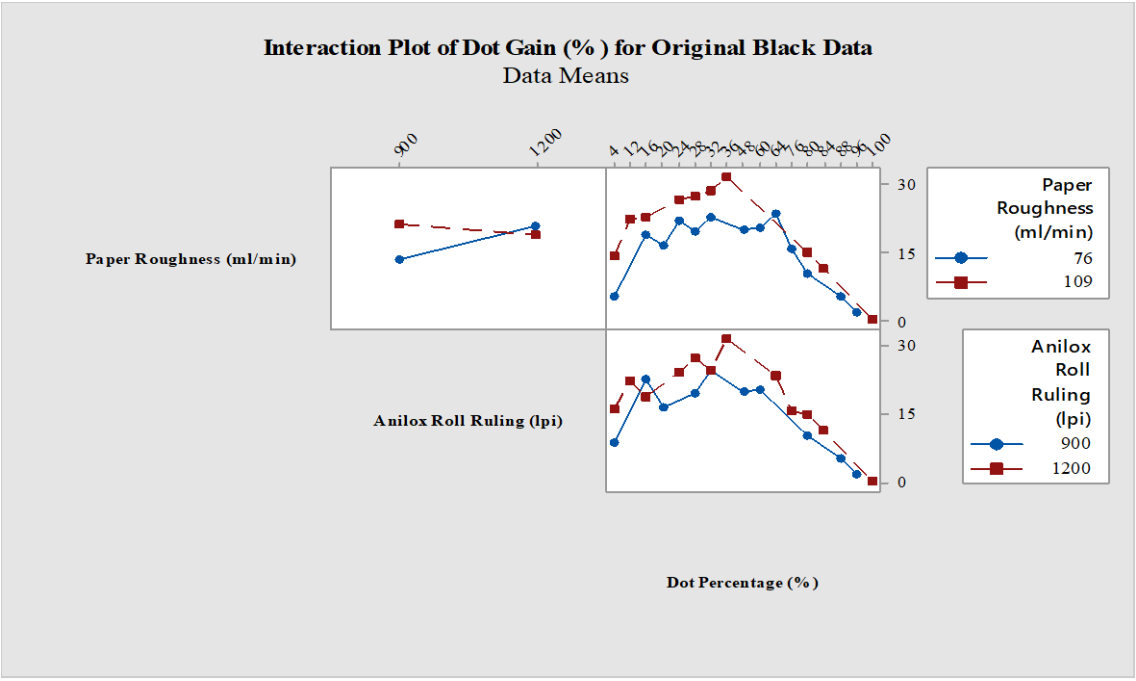

Figure 5.34: Interaction plot of dot gain for original black data

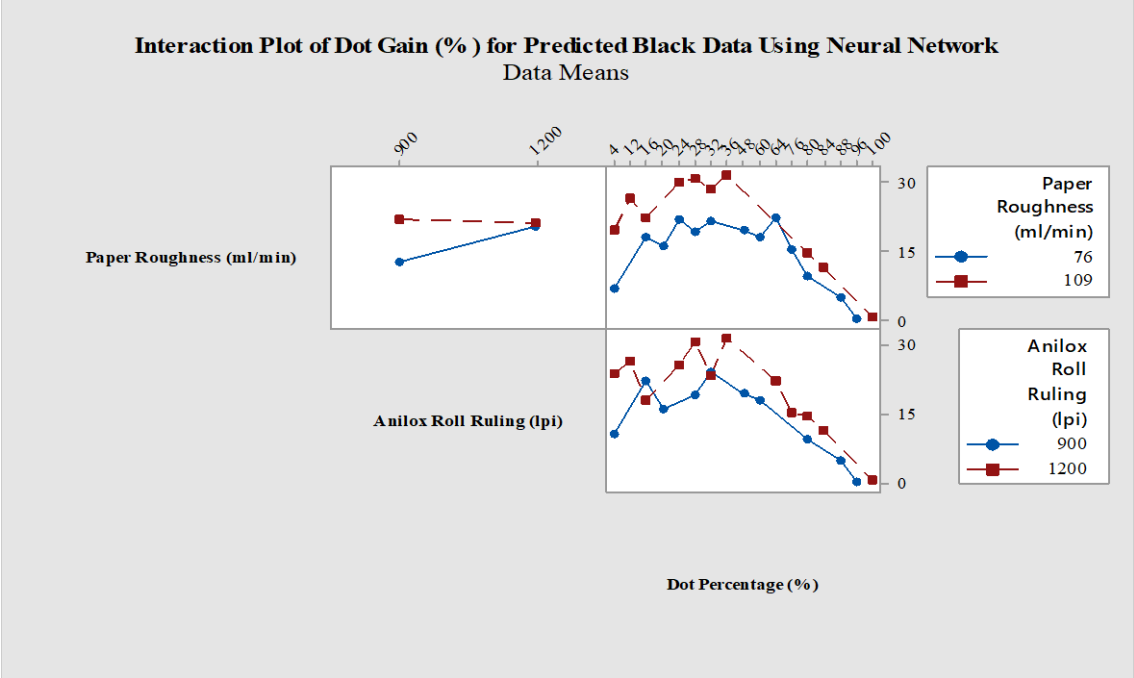

Figure 5.35: Interaction plot of dot gain for predicted black data using neural network

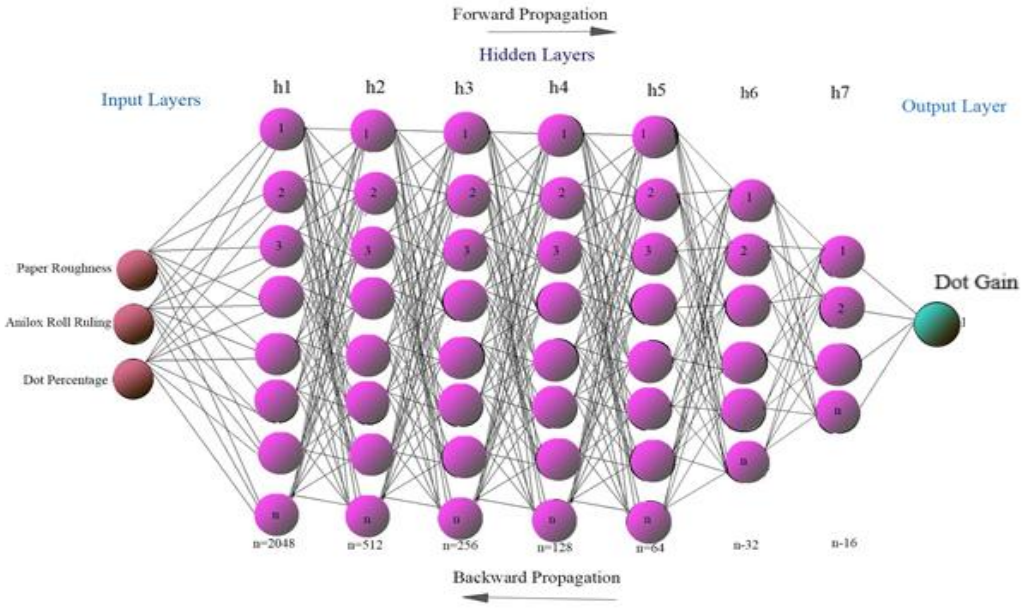

Figure 5.36: Neural network architecture in the study

5.2.2.5 Discussions

In recent years, machine learning has rapidly grown inside the computing and data analysis framework, which typically allows programs to function intelligently. A few

machine learning techniques have been applied in this work to evaluate the dot gain of four color flexography printing.

The summary of loss functions attained for several machine learning models in dot gain prediction is shown in Tables 5.11-5.16. It is discovered through the execution of python program that the neural network (NN) algorithm provides a very notable method for estimating optical dot gain for cyan, magenta, yellow and black colors. This demonstrates that neural networks outperform tested algorithms like SVM, XG boost regression, random forest, decision tree and linear regression in the prediction process. With its unique properties such as a somewhat higher number of hyper parameters, epochs, layers, etc., than other algorithms, the neural network performs exceptionally well.

The main effects plot of original data as well as predicted data for cyan, magenta, yellow and black reproductions with dot gain are shown from Figures 5.20-5.27 and the interaction plots of original data and predicted data are illustrated by the Figures 5.28-5.35. The results of these plots indicate that the dot gain is comparatively less with coated paper than uncoated paper. As the anilox line frequency increases the dot gain tends to decrease. The lower anilox screen frequency together with the uneven texture of uncoated paper accelerates the dot gain effects considerably.

Figures 5.20-5.27 show the nature of the output response (dot gain) of main effects plot with respect to paper roughness and anilox roll ruling (lpi) is more or less similar in both the original data and predicted data.

Interaction plots represented by Figures 5.28-5.35 of original data and predicted data obtained by neural networking machine learning shows the nature of the curve is almost similar.

Figure 5.36 shows that the suggested design of the neural network (NN) algorithm in this study has three input layers, one output layer, seven hidden layers, and 5000 epochs. This method of operation enhanced its level of automation and general effectiveness.

5.2.2.6 Conclusions

The goal of this research is to develop a machine learning model for predicting dot gain effect associated with flexography four process color printing. This paper's primary sections are as follows: a theoretical review of the history of flexography printing and machine learning, python programming using some key machine learning algorithms, performance assessment and outcome analysis. The different machine learning techniques are implemented and assessed using neural network, XG boost regression, SVM regression, random forest regression, decision tree regression and linear regression. The result shows that when compared to all other evaluated algorithms, neural network (NN) algorithm performs noticeably better due to the superior properties of neural networks.

5.2.3 Flexography Color Prints for Hue Error

5.2.3.1 Objective of the Study

The purpose of this study is to establish a machine learning algorithm to predict the hue error in the process color inks used in flexography printing.

5.2.3.2 Experimental Methods

The flexography printing was obtained on different grades of paper with different process colors such as cyan, magenta, yellow and black. Three input variables were chosen for the work and it is shown in the Table 5.17. One of the print quality assessment parameters such as hue error is taken as the response variable throughout the analysis process. Hue error depends on substrate type, ink formulation, anilox roll condition and printing conditions like temperature and pressure.

Table 5.17: Parameters background at printing

Factors	Unit	Symbol	Levels	Response
Anilox Ruling	Lines per inch (lpi)	A	900, 1200	Hue

Paper Roughness	Millilitre per minute (ml/min)	B	76, 109	Error
Dot Percentage	Percentage (%)	C	4% to 100 % with 4% increments	
Halftone dot shape	-	D	Square shaped AM dot	

The lines per inch (lpi) for the anilox roller rulings employed in the work are 900 and 1200. The selected paper roughness values are 76 ml/min and 109 ml/min. The anilox roller cells with engravings have a 60^0 hexagonal shape. For the printing, flexography printing machine Gallus ECS with process color ink of cyan (C), magenta (M), yellow (Y) and black (K) are used. The printing image carrier is a photopolymer plate (manufacturer – Dupont, type of the plate – digital solid photopolymer) with a 1.14 mm thick magnetic backing. Throughout the printing process, all of the parameters such as the ink features (uv ink, viscosity – 300 cp), room temperature (23^0c), printing speed (35 m/min) and nip pressure (3 mm) are maintained constant.

5.2.3.2.1 Measurements and Data Collection

The output response was used to calculate the print quality score. Consequently, a Spectro-densitometer, such as the X-Rite Spectro Eye device was used to measure the output parameters quantitatively. A digital microscope such as the LEICA-S8APO was used to visually inspect the printed region. The readings of 100 prints of input datasets for each color were used with the machine learning algorithms. The training to test dataset split ratio is assumed to be 7:3. The python software receives the gathered data and uses machine learning methods to process it.

5.2.3.3 Dataset

Some samples of cyan, magenta, yellow and black dataset have been given in Tables 5.18-5.21.

Table 5.18: Cyan dataset

Paper_Roughness	**Anilox_Roll_Ruling**	**Dot_Percentage**	**Hue_Error**
76	900	4	50
76	1200	4	50
109	900	4	20
109	1200	4	40
76	900	8	50
76	1200	8	43
109	900	8	13
109	1200	8	38
76	900	12	33
76	1200	12	40
109	900	12	18
109	1200	12	23

Table 5.19: Magenta dataset

Paper_Roughness	Anilox_Roll_Ruling	Dot_Percentage	Hue_Error
76	900	4	50
76	1200	4	33
109	900	4	33
109	1200	4	60
76	900	8	71
76	1200	8	50
109	900	8	50
109	1200	8	78
76	900	12	60
76	1200	12	55
109	900	12	54
109	1200	12	57

Table 5.20: Yellow dataset

Paper_Roughness	Anilox_Roll_Ruling	Dot_Percentage	Hue_Error
76	900	4	25

76	1200	4	25
109	900	4	20
109	1200	4	14
76	900	8	13
76	1200	8	14
109	900	8	11
109	1200	8	10
76	900	12	17
76	1200	12	9
109	900	12	8
109	1200	12	7

Table 5.21: Black dataset

Paper_Roughness	**Anilox_Roll_Ruling**	**Dot_Percentage**	**Hue_Error**
76	900	4	67
76	1200	4	75
109	900	4	67

109	1200	4	67
76	900	8	50
76	1200	8	75
109	900	8	67
109	1200	8	67
76	900	12	67
76	1200	12	75
109	900	12	50
109	1200	12	67

5.2.3.4 Results

The result obtained at the output of machine learning algorithms are given at Tables 5.18-5.21 for each C, M, Y and K process colors. The loss functions of various algorithms for each color is taken as the assessment tool for comparison. Performance accuracy is measured on the basis of loss functions which indicates the ability of established model to predict the outcome based on the input variables provided and is given in Tables 5.23-5.28. The Table 5.22 shows the splitting of dataset.

Table 5.22: Splitting of dataset

Shape of data:	(100, 4)
Shape of split data:	The shape of X_train: (75, 3)

	The shape of X_test: (25, 3)
	The shape of Y_train: (75, 3)
	The shape of Y_test: (25, 3)

Table 5.23: Loss functions of hue error with linear regression algorithm

Process Color	**Linear Regression (LR)**			
	MSE	RMSE	MAE	R^2
Cyan	28.1653	5.3071	3.5038	0.5947
Magenta	40.06	6.3293	4.1471	0.0183
Yellow	14.8179	3.8494	2.3847	0.3432
Black	101.2197	10.0608	8.1093	-0.2188

Table 5.24: Loss functions of hue error with decision tree regression algorithm

Process Color	**Decision Tree Regression (DT)**			
	MSE	RMSE	MAE	R^2
Cyan	13.5844	3.9857	2.8461	0.7714
Magenta	65.4788	8.0919	4.8333	-0.6046
Yellow	7.4273	2.7253	1.6423	0.6708
Black	75.2643	8.6755	5.5	0.0937

Table 5.25: Loss functions of hue error with random forest regression algorithm

Process Color	**Random Forest Regression (RF)**			
	MSE	RMSE	MAE	R^2
Cyan	9.4218	3.0695	2.2604	0.8644
Magenta	32.1818	5.6729	4.0679	0.2113
Yellow	3.7648	1.9403	1.4114	0.8331
Black	57.1929	7.5626	5.6389	0.3113

Table 5.26: Loss functions of hue error with XG boost regression algorithm

Process Color	**XG Boost Regression (XGB)**			
	MSE	RMSE	MAE	R^2
Cyan	9.3758	3.062	2.2547	0.865
Magenta	65.0265	8.0639	5.3306	-0.5935
Yellow	5.7188	2.3914	1.3837	0.7465
Black	49.1653	7.0118	4.3691	0.4079

Table 5.27: Loss functions of hue error with support vector machines regression algorithm

Process Color	**Support Vector Machines Regression (SVM)**			
	MSE	RMSE	MAE	R^2
Cyan	40.5616	6.3688	3.3569	0.4163
Magenta	35.7915	5.9826	4.1265	0.1228
Yellow	17.7679	4.2152	2.2424	0.2124
Black	112.3197	10.5981	8.1154	-0.3525

Table 5.28: Loss functions of hue error with neural network algorithm

Process Color	**Neural Network (NN)**			
	MSE	RMSE	MAE	R^2
Cyan	9.0505	3.0084	2.2154	0.8843
Magenta	30.217	5.497	3.9418	0.2423
Yellow	3.7091	1.9259	1.401	0.8405
Black	53.1164	7.2881	5.4342	0.3476

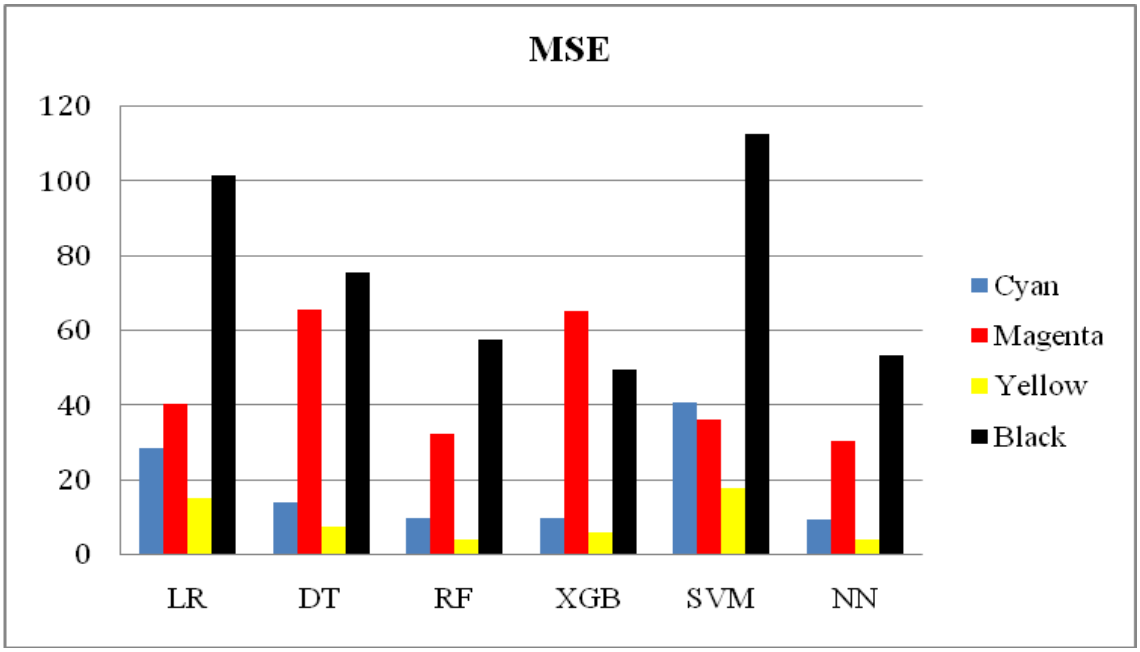

Figure 5.37: Bar chart of MSE values for different machine learning algorithms

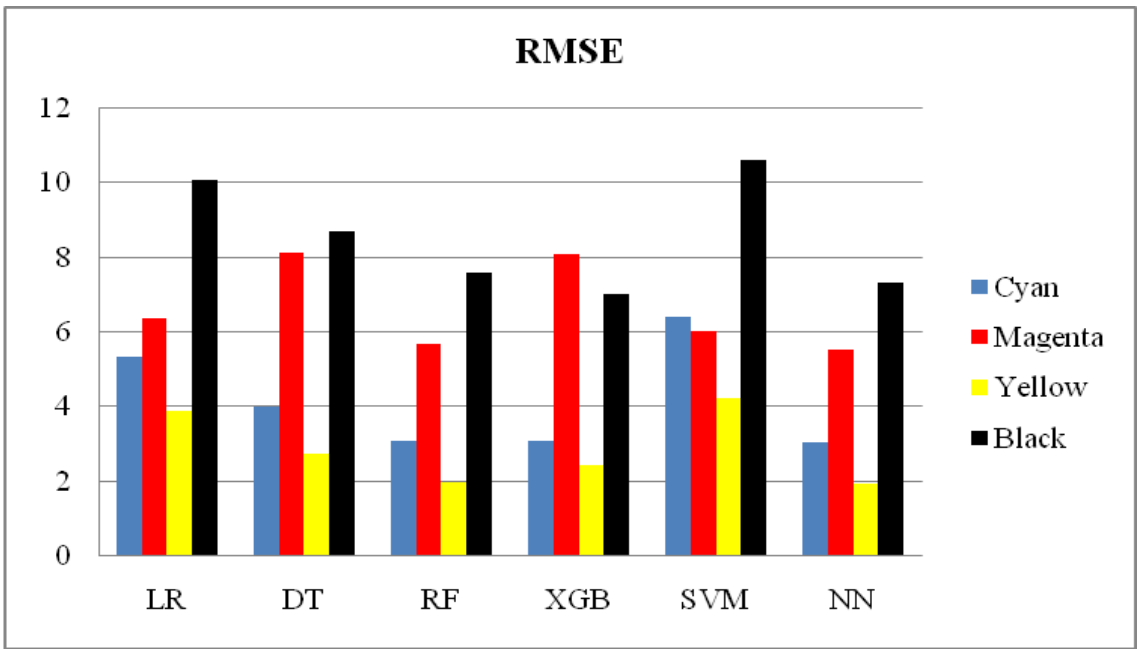

Figure 5.38: Bar chart of RMSE values for different machine learning algorithms

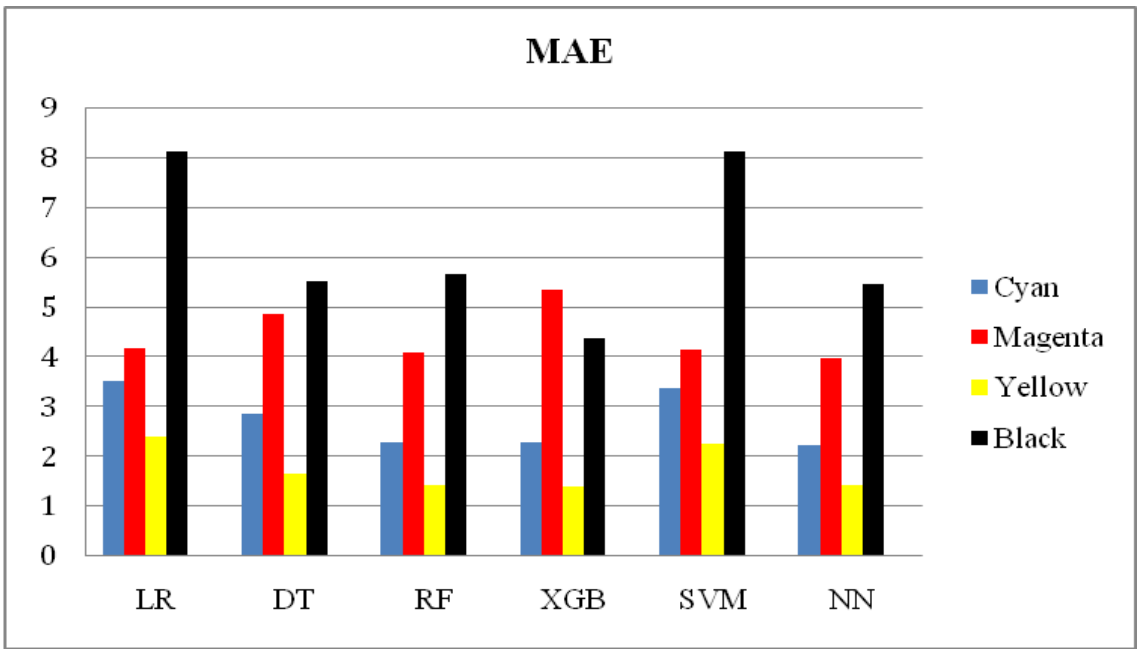

Figure 5.39: Bar chart of MAE values for different machine learning algorithms

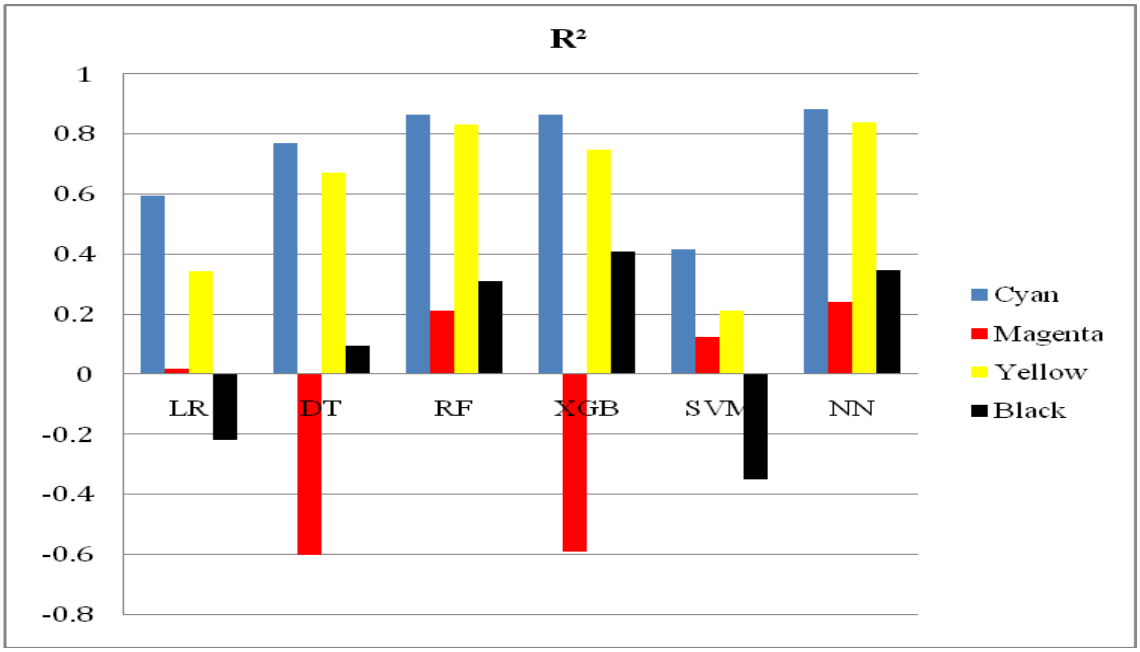

Figure 5.40: Bar chart of R^2 score for different machine learning algorithms

Figure 5.37 represents the Mean Squared Error (MSE) for the different machine learning algorithms adopted for prediction of hue error in flexography printing process. MSE signifies the average squared difference between the actual values and predicted values by a model. A lower value of MSE indicates the accuracy of the model to be used for prediction. It has been found that MSE is lowest in neural network (NN) which implies it is the best model for prediction out of the models considered.

Figure 5.38 shows the Root Mean Squared Error (RMSE) for the different machine learning algorithms. The differences between the predicted values and actual values are quantified by RMSE. It has been found that RMSE is least for neural network (NN) which indicates it is best for this prediction.

Figure 5.39 represents the bar chart of Mean Absolute Error (MAE) for the different machine learning algorithms adopted for prediction. The average absolute differences between the actual and the predicted values are measured by MAE. It has been observed that MAE value is the lowest for the neural network (NN). This indicates that neural network (NN) is the best of all the machine learning algorithms considered for the prediction of hue error in the present work.

Figure 5.40 illustrates the bar chart of R^2 values for the different machine learning algorithms adopted for the prediction of hue error. It implies the percentage of variation in the target variables that can be obtained by the independent variables. The maximum value of R^2 is 1. The more the R^2 value the better is the prediction. It has been observed that R^2 value for the neural network (NN) method is maximum and close to 1 which means that this method is the best for the prediction of hue error in the current investigation. The values of loss functions of different machine learning algorithms shown in Tables 5.23-5.28 were derived by considering the values given in Figures 5.37-5.40.

5.2.3.4.1 Graphical Analysis

The graphical representations show the status of residual data revealed during the analysis phase, the nature of the dataset distribution and the interaction between different parameters involved in the experimental process. The Figures 5.41-5.52 have been plotted using Minitab 17 statistical software.

Figures 5.41-5.44 represent the residual plot of hue error of C, M, Y and K in neural network (NN) machine learning model.

Figures 5.45-5.48 show the main effect plot of hue error for C, M, Y and K adopting neural network (NN) machine learning model.

Figures 5.49-5.52 represent the interaction plot of hue error for C, M, Y and K using neural network (NN) machine learning model which provides the best fit for this case as shown in Tables 5.23-5.28.

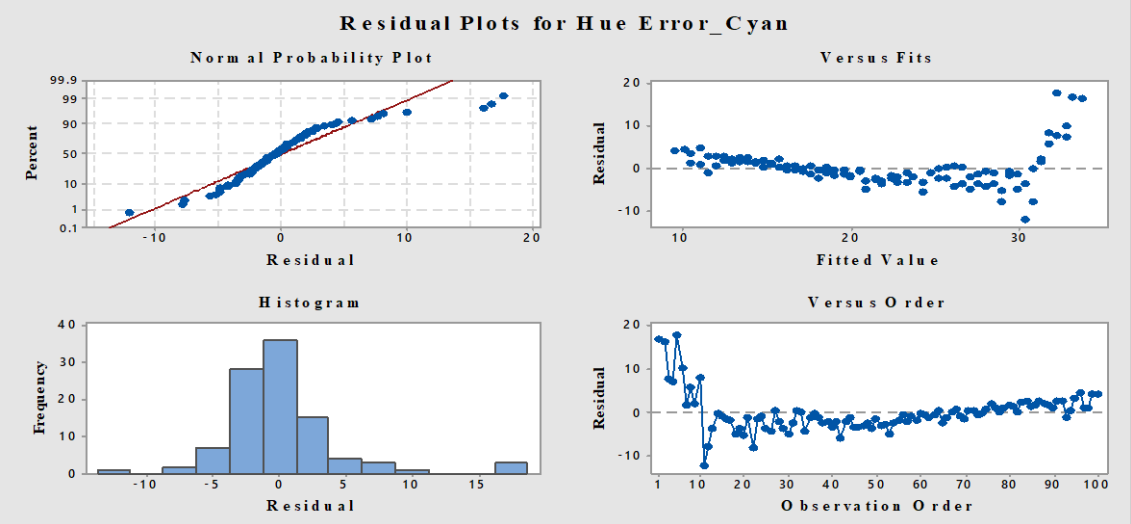

Figure 5.41: Residual plots of hue error for cyan

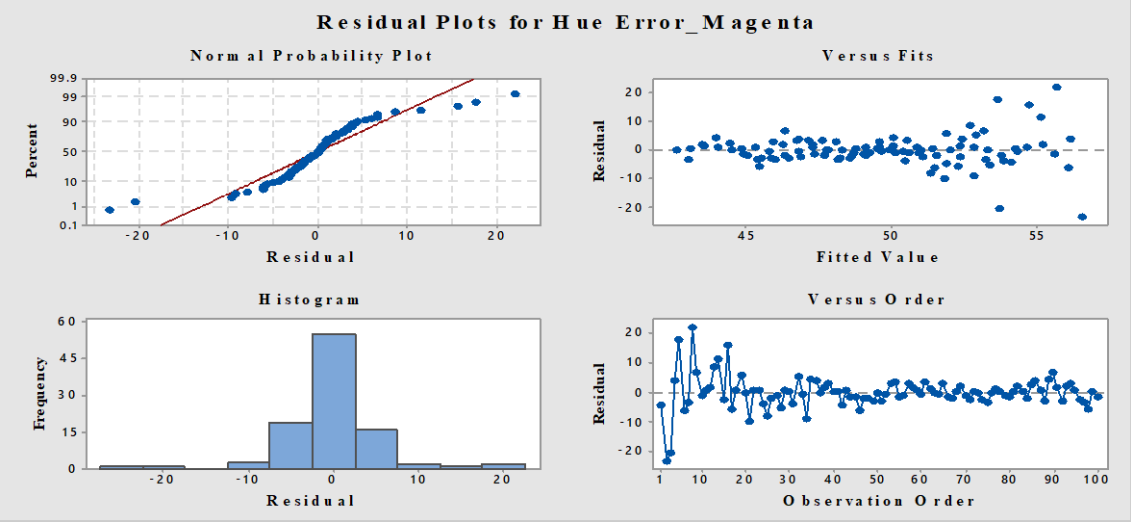

Figure 5.42: Residual plots of hue error for magenta

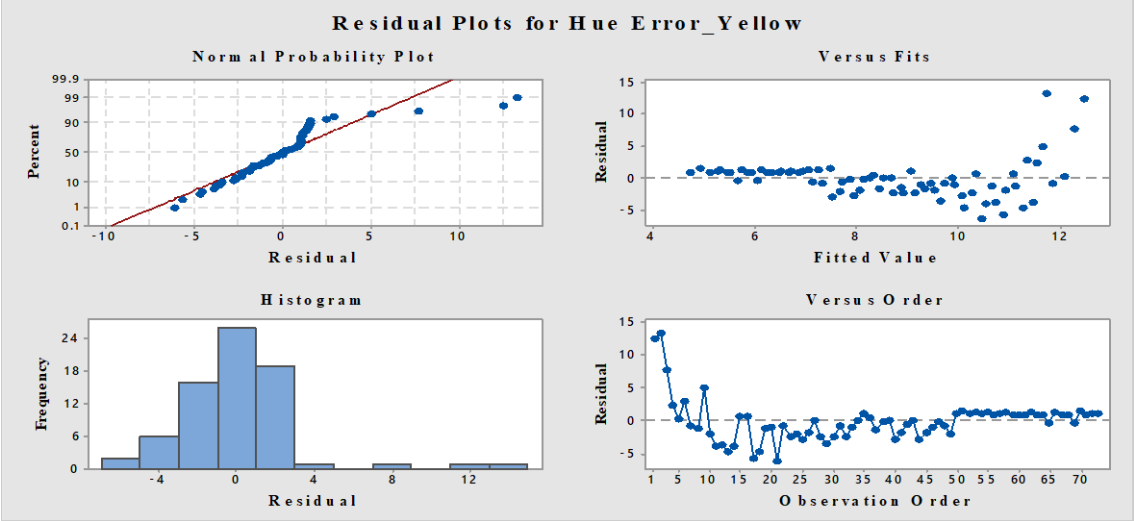

Figure 5.43: Residual plots of hue error for yellow

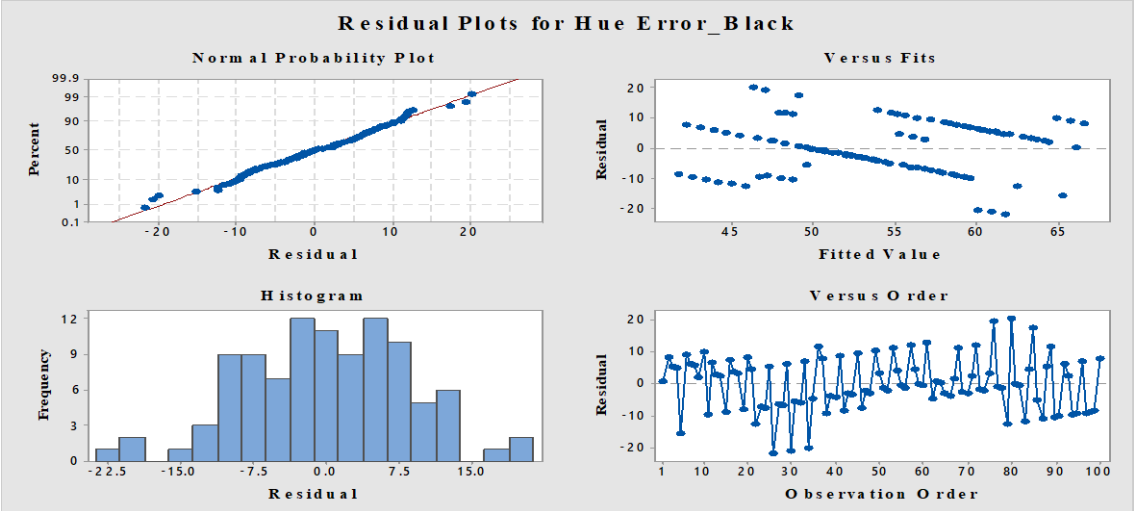

Figure 5.44: Residual plots of hue error for black

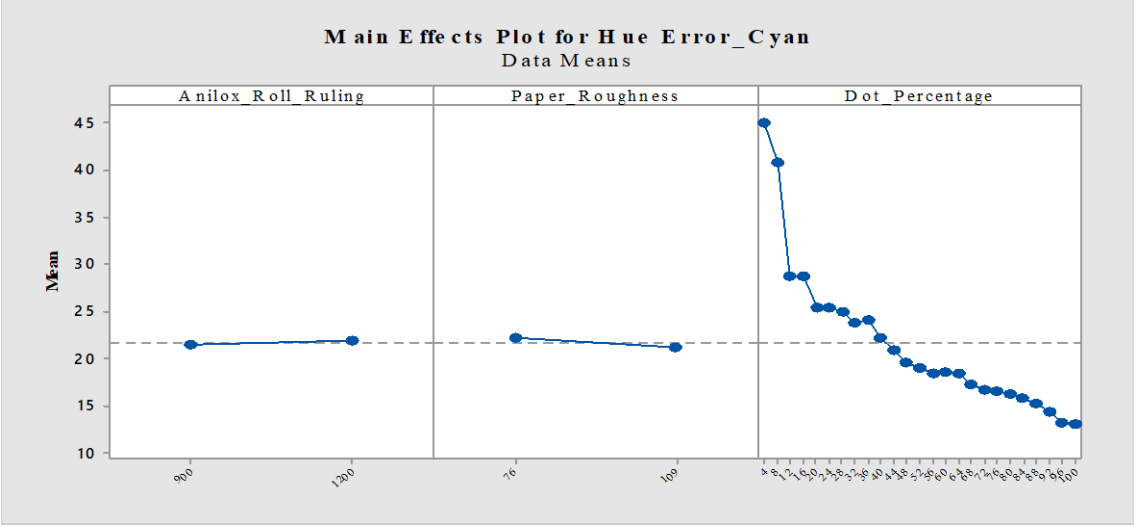

Figure 5.45: Main effects plot of hue error for cyan

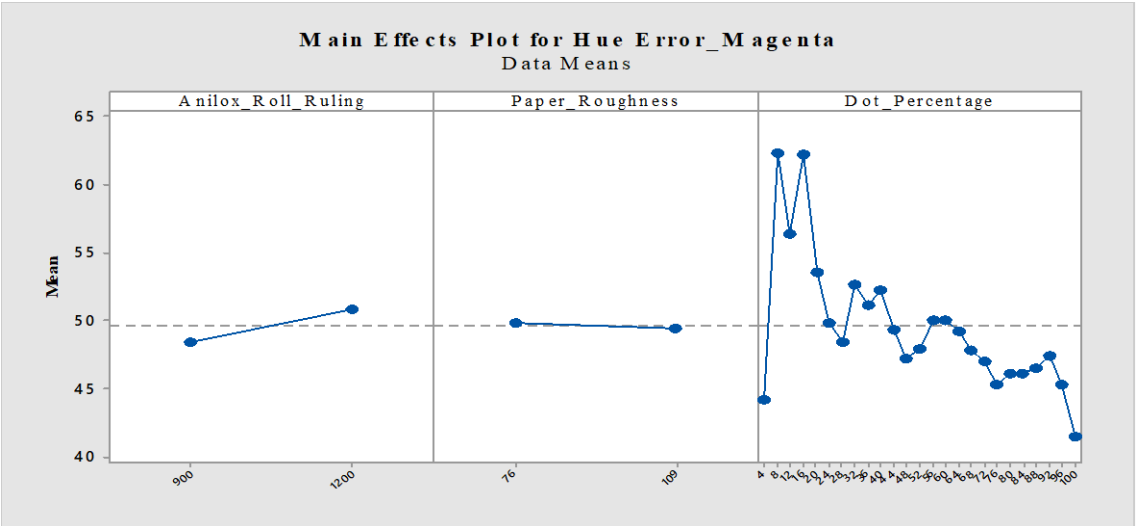

Figure 5.46: Main effects plot of hue error for magenta

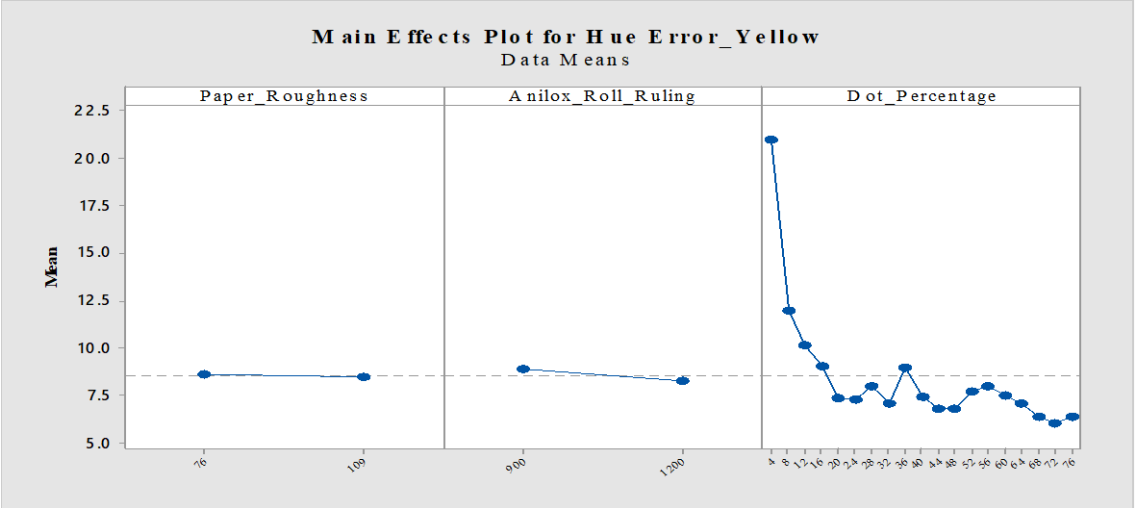

Figure 5.47: Main effects plot of hue error for yellow

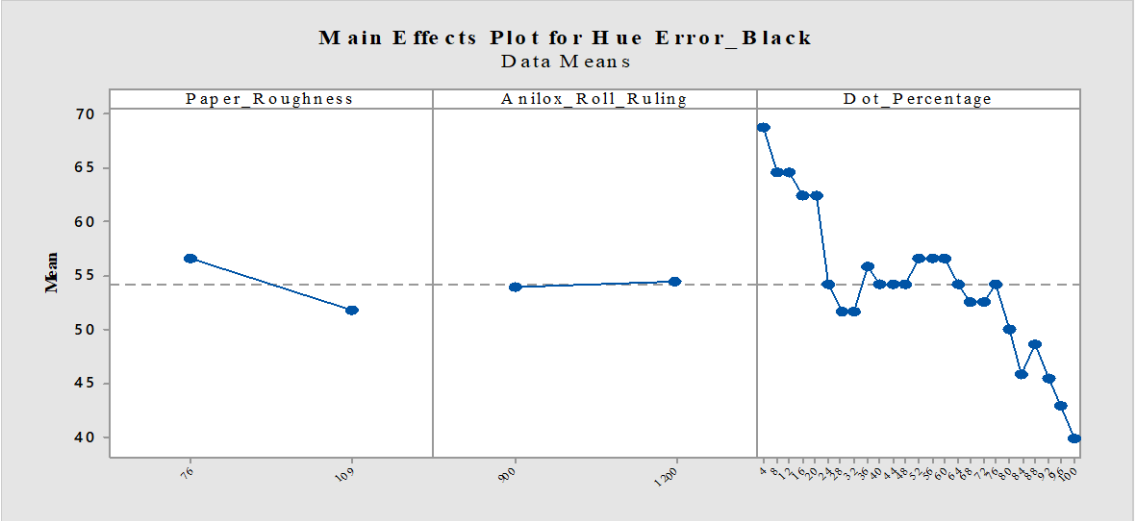

Figure 5.48: Main effects plot of hue error for black

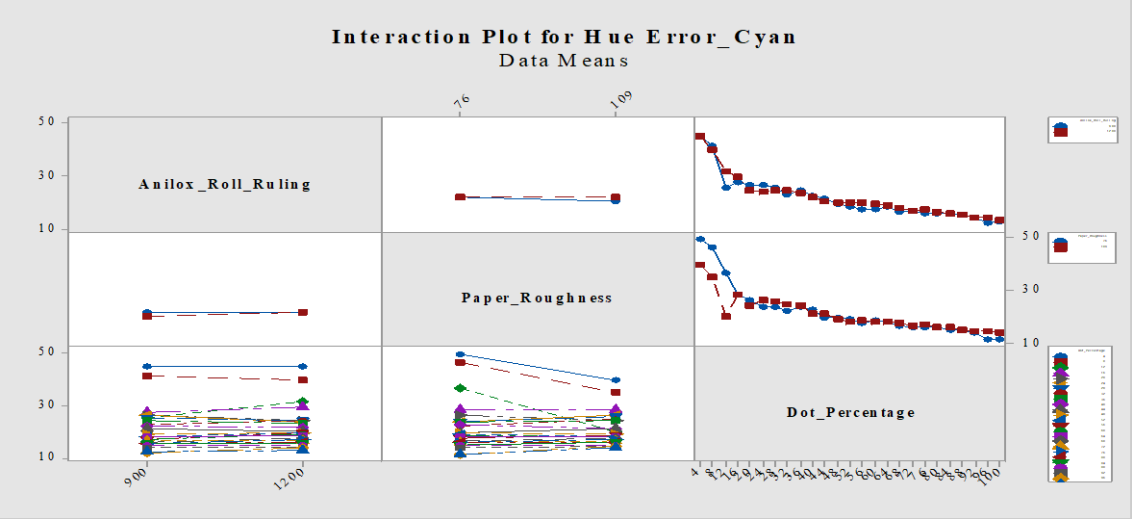

Figure 5.49: Interaction plot of hue error for cyan

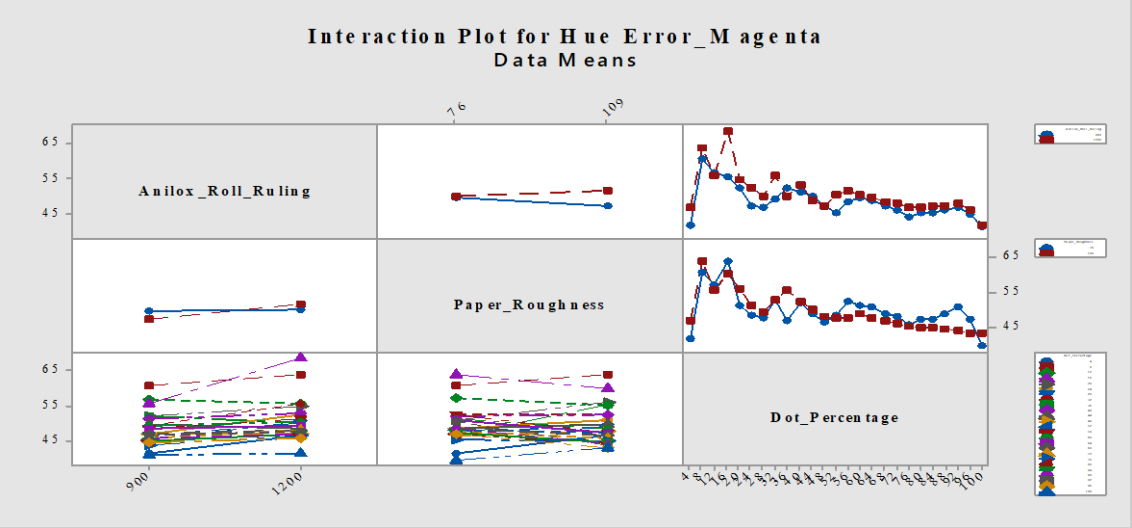

Figure 5.50: Interaction plot of hue error for magenta

Figure 5.51: Interaction plot of hue error for yellow

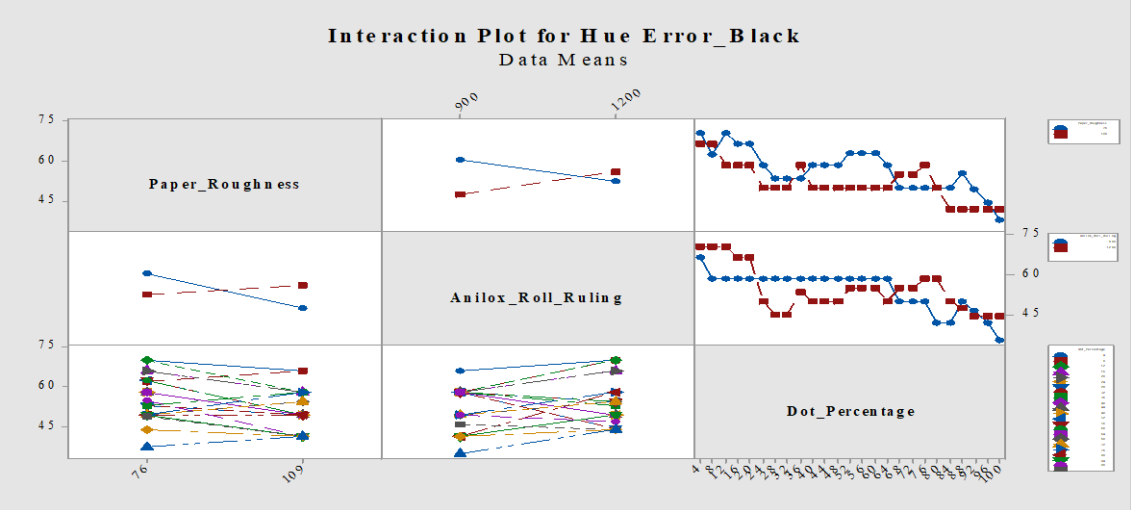

Figure 5.52: Interaction plot of hue error for black

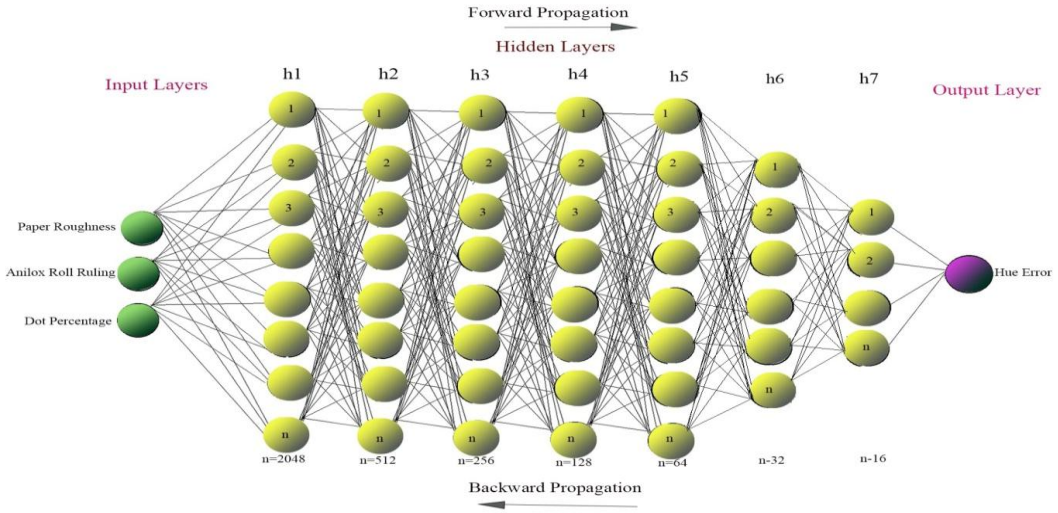

Figure 5.53: Machine learning algorithm of neural network architecture in the study

5.2.3.5 Discussions

The machine learning has expanded quickly in recent years within the framework of computing and data analysis which usually enables the applications to operate intelligently. This work has implemented some machine learning algorithms in the hue error assessment of four color flexography printing work.

The Tables 5.23-5.28 represents the summary of loss functions obtained for various machine learning models in the prediction of hue error. Through python program execution, it is found that the estimation of hue errors obtained for cyan, magenta, yellow and black colors with neural network (NN) algorithm is better than other

machine learning methods. This confirms that the neural network (NN) is a better technique in the prediction process than that of the tested algorithms such as linear regression (LR), decision tree (DT), random forest (RF), XG boost regression, SVM etc. The neural network (NN) is superlative in performance with its special features like comparatively more number of hyper parameters, epochs, layers etc. than that of other algorithms.

The result shown in Tables 5.23-5.28 indicates the nature of inconsistencies occurred in the dataset among different process colors. Thus measuring and managing the color and contamination of printing ink is a crucial step in printing. There are many reasons behind the occurrence of hue error in multi color printing work. The reasons behind this contamination may be due to the manufacturing defects of printing ink, printing practices with lack of knowledge on color reproduction, the halftone dot reproduction with undesirable dot gain issues, the anilox roller screen rulings and geometry of anilox cells, the trapping of contaminating ink particles in the anilox roller cells, the paper and ink characteristics, printing sequence of process colors etc. Considering all these factors, the chance of hue error among the process colors is most common thing in the printing practices.

In this research work the printing sequence are executed as Y, C, M and K and this sequence promotes the chance of hue error variations is minimum in process colors. The ink contamination during the printing process or within the machine can be minimized by setting up the process color sequence accordingly as per the features of image to be printed as well as the characteristics of printing ink used.

The hue error issues are more dynamic in nature with the undesirable dot gain and dot loss associated with each of the process colors. The dot gain issues are also there in the work.

The Figures 5.41-5.44 indicates the residual data existed in each process color dataset. There are several areas where the typical distribution of residuals appears to be asymmetrical. The normal probability plot provides visual information about the diversion of response from the normal distribution. The versus fit plot which illustrates the non-linearity, outliers, and undesired errors related to the dataset discovered throughout the experiment. The histogram in residual plot shows the frequency of

residuals found in the work. The suitability of data collection and the serial correlation of mistakes in the experimental sequence are depicted with versus order plot.

The higher the screen count smaller may be the cell size, so that the chance of clogging will be more with the cells. The hexagonal geometry of the cell enhances optimal ink discharge and thus minimizes the chance of ink clogging. Also, the flexography inking with lower anilox ruling considerably promotes higher ink deposit on to the substrate at printing that may accelerates the visual effect of hue error to some extent if the ink is contaminated. At the same time, the higher screen ruling of anilox meters the ink precisely and as a result the visual recognition of hue error will be suppressed.

The hue error also has influence in the various tonal ranges of the printed image. The contamination will shift the ink hue towards an unwanted hue. This effect will be more prominent at various tonal regions. The color shift in the highlight areas is more than that of shadow areas. If the contamination is towards the complementary hue in the printing, purity will be lost. If the shift is analogous in nature the printed hue will shift towards the contaminated hue.

Practically, the yellow ink is least transparent in nature. Also, with wet on wet printing sequence, the contamination propensity for yellow is more when compared to other process color inks. Due to these reasons, the yellow is printed first. For this reason, the yellow ink in this case possesses the least hue error.

In addition, the surface properties of paper, particularly its roughness and absorptivity, have an impact in color reproduction. More irregular paper surfaces will disperse light more unevenly, and more the absorptivity of paper more will be the absorption of either pigment and/or ink carriers, resulting in reducing gloss, or in an unexpected hue shift. Based on the characteristics of the paper and ink, the droplet will begin to spread and wet the surface as soon as it comes into contact with it. The colorant deposition will vary based on the formulations utilized. Improvements in optical density, saturation, and color may be achieved with a more consistent hue when the right whiteness values, sizing agent, filler content and surface finishing technique are used.

The main effects plot for cyan, magenta, yellow and black reproductions with hue error are shown from Figures 5.45-5.48 and the interaction plots are illustrated from the Figures 5.49-5.52. The results of these plots indicate that the hue error is lesser in

uncoated paper than coated paper. As the anilox line frequency increases the hue error also increased except for yellow which is printed as first color. This may be due to the unwanted clogging of ink particles within the tiny cells than that of the coarser lower line frequency. The dot percentage at various tonal levels shows higher hue error at highlight area than that of middle-tones and shadows. As the tonal value increases the hue error effect is diminishing in nature.

The Figure 5.53 represents that three input layers, one output layer and seven hidden layers. A deep feedforward neural network was designed using Keras to model the regression task. The network architecture begins with an input layer of 3 features, followed by a series of fully connected (dense) layers with decreasing units: 2048, 512, 256, 128, 64, 32, and 16 neurons respectively. Each hidden layer utilizes the Leaky ReLU activation function (with a negative slope coefficient of 0.01) to mitigate the dying ReLU problem and maintain small gradients for negative inputs. A dropout layer with a dropout rate of 0.1 was included after the 256 neuron layer to prevent overfitting by randomly deactivating a subset of neurons during training. The final output layer comprises a single neuron with a linear activation function to produce continuous-valued predictions. The model was compiled with the Mean Squared Error (MSE) loss function and optimized using the Adam optimizer with a learning rate of 4e - 5. To enhance generalization performance and prevent overfitting, 20% of the training data was reserved for validation using the validation_split parameter. Furthermore, early stopping was employed by monitoring the validation loss and halting the training process if no improvement was observed over a fixed number of epochs (50). This strategy ensures that the model does not over-train and remains robust to unseen data.

5.2.3.6 Conclusions

This research work study is focussed on to establish a machine learning model for the prediction of hue error related with four process colors printing in flexography. The main segments of this paper are settled as: the theoretical overview on the flexography printing and machine learning background, python programming with some important machine learning algorithms, performance evaluation and analysis of the results. The various machine learning approaches with linear regression, decision tree regression, random forest regression, XG Boost regression, SVM regression and neural networks are executed and evaluated. The outcome indicates that with the superlative features of

neural network (NN). This algorithm is better in the performance than that of all other tested algorithms. By using neural network (NN) machine learning algorithm, it can be possible to predict the quality of the print under specified conditions considering hue error as the print quality parameters.

5.3 Screen Printing

5.3.1 Screen Printing Black and White Prints for Dot Gain

5.3.1.1 Objective of the Study

The main objective is to establish a machine learning system to predict black and white dot gain in the screen printing. For this purpose different machine learning techniques such as linear regression, decision tree regression and random forest regressions were used.

5.3.1.2 Experimental Methods

The screen printing were carried out with three input variables such as paper substrates with two different roughness levels, screen mesh ruling with three different line rulings and AM and FM halftone dots with 114 dot area levels. The screen mesh rulings were chosen as 100 lpi, 120 lpi and 140 lpi. The paper roughnesses were selected as 36ml/min and 182 ml/min. The printing work was executed in screen printing machine such as ATOM 1520, APL Machinery Pvt. Ltd. with black ink. The parameters such as printing pressure, room temperature and ink features were kept constant throughout the printing process.

5.3.1.2.1 Measurements and Data Collection

The output response was taken as dot gain for the assessment of black and white prints. As a result, the output parameters were quantitatively measured using the Spectro-densitometer such as X-Rite Spectro Eye instrument. The input datasets for the machine learning algorithms were created from the readings of 114 print trials. The split ratio of training to test dataset was taken as 7:3. The collected data were given as input to the python program to process different machine learning algorithms. The Table 5.29 shows the parameters background at screen printing to assess the dot gain.

Table 5.29: Parameters background at screen printing

Factors	Unit	Symbol	Levels	Response
Screen Mesh Ruling	Lines per inch (lpi)	A	100, 120, 140	Dot Gain
Paper Roughness	Millilitre per minute (ml/min)	B	36, 182	
Dot Percentage	Percentage (%)	C	5% to 100 % with 5% increments	
Halftone Screening Type	-	D	AM, FM	

5.3.1.2.2 Programming to Train the Model

The programming codes were used to perform the machine learning algorithms such as linear regression, decision tree and random forest using python program. The influence of different input parameters over the output response are assessed with machine learning algorithms and loss functions are compared with each technique.

5.3.1.3 Dataset

Some samples of black dataset have been shown in Table 5.30.

Table 5.30: Black dataset for dot gain

Paper_Roughness	Screen_Mesh_Ruling	Dot_Percentage	Halftone_Screening_ Type	Dot_Gain
36	100	5	AM	12
36	120	5	AM	-4
36	140	5	AM	-5

182	100	5	FM	18
182	120	5	FM	-2
182	140	5	FM	-5
36	100	10	AM	19
36	120	10	AM	-7
36	140	10	AM	-10
182	100	10	FM	34
182	120	10	FM	13
182	140	10	FM	11

5.3.1.4 Results

The results obtained by using python programming at the different machine learning algorithms are given at Table 5.32. The summary of dataset as Table 5.31 is given. Performance accuracy of different machine learning algorithms are assessed by analyzing the loss functions.

Table 5.31: Splitting of dataset

	Paper_Roughness	**Screen_Mesh_Ruling**	**Dot_Percentage**	**Dot_Gain**
count	114	114	114	114
mean	109	120	50	22.921053
std	73.322297	16.402029	27.507039	11.940964
min	36	100	5	-10

30%	36	100	25	16.25
50%	109	120	50	23
70%	182	140	75	31
max	182	140	95	50
Shape of data	(144, 4)			
Shape of split data	The shape of X_train: (85, 3)			
	The shape of X_test: (29, 3)			
	The shape of Y_train: (85, 3)			
	The shape of Y_test: (29, 3)			

Table 5.32: Loss functions of various machine learning techniques

Machine Learning Algorithm	**MSE**	**RMSE**	**MAE**	**R^2**
Linear Regression (LR)	141.3454	11.8889	9.4178	0.1830
Decision Tree Regression (DT)	29.3017	5.4131	3.5992	0.8306
Random Forest Regression (RF)	12.2104	3.4943	2.4612	0.9294

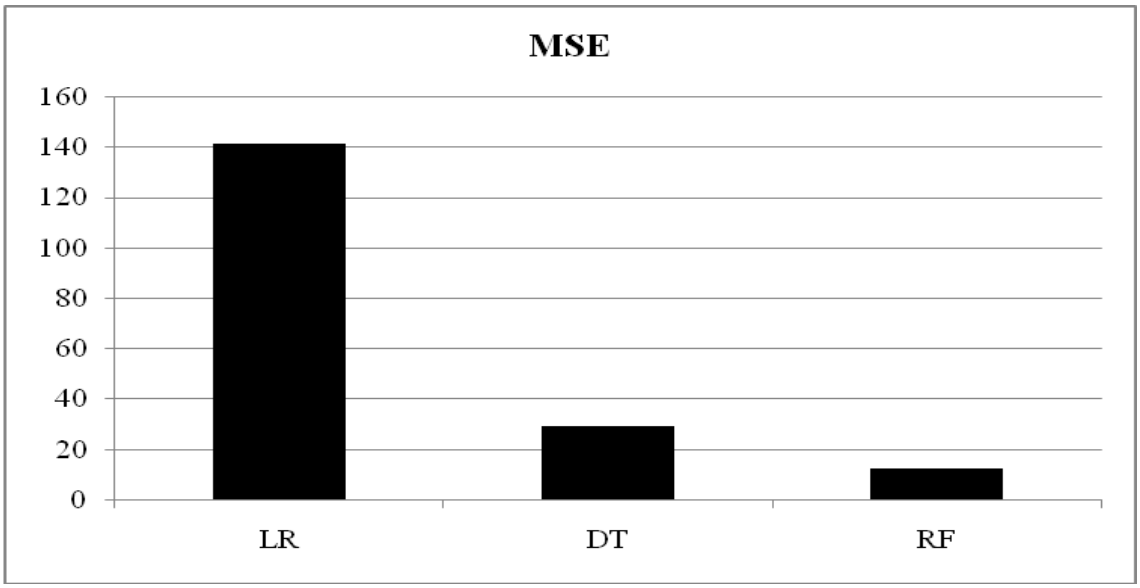

Figure 5.54: Bar chart of MSE values for different machine learning algorithms

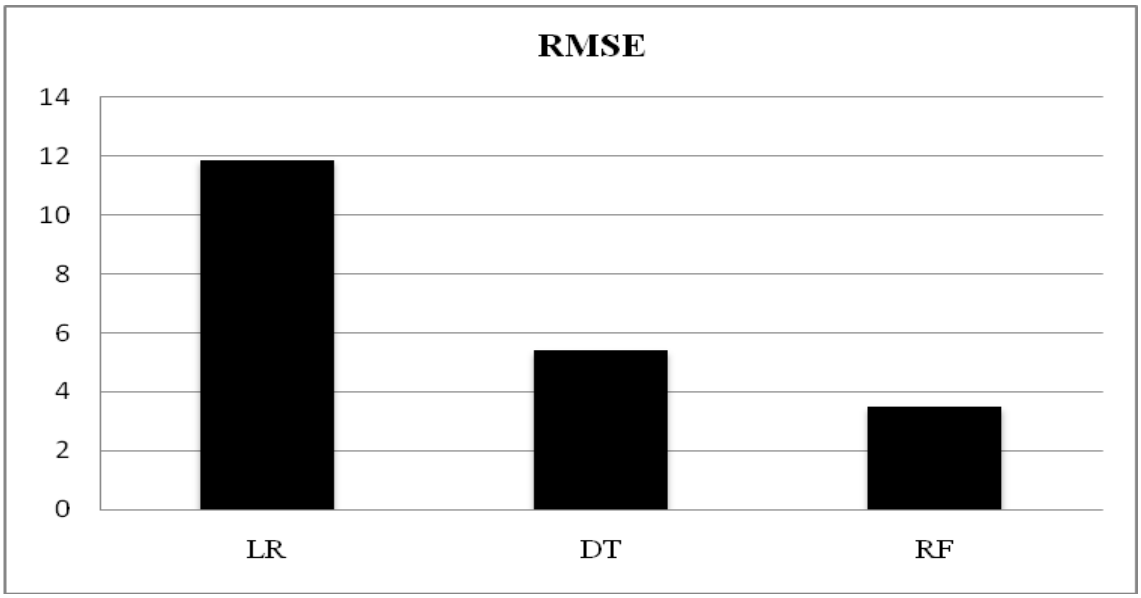

Figure 5.55: Bar chart of RMSE values for different machine learning algorithms

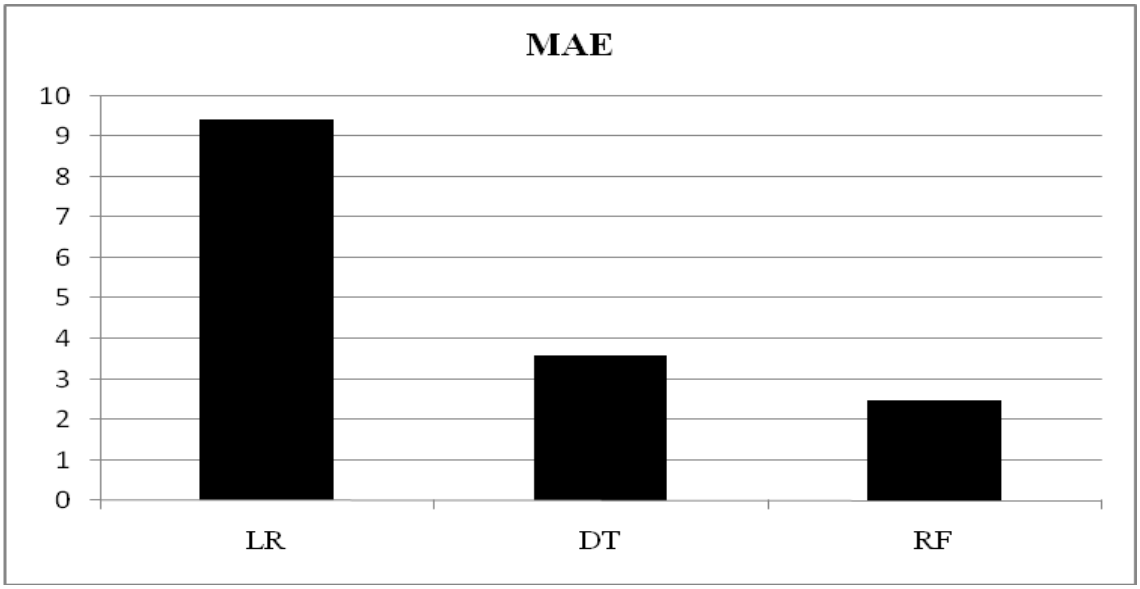

Figure 5.56: Bar chart of MAE values for different machine learning algorithms

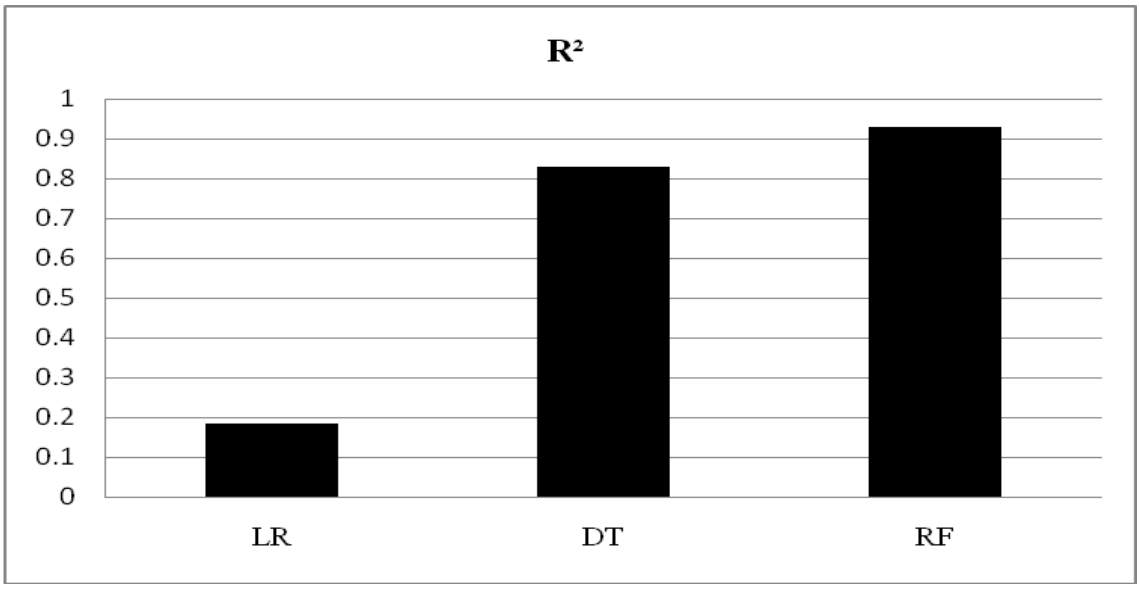

Figure 5.57: Bar chart of R^2 score for different machine learning algorithms

Figure 5.54 shows the Mean Squared Error (MSE) for the different machine learning algorithms adopted for prediction of dot gain in black and white screen printing process. MSE signifies the average squared difference between the actual values and predicted values by a model. A lower value of MSE indicates the accuracy of the model to be used for prediction. It has been found that MSE is lowest in random forest (RF) which implies it is the best model for prediction out of the models considered.

Figure 5.55 represents the Root Mean Squared Error (RMSE) for the different machine learning algorithms. The differences between the predicted values and actual values are quantified by RMSE. It has been found that RMSE is least for random forest (RF) which indicates it is best for this prediction.

Figure 5.56 illustrates the bar chart of Mean Absolute Error (MAE) for the different machine learning algorithms adopted for prediction. The average absolute differences between the actual and the predicted values are measured by MAE. It has been observed that MAE value is the lowest for the random forest (RF). This indicates that random forest (RF) is the best of all the machine learning algorithms considered for the prediction of dot gain in the present work.

Figure 5.57 shows the bar chart of R^2 values for the different machine learning algorithms adopted for the prediction of dot gain. It implies the percentage of variation in the target variables that can be obtained by the independent variables. The maximum value of R^2 is 1. The more the R^2 value the better is the prediction. It has been observed that R^2 value for the random forest (RF) method is maximum and close to 1 which means that this method is the best for the prediction of dot gain in the current investigation. The values of loss functions of different machine learning algorithms shown in Table 5.32 were derived by considering the values given in Figures 5.54-5.57.

5.3.1.4.1 Graphical Analysis

The graphical plots Figures 5.58-5.68 using Minitab 17 statistical software, represent the nature of distribution of datasets, residuals found at the analysis portion and the relationship among various parameters connected with the experimental process.

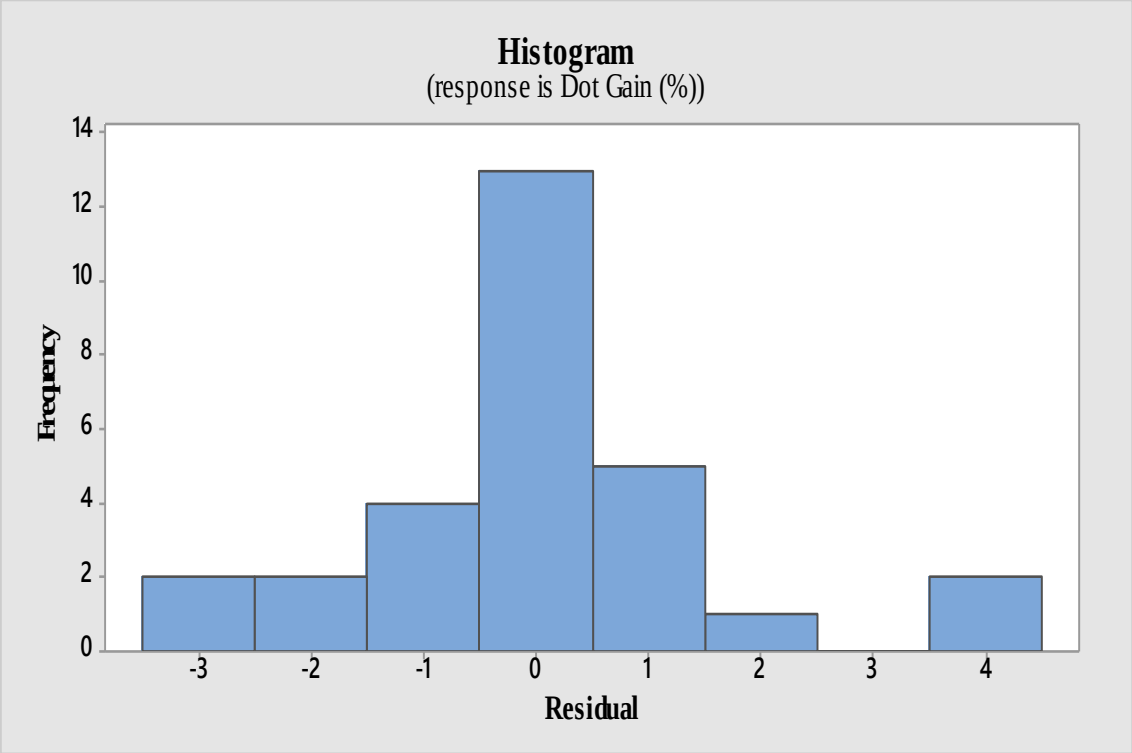

Figure 5.58: Residual plot for dot gain in histogram

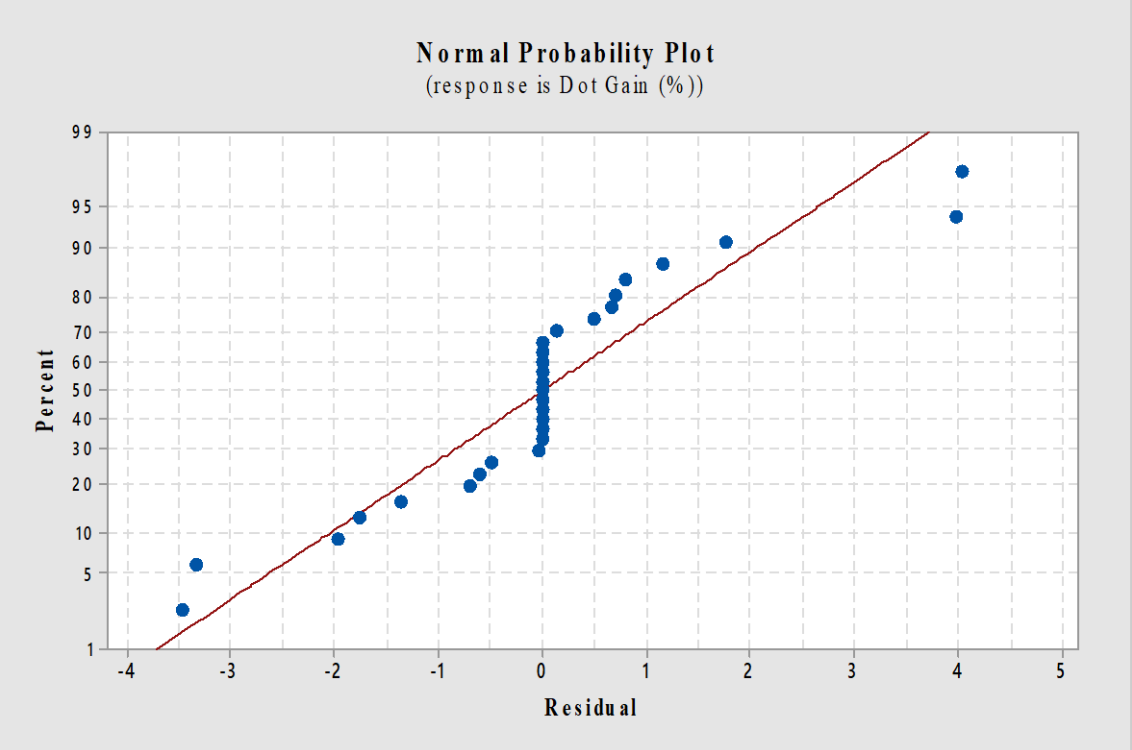

Figure 5.59: Normal probability plot for dot gain

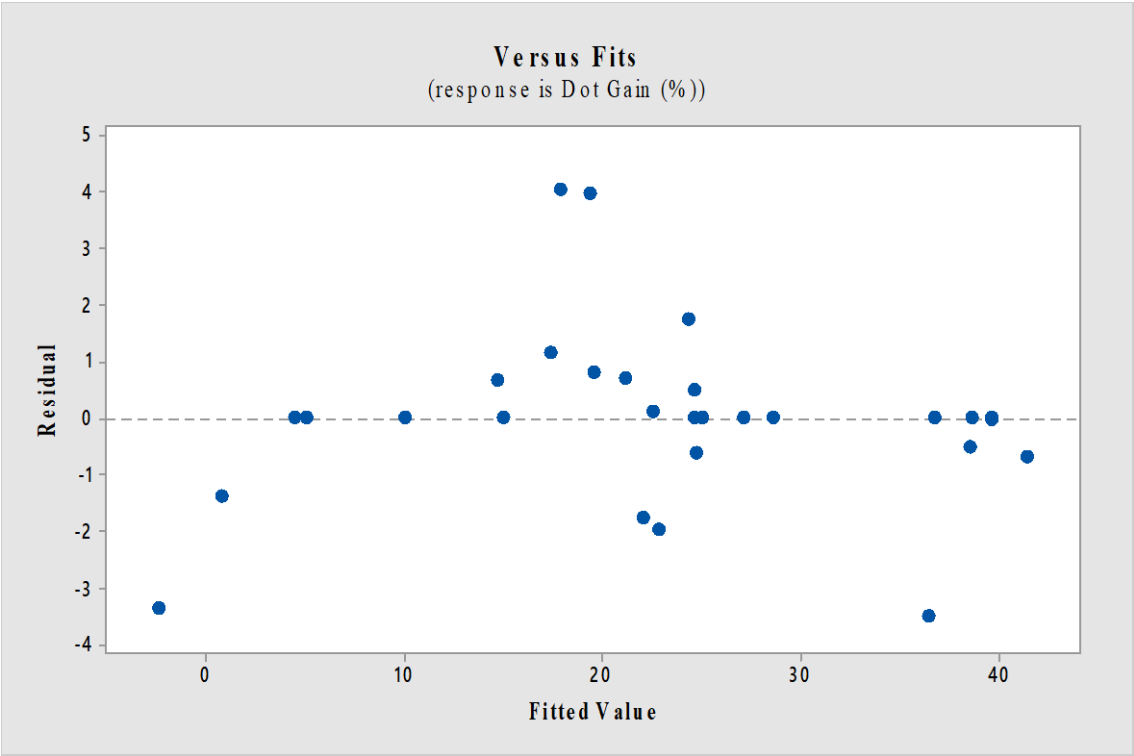

Figure 5.60: Versus fit plot for dot gain

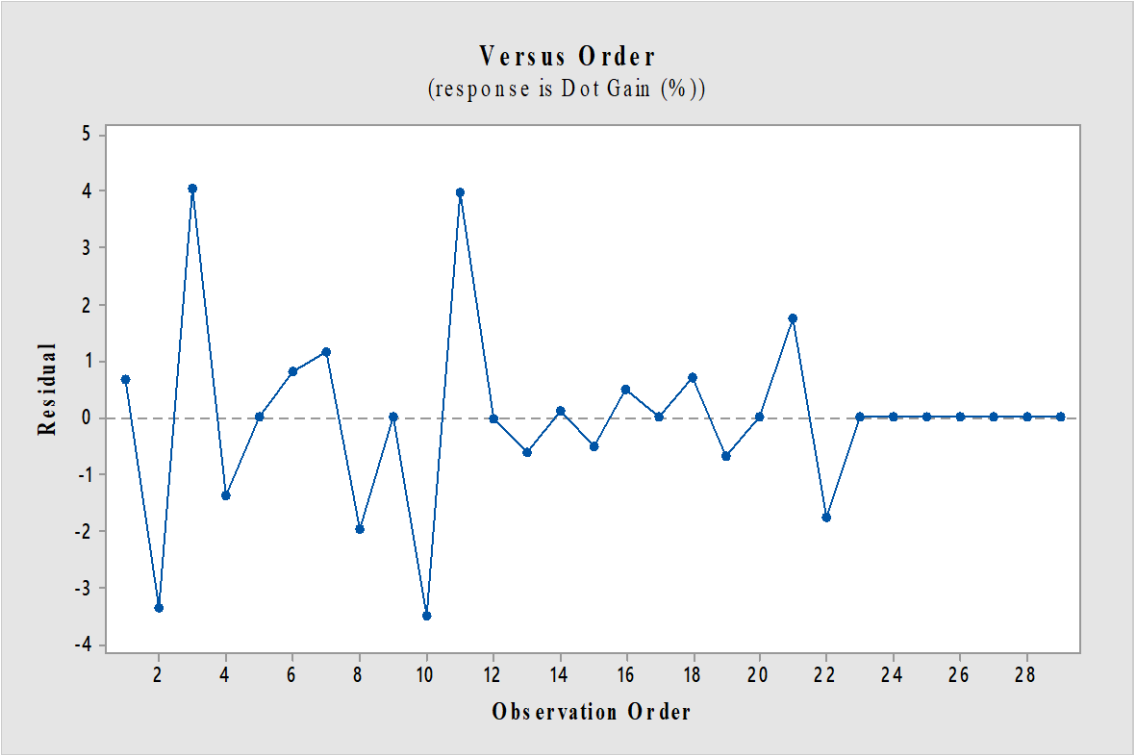

Figure 5.61: Versus order plot for dot gain

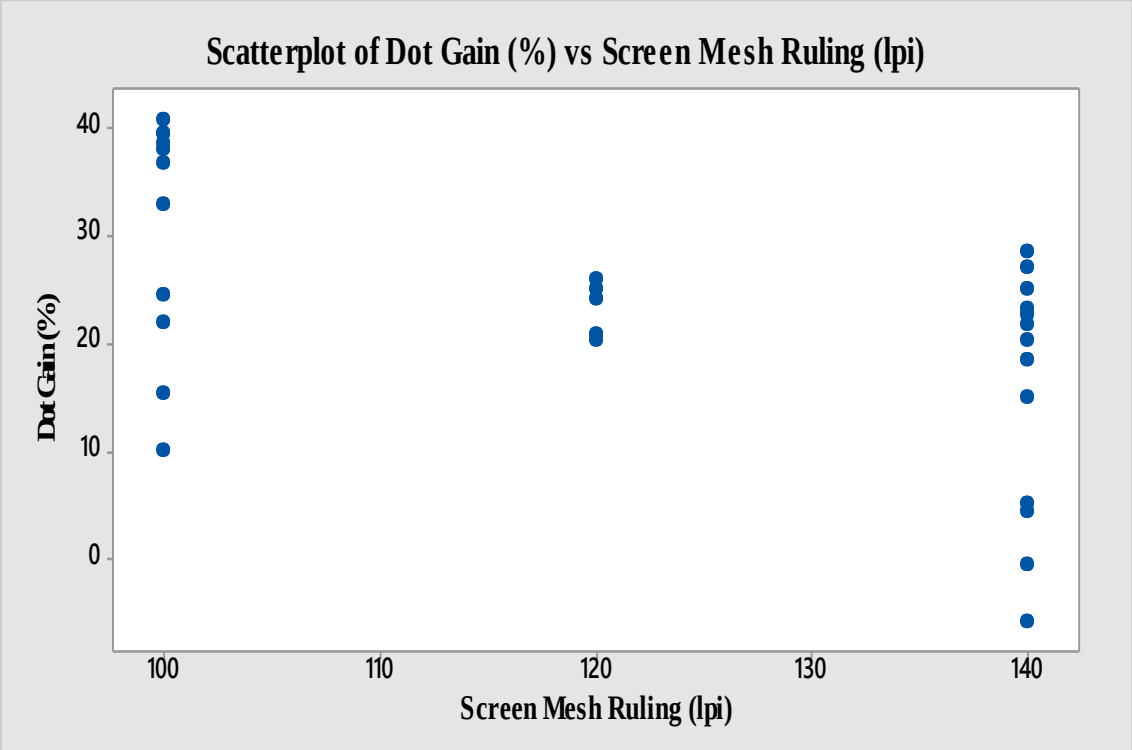

Figure 5.62: Scatterplot of dot gain vs screen mesh ruling

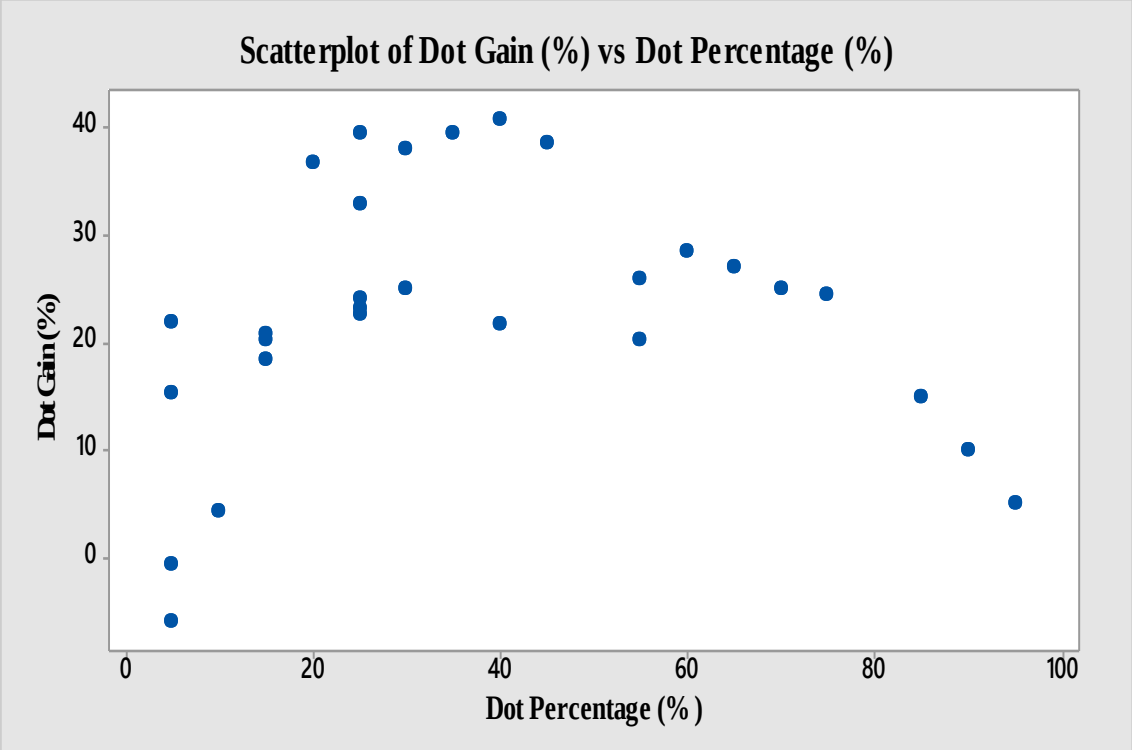

Figure 5.63: Scatterplot of dot gain vs dot percentage

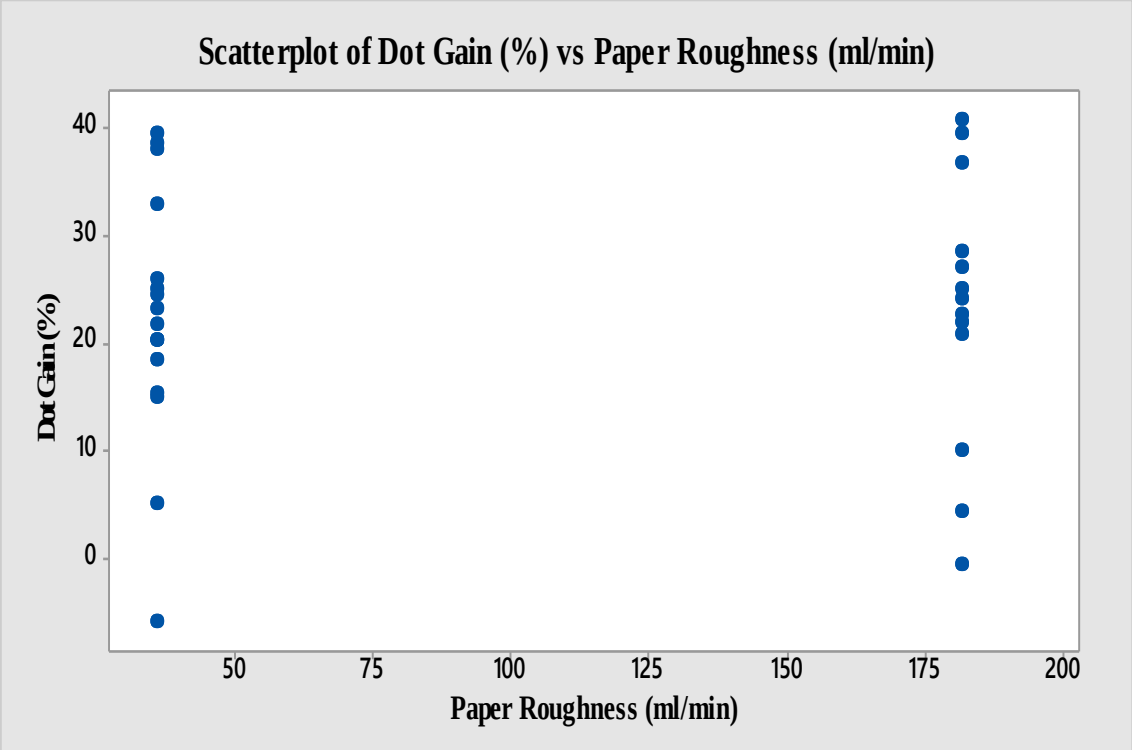

Figure 5.64: Scatterplot of dot gain vs paper roughness

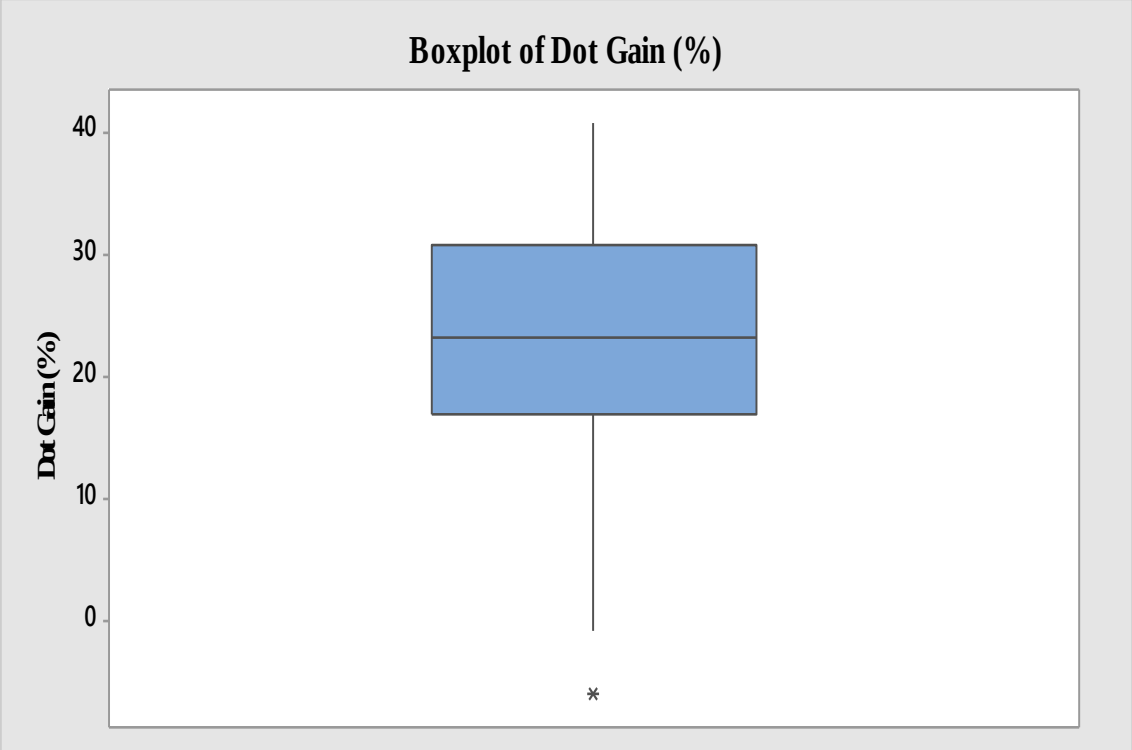

Figure 5.65: Boxplot of dot gain

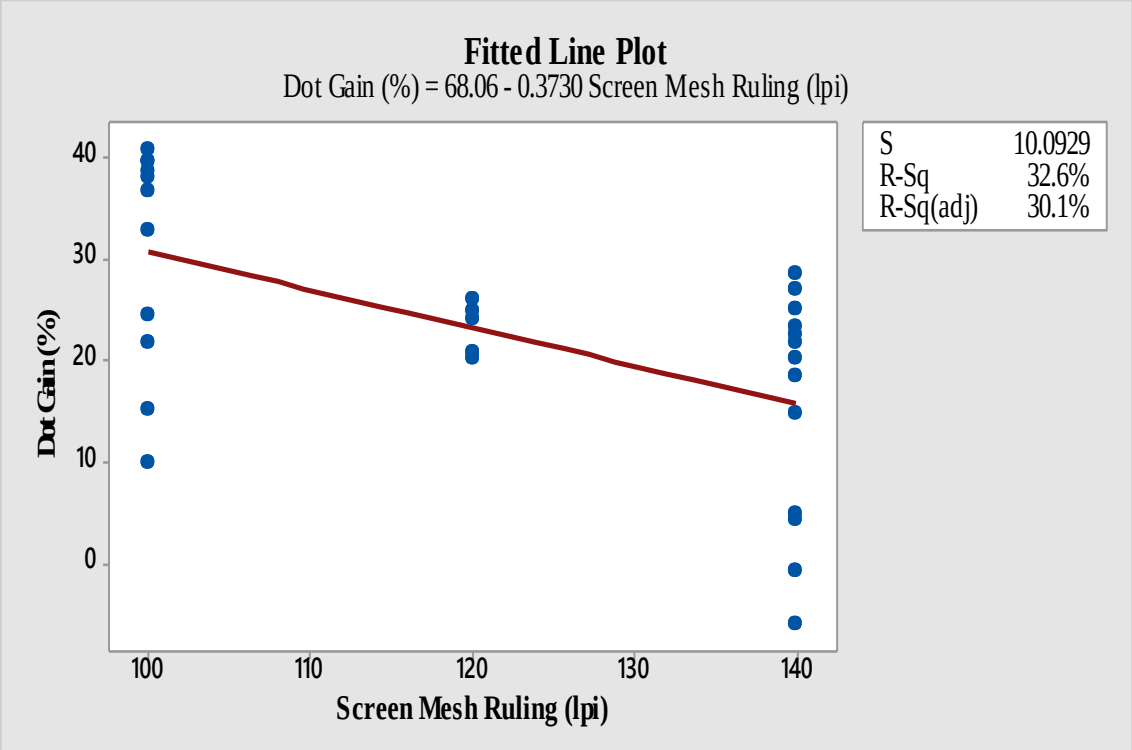

Figure 5.66: Fitted line plot for dot gain vs screen mesh ruling

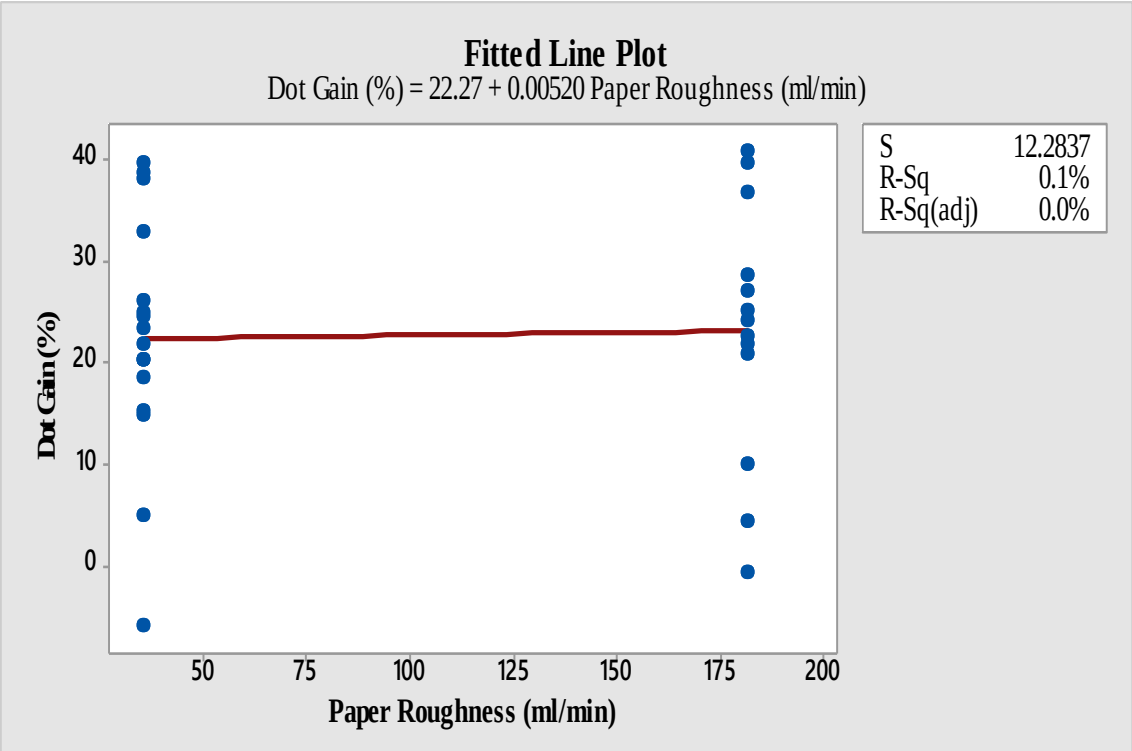

Figure 5.67: Fitted line plot for dot gain vs paper roughness

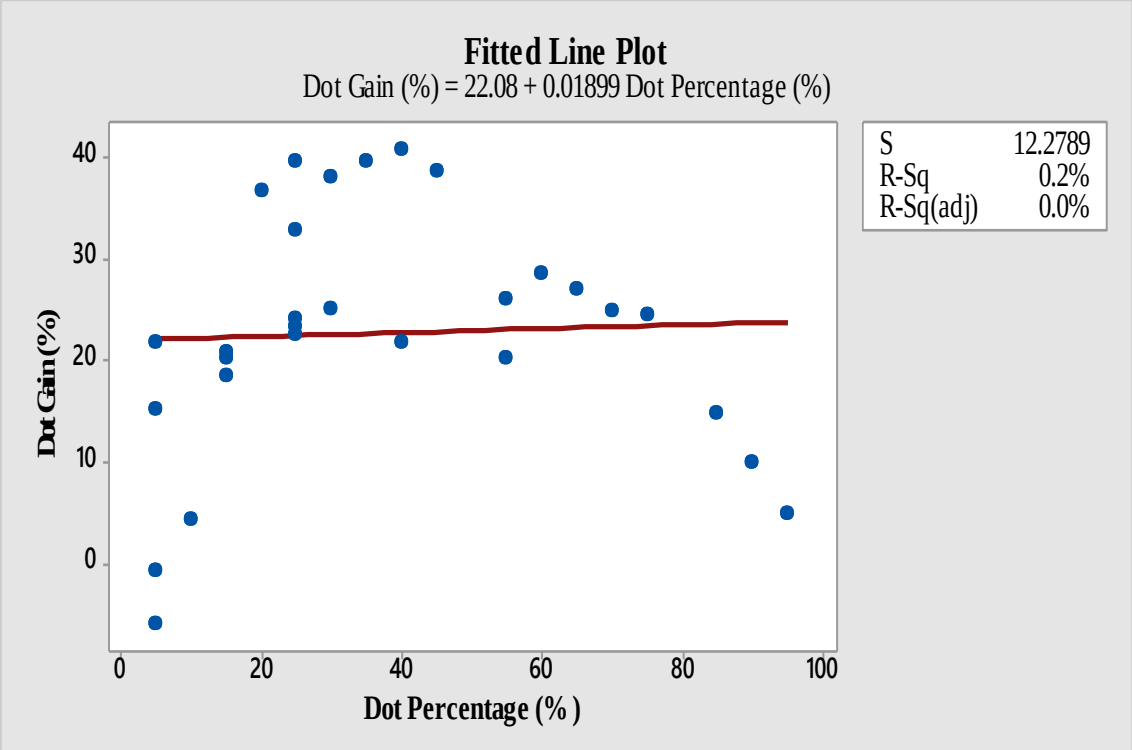

Figure 5.68: Fitted line plot for dot gain vs dot percentage

5.3.1.5 Discussions

The Table 5.32 contains the result of loss functions that shows the random forest regression algorithm is comparatively better in the prediction of dot gain than linear regression and decision tree regression algorithms. The random forest generally combines the predictions of multiple individual models which are decision trees to improve the overall performance. The common problem of individual decision trees is overfitting which can be reduced by using random forest regression as it ensembles nature and introduces randomness. In comparison to single model, random forest gives more accurate predictions due to combination of multiple diverse trees. Random forest regression can handle high dimensional datasets containing a large number of features. From this large number of features, it can identify the features which contribute most to the predictions. Random forest can also handle missing data without any accusation.

The Figure 5.58 shows the histogram plot for the residuals found during the analysis. Residuals at near zero suggest model predictions accuracy. Also found that the normal distribution of residuals is somewhat asymmetrical at some points.

The Figure 5.59 is the normal probability plot that represents the visual data regarding the deviation of response from normal distribution. The presence of outliers indicates the variability in the printing process may not be captured by the model.

The Figure 5.60 represents the versus fit plot that shows the non-linearity, outliers and undesirable errors may be due to the dataset found from the experimental process.

The Figure 5.61 is the versus order plot that indicates the residuals fluctuate around 0 and serial correlation of errors in the experimental sequence. The model performance is stable over the sequence of observations.

The Figure 5.62 shows the scatterplot of dot gain (%) vs screen mesh ruling (lpi) that indicates the possibility of decreasing dot gain with increasing screen mesh ruling. Dot gain is maximum at 100 lpi screen mesh ruling and minimum at 140 lpi screen mesh ruling.

The scatterplot of dot gain (%) vs dot percentage (%) of Figure 5.63 shows the maximum occurrence of dot gain is at the middle-tone regions of the print. Dot gain is maximum for FM dots than for AM dots.

From the scatterplot of dot gain (%) vs paper roughness (ml/min) of Figure 5.64, it is found that the dot gain is dependent on paper roughness structure. The dot gain will be more if the substrate has high porous structure.

The Figure 5.65 is a boxplot of dot gain in screen printing which shows the skewness and spread of data through their quartiles. The whiskers extending from the box tells the variability outside the quartiles. The presence of an outlier with negative dot gain represents occasional dot loss or measurement irregularities during printing.

The Figures 5.66-5.68 are the fitted line plots between dot gain and different input variables such as screen mesh ruling, paper roughness and dot percentage. In Figure 5.66, the value of R-sq is 32.6% which indicates the screen mesh ruling explains about 32.6% of the variation in dot gain. The value of R-sq (adj) is 30.1%, it means adjusted for the number of predictors, slightly lower but consistent. S tells the standard error which is 10.09, that represents the average distance that the observed dot gain values fall from regression line.

The Figures 5.66-5.68 actually represents the estimated value of regression function between response and input variables.

5.3.1.6 Conclusions

The contributions in the screen printing are used as background information for machine learning using python programming and Minitab 17 software. The implementation of three different machine learning algorithms such as linear regression, decision tree and random forest regression are used. The proposed models for data analytics, performance evaluation and result analysis show that the random forest regression provides better efficiency to predict the accuracy of the model.

The Minitab 17 software has been utilized in the graphical plots which indicate the nature of distribution of datasets and the relationships between output response as dot gain and different input variables related to the screen printing experiment.

Chapter 6

Conclusions and Future Scopes

6.1 Flexography Printing

In the present work, the research was conducted on flexography printing with three variable factors: coated and uncoated paper, round and square shaped halftone dots and three different anilox roller screen rulings. Considering the results of Taguchi's grey relational analysis, it has been observed that optimum print quality is obtained when print is taken on coated paper adopting 700 lpi anilox roller screen rulings if the image is made of round dot where dot gain is taken as a factor affecting print quality.

It is also found that if hue error is considered as print quality index, optimum result can be obtained on uncoated paper using square dot but it behaves differently in different percentage dot areas so far as print contrast is concerned, coated paper printed with 700 lpi screen ruling will produce highest print quality. As a whole, 700 lpi anilox roller screen ruling will produce highest print quality on coated paper if the image is composed of round dots. The print quality has been analyzed on the basis of the assessment of print parameters such as solid ink density, dot gain, hue error and print contrast using Taguchi's grey relational analysis. The results showed that the flexography print quality is dependent on the factors such as surface characteristics of substrate [14, 17], geometrical shape of the halftone dots used and the anilox roller screen rulings [8]. Also, this study showed the scope of implementation of Taguchi's grey relational analysis in the decision making process associated with the print quality assessment in flexography.

A mathematical model with three factors based on Box Behnken Design was utilized to optimize the process parameters for flexography printing's evaluation of print contrast and dot gain. The BBD model permits an easy way to generate a higher order response surface methodology using fewer experimental runs. A total of fifteen experimental runs were carried out and both the dot gain and print contrast responses were recorded. The BBD was executed with Minitab 17 statistical software and the graphical analysis and regression analysis were done. The graphical analysis shows the influence of

different factors over dot gain and print contrast. The result is analysed in detail with main effects plot, interaction plot, contour plots, surface plots etc. In the regression analysis part, main, squared, and interaction components are created. To identify which of the components are more important, a 95% confidence level was used.

The influence of paper roughness and anilox roller screen rulings on the dot gain of flexography print were also analyzed. The dot area percentage with square dots at middle-tone areas are found more sensitive to dot gain. It has been found that the effect will be more with the choice of low anilox roller screen rulings together with rough textured substrate in the printing process as controlled transfer of a liquid ink is essential to the flexography printing. The optimum level of process parameters were identified as anilox roller with higher screen rulings and substrate with smooth surface finish would be better for halftone dot reproduction in flexography. It has also been found that print contrast would be affected by the choice of anilox roller screen rulings, paper roughness and percentage dot area. It has further been found that print contrast varies from 40%-60% which indicates good tonal range and well reproduced image details at shadow areas. The roughness of the paper also influences the print contrast [16]. Higher the paper roughness, lower will be the print contrast. The square dot around 50% tonal regions promotes dot gain in an undesirable way, and so the dot shapes other than square dots will be a better choice around 50% tonal regions.

Prediction of image quality using different machine learning techniques has been performed. The work has been carried out both in single color prints and four color prints in flexography printing process.

In single color prints, input parameters that vary were anilox roller screen rulings, paper roughness, dot percentage and dot shape. These data were used to train the system and the predicted output variable was dot gain. It has been observed that random forest regression is comparatively better out of the three machine learning techniques considered in single color prints.

In case of four color prints, the input variables were anilox roller screen rulings, paper roughness, dot percentage and halftone dot shape and output (predicted) responses were dot gain and hue error. The machine learning techniques considered for prediction was LR (Linear Regression), DT (Decision Tree) regression, RF (Random Forest)

regression, XG (Extreme Gradient) boost regression, SVM (Support Vector Machines) regression and NN (Neural Network). It has been observed that overall accuracy of prediction is the best in the case of Neural Network both in dot gain and hue error predictions. It is to be mentioned that Neural Network machine learning can predict dot gains and hue errors with better accuracy in all the process colors such as cyan, magenta, yellow and black in comparison to other methods considered. It has also been found that printing sequence of yellow, cyan, magenta and black promotes minimum chances of hue error variations.

6.2 Screen Printing

The experimental study conducted with this research work was designed in such a way to find the influence of AM and FM dots on coated and uncoated paper under three different screen mesh ruling in the screen printing. The print quality assessment was done through the scientific approach of Taguchi's grey relational analysis by considering the major factors influencing the print quality such as solid ink density, dot gain, hue error and print contrast. The tonal reproduction curve at 5% to 100% dot coverage is plotted for dot area, dot gain, hue error and the print contrast. Moreover, this research work employed the systematic implementation of Taguchi's grey relational analysis technique in the print quality assessment in a most reliable and meaningful way.

It has been found that the screen printing quality is dependent on the screen mesh count. Printing with a high screen mesh count on smooth surface paper will give the best result in screen printing. The AM dots will work better in the middle-tone region with a good tonal value transition from highlight to shadow region. It has also been found that the FM dots are also capable to give the vibrant color especially at the solid density regions than that of AM dots but fail to reproduce the middle-tone densities with a smooth tonal transition [31]. A huge shift of tonal value has been observed at the middle-tones for FM dots. The accurate reproduction of FM dots in screen printing is dependent on the mesh count and some other crucial factors like adaptation with proper stencil making process, adhesion with screen mesh, squeegee pressure, ink parameters etc. The printing on uncoated paper with low mesh count will leads to high dot gain and it is a poor choice for high quality precision works.

In order to improve the process parameters for the evaluation of print contrast and dot gain in screen printing, a mathematical model comprising three elements based on Box Behnken Design (BBD) was employed. With fewer experimental runs, a higher order response surface methodology can be easily generated through the BBD model. The dot gain and print contrast responses were recorded throughout a total of fifteen experimental runs. Minitab 17 software was used to carry out the BBD, and regression and graphical analysis were performed. The graphical analysis was done to find relation among parameters that affect print contrast and dot gain. Using surface, contour, interaction, main effect and other plots, the outcome was thoroughly analyzed.

The screen mesh ruling plays a major role in the occurrence of dot gain in screen printing. It has been found that higher the screen mesh ruling, higher will be the dot gain especially for FM halftone dots. The mesh opening size must be capable to carry each individual halftone dots of the stencil for the accurate result in printing; otherwise, the dot loss over the screen mesh will occur and it further causes dot gain and also it will influence the print contrast too. The undesirable tonal shift from highlight to middle-tones and immediately to the shadow areas were also observed with the screen printing result with FM dots. Also, the dot gain and print contrast were found to be influenced by the surface roughness level of the substrates used [28]. The roughness of the surface can accelerate the rate of ink absorption and increase of dot gain. In the present work, a substrate with smoother surface finish and a higher screen mesh ruling would be the ideal levels of process parameters which may be used with the screen printing in order to get a good quality print.

Prediction of image quality using three different machine learning algorithms has been done in single color prints in screen printing process.

In black and white prints, input parameters which vary are screen mesh ruling, paper roughness, dot percentage and halftone screening type. The experimental data were fed to train the system and the output response as dot gain was found. It has been noticed that random forest regression (RF) gives better output in comparison to linear regression (LR) and decision tree regression (DT) in single color screen prints.

The major contribution of the research work is that the different models like Taguchi Grey Relational Analysis and Box Behnken Design are generally not considered in

flexography and screen printing quality evaluation. But these models as well as Machine Learning have been applied as far as possible in accomplishing of this research work. This can open a completely new avenue in assuring and predicting the print quality. Besides, it is to be mentioned that the results obtained using Taguchi Grey Relational Analysis, Box Behnken Design and Machine Learning are more or less consistent to attain the research goal.

6.3 Future Scopes

This research work in flexography printing may be extended by varying the different parameters such as halftone dot shapes, anilox roller cell shapes, cell angles, cell depth, varying ink viscosities, the printing speed, different surface textures of the substrates, printing atmospheric conditions etc. and their effects on the print quality.

This research work in screen printing may be extended by varying the different parameters such as halftone dot shapes, screen mesh rulings, varying ink viscosities, squeegee angles, squeegee profiles, different substrates and also the printing speed.

Bibliography

Flexography Printing

[1] Adams, Faux & Rieber (1995), Printing Technology, GATF.

[2] Crouch, P. J. (1998). Flexography Primer, GATF.

[3] Kipphan, H. (2001). Handbook of Print Media: Technologies and Production Methods, Springer.

[4] Flexography: Principles & Practices (2013). Foundation of Flexographic Technical Association, ISBN-10: 0989437418.

[5] Leach, H. R., Pierce, J. R., Hickman, P. E., Mackenzie, J. M., & Smith, G. H. (1993). The Printing Ink Manual, Springer, ISBN: 978-0-948905-81-0.

[6] Żołek-Tryznowska, Z., Rombel, M., Petriaszwili, G., & Kasikovic, N. (2020). Influence of Some Flexographic Printing Process Conditions on the Optical Density and Tonal Value Increase of Overprinted Plastic Films. Coatings, 10(9), 816. https://doi.org/10.3390/coatings10090816.

[7] Kirwan, M. J., (2008). Paper and Paperboard Packaging Technology, Wiley-Blackwell, ISBN: 978-1-405-16845-8.

[8] Dendge, R.R. (2023). Analysis of Dot Gain produced by interactions of flexographic plate and anilox roll screen frequencies. *Acta Graphica,* 31(1).

[9] Gooran, S. (2005). Hybrid halftoning, a useful method for Flexography. *Journal of Imaging Science and Technology*, 49(1). https://library.imaging.org.

[10] Youssef, T.K. (2015). The impact of FM-AM hybrid screening and AM screening on flexographic printing quality. *International Design Journal*, 5(4), pp. 1471–1476.

[11] Vandana., & Jangra, V. (2018). The evolution and revolution of screening technology: A review. *Global Journal of Engineering Science and Researches*, ISSN 2348–8034. https://doi.org/10.5281/zenodo.1343474.

[12] Hsieh, Y.C., Cheng, H.W., Cheng, Y.H., Chen, S.Y., & Ng, S.V. (2008). Flexible hybrid screening solutions for flexography. *International Conference on Computer Science and Software Engineering*. https://doi.org/10.1109/CSSE.2008.1390.

[13] Valdec, D., Hajdek, K., Vragovic, L., & Gecek, R. (2021). Determining the print quality due to deformation of the halftone dots in flexography. *Applied Sciences*, 11, 10601. https://doi.org/10.3390/app112210601.

[14] Tomasegovic, T., Pibernik, J., Poljacek, M.S., & Madzar, A. (2021). Optimization of flexographic print properties on ecologically favourable paper substrates. *Journal of Graphic Engineering and Design*, 12(1), pp. 37–44. https://doi.org/10.24867/JGED-2021-1-037.

[15] Dharavath, N.H., Bensen, M.T., & Gaddam, B. (2005). Analysis of print attributes of Amplitude Modulated (AM) vs. Frequency Modulated (FM) screening of multicolor offset printing. *Journal of Industrial Technology*, 21(3). www.nait.org.

[16] Lychock, G. (1996). Explanation of hue error and grayness. *X-rite: Ga00034a_HueError_Grayness_EN*. https://www.xrite.com.

[17] Valdec, D., Miljkovic, P., & Augustin, B. (2017). The influence of printing substrate properties on colour characterization in flexography according to the ISO Specifications. *Tehnicki Glasnik*, 11(1). ISSN 1846–6168 (Print), ISSN 1848–5588 (Online).

[18] Joshi, V.A. (2022). Optimization of flexo process parameters to reduce the overall manufacturing cost. *An International Journal of Optimization and Control: Theories & Applications*, 12(1), pp. 66–78. https://doi.org/10.11121/ijocta.2022.1137.

[19] Bould, C.D., Hamblyn, M.S., Gethin, T.D., & Claypole, C.T. (2010). Effect of impression pressure and anilox specification on solid and halftone density. *Journal of Engineering Manufacture*. https://doi.org/10.1177/2041297510394072.

[20] Kajondecha, P. & Hoshino, Y. (2008). Halftone dot size variation in offset, electrophotographic, and flexographic printing and its perception. *Journal of Imaging Science and Technology*. 52(6). https://doi.org/10.2352/(2008)52:6(060503).

[21] Gencoglu, N.E. (2012). Influence of ink viscosity on dot gain and print density in flexography. *Asian Journal of Chemistry*. Vol. 24, No. 5. https://www.asianjournalofchemistry.co.in.

[22] Bhattacharya, A., Bandhyopadhyay, S. & Green, P. (2016). Characterizing coated paper surface for modelling apparent dot area of halftone prints. *OPTICS EXPRESS 1708*, Vol. 24, No. 2. https://doi.org/10.1364/OE.24.001708.

[23] Theohari, S., Fraggedakis, E., Tsimis, D., Tsigonias, M. & Mandis, D. (2014). Effect of paper properties on print quality by flexographic method. https://www.researchgate.net/publication/263847022.

[24] X-rite, L7-158, *Color Basics EN*. (1996). https://www.xrite.com.

[25] ECTran71. Anilox roll cell structure. Available at: https://en.wikipedia.org/wiki/File:Anilox_cells.png

Screen Printing

[26] Ingram, S. (1999). Screen Printing Primer, GATF.

[27] Dina, B. R., Uddin, M. Z. & Fatema, K. U. (2020). Effect of mesh count on dot design and quality of screen printing in knit fabric. *Journal of Textile Engineering and Fashion Technology.* 6 (4), 122–131. https://doi.org/10.15406/jteft.2020.06.00240.

[28] Viorica, C., Jana, C., Balan, E. & Mohora, C. (2018) The study of the screen printing quality depending on the surface to be printed. In: 22nd International

Conference on Innovative Manufacturing Engineering and Energy, IManE&E 2018, 31 May–2 June 2018, Chisinau, Republic of Moldova. Les Ulis, EDP Sciences - Web of Conferences. https://doi.org/10.1051/matecconf/201817803015.

[29] Kipphan, H. (2001). Handbook of print media: technologies and production methods, Berlin, Springer. https://doi.org/10.1007/978-3-540-29900-4.

[30] Dharavath, N. H., Bensen, M. T. & Gaddam, B. (2005). Analysis of Print Attributes of Amplitude Modulated (AM) vs. Frequency Modulated (FM) Screening of Multicolor Offset Printing. *Journal of Industrial Technology.* 21 (3), 2-10.

[31] Poljacek M. S., Mandic, L., Agic, D. & Gojo, M. (2005). A Contribution to the AM and the FM screening in the graphic reproduction process. In: Katalinic, B. (ed.) DAAAM International Scientific Book 2005. Vienna, DAAAM International Vienna, pp. 395-404.

[32] Novaković, D., Kašiković, N., Vladić, G. & Pal, M. (2016). 15 – Screen Printing. In: Izdebska, J. and Thomas, S. (eds.) Printing on Polymers. Amsterdam, Elsevier, pp. 247-261. https://doi.org/10.1016/B978-0-323-37468-2.00015-4.

Taguchi Grey Relational Analysis

[33] Karna, K.S., & Sahai, R. (2012). An overview on Taguchi Method. *International Journal of Engineering and Mathematical Sciences*, 1, pp. 11–18.

[34] Patil, A.N., Walke, G.A., & Gawkhare, M. (2019). Grey Relation Analysis methodology and its application. *Research Review International Journal of Multidisciplinary*, 4(2). ISSN 2455-3085. www.rrjournals.com.

[35] Kumar, S., & Baral, A.K. (2023). Taguchi's Grey Relationship Analysis (GRA) for comparing the performance of various inkjet printheads for tone value increase on uncoated paper substrates. *International Journal on Recent and Innovation Trends in Computing and Communication*. http://www.ijritcc.org.

[36] Kumar, V. (2020). Taguchi Method Experimental Design Technique.*International conference on Science, Technology and Management,* ISBN:978-81-944855-1-3. www.conferenceworld.in.

[37] Roy, K.R. (2010). *A Primer on the Taguchi Method-2nd Edn*, ISBN 13: 978-0-87263-864-8, 0-87263-864-2. www.sme.org/store.

Box Behnken Design

[38] Iwundu, P.M. & Cosmos, J. (2022). The efficiency of seven-variable box-behnken experimental design with varying centre runs on full and reduced model types. *Journal of Mathematics and Statistics.* Vol. 18(2022): 196.207. https://doi.org/10.3844/jmssp.2022.196.207.

[39] Salagarkar, S., Salunkhe, S. & Doke, C. (2023). A review on Box-Behnken design for analytical method development. *International Research Journal of Modernization in Engineering Technology and Science.* Vol. 05, Issue 12. https://www.irjmets.com.

[40] Sz.Gulyas, N., Al-Tayawi, N.A., Horvath, Z., Laszlo, Z., Kertesz, S. & Hodur, C. (2023). Methods for experimental design, central composite design and the Box–Behnken design, to optimize operational parameters: A review. *Journal of Acta Alimentaria.* https://doi.org/10.1556/066.2023.00235.

[41] Ferreira, C.L.S., Bruns, E.R., Ferreira, S.H., Matos, D.G., David, M.J., Brandao, C.G., da Silva, P.G.E., Portugal, A.L., dos Reis, S.P., Souza, S.A. & dos Santos, L.N.W. (2007). Box-Behnken design: An alternative for the optimization of analytical methods. *Journal of Analytica Chimica Acta.* 597. https://doi.org/10.1016/j.aca.2007.07.011.

[42] Aziz, A.R.A. & Aziz, A.S. (2018). Application of Box Behnken Design to optimize the parameters for kenaf-epoxy as noise absorber. *IOP Conference Series: Materials Science and Engineering.* 454 (2018) 012001. https://doi.org/10.1088/1757-899X/454/1/012001.

[43] Rai, V.H., Modi, K.Y. & Pare, A. (2018). Process parameter optimization for tensile strength of 3D printed parts using response surface methodology. *IOP Conf. Series: Materials Science and Engineering.* 377 (2018) 012027. https://doi.org/10.1088/1757-899X/377/1/012027.

[44] Kechagias, D.J. & Nectarios, V. (2022). Parametric optimization of material extrusion 3D printing process: an assessment of Box-Behnken vs. full-factorial experimental approach. *The International Journal of Advanced Manufacturing Technology, 121*. https://doi.org/10.1007/s00170-022-09532-2.

[45] Manohar, M., Joseph, J., Selvaraj, T. & Sivakumar, D. (2013). Application of Box Behnken design to optimize the parameters for turning Inconel 718 using coated carbide tools. *International Journal of Scientific & Engineering Research.* Vol. 4, Issue 4. http://www.ijser.org.

[46] Ghasemi, M.S., Ghaderpoori, M., Moradi, M., Taghavi, M. & Karimyan, K. (2020). Application of Box–Behnken design for optimization of malachite green removal from aqueous solutions by modified barley straw. *Journal of Global NEST.* Vol. 22, No. 3. https://doi.org/10.30955/gnj.003089.

[47] Aliemeke, G.N.B. & Oladeinde, H.M. (2020). Box-behnken design optimization of sand casting process parameters. *International Journal of Engineering Technologies-IJET*, Vol.6, No.2. https://doi.org/10.19072/ijet.714473.

[48] Ishraq, F., Ahmed, R. & Joytun, N.J. (2021). Fabrication and process parameter optimization of a 3D printer using response surface methodology. *International journal of research in industrial engineering. 10* (3). https://www.riejournal.com.

Machine Learning

[49] Abusaq, Z., Zahoor, S., Habib, S.M., Rehman, M., Mahmood, J., Kanan, M. & Mustaq T.R., (2023). Improving energy performance in flexographic printing process through lean and AI techniques: A Case Study. *Journal of MDPI. Energies 2023*, 16(4), pp.1972. https://doi.org/10.3390/en16041972.

[50] Chandel, M., Silakari, S., Pandey, R., & Sharma, S. (2022). A study on machine learning and Python's framework. *International Journal of Computer Sciences and Engineering*, Vol. 10, Issue 5. https://doi.org/10.26438/ijcse/v10i5.5864.

[51] Çelik, Ö., & Altunaydin, S.S. (2018). A research on machine learning methods and its applications. *Journal of Educational Technology and Online Learning*, Vol. 1, Issue 3, pp.25-40. http://doi.org/10.31681/jetol.457046.

[52] Jin, W. (2020). Research on machine learning and its algorithms and development. *Journal of Physics Conference Series*. 1544(1):012003. http://doi.org/10.1088/1742-6596/1544/1/012003.

[53] Sisodia, P. & Seth, B. (2022). An implementation on Python for data science and machine learning. *International Journal of Creative Research Thoughts*. Vol. 10, Issue 3, pp.a903-a907. https://www.ijcrt.org.

[54] Sodhi, P., Awasthi, N., & Sharma, V. (2019). Introduction to machine learning and its basic application in Python. *SSRN Electronic Journal*. https://doi.org/10.2139/ssrn.3323796.

[55] Turing, A. M. (1950). Computing Machinery and Intelligence. *Mind*, 59(236), 433-460.

[56] Mitchell, T. M. (1997). Machine Learning, McGraw-Hill.

[57] Bishop, C. M. (2006). Pattern Recognition and Machine Learning, Springer.

[58] Hastie, T., Tibshirani, R., & Friedman, J. (2009). The Elements of Statistical Learning: Data Mining, Inference, and Prediction, Springer.

[59] Goodfellow, I., Bengio, Y., & Courville, A. (2016). *Deep Learning*, MIT Press.

[60] Chapelle, O., Scholkopf, B., & Zien, A. (2006). *Semi-Supervised Learning*, MIT Press.

[61] Van Engelen, J. E., & Hoos, H. H. (2020). A survey on semi-supervised learning. *Machine Learning*, 109(2), 373-440.

Soumen Basak
10.10.2025